Hydraulic and Chemico-Osmotic Performance of Polymer Treated Clays

Gemmina Di Emidio

Promotoren: prof. dr. ir. W. Van Impe, dr. ir. F. Mazzieri
Proefschrift ingediend tot het behalen van de graad van
Doctor in de Ingenieurswetenschappen: Bouwkunde

Vakgroep Civiele Techniek
Voorzitter: prof. dr. ir. J. De Rouck
Faculteit Ingenieurswetenschappen
Academiejaar 2009 - 2010

ISBN 978-90-8578-371-8
NUR 956, 973
Wettelijk depot: D/2010/10.500/47

Universiteit Gent
Faculteit Ingenieurswetenschappen
Vakgroep Civiele Techniek

Supervisors:	prof. dr. ir. William F. Van Impe (TW15)
	dr. ir. Francesco Mazzieri (Univpm, Italy)
Examining Board:	
Chairman:	prof. dr. ir. Luc Taerwe (Dean FirW)
Reading Committee:	prof. dr. ir. Mario Manassero (Polito, Italy)
	prof. dr. ir. Peter Troch (TW15)
	prof. dr. ir. William F. Van Impe (TW15), Supervisor
	prof. dr. Eric Van Ranst (WE13)
Other members:	dr. ir. Andrea Dominijanni (Polito, Italy)
	prof. dr. ir. Evelina Fratalocchi (Univpm, Italy)
	dr. ir. Francesco Mazzieri (Univpm, Italy), Supervisor
	prof. dr. ir. Greet Van Eetvelde (TW15), Secretaris
	dr. ir. Peter Van Impe (TW15)

Ghent University
Faculty of Engineering
Laboratory of Geotechnics (IR15)
Technologiepark 905,
B-9052 Zwijnaarde,
Belgium
Tel.: +32-9-264.57.17
Fax.: +32-9-264.58.49

Acknowledgements

I would like to thank my supervisor Prof. William Van Impe for his support, encouragement and helpful comments throughout the course of this research. I would also like to thank the co-supervisor Dr. Francesco Mazzieri for his continuous guidance and dedication.

I would like to thank all the members of my Guidance Committee, Prof. Mario Manassero, Prof. Evelina Fratalocchi, Dr. Andrea Dominijanni and Dr. Peter Van Impe for the enlightening discussions and suggestions. In particular, I would like to thank Dr. Andrea Dominijanni for his supervision and cooperation during the development of the theoretical modeling.

I would like to thank the Department of Geotechnics of the Ministry of Public Works, Prof. Paul Van der Meeren (Faculty of Bioscience Engineering) and Prof. Eric Van Ranst (Faculty of Soil Science) for making available equipment and expertise. Financial support was provided by Ghent University through GOA funding (grant No. 12.058.598) and through the Scientific Research Committee funding for Assistants (CWO-Firw funding).

I would like to thank the personnel of the Laboratory of Geotechnics: the secretaries, the technicians, the thesis students, my colleagues and friends, for their help and for the pleasant time spent together.

I would like to thank my parents, Mauro and Quinta, my nephew, Alessio, my brothers and my friends for their support and encouragement.

Finally, I deeply thank Daniel for his kindness and dedication. This work could not have been possible without him.

Ghent, June 2010
Gemmina Di Emidio

Table of Contents

List of Acronyms and Symbols

e	[-]	void ratio
n	[-]	porosity
k	[m/s]	hydraulic conductivity
w	[%]	water content
σ'	[kPa]	effective stress
PV	[-]	Pore Volumes of flow
CEC	[meq/100g]	Cation Exchange Capacity
EC	[mS/cm]	Electrical Conductivity
Na-CMC	[-]	Sodium-Carboxymethyl Cellulose
Na-PAAS	[-]	Sodium-Polyacrylate
GCL	[-]	Geosynthetic Clay Liner
CCL	[-]	Compacted Clay Liner
DPH GCL	[-]	Dense Prehydrated GCL
MSB	[-]	Multiswellable Bentonite
NB	[-]	Non-treated Bentonite
PC	[-]	Propylene Carbonate
Eh	[mV]	Redox Potential
Gs	[-]	Specific gravity of soil solids
XRD	[-]	X-ray diffraction
SEM	[-]	Scanning Electron Microscopy
d	[nm]	Basal spacing
θ	[$^\circ$]	Incident beam angle
C	[M]	Concentration
$C_{t,i}$	[M]	Top inlet concentration
$C_{b,i}$	[M]	Base inlet concentration
$C_{t,o}$	[M]	Top outlet concentration
$C_{b,o}$	[M]	Base outlet concentration
ΔC	[M]	Salt concentration gradient
$C_{b,j}$	[M]	Concentration of solute species j at the bottom
$C_{t,j}$	[M]	Concentration of solute species j at the top
ΔP	[kPa]	Differential Pressure
$\Delta\pi$	[kPa]	Theoretical chemico-osmotic pressure
ω	[-]	Chemico-osmotic efficiency
R	[J mol^{-1} K^{-1}]	Universal gas constant
T	[K]	Absolute temperature

ν	[-]	Number of ions per molecule
Q_t	[kg m^{-2}]	Cumulative mass per unit area
A	[m^2]	Cross-sectional area of the specimen
m	[kg]	Mass
V	[m^3]	Volume
t	[s]	Time
t_{ss}	[s]	Time to steady state
t_L	[s]	Time lag
L	[m]	Specimen thickness
J	[s^{-1} mol m^{-2}]	Diffusive flux
D_0	[m^2 s^{-1}]	Diffusivity in free solution
D^*	[m^2 s^{-1}]	Bulk diffusion coefficient
τ	[-]	Tortuosity factor
R_d	[-]	Retardation factor
ψ	[V]	Donnan potential
Ψ	[s^{-1}]	Hydraulic permittivity
DDL	[-]	Diffuse double layer
SI	[ml/2g]	Swell index
P	[kPa]	Fluid pressure in the external solution
$\bar{P}$	[kPa]	Fluid pressure in the pore solution
z_i	[-]	Electrochemical valence of the i^{th} ion
C_i	[M]	Concentration of the i^{th} ion in the external solution
$\bar{C_i}$	[M]	Concentration of the i^{th} ion in the pore solution
Π	[kPa]	Osmotic pressure in the external solution
$\bar{\Pi}$	[kPa]	Osmotic pressure in the pore solution
$\Gamma_{\underline{i}}$	[-]	Partition coefficient of the i-th ion
$C_{\underline{x}}$	[M]	Fixed charge concentration
C_{xo}	[M]	Fixed charge concentration divided by e
ϕ_X	[-]	Fixed charge coefficient
ρ_s	[kg m^{-3}]	Density of solid particles
f_{Stern}	[-]	Fraction of electric charge compensated by cations specifically adsorbed in the Stern Layer
σ	[C m^2]	Surface charge
N	[-]	Number of clay platelets per aggregate
S	[m^2/g]	Total specific surface of the clay
S'	[m^2/g]	External specific surface aorun the clay aggregate
e'	[-]	Void ratio referred to the void space between clay aggregates
S_π	[kPa]	Swell pressure
q	[m^3 s^{-1}]	Volumetric flux
F	[C mol^{-1}]	Faraday constant
Φ	[V]	Electric potential within the clay

d_h	[-]	Mechanical permeability at zero electric gradient
ϖ	[-]	Sign of the fixed charge
$\bar{\kappa}$	[mS/cm]	Equivalent electrical conductivity of the solution within the membrane
$\bar{t}_i$	[-]	Transference (or transport) number of the i^{th} ion within the membrane
I_e	[A]	Electric current
u	[-]	Normalized concentration

Samenvatting

Vloeibare afvalstoffen in het milieu kunnen afkomstig zijn van verschillende bronnen: het ongecontroleerd dumpen van zuivere oplosmiddelen, lekkages of percolaat van stortplaatsen enz. De hedendaagse internationale voorschriften geven aan dat, om besmetting van de omgeving te voorkomen, stortplaatsen uit samengestelde afdichtende lagen met zeer specifieke eigenschappen moeten worden opgebouwd. Bentonietklei wordt hierbij op grote schaal, als hydraulisch weerstandbiedend element in de afdichtende systemen van stortplaatsen aangewend, vooral vanwege de geringe hydraulische geleidbaarheid, lage diffusiecoëfficiënt en zelfhelende eigenschappen van die klei. Blootstelling aan elektrolytische en organische oplossing kan echter leiden tot een ongewenste significante stijging van de hydraulische geleidbaarheid en diffusiecoëfficiënt, omwille van de vermindering van de dikte van de dubbele elektronenlaag. De mate waarin dit optreedt, is afhankelijk van het type en de concentratie van dergelijke ionen.

Het voornaamste doel van dit onderzoek was een verbeterd kleimateriaal te ontwikkelen met meer performante hydraulische prestaties. De HYPERklei werd hier ontwikkeld door behandeling van een natuurlijke bentonietklei met anionische polymeren; daarnaast werden ook twee commercieel reeds verkrijgbare, met polymeren behandelde kleimaterialen, bestudeerd: de Multiswellable Bentonite (MSB) en de Dense Prehydrated GCL (DPH GCL). Om de potentiële voordelen van dergelijke behandeling met polymeren te evalueren, werden zowel de fysische en chemische eigenschappen van het behandelde materiaal, evenals de zweleigenschappen onderzocht. Daarbij werden ook doorlatendheidsproeven en chemico-osmotische proeven uitgevoerd op behandelde en op onbehandelde kleimonsters, om de efficiëntie van de materialen in aanwezigheid van agressieve elektrolytoplossingen te evalueren. Ten slotte interpreteert men in dit werk de experimentele resultaten via een nieuw voorstel van numeriek model.

De experimentele en analytische conclusies van dit proefschrift kunnen worden samengevat als volgt:

- De interactie van de klei met de polymeren werd bestudeerd door fysische en chemische analyse van het materiaal. Dergelijke analyse suggereert dat het polymeer zich uiteindelijk zal bevinden tussen de zogeheten platelets van de klei. Daardoor veroorzaken de polymeren een veel meer disperse structuur van de kleimineralen met een verhoogde capaciteit voor wateradsorptie, zelfs in aanwezigheid van elektrolytoplossingen. De hydraulische efficiëntie van de behandelde klei valt hierdoor voordeliger uit.

- Het zwelvermogen van de behandelde klei werd onderzocht via zwelindex-proeven en metingen van de zweldruk. Beide proeftechnieken leidden tot de conclusie dat de behandeling van de klei met een anionen-polymeer het zwelvermogen verbetert.
- Doorlatendheidsproeven onder hydraulische gradiënt werden zowel op onbehandelde als behandelde kleimonsters uitgevoerd. De hydraulische conductiviteit verhoogt voor een onbehandeld kleimateriaal met toenemende concentratie van de elektrolytoplossing, als gevolg van de samendrukking van de diffuse dubbellaag van de kleistructuur. Dit is een volkomen logisch te verwachten uitkomst. Integendeel, wanneer de klei wordt behandeld met polymeren vermindert de hydraulische conductiviteit als men oplossingen van calciumchoride of zelfs zeewater aanwendt.
- Voor onbehandelde kleien wordt, als gevolg van ionendiffusie en samendrukking van de diffuse dubbellaag, een afname in de tijd van de chemico-osmotische efficiëntie vastgesteld. Daar- tegenover staat dat de met anionen-polymeren behandelde klei ook voor chemico-osmotisch doorstroomgedrag veel beter presteert. Het is dus alsof deze polymerenbehandeling de klei beschermt tegen de destructieve rol van de contaminantendiffusie.
- Het blijkt dat de op die manier behandelde kleien daarenboven ook op lange termijn hun osmotische efficiëntie blijven behouden. Wellicht zorgen de polymeren inderdaad voor een versterking van de kleistructuur tegen samendrukking van de diffusie dubbellaag.

Deze proefresultaten van het zweldrukgedrag en de chemico-osmotische performantie van de behandelde klei werd hier geïnterpreteerd, gebruik makend van een nieuw multi-ionen numeriek model. Deze theoretische ontwikkeling is gebaseerd op het model voorgesteld door Dominijanni (2005) voor het geval van een 2-ionen systeem. We ontwikkelden een uitbreiding van het model van Dominijanni van een 2 ionen systeem tot een meer realistische 3 ionen systeem. Dit werd uitgevoord in samenwerking met de Politecnico di Torino.

Met deze uitbreiding werden alle experimentele resultaten van zwellingdruk en chemico-osmotic proeven op zowel onbehandelde als behandelde kleien geanalyseerd.

Uit de 3 ionen model heeft men de zwellingdruk van een kleimonster benaderd. Men ging ervan uit dat het aantal platelets per kleideeltje blijft constant onafhankelijk van de ionen concentratie en valentie.

We waren in staat om het effect van toevoeging van polymeren en verdichting op de zwellingdruk te analyseren d.m.v. de uitkomst van het model. Deze interpretatie heeft aangetoond dat de behandeling met polymeren verhoogt de netto negatieve lading van de klei (C_{X0}) en beperkt de aggregatie van klei deeltjes; met als gevolg een verbetering van de zwellingvermogen van de klei. Ook het verdichten van een klei verhoogt de zwellingdruk. Om deze redenen kan de gelijktijdige werking van polymeer behandeling en verdichting de zwellingvermogen van de klei aanzienlijk verbeteren.

In dit werk werd het vernoemde numerieke model daarenboven ook aangewend voor de analyse van de chemico-osmotische proefresultaten. Daardoor heeft men de sensitiviteit van dergelijk kleigedrag voor het aantal platelets per kleideeltje en voor gegeven vaste ladingsconcentratie, geëvalueerd. Dit blijkt zeer goed aan te sluiten bij de interpretatie van de specifieke proefresultaten in dit werk. Ook deze theoretische benadering via modellering suggereert dus dat het hier aangewende anionenpolymeer de kleistructuur openhoudt en de negatieve lading van de klei verhoogt.

Abstract

The purpose of hydraulic clayey barriers is to isolate waste liquids from the environment. Bentonite clay is widely used in hydraulic barriers because of its elevated sealing capacity in presence of water. However, exposure to high concentrations of inorganic solutions can change the clay fabric increasing its hydraulic conductivity, with a consequent enormous harm to the environment.

The main purpose of this research was to develop a superior clay with enhanced Hydraulic Performance. An engineered clay (HYPER clay) was developed through treatment of a natural bentonite with an anionic polymer. Furthermore, two commercially available polymer treated clays were studied: a Multiswellable Bentonite (MSB) and a Dense Prehydrated GCL (DPH GCL). To demonstrate the potential benefits of polymer treatment material characterization and swelling tests were performed. Subsequently, hydraulic and chemico-osmotic tests were executed on treated and untreated clays to evaluate the modified clays resistance to chemical attack. Finally a theoretical interpretation of the experimental results was conducted with a newly developed multi-ion system approach.

All experimental and theoretical conclusions of this PhD thesis can be summarized as follows.

The effect of polymers adsorption on clays was studied by physical and chemical analysis that demonstrated the potential benefits of polymers on the sealing, hydraulic and membrane properties of clays. Physical and chemical characterization results proved that the polymer intercalates in the interlayer region of the bentonite inducing a dispersed clay structure and increases the water adsorption capacity of the clay in electrolyte solutions with a consequent potential benefit on the hydraulic performance.

The swelling ability of the treated clays was quantified by means of standard swell index test and swelling pressure tests. Both showed that the treatment with the anionic polymer studied here improved the swelling ability of the untreated clay. The swelling pressure test, compared to the standard swell index test, showed more efficiently the swelling ability of polymer treated clays. Swelling pressure increased also with increasing polymer dosage up to an optimum value.

Hydraulic conductivity tests were conducted on untreated and polymer treated clays. As expected, the hydraulic conductivity of untreated clays increased by permeating the samples with electrolyte solutions due to the compression of the double layer thickness. Conversely, polymer treatment maintained low hydraulic conductivity of the clays to $CaCl_2$ and to sea water in the long term.

The prehydration with addition of polymers and the densification of the com-

mercial product (DPH GCL) preserved low hydraulic conductivities even in presence of aggressive electrolyte solutions such as $CaCl_2$ solutions and sea water.

The low permeability protracted in the long term observed in the polymer treated clays suggested that also the chemico-osmotic efficiency could be maintained with time in presence of aggressive solutions. For this reason, chemico-osmotic efficiency tests were also carried out.

The effect of partial or complete destruction of chemico-osmotic behavior due to diffusion was observed in untreated clays. The clay showed in fact initial membrane behavior, that gradually decreased due to the gradual compression of the double layer thickness due to diffusion of invading cations.

On the other hand, the polymer treatment with the anionic polymer protected the clay against the destructive role of diffusion, maintaining the initial osmotic efficiency in the long term. The polymer treatment modified the bentonite structure such that the double layer thickness of the clay resisted collapse and the membrane efficiency was sustained.

The Swell Pressure and Chemico-osmotic tests results were interpreted theoretically in a newly developed multi-ion system approach. The theoretical development presented here was based on the model proposed by Dominijanni (2005) for 2-ion systems. We developed, in cooperation with the Politecnico di Torino, an extension of the model to allow for multi-ion systems.

With this extension we back analized all experimental data of swelling pressure and chemico-osmotic tests conducted on untreated and polymer treated clays.

We have calculated the swelling pressure of bentonites for 3-ion systems based on the Donnan model and the electroneutrality conditions. We assumed that the number of platelets per aggregate were constant independently of the ion concentration and valence.

We were able to compare the effect of polymer addition and densification based on the back analysis of the swelling pressure tests. Interpreting the experimental data with the model, we demonstrated in fact that the polymer treatment increased the net negative charge of the clay (C_{X0}) and limited the aggregation between clay platelets with a consequent improvement of the swelling ability of the clay. Also the densification of a clay increased its swelling pressure. For this reasons, the simultaneous effect of polymer treatment and densification improved considerably the swelling ability of the clay.

For the analysis of the chemico-osmotic tests results we develop an extention of the general model proposed by Dominijanni (2005). In cooperation with Politecnico di Torino, we solved the transport equations for a 3-ion systems in order to interpret correctly the actual multi-ion scenario expected in the site.

The interpretation of the results based on the new model were performed. A parametric study was intended to analyze the impact of the fixed charge concentration of the clay and the impact of the number of clay particles per aggregate on the chemico-osmotic efficiency coefficient vs. time. Whereas, the back analysis of the experimental data allowed to define the fixed charge concentration for both the untreated and polymer treated clays.

The fixed charge concentration of the HYPER clay was higher C_{X0} than that of

the untreated clay, whereas, the number of platelets per aggregate was lower. This theoretical interpretation suggests that not only the anionic polymer maintains the interlayer open but also it increases the negative charge concentration of the clay.

1 Introduction

1.1 Problem statement

Waste liquids in the environment may result from several sources, e.g., uncontrolled dumping of pure solvents, spills, or infiltration of water through solid waste in landfill disposals resulting in contaminated leachate. Contaminants contained in this leachate can lead to significant damage to the environment and to the human health due to their mobility and solubility. To isolate those harmful contaminants from the environment, clay barrier systems are often used.

According to international regulations, landfills must be constructed with containment systems with low hydraulic conductivity in order to avoid contamination of groundwater and soil. Usually, a compacted clay liner (CCL) is used in cover systems and bottom liners for landfills. CCLs are natural clay material compacted in situ with a minimum thickness prescribed by national regulations. Over the past decades, geosynthetic clay liners (GCLs), which are factory-manufactured clay liners consisting of a thin layer of bentonite encased by geotextiles or glued to a geomembrane, have gained widespread popularity as a substitute for compacted clay liners.

Design engineers and environmental agencies have shown a growing interest in the use of GCLs due to their relatively low cost, their low hydraulic conductivity to water, their reduced thickness that allows an increase of waste storage volume and an easy installation with consequent relative low costs. As a result, they are being investigated intensively, especially with regard to their hydraulic

and diffusion characteristics, chemical compatibility, self-healing capacity, long term performance, etc. (Shackelford et al., 2000; Egloffstein, 2001; Bouazza, 2001; Kolstad et al., 2004; Katsumi and Fukagawa, 2005).

Bentonite clay is widely used in barriers for landfill systems because of its elevated sealing capacity in presence of water. However, exposure to polluted leachate can cause loss of efficiency of the clay as hydraulic barrier (Mitchell, 1993), with a consequent enormous harm to the environment.

1.2 Modified clays proposed as barrier materials

Modified bentonites have been recently introduced in barrier applications to improve their chemical resistance to aggressive permeants (Kondo, 1996; Flynn and Carter, 1998; Simon and Müller, 2005; Ashmawy et al., 2002). Among these treated soils, the clays treated with cationic polymers showed higher or slightly lower permeability compared to untreated clays (Ashmawy et al., 2002; McRory and Ashmawy, 2005).

Organoclays treated with organic molecules showed higher retention capacities than untreated clays, but slightly higher permeabilities (Lorenzetti et al., 2005).

Multiswellable bentonite (MSB), that is a manufactured bentonite clay modified with an organic compound, the propylene carbonate (Kondo, 1996), showed high swelling capacity and low hydraulic conductivity values for monovalent and bivalent solutions (Katsumi et al., 2008). On the other hand, this material showed a hydraulic conductivity to electrolytes solutions after prolonged permeation with deionised water, comparable to untreated bentonites, probably as a result of amendment loss with time (Mazzieri and Pasqualini, 2006).

Conversely, hydraulic permeability tests on a Dense PreHydrated Geosynthetic Clay Liner (DPH GCL) showed excellent results in aggressive solutions in the long term (Kolstad et al., 2004; Katsumi et al., 2008). This DPH GCL is treated with specific anionic polymers (such as CMC and Sodium Polyacrylate), prehydrated and densified to a dry bentonite content much higher than standard GCLs (Flynn and Carter, 1998).

Therefore, in view of pollutant containment applications, it is of great interest to evaluate the potential benefits of anionic polymers treatment on clays, their transport parameters, treatment techniques more suitable to preserve the polymer benefits in the long term.

1.3 Objectives of this work

The main purpose of this research is to develop a superior clay with enhanced hydraulic performance (HYPER clay) and to investigate the influence and mecha-

nisms through which the polymers and organic molecules can improve the sealing capacity, hydraulic and chemico-osmotic efficiency of bentonites for barrier applications.

Engineered clays were developed for this purpose by adsorbing an anionic polymer to the surface of an untreated bentonite. Furthermore, two commercially available polymer treated clays were studied: the Multiswellable Bentonite (MSB) and a Dense Prehydrated GCL (DPH GCL).

To demonstrate the benefits of polymer treatment and to determine the impact of different preparation techniques, physical and chemical characterization of the materials was performed. Then, standard swell index tests and alternative swell pressure tests were carried out with a specially designed apparatus in order to study the self-sealing capacity of these treated clays in presence of various aggressive solutions. Subsequently, hydraulic and chemico-osmotic tests were executed to study the impact of a number of parameters (such as polymer treatment, polymer dosage, prehydration, densification, ion concentration and valence) on the hydraulic and chemico-osmotic performance of these enhanced clays for containment systems. Finally the theoretical interpretation of the experimental results was conducted with a newly developed (3-ion system) model.

1.4 Outline of this doctoral thesis

This research was carried out at the Laboratory of Geotechnics, Ghent University. The results of the experimental and theoretical study of polymer treated clays can be grouped in five research stages:

- Stage 1: Material characterization was performed at the Laboratory of Geotechnics, the Laboratory of Soil Science and the Laboratory of Applied Analytical and Physical Chemistry of Ghent University. This stage includes the analysis and development of innovative polymer treated clays as barrier materials by analyzing the impact of the polymers on the clay structure and its behavior in presence of various ionic solutions.

- Stage 2: Self-sealing ability was tested by means of standard swell index tests and an alternative swell pressure test. Swell index tests, usually used to evaluate qualitatively the swelling abilities of clays, show some limitations to evaluate the swelling abilities of polymer treated clays. For this reason a special frame was designed in order to perform swell pressure test measurements as an alternative of swell index tests, representing better the swelling abilities of treated clays in aggressive conditions.

- Stage 3: Hydraulic performance of polymer treated clays was tested by means of long-term permeability tests. The influence on the hydraulic con-

ductivity of parameters such as polymer treatment, polymer dosage, prehydration, densification, ion concentration and valence were examined. The hydraulic conductivity of the overlapped area of GCLs is crucial for the overall performance of containment barriers. For this reason simultaneously to small scale hydraulic conductivity tests on newly developed polymer treated clays, large scale hydraulic conductivity tests were also conducted on overlapped manufactured DPH GCL samples.

- Stage 4: Chemico-osmotic performance and transport parameters of polymer treated clays were determined. A special apparatus was used following the testing methods of previous studies (Olsen, 1969; Malusis et al., 2001; Mazzieri et al., 2003). This stage illustrates the potential benefits of prehydration, polymer treatment and compression on the Chemico-osmotic efficiency and Diffusion Coefficient of the treated clays.

- Stage 5: Finally the theoretical framework for the interpretation of the swelling pressure of clays and of the chemico-osmotic tests was developed in cooperation with Dr. ir Andrea Dominijanni. He is part of the research group of Prof. Dr. ir Mario Manassero at DITAG Department of Politecnico di Torino, Italy. The theoretical results have been analyzed on the basis of the Fixed Charge Model and Donnan's Equations.

2

State of the art

2.1 Background and overview of Geosynthetic Clay Liners

Over the past decades, Geosynthetic Clay Liners (GCLs), which are factory - manufactured clay liners consisting of a thin layer of bentonite encased by geotextiles or glued to a geomembrane, mechanically held together by needling, stitching, or chemical adhesives, have gained widespread popularity as a substitute for compacted clay liners.

Since their introduction in the mid-1980's, GCLs have been utilized greatly as the lower portion of geomembrane/GCL composites in both landfill liners and final covers. They have also been used in other containment applications, such as in roads construction, railways, secondary containment for above ground tank farms, dams, canals, ponds, rivers and lakes. They are also used for waterproofing of buildings and other similar structures.

Design engineers and environmental agencies have shown a growing interest in the use of GCLs because their relatively low cost, their low hydraulic conductivity to water, their reduced thickness that allows an increase of waste storage volume and an easy installation with consequent relative low costs. As a result, they are being investigated intensively, especially in regard to their hydraulic and diffusion characteristics, chemical compatibility, self-healing capacity, long term performance, etc (Shackelford et al., 2000; Egloffstein, 2001; Bouazza, 2001; Katsumi et al., 2008).

Since Geosynthetic Clay Liners, or GCLs, are composite materials consisting of bentonite clay contained within geotextiles it is necessary to describe each of the component parts before considering the manufactured product.

Bentonite

Bentonite is a well-known member of the clay family of geologically cohesive materials having extremely low hydraulic conductivity, or permeability, to liquids and gases. Of the various types, sodium bentonite is known to have the lowest permeability of any naturally occurring geologic material. It is only available in large quantities in Wyoming and North Dakota in the U.S. The transportation costs of moving bentonite from these locations to worldwide factories for GCL manufacturing are relatively high. An alternative can be found in the large natural deposits of higher permeability calcium bentonite, which is much more available on a worldwide basis. By using sodium hydroxide to treat the calcium bentonite, a replacement of the calcium ions occurs, decreasing the permeability to that of the naturally occurring sodium bentonite. The process is sometimes called peptizing and is worldwide in its usage. Although not fully established, this trend will probably increase in the future.

Regarding, identification of the bentonite, X-ray diffraction is a precise method of determining the composition of clays. Although not as accurate, the American Petroleum Institute's methylene blue analysis is easy to perform and is thought to give conservative results. A more complete treatment of bentonite properties is treated in Section 2.2.

Geotextiles

Geotextiles are generally used as the carrier material beneath the bentonite and the cap (or cover) fabric above it. The geotextiles can be nonwoven, woven, or composite nonwovens with a woven scrim. Presently, most of the geotextiles are made from polypropylene resins with minor additions of additives such as high temperature processing aids, ultraviolet light stabilizers, and long-term durability additives. Woven geotextiles are either of the slit-film or spunlaced variety which have excellent strength and stiffness characteristics, but must be of a sufficiently tight weave so as not to allow bentonite to squeeze through the openings.

The properties of the geotextiles are an important consideration. In addition to opening size, the mass per unit area, tensile strength, tensile elongation, and installation survivability properties are all important.

Other associated materials

In addition to the possible adhesives added to the bentonite as just mentioned, very thin polymer films (0.10 mm thick), i.e., geofilms, have been added to the

composite material for further reduction of permeability. Such films are placed either above or below the cap geotextile to lower its permeability from the as-manufactured condition.

A different approach in achieving very low permeability than using a geofilm is to polymer treat the cap geotextile to lower its permeability from the as-manufactured condition. Both of these approaches are often recommended when using GCLs as a sole barrier material for noncritical and/or temporary applications. (For landfill and hydraulic applications, GCLs are invariably covered by a geomembrane).

Lastly, it is also possible to polymer modify the bentonite particles themselves within their molecular structure or adhere polymers to the outside of the platelets. This subset of nano-technology gives rise to the terms of internal or external bentonite modification. Such processes, however, are not widespread and presently the low permeability component of GCLs is mainly bentonite.

GCL manufacturing

There are currently two structurally different GCL types distinguished by the method of manufacturing the composite material: nonreinforced and (internally) reinforced. The two forms are based on the realization that hydrated bentonite is extremely low in its shear strength. Thus, nonreinforced GCLs are used on very flat surfaces and reinforced GCLs (by needle punching or stitch bonding) are used on relatively steep slopes. Each type has a number of subvariations.

Nonreinforced GCLs are either geotextile-related, geotextile/polymer-related, or geomembranerelated. The geotextile-related types have geotextiles on both surfaces and an adhesive mixed with the bentonite for bonding purposes, as shown in Figure 2.1(a). The geotextile/polymer-related types are similar but have a polymer impregnated in the upper geotextile to decrease the permeability lower than the bentonite itself. The geomembrane-related types have the bentonite adhesively bonded to a geomembrane (see Figure 2.1(b)). The geomembrane can be of any type, thickness, or surface texture.

More common than the above are reinforced GCLs. The usual method of reinforcement is by needle punching from a nonwoven cap geotextile through the bentonite and opposing geotextile, which creates a labyrinth of fibers throughout (see Figure 2.1(c)). Alternatively, we can stitch bond between two woven geotextiles through the sandwiched bentonite layer (see Figure 2.1(d)). Further variations of reinforced GCLs are geotextile-related, geotextile/polymer-related, and geotextile/geofilm-related. The geotextile-related types have various geotextiles on both surfaces. The geotextile/polymerrelated types have a polymer impregnated in the upper geotextile to lower the permeability beyond the bentonite itself. The geotextile/film-related types have a thin plastic film either above or beneath the cap geotextile. After needle punching, this film becomes part of the composite material and decreases the permeability much lower than the bentonite itself.

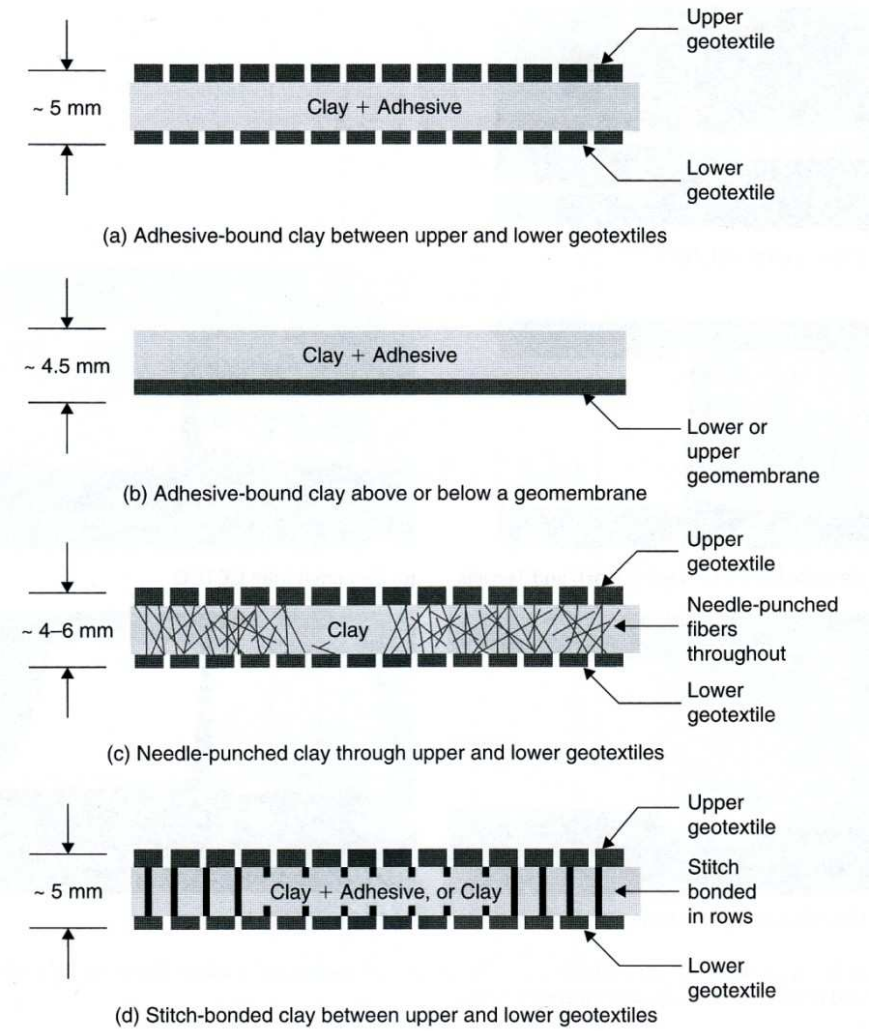

Figure 2.1: Cross sections of currently available GCLs (Koerner, 2005)

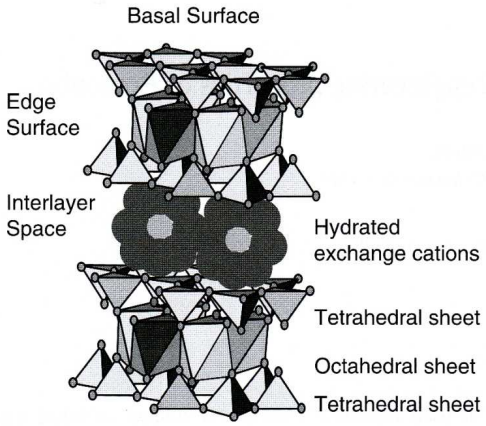

Figure 2.2: Montmorillonite structure

2.2 Mineralogy of bentonite

Smectite is a class of hydrated 2:1 layer silicate minerals that form stable colloidal suspensions and have an expandable volume due to the retention of hydrated cations. These attributes arise from the unique structural chemistry of the mineral. High quality bentonites contain greater than 70% smectite by mass. Minor constituents may include quartz, volcanic glass, opaline silica, feldspar, zeolite, and carbonate, as well as discrete kaolin, mica, or illite or mixed-layer clay minerals such as illite-smectite and kaolin-smectite. It is the smectite component, however, with its large specific surface area (as high as 850 m^2/g), cation exchange capacity (80-150 meq/100 g), and capability for interlayer swelling, that is responsible for the desirable physical and chemical attributes that make the use of bentonite ubiquitous in many industrial, commercial, and engineering applications.

Crystalline structure

As illustrated in Figure 2.2, the basic structure of minerals in the smectite group is characterized by having one octahedral sheet joined on either side by two silica tetrahedral sheets (thus the term 2:1 layer silicate) forming a unit layer (Brindley and Brown, 1980; Newman, 1987; Moore and Reynolds, 1997). In an ideal 2:1 layer, aluminum (gibbsite-like) or magnesium (brucite-like) octahedra are coordinated with four oxygen atoms and two hydroxyl ions. The tetrahedra are comprised of silicon atoms coordinated with four oxygen atoms; one of these, the apical oxygen, is also bonded to the octahedra.

If the central cations in the octahedral sheet are predominantly trivalent (e.g. Al^{3+}) then only two thirds of the cation sites (2 of 3) need to be occupied for

electroneutrality and the structure is termed dioctahedral. Dioctahedral smectites include the montmorillonite, beidellite, and nontronite species. If the cations in the octahedral sheet are predominantly divalent (e.g. Mg^{2+}) then all of the cation sites (3 of 3) need to be occupied and the structure is termed trioctahedral. Trioctahedral smectites include the saponite, hectorite, and sauconite species. Montmorillonite is the most common naturally occurring species in the smectite group, and the following discussion will be limited to montmorillonite unless other minerals are specifically mentioned.

Oxygen anions are shared between the central octahedral sheet and the two tetrahedral sheets, thus forming a strong bond that preserves the 2:1 unit layer. The thickness of the interlayer plus one unit layer (i.e. the structural repeat distance) is variable and is referred to as basal spacing, indexed as $d_{(001)}$. Several tens or even hundreds of unit layers constitute a crystallite. Many million layers and thousands of crystallites form montmorillonite particles with sizes of the order of 2 μm effective spherical diameter.

Adjacent montmorillonite layers are separated by an interlayer space that spans the distance between opposing basal or interlayer surfaces (see Fig. 2.2). These surfaces are elongated flat plates and constitute the largest surface area in smectites. The interlayer surfaces are also where most of the layer charge of the mineral is expressed and where exchangeable cations required to balance the layer charge reside. The high hydration energies of the exchange cations enable montmorillonite to absorb large amounts of water. While bonding between unit layers arising from electrostatic and short-range van der Waals attractive forces is relatively weak, the interaction of water with exchangeable cations within the interlayer space can be strong enough to allow partial or complete disassociation of smectite unit layers in aqueous solution, a phenomenon referred to as interlayer swelling.

Depending on the extent of interlayer disassociation, smectite particles range in thickness from individual unit layers, upward to thicknesses corresponding to several tens, hundreds, or thousands of stacked unit layers. Detecting changes in basal spacing associated with interlayer sorption of water or other polar sorbates is one of the key processes by which the presence of smectite in a mineral mixture is identified using X-ray diffraction (XRD).

Morphology and fabric

The morphology of smectite often resembles a thin, crumpled film or flake and it can be difficult to differentiate one particle from another. Multiple levels of scale and multiple types of mineral interactions must be considered. The volume fraction, arrangement, and orientation of the solids and pore spaces on these multiple levels of scale define the fabric of the system. This fabric (also referred to as texture or microstructure) influences bulk physical properties of the bentonite

such as swelling, sealing, and hydraulic conductivity, and is critically important in governing the corresponding performance of bentonite as a barrier material.

Individual crystallites comprised of multiple unit layers interact in face-face, overlapping face-face, edge-face and edge-edge associations to form quasi-crystals (Likos et al., 2010). A quasi-crystal is an equilibrium structure smectite gels adopt that reduces the net potential energy of particle interaction. Attractive van der Waals force interactions between quasi-crystals enable the formation of larger, interconnected clay domains. Clay domains can have various size and durability, depending on the surrounding environment (Lagaly, 2006).

The number of layers that constitute a quasi-crystal, its size, shape and interaction with other quasi-crystals is generally dependent on the layer charge characteristics of the mineral, electrolyte concentration, and identity of the exchange cation. The average thickness of Na-smectite quasi-crystals is small; typically lower than 100 individual layers, but they generally have a large aspect ratio (Tessier, 1990). The resulting gel fabric or micro-structure has a distribution of inter-particle pore sizes, which optimizes water retention, inhibits water flow (Egloffstein, 2001), and influences how interlayer swelling translates to corresponding bulk volume changes (Likos et al., 2010). On the other hand, Ca-smectite gels are typically composed of larger crystallites made up of as many as several hundred individual layers (Tessier, 1990). This results in a fabric with a pore size distribution more conductive to water (Egloffstein, 2001) and which more efficiently translates interlayer volume change to bulk volume change (Likos et al., 2010).

Swelling clays can absorb higher than 200% their mass in water and increase their original volume many fold. The clay fabric at high water content is instrumental in translating properties from the individual mineral layer or crystallite level to the macro-scale level. When under confinement, as is the usual condition in geotechnical applications, a Na^{+} clay fabric will seal because domains of quasi-crystals will necessarily have to re-arrange and expand into the available inter-particle pore space during wetting. This results in a reduction in void sizes and inter-connectivity of pores with an associated increase in tortuosity. The highly flexible nature of clay platelets enables overlapping face-face associations to dominate the fabric of Na^{+} saturated smectite gels. These particle interactions are relatively unimportant in Ca^{2+} smectite gels, where quasi-crystals are generally larger and more rigid (Likos et al., 2010).

Layer charge

Smectite is characterized by extensive isomorphous substitution that results in charge deficiencies within the crystalline structure. Substitution may occur either in the octahedral layer (e.g. Mg^{2+} for Al^{3+}) or in the tetrahedral layer (e.g. Al^{3+} for Si^{4+}), such that the overall structure carries a net negative layer charge. The negative layer charge must be neutralized by cations residing in the interlayer,

which in the case of smectites, are hydrated and exchangeable.

Exchangeable cations

The net negative charge arising from isomorphous substitution is offset by exchangeable interlayer cations. These cations are predominantly located between the unit layers within the interlayer space, but can also exist between particles or crystallites within the interparticle pore space. The cations are referred to as exchangeable because they may be replaced by other cations from solution under energetically favorable conditions. Exchangeable cations in naturally occurring clay minerals are primarily Ca^{2+}, Mg^{2+}, Na^{+}, and K^{+}, usually in that decreasing order of abundance (Mitchell, 1993).

The predominant type of exchangeable cation may be used as a qualifier for differentiating one form of the same mineral from another. We refer, for example, to Na-bentonite (or the Na^{+} form of bentonite) if Na^{+} is the predominant type of exchangeable cation. Ca^{2+} forms of bentonite are common as well.

The exchangeability of exchange cations is governed by their valence, size, hydration energies and concentration (Mitchell, 1993). For equivalent concentrations, the propensity for one type of cation to replace another follows the sequence:

$$Li^{+} < Na^{+} < K^{+} < Mg^{2+} < Ca^{2+} < Al^{3+} < Fe^{3+}$$

The higher affinity for polyvalent cations (e.g. Ca^{2+} over Na^{+}) leads to important considerations regarding ion exchange and the corresponding changes in engineering behavior (e.g. increases in hydraulic conductivity).

The magnitude and equivalency of charge in montmorillonite is usually quantified by cation exchange capacity (CEC) rather than by layer charge. In an ideal case, these measures should be identical, but since the CEC is an operationally defined measure (it depends on the method used) there is usually some disparity between CEC and layer charge measured values.

2.3 Adsorption and swelling behavior

The primary function of the bentonite layer in a GCL is to impede the flow of migrating liquids and dissolved chemical species. This is achieved by its low hydraulic conductivity, which is of the order of $1\times E^{-10}$ m/s to $1\times E^{-12}$ m/s. This low hydraulic conductivity results primarily from the smectite component's small particle size, large surface area, swelling potential, and capability to adsorb and effectively immobilize pore water through a variety of short-range and long-range hydration mechanisms. The adsorption and swelling behavior of bentonite is affected by many factors that are inherent to the bentonite in its natural state. These

include: layer charge (CEC), the location of layer charge, exchange cation identity, the clay fabric in its natural state, and impurities present.

Short-range hydration mechanisms

Colloidal clay minerals in general, and smectite in particular, are capable of significant interactions with water. Interactions occur on the external particle surfaces and, for swelling clay minerals, on the interlayer surfaces as well. The surface area and the surface charge properties of the mineral dictate the extent and range of the interactions. The large specific surface area of smectite is clear indication of the importance of solid-liquid interaction in governing its behavior.

The initial hydration of a clay mineral surface involves four basic short-range interaction mechanisms: (i) hydrogen bonding, (ii) dipole-charged surface attraction, (iii) van der Waals attraction, and (iv) hydration of exchangeable cations (Mitchell, 1993). Hydrogen bonding occurs between water dipoles and oxygens along the surface of the inter-layer, coordination under-saturated oxygen at crystallite edges and most importantly between water molecules. Interlayer surfaces have a permanent, but low residual charge, thus water interacts with these surface via the proton. At high pH, water interacts with the edge surfaces via the proton, but at low pH, water interacts with the protonated edge surfaces via the oxygen. Charged surface-dipole attraction occurs as water dipoles become attracted to and oriented with the negative electrical field emanating from the mineral surface. Van der Waals attractive fields arise from instantaneous atomic interactions between the atoms comprising the mineral surface and the atoms comprising the pore water.

Most importantly for montmorillonite, hydration of exchangeable cations occurs as the positively charged ions attract water dipoles, which form a hydration shell surrounding the cation. Because the cations are restrained by the layer charge field, their water of hydration shell is restrained as well. The energy associated with cation hydration is a function primarily of the cation size and valence, where small size, yet low valence provides favorable energetics for hydration. Secondary layers of water can H-bond with the primary layer of hydration water, forming multiple hydration shells. These H-bonds decrease in strength rapidly with the number of layers. Beyond two or three layers, the water of these shells behaves as bulk water.

Ions with small ionic radii have a high charge potential emanating from their surface. They interact strongly with water and therefore attract more water within the interlayer of clays than larger ions of similar valence. While the size of hydrated Ca^{2+} is larger than Na^{+}, its higher valency enables a greater attraction to the clay surface. Greater attraction energy enables cations like Ca^{2+} to interact strongly with both surfaces of adjacent clay layers, therefore Ca^{2+} is retained more strongly than Na^{+}. The ratio of the difference in ionic and hydrated radii to the cation valence (Δradius/valence) provides a measure of this interaction.

The physical consequence of these short-range solid-liquid interaction mechanisms is to attract, align, and impart some order into the molecular arrangement of the vicinal (near surface) pore water. The potential of the vicinal water, therefore, is reduced relative to the potential of free (bulk) pore water. This local gradient in potential serves to drive additional water into the interlayer, but is highly dependent on the properties of the interlayer cation, as described above. For some cations, for example Na^+ and Ca^{2+}, the attraction of additional water results in volume change phenomena known as crystalline swelling at relatively low water contents and osmotic, swelling at higher water contents. Crystalline swelling can occur for most cations, but osmotic swelling is limited to Na^+ and Li^+ (and possibly Be^{2+}) where the Δradius to valence ratio is greater than 300, and more than 3 hydration shells can occur.

Crystalline and osmotic swelling regimes

Norrish (1954) applied XRD techniques to observe basal spacing up to about 130 *Å* in Na- montmorillonite within the gelled phase at high water content. Interlayer swelling is generally divided into two stages: in the first stage, or within the crystalline swelling regime, basal spacing increases in a step-wise fashion as molecular layers of H_20 are sequentially adsorbed in the interlayer around the interlayer cations. Total water content corresponding to the upper limit of crystalline swelling (three or four water layers) is less than about 25% by mass. Transition into an osmotic swelling regime is manifested as a jump in basal spacing from ≈20 *Å* to ≈40 *Å*, where upon a significant amount of water is adsorbed, disassociation of the crystallites continues, and the system enters a gelled phase.

Crystalline swelling

Crystalline swelling is a process whereby expandable 2:1 phyllosilicates sequentially intercalate one, two, three, or four discrete layers of H_20 molecules between the mineral interlayers (Norrish, 1954). This process, which has also been referred to as Type I swelling, occurs prior to osmotic (Type II) swelling associated with longer-range electrical diffuse double layer effects.

Crystalline swelling is the result of the balance between forces of attraction and repulsion operating between adjacent interlayer surfaces (Norrish, 1954). The net potential energy of interaction (Laird, 1996) is dominated by electrostatic attraction between the exchange cations and the basal surfaces of the clay. The positively charged cations act as charge bridges or links between adjacent negatively charged clay layers. The net potential energy of repulsion, on the other hand, is dominated by the hydration energy of the exchange cations. The exchange cations can exist within the interlayer in partially hydrated, thermodynamically stable phases that interact strongly with their surroundings: they will attract or release water

of hydration until the net potential energies of attraction and repulsion are balanced. Unsaturated conditions or saturated conditions with high electrolyte concentrations favor the dominance of net forces of attraction, while fully saturated conditions of low electrolyte concentration favor the dominance of net forces of repulsion.

For divalent mineral forms where relatively large interlayer attractive forces must be overcome (e.g. Ca-smectite), crystalline swelling ceases at three or possibly four molecular water layers, thus forming stable quasi-crystals. Because interlayer sorption is limited, corresponding bulk volume changes of Ca-smectite are relatively small. Limited interlayer sorption in Ca-smectite is also reflected in engineering indexes such as Atterberg limits, which although high by comparison with other minerals, are small by comparison with smectite having sodium as the predominant type of interlayer cation.

For monovalent mineral forms such as Na-smectite, where the interlayer attractive forces are relatively weak, interlayer sorption may continue beyond the three or four layers of water associated with crystalline swelling. Additional interlayer separation continues under an osmotic mechanism driven by a gradient in chemical potential between the interlayer water and bulk pore water residing in the interparticle pore space. It is this transition into the osmotic swelling regime that allows for more complete disassociation of the mineral interlayers, large macroscopic volume changes, high Atterberg indexes, and gelling behavior partly responsible for the self-healing and low hydraulic conductivity characteristics required for barrier applications.

Laird (2006) discussed the dependence of crystalline swelling of hydrated smectites on their surface charge characteristics. At equal-molar electrolyte concentrations, low charge smectites tend to swell more than high charge smectites. Because swelling underpins smectite performance in GCLs, it follows that those GCLs containing bentonites with moderate to low CEC, such as the Wyoming bentonites, will most likely have greater swelling indexes than those with higher CEC.

Osmotic swelling

Osmotic swelling occurs as the result of pore water flow driven by a gradient in dissolved solute concentration between the interparticle pore fluid and the interlayer pore fluid. Figure 2.3 shows a schematic for the distribution of ions relative to a charged surface in aqueous solution. The charge field emanating from charge deficiencies in the clay mineral is greatest at the surface and decays with increasing distance. As a result, cations are concentrated near the surface and tend to be diffuse at distance.

A common model for this distribution is the Gouy-Chapman theory of a diffuse double layer (DDL), which models the decay exponentially (Mitchell, 1993). The

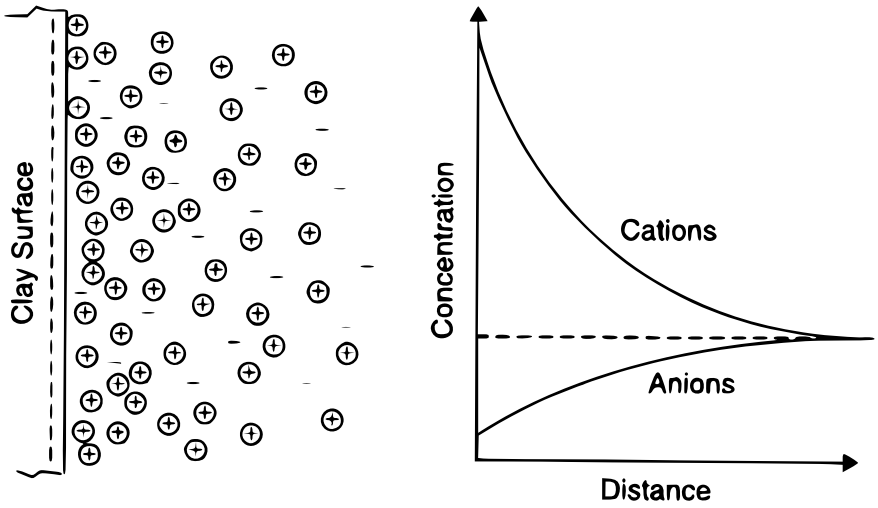

Figure 2.3: Schematic of the clay-water-ion double layer system (Mitchell, 1993)

thickness (1/K) of the diffuse double layer is:

$$\frac{1}{K} = \sqrt{\frac{\varepsilon_0 DkT}{2n_0 e^2 v^2}} \tag{2.1}$$

where ε_0 is the permittivity of vacuum, D is the dielectric constant of the pore fluid, k is the Boltzmann constant, T is absolute temperature (K), n_0 is the far-field (bulk pore fluid) ion concentration (ions/m3), e is the electronic charge, and v is the ion valence. Equation 2.1 is instructive because it allows one to appreciate the impact of changes in the system variables on the thickness of the double layer. For example, a double layer will generally decrease in thickness, or collapse, if the ion concentration is increased, if the ion valence is increased (e.g. if Na^+ is replaced with Ca^{2+}), or if the dielectric constant of the pore fluid is decreased. This affects the net interlayer and interparticle interaction force, the corresponding particle and pore fabric, and ultimately, the engineering behavior of the clay.

When two charged surfaces in an electrolyte solution approach one another, their electrical double layers at some point begin to interact. If the energetics of the two surfaces favor attraction, the double layers will overlap. Overlapping double layers are the normal condition governing the behavior of clay-water systems of geotechnical importance, such as hydrated GCLs. Overlapping double layers in clay-water-ion systems may occur on both the particle scale (i.e. between adjacent parallel or non-parallel particles in the interparticle pore space) and on the sub-particle scale (i.e. between quasi-crystals, crystallites, and ultimately unit layers in the interlayer pore space). The region of overlapping double layers is marked

by a relatively high concentration of cations because they are effectively restrained from diffusing to other regions of the pore fluid. This concentration gradient results in osmotic pressure that acts to drive additional water into the interlayer, resulting in disassociation of the unit layers, large bulk volume change, and the formation of a gelled fabric.

Osmotic swelling can be better understood by considering a simple experiment. Free water is in contact with a solute solution through a semi-permeable membrane that is permeable to water molecules but not to the solute. The dissolved solutes decrease the potential of the solution in a left-hand reservoir by an amount dependent on the solute concentration, thus creating a gradient that acts to drive water through the membrane from a right-hand reservoir. Equilibrium is reached when the pressure head in the left reservoir (h_0) balances the osmotic forces tending to cause inflow. This pressure head is the osmotic pressure, π, which, if the solute solution is ideal and dilute, may be approximated by the van't Hoff equation:

$$\pi = \rho_s g h_0 = RTC_s$$

where ρ_s, is the density of the solute solution, g is gravitational acceleration, R is the universal gas constant, T is absolute temperature, and C_s, is the molar concentration of the solution. Osmotic pressure, therefore, is directly proportional to the concentration difference between the reservoirs.

In clays, the effect of an imperfect semi-permeable membrane is introduced by the restraint in ion mobility that the negatively charged mineral surfaces impose on the interlayer cations in overlapping double layers. Once sufficient separation distances between unit layers are achieved during crystalline swelling (for Na-smectite, this is $\approx$20 $\dot{A}$), attractive forces no longer dominate, and the interlayer can be considered a region of high electrolyte concentration compared to the external bulk solution. If cations are retained in the interlayer space in concentrations greater than in the bulk pore fluid, osmotic pressure arises from the difference in ion concentration, thus causing water to be drawn into the zone of relatively high concentration. The volume change associated with this process is referred to as osmotic swelling (Bolt, 1956; Warkentin and Schofield, 1958; Quirk and Marcelja, 1997).

During osmotic swelling, smectites can form a stable gel phase. A gel phase is a borderline equilibrium state where both crystalline and osmotic swelling as well as dispersion may occur during further uptake of water on the one hand, and shrinking, flocculation and fabric rearrangement occur during water loss on the other hand. Stated another way, a gel phase is a transitional hydrous (saturated) phase existing between the condensed (plastic-like) phase and the dispersed (fluid-like) phase. Typically clay gels are materials having reduced void sizes and minimal inter-connectivity of pores, and therefore exhibit increased tortuosity of

flow path. In order to effectively seal under confinement, domains of quasi-crystals must be able to re-arrange and expand into the available inter-particle pore space during wetting. Typically wetting with low ionic strength solutions forms optimal bentonite gels. Low solution concentrations of counter ions fail to fully shield repulsive forces operating between adjacent clay layers, thus enabling repulsive forces to override the attractive forces. A stable gel phase then results. Conversely, higher counter ions tend to shield the repulsive forces and result in attractive forces within the gel becoming dominant. This results in collapse of the gel phase to a plastic phase.

2.4 Hydraulic Conductivity of GCLs

The hydraulic conductivity of GCLs depends in most cases on the hydraulic conductivity of the bentonite. The only exceptions are GCLs containing a geomembrane. The hydraulic conductivity of clays is determined by the cross-section of flow and by the tortuosity of the flow pathways in the clay. These parameters are dependent on the size, shape and microstrutture of the clay particles, as well as their density and water content. The best density properties are possessed by the clay minerals with optimal parallel bedding, perpendicular to the direction of flow and small particle thickness (few platelets per aggregate), as this is where only narrow structural pores result.

The large specific surface of montmorillonite (800 m^2/g) combined with its large net negative charge result in adsorption of a large number of hydrated cations as well as adsorption and water molecules, and interlayer separation during hydration (Mitchell, 1993). These adsorbed water molecules and cations can comprise a significant fraction of the pore space, and are essentially immobile (Mesri and Olson, 1971; Mitchell, 1993). As a result, the portion of the pore space occupied by bulk water (i.e., non-adsorbed water that is free to flow) is relatively small, and the pathways formed by the bulk water have irregular shapes (Mesri and Olson, 1971). Consequently, the hydraulic conductivity of montmorillonite to water typically is very low. Also, the large affinity of montmorillonite for water molecules and hydrated cations results in significant swelling of montmorillonite (5 to 10 times the dry volume) when hydrated under low effective stress.

The low hydraulic conductivity of montmorillonite to water is responsible for the low hydraulic conductivity of bentonites and GCLs when permeated with water. As a result, the amount of montmorillonite should affect the hydraulic conductivity of a soil or GCL (Shackelford et al., 2000).

Since the low hydraulic conductivity of bentonite is primarily due to adsorbed molecules associated with the montmorillonite restricting the pore spaced active in flow, bentonites are particularly sensitive to changes in the composition of the pore fluid that influence the thickness of the adsorbed layer. In particular, liquids

that cause the adsorbed layer to collapse also cause the hydraulic conductivity to increase (Mesri and Olson, 1971). Thus, GCLs containing bentonite with a greater montmorillonite content are potentially more vulnerable to chemical attack and incompatibility.

GCLs often are used to contain liquids other than water. Hydraulic conductivity to the actual permeant liquid is usually assessed via a compatibility test where the specimen is permeated with the liquid to be contained or a liquid simulating the anticipated liquid.

Factors dominantly affecting the hydraulic conductivity are considered to be: (1) the quality of the bentonite, (2) the size, the shape and the geometrical arrangement, (3) the bentonite mass per unit area, (4) the confining stress and/or the void ratio, (5) the ion concentration and valence, and the dielectric constant of the permeating liquid, (6) the prehydration water content. In this Section we will describe in detail the main factors affecting the hydraulic conductivity of particular interest for this thesis.

2.4.1 Factors affecting the hydraulic conductivity of GCLs

Influence of valence and concentration

The adsorbed layer, referred to as the diffuse double layer (DDL), is commonly described using the Stern-Gouy model (Mitchell, 1993; Shang et al., 1994). According to the Stern-Gouy model, a thin film called the Stern layer consisting of oriented water dipoles and fixed hydrated cations is directly adjacent to the clay surface, while a diffuse layer of hydrated cations attracted to the clay surface resides immediately adjacent to the Stern layer (Shang et al., 1994). The concentration of cations in the diffuse layer is a function of the electrical potential of the negatively charged clay surface, which decreases with distance from the clay surface.

As indicated by equation 2.1, the electrolyte concentration, cation valence, and dielectric constant affect the thickness of the DDL, 1/K, which, in turn, affects the hydraulic conductivity and swelling of bentonite. A decrease in 1/K will cause a corresponding increase in hydraulic conductivity by increasing the size of the flow paths (Mesri and Olson, 1971; Shang et al., 1994). Therefore, electrolyte concentration, cation valence, and dielectric constant can affect the hydraulic conductivity.

Replacement of sodium in the exchange complex with other ions affect the thickness of the adsorbed layer and, thus, swelling and hydraulic conductivity of the bentonite in GCLs (Shackelford et al., 2000; James et al., 1997; Katsumi et al., 2008). The influence of valence has been shown to be evident in free swell tests conducted on GCL bentonite by Shackelford et al. (2000). The bentonite was hydrated with deionized water and three different 0.025 M chloride solutions. The

results, show the change in swell according to the valence of the cation.

The highest valence cation, Al^{3+}, showed the largest affect on the swelling capacity of the clay, which is consistent with the Gouy-Chapman and Stern-Gouy theories. The swell in deionized water is only slightly larger that in the LiCl, due to the monovalency of the cation. The Li^{+} may replace the Na^{+}, but the little change in swell because the minimal change in double layer thickness due to the 1:1 exchange. Permeability tests were also conducted on the GCL bentonite permeated with the same concentration solutions as above. The findings were consistent with changes in the thickness of the diffuse layer. The hydraulic conductivity reported for the monovalent permeant was 3 orders of magnitude lower than that of the divalent.

Jo et al. (2001) investigated the influence of single-species salt solutions of various concentration on the swelling and hydraulic conductivity of nonprehydrated GCLs. It was found that monovalent cations reduce the swelling to different degrees depending on the hydrated radius of the cation. Divalent cations decreased the swell more notably than the monovalent (Fig. 2.4), however the species was found to be less influential on the degree of swell. Valence and concentration were found to have analogous effects on swelling and hydraulic conductivity (Fig. 2.5).

Finally, Jo et al. (2001) found a strong inverse relationship between hydraulic conductivity and swell index (both normalized to their value in deionized water), as shown in Fig. 2.6. For swell index ratio lower than 20, the hydraulic conductivity increases dramatically with decreasing swell index. This result indicates that free swell tests can be valuable for estimating how inorganic aqueous solutions affect the hydraulic conductivity of nonprehydrated GCLs.

Ruhl and Daniel (1997) described the response of geosynthetic clay liners to permeation with various chemical solutions and leachates. Ca^{2+} solutions were found to be far more aggressive to the GCLs than real leachates due to the lower concentration of cations. Contaminant resistant bentonites produced variable results, as some are more resistant to specific chemicals.

Experimental results have shown that Ca^{2+} from dilute solutions can gradually exchange the naturally occurring Na^{+} on the exchange complex, resulting in gradual compression of the adsorbed layer and consequent gradual increase in hydraulic conductivity (Shackelford et al., 2000). This is shown to occur at very large pore volumes of flow, which indicates that the cation exchange can occur over a long period of time.

When multivalent cations replace the Na^{+} ions, the volume of water bound to the montmorillonite surface (immobile water) decreases and the volume of free (mobile) water increases (Van Olphen, 1991; McBride, 1994), resulting in shrinkage of montmorillonite aggregates. Under modest confinement, this change in aggregate size results in larger interaggregate pores (the pores conducting flow) and higher hydraulic conductivity (Mesri and Olson, 1971; Jo et al., 2001). Con-

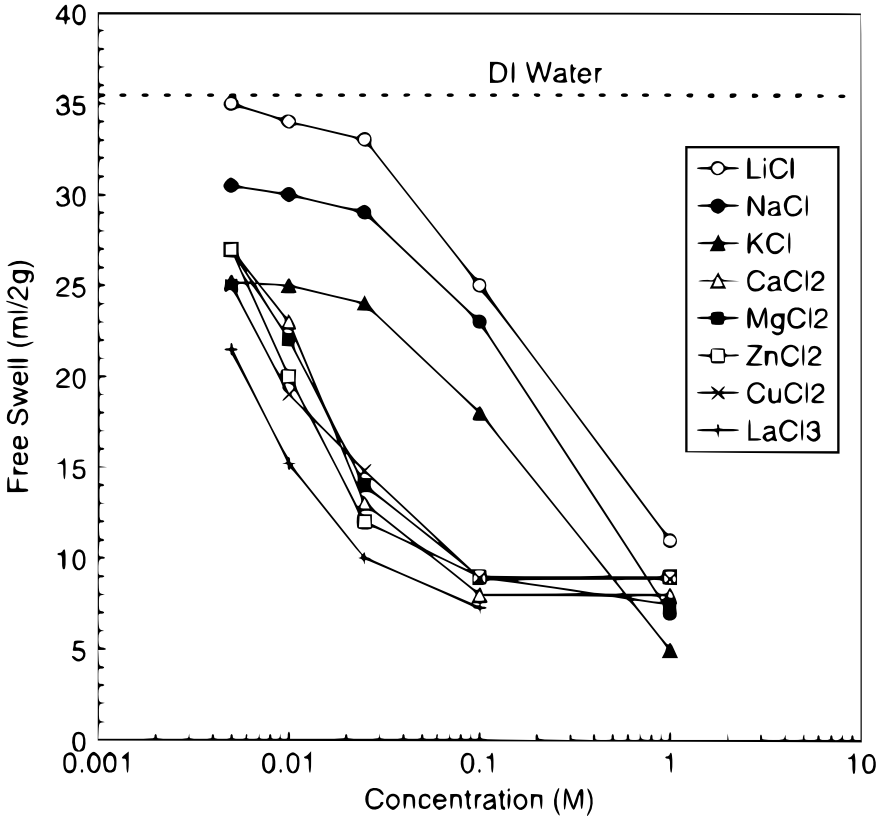

Figure 2.4: Effect of Concentration on Swelling of Sodium Bentonite from GCL (Jo et al., 2001)

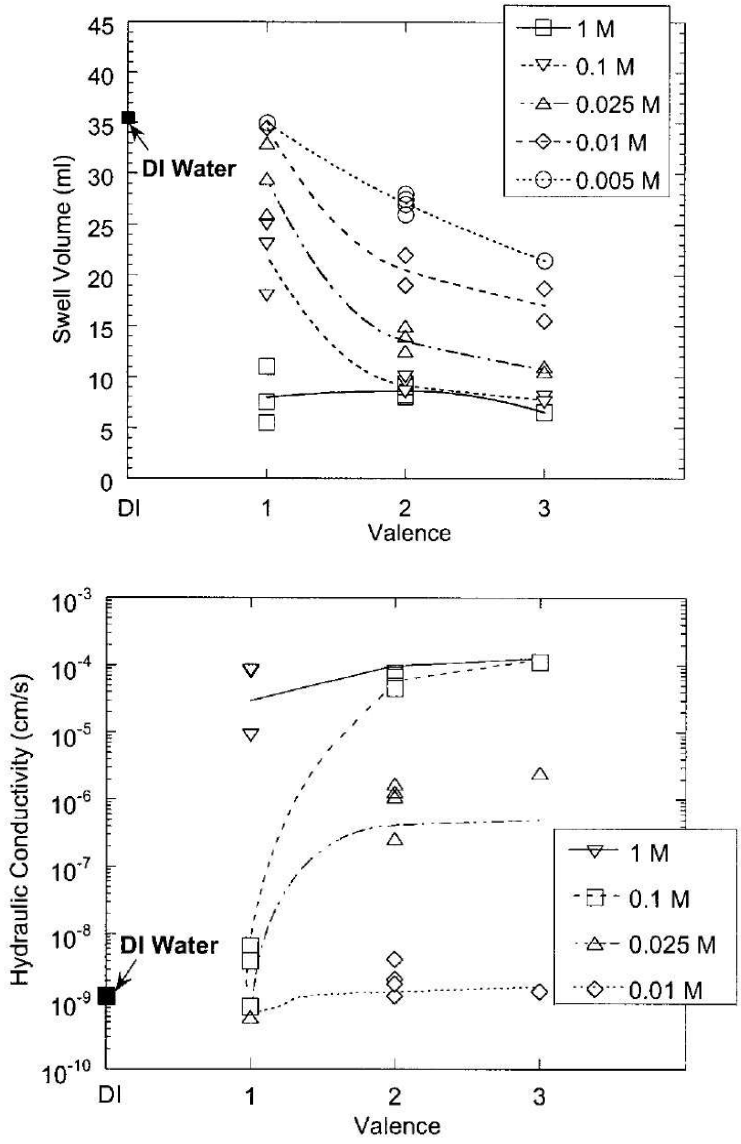

Figure 2.5: Effect of valence of cations on swelling and hydraulic conductivity of sodium bentonite from GCL (Jo et al., 2001)

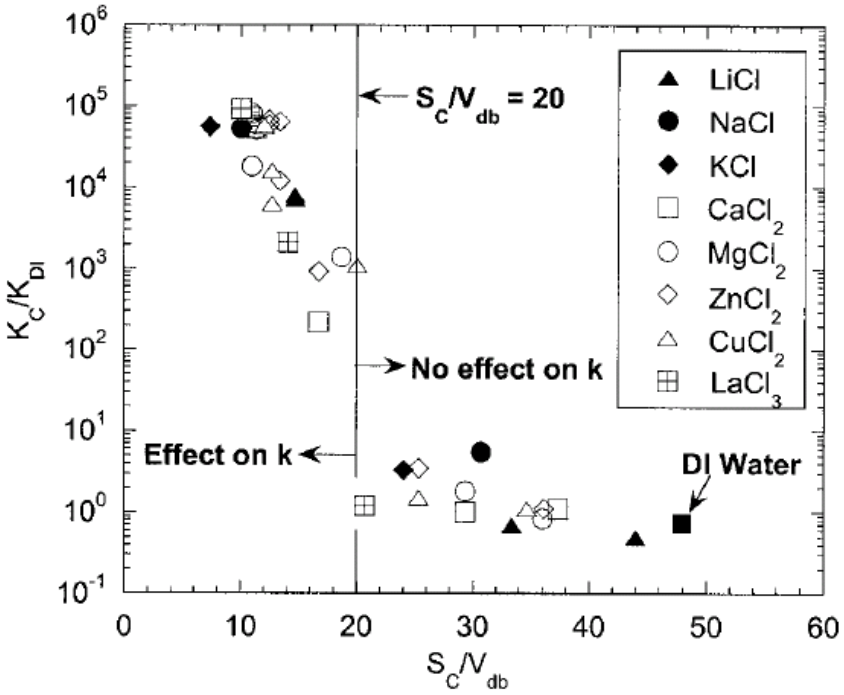

Figure 2.6: Inverse relationship between hydraulic conductivity ratio and swell index ratio (Jo et al., 2001)

versely, if the permeant solution contains only monovalent cations, or if there is no cation exchange, the volume of bound water increases or decreases depending on the cation concentration in the permeant solution. This effect causes expansion or contraction of the montmorillonite aggregates and interaggregate pores, resulting in changes in hydraulic conductivity. A variety of researchers studying the hydraulic conductivity of GCLs to salt solutions have observed these effects (Petrov et al., 1997; Shackelford et al., 2000; Egloffstein, 2001; Vasko et al., 2001).

Influence of prehydration

Several investigators have reported that the order that permeant liquids are introduced to bentonitic barrier materials can have a significant effect on their final hydraulic conductivity (Daniel et al., 1993; Didier and Comeaga, 1997; Petrov et al., 1997; Ruhl and Daniel, 1997).

In particular, hydration of the bentonite with water before permeation with a chemical solution results in a lower hydraulic conductivity than that obtained by direct permeation with the chemical solution. This effect is evident in the data reported by Petrov et al. (1997). Direct permeation of sand-bentonite mixtures results in hydraulic conductivities greater than those obtained by initial permeation with deionized water followed by permeation with the salt solution.

Ruhl and Daniel (1997) performed hydraulic conductivity tests on five GCLs using seven permeant liquids and three conditions of hydration. The condition of hydration was found to be very important: much lower hydraulic conductivity generally resulted when the first wetting liquid was water rather than the chemical solution or leachate. The GCLs had a high hydraulic conductivity when permeated directly with: simulated municipal solid waste (MSW) leachate that was rich in calcium; a strong acid solution; or a strong base solution. However, permeation of the prehydrated sample did not continue long enough for the sodium in the bentonite to be fully replaced with calcium, and permeation over a much longer period (years) would have eventually caused calcium replacement and probably an increase in hydraulic conductivity.

Influence of void ratio and effective stress

Terzaghi (1923) emphasized the importance of the nonuniformity of the voids on clay permeability and the substantial dependence of the permeability on the void ratio. He considered that the physical properties of the pore water changed in the immediate vicinity of the clay surfaces.

Grace (1953) demonstrated that improved dispersion is the main reason for the marked reduction of permeability caused by use of certain electrolytes and he pointed out the importance of particle reorientation as consolidation progressed.

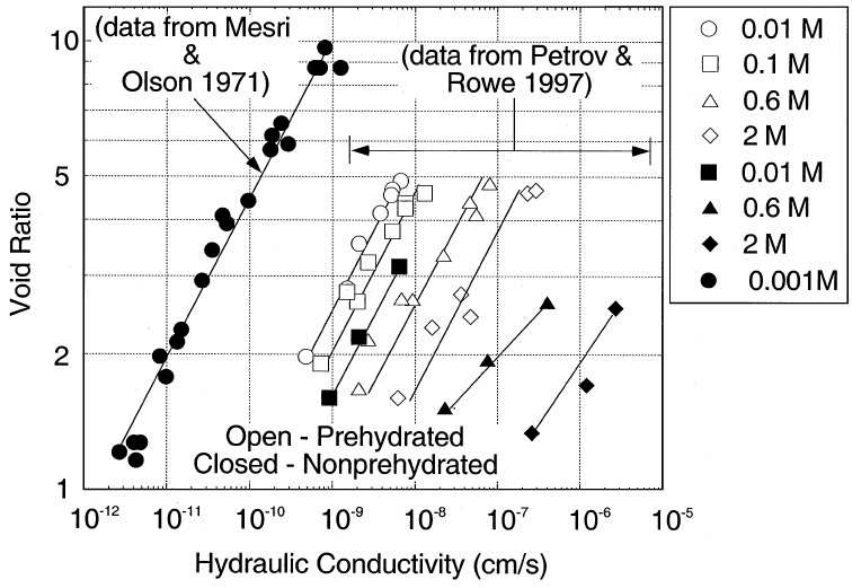

Figure 2.7: Hydraulic conductivity of bentonites permeated with various NaCl solutions as a function of the logarithm of void ratio (Shackelford et al., 2000)

Olsen (1960) measured hydraulic flow rates, electrical conductivities, and streaming potentials for flow through kaolinite, illite, and Boston blue clay, and concluded that electro-osmotic counterflow, high viscosity, and tortuous flow paths failed to account for the permeability characteristics he measured. He concluded that unequal pore sizes was the most important variable.

Mesri and Olson (1971) stated that the foregoing studies indicate that the most important variable influencing the permeability of clays is flocculation of the clay particles, which influences the distribution of void sizes and shapes.

Mesri and Olson (1971) showed also that a direct linear relationship exists between the logarithm of hydraulic conductivity (log k) and the logarithm of void ratio (log e) for homoionized bentonites permeated with various aqueous solutions. As shown in Fig. 2.7, the data from the GCLs tested by Petrov and Rowe (1997) exhibit a similar relationship, although Petrov and Rowe (1997) indicated that an equally good linear relationship exists between the logarithm of the hydraulic conductivity, log k, and the void ratio, e. The log k versus log e lines (Fig. 2.7) shift towards higher hydraulic conductivity as the NaCl concentration increases and, for all but the strongest NaCl solutions, the lines have similar slope.

The data in Fig. 2.7 show that both void ratio and cation concentration influence the hydraulic conductivity. Void ratio, which is controlled by the state of

stress, describes the total amount of void space in the specimen. The fraction of the total void space that conducts flow is controlled by the thickness of the adsorbed layer, which is influenced by the cation concentration (Eq. 2.1). The data in Fig. 2.7 suggest that changes in void ratio have similar effect on hydraulic conductivity regardless of the cation concentration or the thickness of the adsorbed layer. That is, the effect of varying the total void space appears to be independent of the effect of changing the thickness of the adsorbed layer.

2.4.2 Overlapping Geosynthetic Clay Liners

GCLs are manufactured in panels and are installed by unrolling and overlapping the panels. Therefore, in addition to the hydraulic performance of intact GCLs, the hydraulic performance of unavoidable overlapping is also important. In fact, the hydraulic conductivity of overlaps is crucial to the overall performance of GCL as hydraulic barrier. Large-scale testing equipment able to accommodate a full-scale overlap seam is necessary to evaluate correctly the efficiency of the seams. Daniel et al. (1997) described overlap tests in a GCL flowbox (a large scale laboratory permeameter, in Fig. 2.8).

The efficiency of the seams depends on:

1. swelling ability of bentonite; the bentonite must sufficiently swell to seal the two overlapping panels

2. GCL type; Estornell and Daniel (1992) observed that for GCLs with geotextiles on both sides, problems with migration of bentonite into the underlying drainage layer may be encountered when inadequate filtration is provided

3. correct placement; e.g. appropriate overlap width (Estornell and Daniel, 1992; Satoshi and Mitsuji, 1996)

4. use of bentonite paste/powder in the overlapping area; Benson (2002) illustrated that leakage rates of GCL overlaps are lower if bentonite paste is used to seal the seam

5. the effective stress (Estornell and Daniel, 1992; Schroeder et al., 2001)

Estornell and Daniel (1992) performed large scale hydraulic conductivity tests on three conventional GCLs to determine the self sealing capacity using tap water as permeant. Except for the case where low effective stress was employed, they found a hydraulic conductivity of overlapped GCLs almost identical to values of intact GCLs.

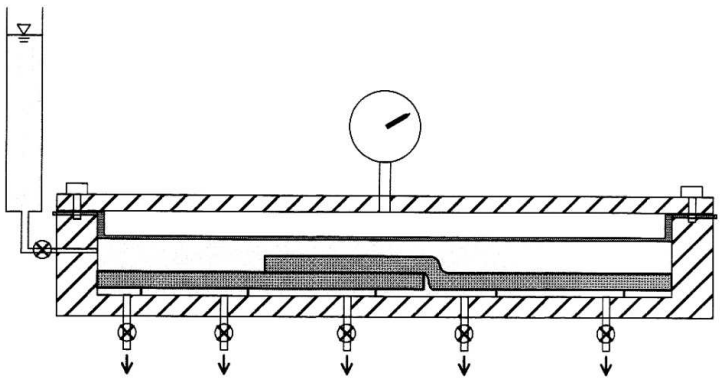

Figure 2.8: Flow box experimental apparatus (Daniel et al., 1997)

2.5 Modified clays proposed as barrier materials

When GCLs are used as hydraulic barrier materials to contain chemical substances, barrier performance deterioration must be closely monitored. For example, the barrier performance of GCLs directly exposed to leachates at waste containment facilities may deteriorate because the bentonite in GCLs has insufficient swelling against electrolytic chemical solutions (Norrish, 1954; Katsumi et al., 2008). Numerous studies have examined the applicability and chemical compatibility of bentonites and GCLs, and have shown that the type and concentration of chemicals affect the hydraulic conductivity. It has been reported that the hydraulic conductivity value increases as the concentration of the electrolytic solution increases (Jo et al., 2001; Kolstad et al., 2004; Petrov et al., 1997; Shackelford et al., 2000; Katsumi et al., 2008).

To improve the chemical compatibility of clays to aggressive permeants, several types of chemically-resistant clays have been recently developed.

Recently an enhancement method to protect the double layer compression of clays from chemical attack is to use large organic molecules that bind to the montmorillonite surface as a prop to hold open the interlayer region in the presence of aggressive liquids. The organic molecules may also bond to the sodium ions in the interlayer space, minimising exchange during permeation with solutions containing divalent or polyvalent cations (Trauger and Darlington, 2000).

Organoclays

Extensive research has been conducted to characterize the sorption of organic compounds onto clay surfaces (Lo et al., 1997; Lorenzetti et al., 2005; Bartelt-Hunt et al., 2005). Organobentonites are clays, typically amended by exchanging quater-

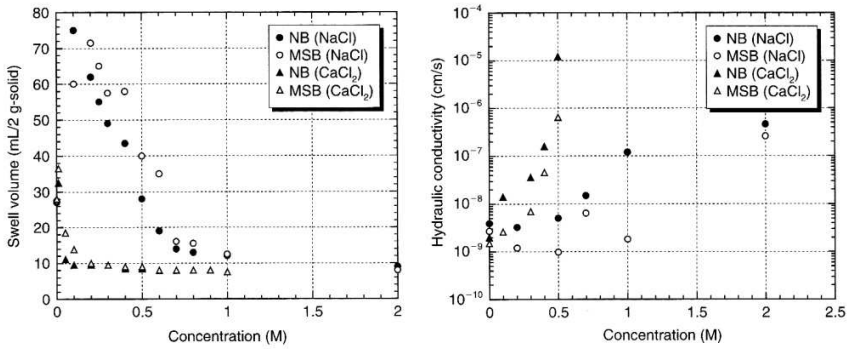

Figure 2.9: Swell volume and Hydraulic conductivity of chemical resistant Multiswellable Bentonite (MSB) versus natural bentonite (NB) for NaCl and $CaCl_2$ solutions (Katsumi, 2010)

nary ammonium cations for the naturally occurring sodium. This process renders the modified clay hydrophobic and highly organophillic. Organically modified clays have been found to be a promising alternative to resist pollutant transport (Lo et al., 1997). Bentonites modified with ammonium compounds (organoclays) have sorption capacities for organic compounds 4-5 times higher than untreated clays (Lorenzetti et al., 2005). However, the hydraulic conductivity of clays may increase significantly upon modification with organics.

Multiswellable Bentonite (MSB)

Multi-swellable bentonite (MSB), developed by Kondo (1996), is a bentonite treated with Propylene Carbonate (PC), an organic compound, to activate the osmotic swelling capacity of the clay. Propylene carbonate is placed in the interlayer of the smectite and attracts numerous water molecules. This results in a strong swelling power even if the permeant contains polyvalent cations or a high concentration of monovalent cations. Figure 2.9 shows values for the swell volume and the hydraulic conductivity of solutions of natural bentonite (NB) and MSB with NaCl and $CaCl_2$ as pore liquids (Katsumi, 2010). For hydraulic conductivity tests using flexible-wall permeameters, NB or MSB granules were placed between the top and the bottom pedestals to achieve a thickness of approximately 1 cm.

This condition simulates the cases where these bentonites are used as GCLs, as well as simply to evaluate the chemical compatibility of the bentonites. Each specimen had a dry density of 0.79 g/cm^3. Under a cell pressure of 20-30 kPa, the bentonite specimens were exposed to the permeant liquid for longer than 24 hours. MSB exhibits higher levels of swell volume than NB for all concentration levels. Most values for the hydraulic conductivity of MSB are one to two orders in

magnitude lower than the values for that of NB for the same concentration levels (Katsumi, 2010).

Trisoplast

Trisoplast is the trade name of a well-defined mixture of sand (lower than 89.1% by dry weight), bentonite (higher than 10.7% by dry weight) and a special polymer (higher than dry 0.2% by weight). A sand-bentonite-mixture used as compacted clay liner has already a good sealing property, which, together with other geotechnical properties, is considerably amended by the polymer additive (Simon and Müller, 2005). The synthetic additive is a high molecular weight, hydrophilic and gel-forming polymer. Therefore, all water transport processes in the mixture are strongly retarded by the polymer. In addition it gives rise to some internal cohesion in the sandbentonite mixture. Trisoplast may have hydraulic conductivity one order of magnitude lower than conventional compacted clay liners (Simon and Müller, 2005).

Clays treated with cationic polymers

Polymers dissolved in solution may adsorb easily to both sand and clay surfaces (Stumm, 1992). Such adsorption in clays can be irreversible and entropy-driven because a cationic polymer chain displaces many water molecules and contains thousands of cations which would need to be displaced simultaneously (Theng, 1982; Ashmawy et al., 2002). For this reason cationic polymers can protect the clay from cation exchange, that is the main reason for the increase of permeability. However, cationic polymer amendments provides no improvement to the hydraulic conductivity of bentonites (McRory and Ashmawy, 2005).

Clays treated with anionic polymers

A product in this category is the Dense PreHydrated GCL (DPH GCL), densified by calendering after prehydration with a polymeric solution containing Na-CMC, sodium polyacrylate and methanol. This DPH GCL showed excellent performance in various aggressive solutions (Schroeder et al., 2001; Kolstad et al., 2004; Katsumi, 2010). Polyacrylate compounds in this DPH GCL can replace the sodium cations of the clay to avoid ion exchange, enhancing the impermeable behaviour under aggressive conditions (Flynn and Carter, 1998).

Adsorption of anionic polymers onto clay surface is promoted by the presence of polyvalent cations which act as bridges between the anionic groups on the polymer and the negatively charged sites on the clay (Mortensen, 1960; Theng, 1982). Qiu and Yu (2007) modified a bentonite with CMC. XRD (X-Ray Diffraction) and FTIR (Fourier Transform Infrared Spectroscopy) analyses showed that the polymer chains had intercalated into the clay sheets, and the strong chemical

interaction between the ether bonds from the polymer and Si-O bonds from the clay was the driving force for intercalation. They demonstrated that treating clay with CMC can increase its water absorbency and water retention ability.

This study evaluates the pollutant containment ability of clays treated with Na-CMC given its high water retention capacity.

2.6 Contaminant transport through GCLs

2.6.1 Diffusion

Diffusion is a chemical process involving contaminant migration from areas of higher concentration to areas of lower concentration even when there is no flow of water. The diffusive behaviour of inorganic contaminants through a GCL has been reported recently by Rowe (1998) and Lake and Rowe (2000). Their main findings can be summarized as follows: (1) void ratio and related confining stress have a strong influence on diffusion coefficient, (2) the solute concentration level can give significant variation in the diffusion coefficients due to the modification of the microstructure of the sensitive mineral component (in particular sodium bentonite). On the other hand, GCL manufacture process was found not to significantly affect the diffusion coefficient.

While the use of GCLs in geoenvironmental containment applications has been based primarily on favorable hydraulic performance and economic benefits, other factors may be important in terms of the overall performance of GCLs in containment applications. For example, the potential for breakthrough of contaminants through GCLs in less than 1 day as a result of solute (liquid-phase) diffusion has been reported (Malusis and Shackelford, 2002b), and the premature arrival of a salt (2.0 N NaCl) front through a needle-punched GCL during permeation at low flow rates has been attributed to the dominance of diffusive transport (Petrov et al., 1997).

Thus, diffusion is an important, if not dominant, process of determining the rate of aqueous miscible contaminant migration through GCLs.

2.6.2 Clay chemico-osmotic behavior

Membrane behavior, or the ability of clay soils to impede the passage of solutes, also could affect contaminant migration through GCLs.

The ability of clay soils to act as membranes that restrict the passage of solutes is well documented (Kemper and Rollins, 1966; Olsen, 1969; Olsen et al., 1990). Restricted movement of inorganic solutes, specifically anions and cations, through the pores of a clay soil has been attributed to electrostatic repulsion of the ions by electric fields associated with the diffuse double layers (DDLs) of adjacent clay particles (Hanshaw and Coplen, 1973; Fritz, 1986; Keijzer et al., 1997).

Nonelectrolyte solutes (uncharged species), such as aqueous miscible organic compounds, also may be restricted from migrating through clay soils due to steric hindrance, i.e., the geometric restriction that results when the solute molecule is greater than the pore size (Grathwohl, 1998). The existence of membrane behavior also results in chemico-osmosis, or the movement of liquid in response to a solute concentration gradient, from lower solute concentration (higher water activity) to higher solute concentration (lower water activity) (Katchalsky and Curran, 1965; Fritz, 1986)

The term semi-permeable pertains to any material that behaves as a membrane. The extent to which clay soils act as semi-permeable membranes traditionally has been quantified in terms of a reflection or osmotic efficiency coefficient, σ (Staverman, 1952; Katchalsky and Curran, 1965; Kemper and Rollins, 1966; Olsen et al., 1990).

In cases where σ represents stress, the osmotic efficiency coefficient has been designated by ω (Mitchell, 1993). Also, in some cases, x has been referred to as the chemico-osmotic efficiency coefficient to distinguish the osmotic flow process in response to a concentration gradient from osmotic flow processes in response to electrical gradients (i.e., electro-osmosis) or thermal gradients (i.e., thermo-osmosis) (Malusis et al., 2001).

In general, ω ranges from zero representing a material that exhibits no solute restriction, to unity representing an ideal or perfect membrane that completely restricts the movement of solutes. In most cases involving membrane behavior in clay soils, only a portion of the pores is restrictive such that $0 < \omega < 1$, and the clay soils are referred to as nonideal or leaky membranes (Kemper and Rollins, 1966; Olsen, 1969; Barbour and Fredlund, 1989; Mitchell, 1993; Keijzer et al., 1997). Both nonideal and ideal membranes are semi-permeable.

Factors affecting clay membrane behavior

The value of ω is affected by several factors, including the state of stress in the soil, the types and amounts of clay minerals comprising the soil, and the types (species) and concentrations of the solutes in the pore water (Kemper and Rollins, 1966; Olsen et al., 1990; Mitchell, 1993; Malusis et al., 2001)

In general, ω increases with increase in the effective stress in the soil (or decrease in void ratio or porosity), increase in the activity of the clay soil, and decrease in the solute charge and/or solute concentration (Kemper and Rollins, 1966; Olsen, 1969; Mitchell, 1993).

In particular, membrane behavior in the presence of common electrolytes (e.g., NaCl) has been illustrated extensively for sodium bentonite (e.g., Kemper and Rollins, 1966; Keijzer et al., 1997; Malusis et al., 2001; Malusis and Shackelford, 2002). These results suggest that membrane behavior is significant in clay soils containing an appreciable amount of sodium montmorillonite. Thus, the existence

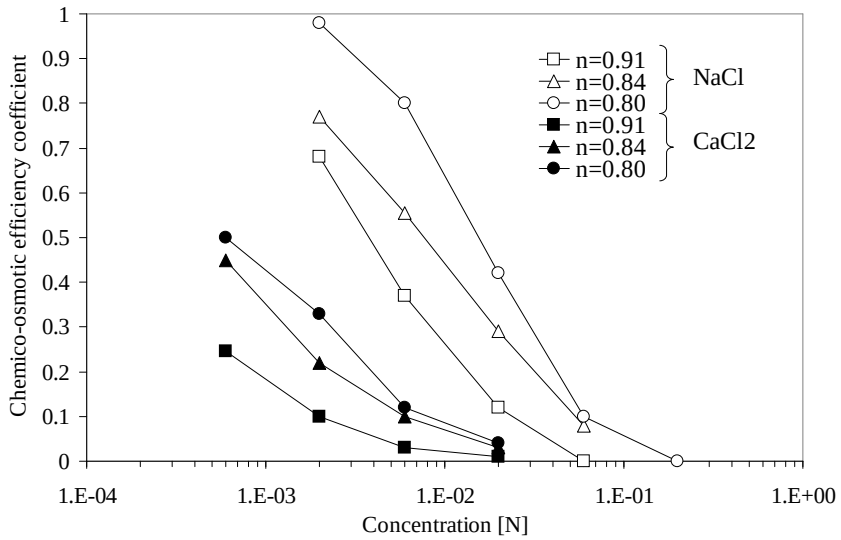

Figure 2.10: Factors influencing the chemico-osmotic behavior: concentration, valence and porosity (Kemper and Rollins, 1966)

of membrane behavior resulting from the sodium montmorillonite content in clay soil barriers may have an effect on the migration of contaminants through such barriers.

For example, ω values for two different types of bentonite specimens are shown in Fig. 2.10. The data in the figure indicate that ω decreases as the salt concentration increases for a given porosity (n) and salt (NaCl or $CaCl_2$) solution. The data in the figure also indicate that ω decreases with an increase in cation valence (Ca^{2+} versus Na^{+}) for a given porosity and average salt concentration. Both of these trends are consistent with expected behavior based on DDL theory in that the thickness of the DDLs of adjacent clay particles and the resulting extent of influence of the ion-restricting electric fields inside the soil pores decreases as the ion concentration and cation charge in the pore water increases.

2.6.3 Chemico-osmosis and solute transport through GCLs: Theoretical background (Dominijanni, 2005)

When a GCL is placed in contact with a bulk solution, the ion concentrations in the pore solution are discontinuous with respect to the ion concentrations in the bulk solution due to the presence of the charge of the solid skeleton. The concentration of the cations (i.e. counter-ions) is higher than that of the bulk solution, whereas the concentration of the anions (i.e. co-ions) is lower. In Figure 2.11, a GCL is

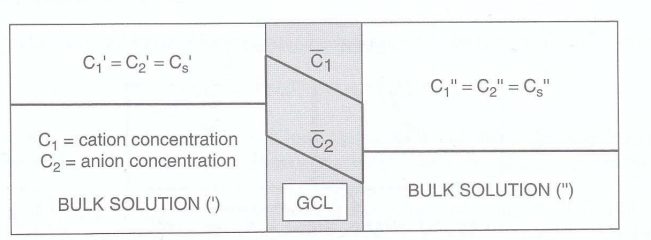

Figure 2.11: Ion concentration profiles within a GCL in contact with two bulk solutions. C, is the concentration of a (1:1) electrolyte in the external bulk solutions; C1, C2 are the concentration of the cation and the anion, respectively, within the GCL.

placed in contact with two bulk solutions containing a 1:1 salt consisting of monovalent ions (e.g. NaCl or KCl). Due to the electro-neutrality requirement, the cation concentration is equal to the anion concentration in the bulk solutions. At the boundaries with the GCL, the ion concentrations are discontinuous. Within the GCL, electro-neutrality must take into account the charge of the solid skeleton or fixed charge (FC) that is negative. As a result, the cation concentration is higher than the salt concentration in the bulk solution, whereas the anion concentration is lower.

The ion partition mechanisms associated with the momentum transfer between the components of the solution and the condition of absence of electric current are responsible for the restricted movement of salt solutions through semi-permeable membranes and chemico-osmosis, i.e. the volumetric flux of the solution in response to a salt concentration gradient.

Thermodynamics of irreversible processes

The coupled transport theory represents the generalization of the classic advective-diffusive theory adopted for modelling the migration of solutes through uncharged porous media. This theory is generally based on the formalism of the Thermodynamics of Irreversible Processes (Staverman, 1952; De Groot and Mazur, 1962; Katchalsky and Curran, 1965).

The approach developed by Staverman (1952) is based on the strongly simplifying assumption that the semipermeable membrane can be idealized as a 'discontinuity' between two bulk solutions. In such an approach, all the variables are referred to the two compartments in contact with the membrane, so it is not necessary to evaluate the phenomena occurring within the membrane. The main advantage of such an approach is that the problem of modelling transport mechanisms through the porous medium is avoided. In the discontinuous version of the Thermodynamics of Irreversible Processes under isothermal conditions, the membrane is considered as a transition region between two homogeneous compartments hav-

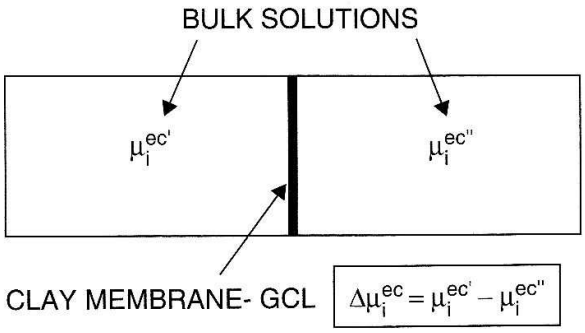

Figure 2.12: Reference scheme for the application of the discontinuous version of the Thermodynamics of Irreversible Processes.

ing the same temperature, and the differences in the thermodynamic potentials across the membrane that represent the driving forces responsible for the corresponding flows are assumed to be small (see Fig. 2.12). Under these conditions, and in the absence of chemical reactions, the dissipation function, Φ, defined as the rate of entropy production multiplied by absolute temperature, may be expressed as follows (De Groot and Mazur, 1962; Katchalsky and Curran, 1965):

$$\Phi = \sum_{i}^{N} J_i \Delta\mu_i^{ec} \tag{2.2}$$

where N = number of the components of the solution, J_i = molar mass flow of the i^{th} component and $\Delta\mu_i^{ec}$ = electrochemical potential difference of the i^{th} component. The electrochemical potential differences are intended as the thermodynamic forces driving the mass fluxes. The finite differences are defined as the values in the 'left' bulk solution minus those in the 'right' bulk solution, as indicated in Figure 2.12. The conventional assumption of the Thermodynamics of Irreversible Processes is that the processes under consideration are sufficiently slow as to make all the fluxes linear functions of all the forces operating in the system. The resulting system of N equations is given as follows:

$$J_i = \sum_{j} L_{ij} \cdot \Delta\mu_i^{ec} \quad i = 1,2...N \tag{2.3}$$

where L_{ij} =phenomenological coefficients. Based on Onsager's law of reciprocity (Onsager, 1931a,b), the matrix of the coefficients L_{ij} is symmetrical, such that:

$$L_{ij} = L_{ji} \tag{2.4}$$

The typical analysis of osmosis and solute transport through a membrane is restricted to the case of a solution containing a binary electrolyte consisting of a counter-ion (charge polarity opposite that of the membrane charge) and a co-ion (same charge polarity as the membrane) (Katchalsky and Curran, 1965; Groenevelt and Bolt, 1969), or:

$$(Counter-ion)_{z_1}^{\nu_1}\,(Co-ion)_{z_2}^{\nu_2} \tag{2.5}$$

where (ν_1, z1) and (ν_2, z2) are the stoichiometric coefficient and the electrochemical valence of the counter-ion (index 1) and co-ion (index 2), respectively.

The salt in solution is assumed to be completely dissociated such that:

$$(Counter-ion)_{z_1}^{\nu_1}\,(Co-ion)_{z_2}^{\nu_2} \longrightarrow \nu_1\,(Counter-ion)^{z1} + \nu_2\,(Co-ion)^{z2}$$

Clay particles generally have a negative charge such that the counter-ions are cations (positive charged ions) and the co-ions are anions (negative charged ions).

The ionic concentrations, C_i, in a bulk solution are related to the salt concentration, C_s, as follows:

$$C_i = \nu_i C_s \tag{2.6}$$

Electro-neutrality in the external or bulk solutions implies that:

$$z_1 C_1 + z_2 C_2 = 0 \tag{2.7}$$

Using Equation 2.6, the electro-neutrality condition (Eq. 2.7) reduces to:

$$z_1 \nu_1 + z_2 \nu_2 = 0 \tag{2.8}$$

For a solution containing a binary electrolyte, the dissipation function (Eq. 2.2) is given by

$$\Phi = J_w \Delta\mu_w + J_1 \Delta\mu_1^{ec} + J_2 \Delta\mu_2^{ec} \tag{2.9}$$

where (J_w $\Delta\mu_w$), (J_1 $\Delta\mu_1^{ec}$), (J_2 $\Delta\mu_2^{ec}$) are the molar mass flux and the electrochemical potential difference of the solvent (water), the counter-ion and the co-ion, respectively. In Equation 2.9, the electrochemical potential difference of the solvent has been assumed to be coincident with the chemical potential difference because the solvent molecules do not have an electrical charge.

The chemical potential difference of the solvent may be related to the hydraulic pressure difference, ΔP, and the osmotic pressure difference, $\Delta\Pi$, by means of the following relation (Katchalsky and Curran, 1965):

$$\Delta\mu_w = \overline{V}_w\,(\Delta P - \Delta\Pi) \tag{2.10}$$

where $\overline{V}_w$ = partial molar volume of the solvent.

The electrochemical potential differences of the ions are given by (Katchalsky and Curran, 1965):

$$\Delta\mu_i^{ec} = \overline{V}_i \Delta P + \Delta\mu_i^c + z_i F \Delta\varphi \tag{2.11}$$

where $\overline{V}_i$ = partial molar volume of the i^{th} ion, $\Delta\mu_i^c$ = chemical part of the chemical potential difference ofthe i^{th} ion, F = Faraday constant (9.648 70104 Cmol^{-1})and $\Delta\varphi$ = electrical potential difference.

The choice of the generalised forces and fluxes is to some extent arbitrary and based on convenience, i.e., based on condition that the product of each conjugate pair has the correct dimensions and the dissipation function is invariant. Substituting equations 2.10 and 2.11 into equation 2.9, the dissipation function becomes:

$$\Phi = q\Delta P - J_w \overline{V}_w \Delta\Pi + J_1 \Delta\mu_1^c + J_2 \Delta\mu_2^c + I_e \Delta\varphi \tag{2.12}$$

where $q = J_w \overline{V}_w + J_I \overline{V}_1 + J_2 \overline{V}_2$ is the total volumetric flux of the solution (or Darcy's velocity of the solution) and $I_e = F(z_1 J_1 + z_2 J_2)$ is the electric current density. The expression of the dissipation function given by Equation 2.12 is particularly convenient when the bulk solutions are not closed electrically, so that the electric current through the membrane has to equal zero (I_e = 0). If the electric current is zero, the last term in Equation 2.12 drops out and the ionic fluxes are related as follows:

$$\frac{J_1}{\nu_1} = \frac{J_2}{\nu_2} = J_s \tag{2.13}$$

where J_s = molar mass flux of the salt. In the absence of an applied electric current, the dissipation function may be written in the following form:

$$\Phi = q\Delta P - J_w \overline{V}_w \Delta\Pi + J_s \Delta\mu_s^c \tag{2.14}$$

where $\Delta\mu_s^c = \nu_1 \Delta\mu_1^c + \nu_2 \Delta\mu_2^c$ is the chemical part of the chemical potential difference of the salt. The osmotic pressure, $\Delta\Pi$, is related to $\Delta\mu_s^c$ as follows:

$$\Delta\Pi = C_{1,ave} \Delta\mu_1^c + C_{2,ave} \Delta\mu_2^c = C_{s,ave} \Delta\mu_s^c \tag{2.15}$$

where $C_{1,ave}$, $C_{2,ave}$ and $C_{s,ave}$ are the average concentrations between the two external solutions of the counter-ion, the co-ion and the salt, respectively.

The average concentrations $C_{1,ave}$, $C_{2,ave}$ and $C_{s,ave}$ are not uniquely defined since various types of averages may be used to evaluate them (e.g. arithmetic, geometric, logarithmic, harmonic, etc.). However, since the concentration differences between the two external solutions are assumed to be small, the difference between the various types of average also should be small. Arithmetic averages will always be used herein to determine the average concentrations. The average salt concentration is given by:

$$C_{s,ave} = \frac{C'_s + C''_s}{2} \tag{2.16}$$

where C'_s and C''_s are the salt concentrations in the left and the right cell, respectively.

For dilute solutions, $J_w \overline{V}_w \approx q$ and Equation 2.12 can be rewritten in the following form:

$$\Phi = q\Delta P + J_s^d \Delta \mu_s^c \tag{2.17}$$

where $J_s^d = J_s - qC_{s,ave}$ represents the diffusive part of the salt mass flux. In Equation 2.17, the number of independent forces and fluxes is reduced from 3 (as in Eq. 2.9) to 2 under the condition of no-electric current. Transforming Equation 2.9 into Equation 2.17, we have changed the generalised flows and forces so as to obtain a more suitable form of the dissipation function for practical applications. In Equation 2.17, the flows are the volumetric flux, q, and the salt diffusive molar mass flux, J_s^d, and the forces are the hydraulic pressure difference, ΔP, and the chemical potential difference of the salt, $\Delta \mu_s^c$. For dilute solutions, $\Delta \mu_s^c$ may be related to the salt concentration difference, ΔC_s, as follows (Katchalsky and Curran, 1965):

$$\Delta \mu_s^c = (\nu_1 + \nu_2) RT \frac{\Delta C_s}{C_{s,ave}} \tag{2.18}$$

where R = universal gas constant (8.3145 J/mol K) and T = absolute temperature.

Using the generalised flows and forces comparing in Equation 2.17, the phenomenological equations are:

$$q = \alpha_{11}\Delta P + \alpha_{12}\Delta \mu_s^c \tag{2.19}$$

$$J_s^d = \alpha_{21}\Delta P + \alpha_{22}\Delta \mu_s^c \tag{2.20}$$

Based on Onsager's law of reciprocity, the matrix of the coefficients α_{ij} is symmetrical, such that:

$$\alpha_{12} = \alpha_{21} \tag{2.21}$$

The phenomenological equations given by Equations 2.19, 2.20 describe the transport of a solution containing a binary electrolyte through a semipermeable membrane. The phenomenological coefficients α_{ij} have to be measured by means of appropriate experiments. In general, these coefficients may depend on the hydraulic pressure and the salt concentration, in addition to the physical properties of the membrane, such as the porosity, the pore size and the membrane charge

density. From a purely phenomenological point of view, only a systematic experimental investigation may characterize a membrane in a complete way, relating the phenomenological parameters to all varying quantities of the system.

The phenomenological coefficients α_{ij} have some special values corresponding to the limiting behaviour of the membrane. If the membrane has no selective ability with respect to the solute, the coefficient α_{12} is equal to zero. In this case, the membrane is not semi-permeable and the flows of solvent and solute are not coupled, such that the volumetric flux is given by:

$$q = \alpha_{11}\Delta P \;\; when\; \alpha_{12} = 0 \tag{2.22}$$

and the salt flux by:

$$J_s = qC_{s,ave} + J_s^d = qC_{s,ave} + \alpha_{22}\Delta\mu_s^c \;\; when\; \alpha_{12} = 0 \tag{2.23}$$

For dilute solutions, $\Delta\mu_s^c$ is given by Equation 2.18 and the salt flux (Eq. 2.23) may be written as follows:

$$J_s = qC_{s,ave} + \frac{\alpha_{22}(\nu_1+\nu_2)RT}{C_{s,ave}}\Delta C_s \;\; when\; \alpha_{12} = 0 \tag{2.24}$$

Comparing Equations 2.22 and 2.24 with the flux equations of the advective-diffusive transport theory, the phenomenological coefficients α_{11} and α_{22} may be related to the parameters usually used in environmental geotechnical engineering for the special case of non-membrane behaviour:

$$\alpha_{11} = \frac{k_h}{\gamma_w L_h} \tag{2.25}$$

$$\alpha_{22} = nD_s^* \frac{C_{s,ave}}{L_h(\nu_1+\nu_2)RT} \quad when\; \alpha_{12} = 0 \tag{2.26}$$

where n = connected porosity, k_h = hydraulic conductivity, γ_w,= unit weight of the solution, L_h = thickness of the membrane, $D_s^* = \tau_m D_{s,0}$ = effective salt diffusion coefficient, τ_m = matrix tortuosity factor and $D_{s,0}$ = free-solution salt diffusion coefficient. τ_m represents the tortuous nature of the actual diffusive pathways through the porous medium due to the geometry of the interconnected pores. The free-solution salt diffusion coefficient is given by:

$$D_{s,0} = \frac{(\nu_1+\nu_2)D_{1,0}D_{2,0}}{\nu_1 D_{2,0} + \nu_2 D_{1,0}} = \frac{(|z_1|+|z_2|)D_{1,0}D_{2,0}}{|z_1|D_{1,0} + |z_2|D_{2,0}} \tag{2.27}$$

where $D_{1,0}$ and $D_{2,0}$ are the free-solution diffusion coefficients of the counter-ion and of the co-ion, respectively.

The relation between α_{11} and k_h (Eq. 2.25) is general and is valid also in the case of membrane behaviour, because the hydraulic conductivity of a semipermeable membrane is defined as ratio between the volumetric flux and the hydraulic

pressure (head) difference under no-electric current and no-concentration difference conditions. On the contrary, the relation between $\alpha_2 2$ and D_s^* (Eq. 2.26) is valid only in the case of non-membrane behaviour, i.e., in the absence of osmotic effects.

When the membrane is an 'ideal' or 'perfect' semipermeable membrane, the salt flux is completely hindered:

$$J_s = qC_{s,ave} + J_s^d = (\alpha_{11}C_{s,ave} + \alpha_{12})\,\Delta P + (\alpha_{12}C_{s,ave} + \alpha_{22})\,\Delta\mu_s^c = 0 \qquad (2.28)$$

Equation 2.28 implies the following conditions:

$$\alpha_{12} = -\alpha_{11}C_{s,ave} \quad for\ non-membrane\ behaviour \qquad (2.29)$$

$$\alpha_{22} = -\alpha_{12}C_{s,ave} \quad for\ non-membrane\ behaviour \qquad (2.30)$$

Using equation 2.29, the volumetric flux, q, is given by:

$$q = \alpha_{11}\,(\Delta P - \Delta\Pi) \qquad (2.31)$$

The actual clay membranes are able to restrict the passage of the solute only partially. In order to characterise completely the transport of the solution through a clay membrane, the three coefficients α_{11}, α_{12} and α_{22} should be measured by means of appropriate experiments. However, some other phenomenological coefficients, related to the α_{ij} coefficients by simple relations, are more convenient for the experimental measurements.

The volumetric flux (Eq. 2.19) may be rewritten as follows:

$$q = \frac{k_h}{\gamma_w L_h}\,(\Delta P - \omega\Delta\Pi) \qquad (2.32)$$

where k_h is related to α_{11} by Equation 2.25 and

$$\omega = -\frac{\alpha_{12}}{\alpha_{11}C_{s,ave}} \qquad (2.33)$$

where ω is the chemico-osmotic efficiency coefficient. The chemico-osmotic efficiency coefficient is also called reflection coefficient and is indicated using the Greek letter σ. The use of the symbol ω is preferred in the engineering literature because the symbol σ typically represents stress or electric conductance (Malusis et al., 2003).

Using Equation 2.19, the hydraulic pressure difference may be expressed as a function of the volumetric flux:

$$\Delta P = \frac{1}{\alpha_{11}}\left(q - \alpha_{12}\frac{\Delta\Pi}{C_{s,ave}}\right) \qquad (2.34)$$

Substituting Equation 2.34 into Equation 2.20, the salt flux, J_s, is given by:

$$J_s = (1-\omega)\, qC_{s,ave} + \frac{nD^*_\omega}{L_h}\Delta C_s \tag{2.35}$$

where

$$D^*_\omega = \left(\alpha_{22} - \frac{\alpha^2_{12}}{\alpha_{11}}\right)\frac{RT\,(\nu_1+\nu_2)\,L_h}{nC_{s,ave}}$$

$$= \alpha_{22}\frac{RT\,(\nu_1+\nu_2)\,L_h}{nC_{s,ave}} - \omega^2\frac{k_h}{\gamma_w n}C_{s,ave}RT\,(\nu_1+\nu_2) \tag{2.36}$$

is the osmotic effective salt diffusion coefficient.

The chemico-osmotic efficiency coefficient, ω, may be determined from Equation 2.32 using one of the following experimental conditions:

$$\omega = \left(\frac{\Delta P}{\Delta\Pi}\right)_{q=0,I_e=0} \tag{2.37}$$

$$\omega = \frac{L_h\gamma_w}{k_h}\left(\frac{q}{\Delta\Pi}\right)_{\Delta P=0,I_e=0} \tag{2.38}$$

The osmotic effective salt diffusion coefficient is defined by the following experimental condition:

$$D^*_\omega = \frac{L_h}{n}\left(\frac{J_s}{\Delta C_s}\right)_{q=0,I_e=0} \tag{2.39}$$

With respect to the more conventional case of non-membrane behaviour, the definition of the diffusive coefficient is more ambiguous, because the two boundary conditions q = 0 and ΔP = 0 cannot be satisfied at the same time in a semipermeable membrane. In Equation 2.35, it is implicitly stated that we have defined the diffusive coefficient as the coefficient that we can measure when the volumetric flux is zero (q = 0).

Using the condition α_{12} = 0 and Equation 2.26, a non-semipermeable membrane is characterised by the following special values of the parameters ω and D^*_ω:

$$\omega = 0 \quad D^*_\omega = D^*_s \tag{2.40}$$

An ideal membrane, instead, is characterised by the following special values of the parameters ω and D^*_ω:

$$\omega = 1 \quad D^*_\omega = 0 \tag{2.41}$$

The chemico-osmotic efficiency coefficient, ω, of a clay membrane is a measure of its effectiveness in causing hydraulic flow under an osmotic gradient (see Eq. 2.32) and of its ability to prevent the passage of ions (see Eq. 2.35). Such a

coefficient is equal to zero (ω = 0) when the membrane is not semipermeable and assumes a maximum value of unity (ω = 1) when the membrane is ideal or perfect. The values of ω are frequently assumed to vary from zero to unity, although there are not thermodynamic restrictions to such a variation such that low negative values also have been measured (Kemper and Quirk, 1972).

Based on Equations 2.40 and 2.41, the osmotic effective salt diffusive coefficient varies with ω. We will discuss the dependency of D^*_ω on ω within GCLs on the basis of experimental evidence and theoretical considerations.

Physical interpretation of transport parameters

One of the most important advantages of the thermodynamic approach is that it doesn't require any specification of the physical phenomena involved in the transport of ions through a semipermeable membrane. This advantage is even more appreciable if we consider that our knowledge of the physico-chemical mechanisms controlling ion distribution within the pores at the microscopic scale is still partial and controversial. However, the experimental observations suggest the existence of some general relations between the phenomenological coefficients. In particular, the relation between the osmotic effective salt diffusion coefficient, D^*_ω, and the chemico-osmotic efficiency coefficient, ω, may be investigated on the basis of a sufficiently general physical model.

It's well known that clays are able to generate a partition of ions due to the negative electric charge of the surfaces of their particles. At the microscopic scale, such a partition may be modelled by the diffuse double layer (DDL) theory. The DDL theory states that the electric potential distribution within the pores is governed by the Poisson-Boltzmann equation. Moreover, other mechanisms, normally not contemplated in the DDL theory, may play a significant role in partitioning ions within clay pores, such as: (i) steric hindrance due to the finite size of ion molecules; (ii) dielectric exclusion due to the polarization of matrix/solvent interface; and (iii) the increase in the solute solvation energy due to possible changes in the properties of solvent in nanopores.

However, apart from the partition mechanism, the actual ion concentrations in the membrane, $\overline{C}_i$, may be related to the virtual or equivalent salt concentration, C_s, by means of a simple relation such as:

$$\overline{C}_i = \nu_i C_s \Gamma_i \quad i = 1,2 \tag{2.42}$$

where Γ_i = partition coefficient of the ith ion. C_s represents the salt concentration of a virtual or equivalent bulk solution that would be in thermodynamic equilibrium with an infinitesimal element of the membrane at the generic position x within the membrane (Dormieux et al., 1995; Yaroshchuk, 1995). At the boundaries (i.e. x = 0 and x = L_h), the virtual solution coincides with the bulk solutions that are in

contact with the clay membrane. The ion partition coefficients represent the interaction of the ion species with the charged solid skeleton of the clay membrane. If the fixed charge (FC) is negative, the anion species are repelled from solid particles and the coefficient Γ_2 varies from zero to unity (i.e. $0 < \Gamma_2 < 1$). Also, the cation is attracted by the solid particles and the coefficient Γ_1, is larger than unity (i.e. $\Gamma_1 \geq 1$).

If the only partition mechanism considered is that associated to electrostatic repulsion of ions from charged pore walls, the partition coefficients may be related to the macroscopic electric potential of the membrane, ψ_m, as follows:

$$\Gamma_i = exp\left(-\frac{z_i F}{RT}\psi_m\right) \tag{2.43}$$

where ψ_m is also called Donnan potential.

In order to relate the macroscopic electric potential, ψ_m, to the physical and chemical properties of the semipermeable porous medium, Teorell (1935, 1937) and (Meyer and Sievers, 1936a,b) proposed to adopt an electro-neutrality condition, taking into account the concentration of the FC, C_x, uniformly distributed within the porous medium, as follows:

$$z_1\overline{C}_1 + z_2\overline{C}_2 + \varpi C_x = 0 \tag{2.44}$$

where ϖ is the sign of the fixed charge (for clays with a negative fixed charge, $\overline{\omega} = -1$).

The fixed charge concentration, C_x, may be assumed proportional to the CEC and inversely proportional to the void ratio, e = n/(1- n), or:

$$C_x = \phi_x \, CEC \, \rho_s \frac{1}{e} \tag{2.45}$$

where ϕ_x is the fixed charge coefficient and ρ_s is the density of the solid phase.

The fixed charge coefficient, $\phi_x = \phi_x(S, \varepsilon_r, r_1, \ldots)$, varies from zero to unity and may account implicitly for the dependency of the FC concentration on the characteristic dimension of the pores through the specific surface, S, and on the relative dielectric constant of the solvent, ε_r. When $S \rightarrow \infty$ or $\varepsilon_r \rightarrow \infty$, the coefficient of the FC tends to 1. However, for real clays with a finite and not negligible microscopic characteristic dimension of pores, the reduction of the ion partition ability is taken into account adopting a value of ϕ_x smaller than 1. Moreover, the parameter ϕ_x accounts for the formation of a Stern layer of immobile cations, specifically adsorbed on the solid surface. The effect of the formation of the Stern layer may be introduced in the macroscopic model by means of an empirical dependency of ϕ_x on the type of cations present in solution through the radius of the cation species, r_1. The formation of a Stern layer reduces the theoretical FC concentration, so that $\phi_x < 1$. Finally, ϕ_x also may be used for taking into account the effect of

'imperfections', i.e. preferential transport paths having a microscopic dimension higher relative to the intact matrix and producing a reduction in effectiveness of the membrane in partitioning the ion species.

Neglecting the effect of inertia on the movement of each component of the solution, the momentum equations for water and ions are (Spiegler, 1958; Gu et al., 1999; Dominijanni and Manassero, 2005):

$$\overline{C}_w \nabla(-\mu_w) = f_{w1}(v_w - v_1) + f_{w2}(v_w - v_2) + f_{wm}(v_w - v_m) \tag{2.46}$$

$$\overline{C}_1 \nabla(-\mu_1^{ec}) = f_{1w}(v_1 - v_w) + f_{12}(v_1 - v_2) + f_{1m}(v_1 - v_m) \tag{2.47}$$

$$\overline{C}_2 \nabla(-\mu_2^{ec}) = f_{2w}(v_2 - v_w) + f_{21}(v_2 - v_1) + f_{2m}(v_2 - v_m) \tag{2.48}$$

where $\overline{C}_w = C_w$ = water concentration, v_w = water filtration velocity, v_1, = cation velocity, v_2 = anion velocity, v_m = velocity of the solid skeleton, f_{ij} = friction coefficient between the components i^{th} and j^{th}. The terms on the left-hand side of Equations 2.46, 2.47, 2.48 represent the forces for unit volume that drive the movement of the components of the solution. The terms on the right-hand side represent the momentum exchanged between the components of the solution. Under the assumption of binary interactions between the components of the system, the matrix of the friction coefficients is symmetric, such that

$$f_{ij} = f_{ji} \quad i, j = 1, 2, w, m \tag{2.49}$$

The assumption of a rigid solid skeleton implies that v_m is equal to zero.

For dilute solutions, the water filtration velocity may be assumed equal to the solution filtration velocity (i.e. $v_w \cong q/n$) and the ion species may be assumed to be sufficiently rarefied, such that the prevalent interaction force that they exchange with the other components of the mixture is that with water. As a result, the interaction forces among ions and between ions and the solid skelton may be neglected in comparison with the interaction force between ions and water (i.e. $f_{ij}, f_{im} << f_{iw} \;\; i, j = 1, 2$).

The gradients of the electro-chemical potential in Equations 2.46, 2.47, 2.48 may be referenced to the virtual solution due to the condition of thermodynamic equilibrium. The momentum equations for dilute solutions may be rewritten as follows:

$$\nabla(-P) - \nabla(\Pi) = f_{1w}(v_w - v_1) + f_{2w}(v_w - v_2) + f_{wm} v_w \tag{2.50}$$

$$\overline{C}_1 \left(RT \frac{\nabla(-C_1)}{C_1} + z_1 F \nabla(-\varphi) \right) = f_{1w}(v_1 - v_w) \tag{2.51}$$

$$\overline{C}_2\left(RT\frac{\nabla(-C_1)}{C_2}+z_2F\nabla(-\varphi)\right)=f_{2w}(v_2-v_w) \tag{2.52}$$

where the hydraulic pressure, P, the osmotic pressure, $\Pi=(\nu_1+\nu_2)RTC_s$, the ion concentrations, $C_i=\nu_i C_s$, and the electric potential, φ, are referenced to the virtual solution. From Equations 2.50, 2.51 and 2.52, the volumetric flux, $q=nv_w$, and the ion mass fluxes, $J_i=n\overline{C}_i v_i$, may be derived as follows:

$$q=nd_h\left[\nabla(-P)-\nabla(-\Pi)+RT\sum_{i=1}^{2}\Gamma_i\nabla(-C_i)+F\nabla(-\varphi)\sum_{i=1}^{2}z_i\Gamma_i C_i\right] \tag{2.53}$$

$$J_i=q\Gamma_i C_i+nD_i^*\Gamma_i\nabla(C_i)+n\Gamma_i C_i D_i^* z_i\frac{F}{RT}\nabla(-\varphi)\quad i=1,2 \tag{2.54}$$

where $d_h=1/f_{wm}$ is the mechanical permeability and $D_i^*=RT\overline{C}_i/f_{iw}$ is the macroscopic effective diffusion coefficient. Neglecting all phenomena due to the coupling between microscopic variations in concentration, velocity and electric potential, the macroscopic effective diffusion coefficient may be assumed constant and related to the free-solution diffusion coefficient, $D_{i,0}$, as follows:

$$D_i^*=\tau_m D_{i,0} \tag{2.55}$$

where τ_m is the tortuosity factor.

In the absence of electric current (i.e. $I_e=0$), the electric potential gradient may be eliminated from Equations 2.53 and 2.54. For a mono-dimensional problem, the fluxes are given by:

$$q=-\frac{k_{h,\lambda}}{\gamma_w}\left[\frac{dP}{dx}-\omega_\lambda\frac{d\Pi}{dx}\right] \tag{2.56}$$

$$J_s=(1-\omega_\lambda)qC_s-nD_{\omega,\lambda}^*\frac{dC_s}{dx} \tag{2.57}$$

where $k_{h,\lambda}$ = local hydraulic conductivity, ω_λ, = local chemico-osmotic efficiency coefficient and $D_{\omega,\lambda}^*$, = local osmotic effective diffusion coefficient (Dominijanni and Manassero, 2005). The local phenomenological parameters are given by the following expressions:

$$\frac{k_{h,\lambda}}{\gamma_w}=\frac{nd_h}{1+d_hRT\frac{(\Gamma_2\Gamma_1)^2\nu_1\nu_2C_s}{\nu_1\Gamma_2D_2^*+\nu_2\Gamma_1D_1^*}} \tag{2.58}$$

$$\omega_\lambda=1-\frac{\nu_1D_2^*+\nu_2D_1^*}{\nu_1\Gamma_2D_2^*+\nu_2\Gamma_1D_1^*}\Gamma_1\Gamma_2=1-\frac{\nu_1D_{2,0}+\nu_2D_{1,0}}{\nu_1\Gamma_2D_{2,0}+\nu_2\Gamma_1D_{1,0}}\Gamma_1\Gamma_2 \tag{2.59}$$

$$D_{\omega,\lambda}^*=(1-\omega_\lambda)D_s^* \tag{2.60}$$

In Equation 2.58, the local hydraulic conductivity at zero electric current, $k_{h,\lambda}$, is dependent on the concentration of the FC and the ions in solution. However, for plausible values of the parameters normally found in clay membranes, such dependency is generally negligible and, as a first approximation, may be assumed as follows:

$$k_{h,\lambda} \cong n d_h \gamma_w = k_h = L_h \gamma_w \left(\frac{q}{\Delta P}\right)_{\Delta\Pi=0, I_e=0} \tag{2.61}$$

The global parameters, measured by means of experiments, are related to the local parameters as follows:

$$w = \left(\frac{\Delta P}{\Delta \Pi}\right)_{q=0, I_e=0} = \frac{1}{\Delta C_s} \int_{C_s''}^{C_s'} \omega_\lambda dC_s \tag{2.62}$$

$$D_\omega^* = \frac{L_h}{n} \left(\frac{J_s}{\Delta C_s}\right)_{q=0, I_e=0} = \frac{1}{\Delta C_s} \int_{C_s''}^{C_s'} D_\omega^* dC_s = (1-\omega) D_s^* \tag{2.63}$$

Based on Equation 2.62, the measured values of the chemico-osmotic efficiency coefficient depend on the salt concentration in the two reservoirs that are in contact with the sample, rather than on the simple average concentration.

For a solution containing a 1:1 electrolyte (i.e. a salt consisting of monovalence ions, such as NaCl or KCl), Dominijanni and Manassero (2005) developed the following analytical expression for ω:

$$\omega = 1 + \frac{C_x}{2\Delta C_s} \left[Z_2 - Z_1 - (2t_1 - 1) \cdot ln \left(\frac{Z_2 + 2t_1 - 1}{Z_1 + 2t_1 - 1} \right) \right] \tag{2.64}$$

where

$$Z_1 = \sqrt{1 + (2C_s'/C_x)^2}$$

$$Z_2 = \sqrt{1 + (2C_s''/C_x)^2}$$

and $t_1 = D_{1,0}/(D_{1,0} + D_{2,0})$ is the cation transport number.

Using Equation 2.64 to interpret the experimental data of Malusis and Shackelford (2002a) for GCL specimens, Dominijanni and Manassero (2005) determined a fixed charge coefficient, ϕ_x, equal to 0.04 (see Fig. 2.13).

Equation 2.59 describes the dependency of the local chemico-osmotic efficiency coefficient on the ion concentrations, the FC concentration, the ion diffusion coefficients and the ion valences. On the basis of Eq. 2.59, ω_λ can assume negative values in the presence of low values of the transport number of the cation, $t_1 = D_{0,1}/(D_{0,1} + D_{0,2})$ (when the anions have a mobility much greater than cations) for 1:1 electrolytes. For example, in Figure 2.14, the dependency of ω_λ on the value of the transport number of the cation and the relative salt concentration, $\chi = C_s/C_x$, is illustrated for a 1:1 electrolyte. When t_1 is smaller than 0.5,

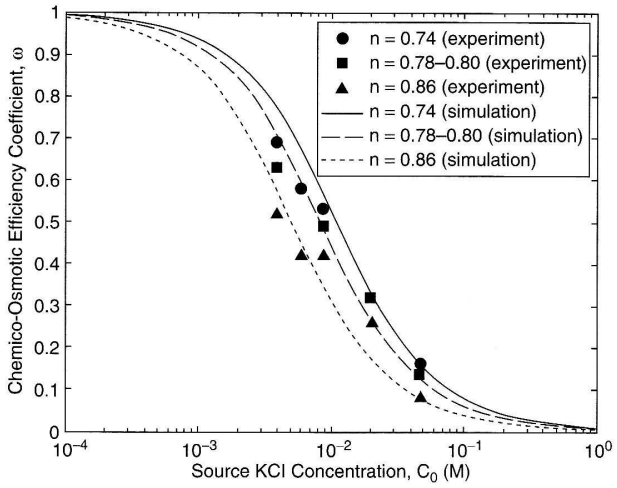

Figure 2.13: Interpretation of the experimental data of Malusis and Shackelford (2002a) assuming a constant fixed charge concentration. In the experiments $C_s' = C_0$ and $C_s'' = 0$

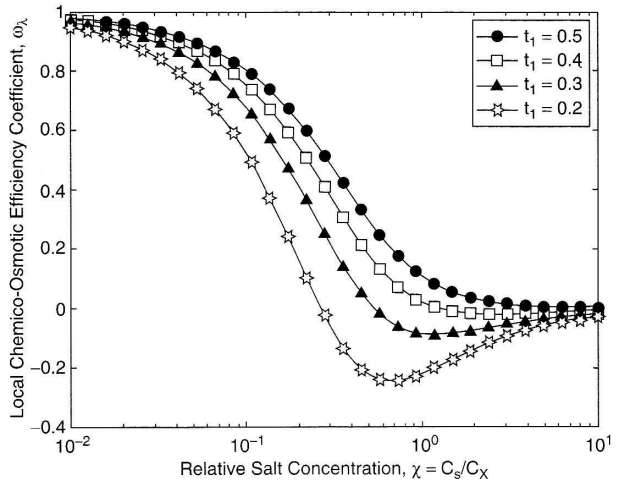

Figure 2.14: Local chemico-osmotic efficiency coefficient ω_λ versus relative salt concentration $\chi = C_s/C_x$, and the cation transport number, $t_1 = D_{0,1}/(D_{0,1} + D_{0,2})$, for a solution containing a (1:1) electrolyte

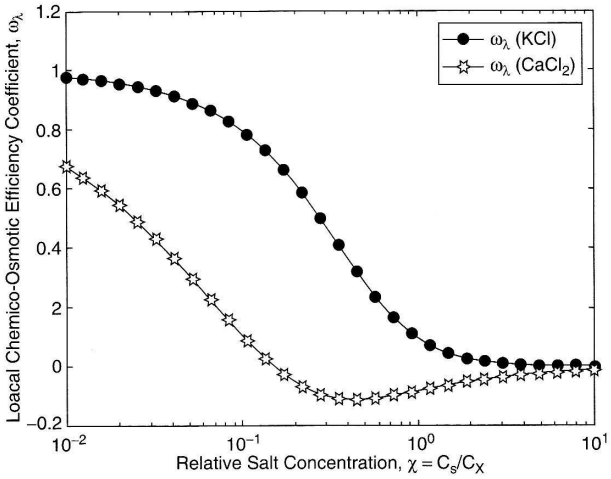

Figure 2.15: Local chemico-osmotic efficiency coefficient ω_λ versus relative salt concentration $\chi = C_s/C_x$, for solutions containing cations with different valence (z_1=+1 for K^+ and z_1=+2 for Ca^{2+})

ω_λ, can assume negative values. When the salt concentration increases or the FC concentration decreases, the parameter ω_λ decreases.

When the solution contains a 2:1 electrolyte, the restrictive capacity of the membrane is reduced. This phenomenon is clearly illustrated in Figure 2.15, where ω_λ is plotted as a function of the relative salt concentration, χ, for the case of KCl and $CaCl_2$ solution.

In order to evaluate the salt flux for steady state conditions, Equation 2.57 may be linearized, assuming as a first approximation that $\omega_\lambda \cong \omega$ and $D^*_{\omega,\lambda} \cong D^*_\omega$ for C_s, varying between C'_s and C''_s. Making such an approximation, the steady state salt flux, J_s, is given by:

$$J_s \cong (1-\omega)q\frac{C'_s exp\left[\frac{(1-\omega)qL}{nD^*_\omega}\right] - C''_s}{exp\left[\frac{(1-\omega)qL}{nD^*_\omega}\right] - 1} \tag{2.65}$$

Equation 2.65 allows a more accurate determination of the steady state salt flux than Equation 2.35. The transient analysis of the transport of the solution should be based on the following coupled mass balances:

$$\frac{\partial(nC_w)}{\partial t} = -\frac{\partial(C_w q)}{\partial x} \tag{2.66}$$

$$\frac{\partial(n\Gamma_i C_i)}{\partial t} = -\frac{\partial(J_i)}{\partial x} \quad i = 1,2 \tag{2.67}$$

where ρ_w = water density.

The analysis has been restricted to clays with only one cation and one anion in the pore solution. However, Equations 2.46, 2.47 and 2.48 may be generalized in order to study systems containing a generic number of ions in solution. Also, the thermodynamic approach of Staverman (1952) may be generalized to a generic number of ions (Yaroshchuk, 1995) defining an appropriate set of phenomenological parameters.

3
Materials

3.1 Laboratory modified clays

3.1.1 HYPER clay

The main purpose of this research is to develop a superior clay with enhanced Hydraulic Performance (a ”HYPER clay”). Engineered clays were developed for this purpose by adsorbing various dosages of an anionic polymer to the surface of an untreated bentonite. Hydraulic and chemico-osmotic performance of representative samples was analyzed.

The reference untreated clay used in this study is a sodium bentonite clay provided by Hojun Corporation, Japan. Physical and chemical properties of this clay are summarized in Table 5.1 in the Results Section. A series of laboratory tests were conducted to classify the geotechnical (physical and chemical) properties of this bentonite.

This reference bentonite clay was treated with an anionic polymer, Sodium-CarboxyMethyl Cellulose (Na-CMC), with various dosages (from 2% up to 16%) by dry weight. The clay was poured in a polymeric solution containing Na-CMC while stirring using a mechanical stirrer. The clay and the polymeric solution were mixed for 30 minutes. These slurries of clay, polymers and water were then oven dried at 105° C. After drying, the bentonites were ground using first a mortar and pestle and then a Retsch Mortar Grinder RM 200, as shown in Fig. 3.1.

Among these treated clays we named HYPER clay the clay treated with 2% Na-CMC. Also the treated clays were examined by physical and chemical analysis

in order to evaluate the impact of the method of preparation on the adsorption ability of the clay and the effect of the polymer on the clay fabric.

Sodium Carboxymethyl Cellulose, Na-CMC

Carboxymethyl cellulose (CMC) is a cellulose derivative with carboxymethyl groups (-CH2-COOH) bound to some of the hydroxyl groups of the glucopyranose monomers that make up the cellulose backbone (Fig. 3.2). It is often used as its sodium salt, Sodium Carboxymethyl Cellulose (Na-CMC).

The CMC is synthesized by the alkali-catalyzed reaction of cellulose with chloroacetic acid. The polar (organic acid) carboxyl groups render the cellulose soluble and chemically reactive. The functional properties of CMC depend on the degree of substitution of the cellulose structure (i.e., how many of the hydroxyl groups have taken part in the substitution reaction), as well as the chain length of the cellulose backbone structure and the degree of clustering of the carboxymethyl substituents.

CMC is used in food science as a viscosity modifier or thickener, and to stabilize emulsions in various products including ice cream. It is also a constituent of many non-food products, such as toothpaste, paints, detergents and various paper products. It is used primarily because it has high viscosity, is non-toxic, and is non-allergenic. In laundry detergents it is used as a soil suspension polymer designed to deposit onto cotton and other cellulosic fabrics creating a negatively charged barrier to soils in the wash solution. CMC is also used in the oil drilling industry as an ingredient of drilling mud, where it acts as a viscosity modifier and water retention agent. Insoluble microgranular carboxymethyl cellulose is used as a cation-exchange resin in ion-exchange chromatography for purification of proteins.

3.2 Factory manufactured materials

The hydraulic and chemico-osmotic performance of two manufactured polymer treated clays was also analyzed: on a Multiswellable Bentonite (MSB) and on a Dense PreHydrated GCL (DPH GCL).

3.2.1 Multiswellable Bentonite

A modified Multiswellable bentonite (MSB, Hojun Corp., Japan), was obtained by treating natural sodium bentonite with 25% of an organic compound (Propylene Carbonate, PC).

MSB exhibits higher swelling capacity and hydraulic conductivity values of one to two orders of magnitude lower than untreated bentonite in various electrolyte solutions (Katsumi, 2010). Onikata et al. (1999) showed that propylene

Figure 3.1: After drying, the treated bentonites were ground using first a mortar and pestle (a and b) and then a Retsch Mortar Grinder RM 200 (c)

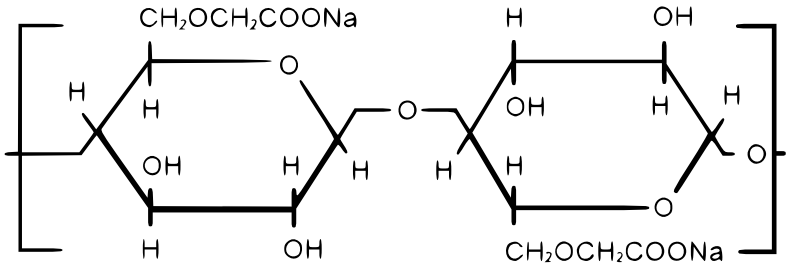

Figure 3.2: Sodium Carboxymethylcellulose, anionic polymer chemical formula

carbonate (PC) forms complexes with montmorillonite by intercalation, and that the PC-montmorillonite complexes exhibit osmotic swelling even in concentrated aqueous electrolyte solutions. Table 5.1 (Results Section) summarizes the main physical and chemical properties of MSB.

A series of laboratory tests were conducted to classify the physical and chemical properties of MSB. These experimental values for material properties are summarized in Table 5.1 and presented in detail in the Results Section.

3.2.2 Dense PreHydrated GCL

The hydraulic and chemico-osmotic efficiency of a manufactured Dense PreHydrated GCL (DPH GCL) was also analysed. This patented GCL (Flynn and Carter, 1998) is prehydrated with a dilute polymer solution containing carboxymethyl cellulose (CMC), sodium polyacrylate (Na-PAAS) and methanol. The sodium-montmorillonite clay is mixed with the liquid in a high speed, high shear mixer (Fig. 3.3, label 18). This mass is then calendered under vacuum into a bentonite sheet with a reduced number of voids (Fig. 3.3, label 24). The bentonite sheet is then sandwiched between one high strength woven polypropylene geotextile and a perforated polyester scrim (Fig. 3.3, labels 32 and 34). Table 5.1 summarizes the main properties of the material analyzed.

The high shear mixing, vacuum calendering and the use of methanol as a solvent enhance the adsorption of polymers in clays encouraging the formation of a complex by intercalation (Filippi et al., 2007; Sinha Ray and Bousmina, 2005; Flynn and Carter, 1998).

In making the DPH GCL both the CMC and the methanol make the mixed and kneaded product more flexible and workable. Whereas, polyacrylate compounds are added to the mixture to enhance the impermeable behaviour of the clay under aggressive conditions such as high electrolyte concentrations and strong leachates. In the sodium-cation form the acrylate can replace the sodium cations coated to the clay to avoid ion exchange with calcium or other ions. The CMC is a fungicidal preserving agent to prevent the growth of mould, and a lubricant to make the

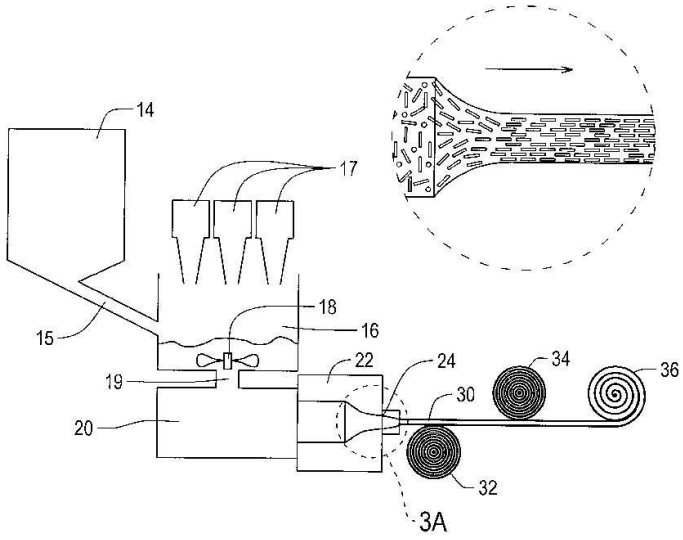

Figure 3.3: DPH GCL method of preparation: a clay is mixed with a polymeric solution in a mixer (18). This mass is then calendered under vacuum into a sheet with a reduced number of voids (24). The bentonite sheet is then sandwiched between two geotextiles (32, 34). (Flynn and Carter, 1998)

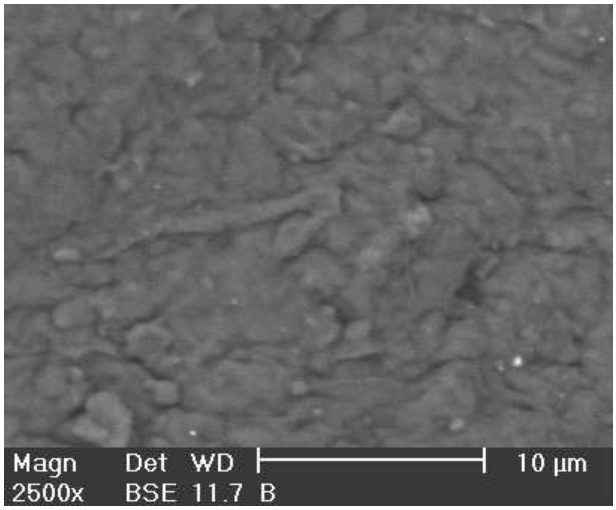

Figure 3.4: Scanning Electron Microscopy (SEM) of the DPH GCL

mixture more flexible and easily extrudable. The CMC, a water-soluble polymer, behaves as bulking agent during manufacturing, then in use dissolves in water providing micropores where more water can penetrate and hydrate the adjacent montmorillonite. The protection by bacterial attack provided by the CMC is important because the bacterial reactions can produce hydrocarbons which react with the sodium ions in the clay.

A bentonite paste provided by the manufacturer of the DPH GCL was used to improve the sealing of the overlapped samples. The bentonite paste is prehydrated with the same polymeric solution used for the DPH GCL. The water content of the bentonite paste is higher than the water content of the DPH GCL sample (144.30 % vs. 44.82 %) in order to enable an easy spreading of the paste.

The DPH GCL is provided with three enhancement methods to prevent or minimize compression of the interlayer and the corresponding increases in hydraulic conductivity (Kolstad et al., 2004). These enhancement methods are:

1. Prehydration
2. Decrease of void ratio
3. Polymer treatment

The first method, prehydration, consists of hydrating the bentonite with a deionized water prior to exposing it to an aggressive solution (Petrov et al., 1997). The second method is to increase the solids content of the bentonite, either by applying a high effective stress or by compressing the bentonite during manufacturing of the

GCL in order to reduce its void ratio (Petrov and Rowe, 1997). This approach is intended to diminish the effect of compression of the interlayer space by replacing void space with mineral solid. A third method is to use large organic molecules that bind to the montmorillonite surface as a prop to hold open the interlayer region in the presence of aggressive liquids (Kolstad et al., 2004).

This study is mainly dedicated to analyze the impact of polymer treatment as enhancement method on the hydraulic performance of clays.

3.3 Electrolyte solutions

The solutions used in this study are deionised water, natural sea water and a series of KCl and $CaCl_2$ solutions with concentration varying from 0.0001 M to 1 M.

The deionised water, used as reference solution, was produced using a water purification system PURELAB Option-R 7/15 (ELGA Vivend Water System Ltd), designed to provide highly purified water. The PURELAB Option-R process links four purification technologies: Reverse Osmosis, adsorption, ion-exchange, photo oxidation and also incorporates a re-circulation for further purification to obtain pump good quality potable water.

The electrolyte solutions were prepared by dissolving salts in deionised water, $CaCl_2 \cdot 2H_2O$ and KCl (>99.7%). Natural sea water was collected in the Adriatic Sea (Ancona, Italy). Chemical composition of the sea water is shown in Table 3.1. These electrolyte solutions were chosen to investigate the impact of their concentration and valence on the Atterberg limits, swelling ability, hydraulic conductivity and chemico-osmotic performance of modified clays. Chemical properties of the electrolyte solutions are shown in Table 3.2.

A 500 ppm DOWICIL QK-20 biocide solution was used as fungicidal to prevent microbial reactions during permeation in some of the hydraulic conductivity tests on the DPH GCL. For hydraulic conductivity tests with high permeability values, the influent solution was spiked with Rhodamine dye (5 g/L) to stain the preferential flow paths.

Ions	concentration [M]	ionic strength [M]	EC [mS/cm]	salinity [-]	pH [-]	Eh [mV]
seawater		0.88	55.0	35.5	7.89	201
Na^+	0.501					
K^+	0.012					
Ca^{2+}	0.011					
Mg^{2+}	0.049					
Cl^-	0.547					
SO_4^{2-}	0.027					
HCO_3^-	0.003					
CO_3^{2-}	0.0003					
NO_3^-	0.0007					

Table 3.1: Chemical composition of the sea water from the Adriatic Sea (Ancona, Italy)

Solution	concentration [M]	EC [mS/cm]	salinity [-]	pH [-]	Eh [mV]
deionized water		0.0039	0.0	7.57	293
KCl	0.0001	0.0142	0.0	6.45	258
	0.001	0.143	0.0	6.22	243
	0.01	1.392	0.5	6.261	304
	0.1	12.760	7.3	6.59	324
	1	112.9			
$CaCl_2$	0.0001	0.0253	0.0	6.35	297
	0.001	0.251	0.0	7.28	330
	0.005	1.211	0.4	6.56	262
	0.01	2.220	0.9	6.69	238
	0.1	18.540	11	6.77	260
	1	144.5			

Table 3.2: Chemical properties of the electrolyte solutions

4 Methods

4.1 Material characterization methods

4.1.1 Specific gravity by water pycnometer

The specific gravity of soil solids (Gs) of the clayey samples was determined by the water pycnometer method following the standard ASTM D854. This method that applies to soils that pass the 4.75 mm sieve is based on the determination of the volume of a known mass of soil by the fluid displacement method. The density of solid particles is calculated dividing the mass of the soil by its volume.

Although mass is easy to measure, the volume of an irregularly shaped sample can be more difficult to determine. One method is to put the sample in a water-filled container and read off how much water it displaces. The surface tension of the water may keep a significant amount of water from overflowing, which is especially problematic for small samples. For this reason it is desirable to use a water container with a small a capillary mouth, such as the water pycnometer (Fig. 4.1).

The dry soil is added to the pycnometer, which is then weighed, giving the weight of the powder sample. The pycnometer is then filled with a liquid of known density (deaired deionized water used to calibrate the pycnometer). The weight of the displaced liquid can then be determined, and hence the specific gravity of the soil. ASTM D854 prescribes to use about 10 g of dry soil. Given the high swellability of bentonites, 2 g of soil were used for this study. Three samples were used and an average of the three densities was recorded.

(a)

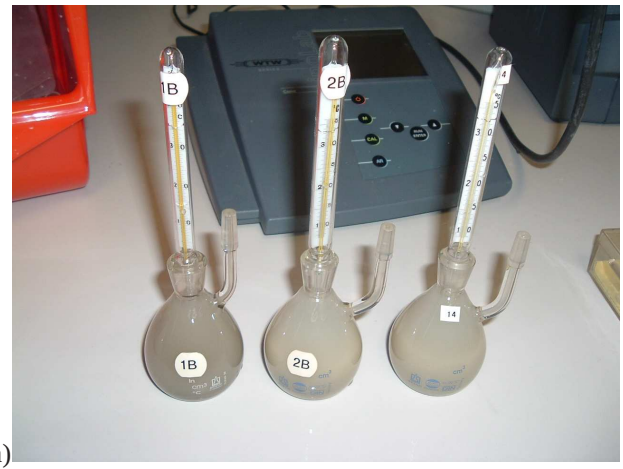

(b)

Figure 4.1: Measurement of the specific gravity of soil solids (Gs) by water pycnometer (ASTM D854): (a) water pycnometers and (b) vacuum chamber

Figure 4.2: Casagrande cup and the tools for the Atterberg limits determination

4.1.2 Atterberg Limits by Casagrande cup and rolling method

The liquid limit, the plastic limit and the plasticity index are measured following the standard test method (ASTM D4318). The liquid limit represents the water content, in percent, of a soil at the arbitrarily defined boundary between the semiliquid and plastic states. The limit liquid can be determined by the Casagrande apparatus that consists of a semispherical brass cup that is repeatedly dropped onto a hard rubber base (Fig. 4.2). The liquid limit is defined as the water content at which a groove cut into the soil placed in the cup will close over a distance of 12.7 mm following 25 blows.

The plastic limit represents the water content of a soil at the boundary between the plastic and semi-solid states. It is determined by rolling a small sample into threads and finding the water content at which threads, of 3 mm of diameter will start to crumble (Fig. 4.2). A number of determinations are made and the average water content is reported as the plastic limit.

The plasticity index is the range of water content over which a soil behaves plastically. Numerically, it is calculated as the difference between the liquid limit and the plastic limit.

Figure 4.2 shows a picture of the Casagrande cup and the tools for the Atterberg limits determination.

4.1.3 X-Ray Diffraction and Scanning Electron Microscopy

X-Ray Diffraction (XRD) analyses were performed on samples oriented on glass slides. XRD was performed on untreated clay, polymer treated clay and on the

Figure 4.3: Philips PW 3710 mpd control (Laboratory of Geology and Soil Science, UGent)

DPH GCL. These tests were carried out at the Laboratory of Soil Science, Department of Geology and Soil Science, UGent. The X-ray diffraction patterns were recorded on a Philips PW 3710 mpd control (Fig. 4.3). The diffraction spectra allow to determine the basal spacing between particles, providing an indication on the interlayer thickness of the material.

Moreover, powder X-ray diffraction analyses were performed on air-dried samples of MSB using a Philips diffractometer (PW1730 X-Ray generator, PW 1050/70 goniometer and Cu K radiation) at the FIMET Department of the Universitá Politecnica delle Marche.

When X-rays encounter any form of matter, they are progressively attenuated as a result of absorption, scattering, and/or diffraction phenomena. Since the atoms are arranged periodically in a lattice of substance, the rays scattered by them have definite phase relationships. Diffraction occurs only at those particular angles of incidence at which the wavelength of the X-rays is of the same order of magnitude as the repeat distance between the scattering centers (atoms) according to the Bragg's law (equation 4.1).

$$n\lambda = 2dsin\theta \tag{4.1}$$

where λ = wavelength of diffracted rays, d = distance between atom planes (basal spacing), θ = angle of incident beam, n = (integer) order of reflection. Figure 4.4 shows how to derive the Bragg's law using the reflection geometry and applying trigonometry.

Also a scanning Electron Microscope (SEM) analysis, was performed on the

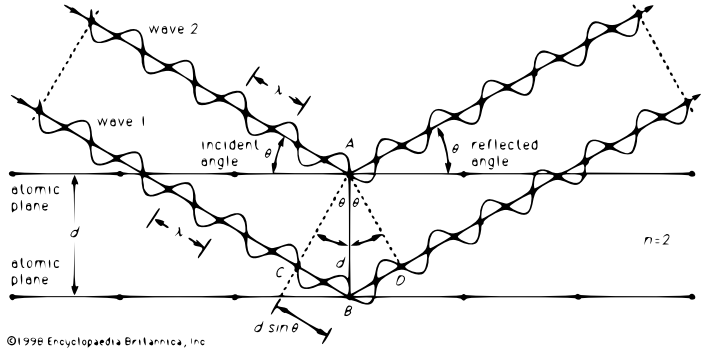

Figure 4.4: Deriving Bragg's law using the reflection geometry and applying trigonometry

DPH GCL with EDX system for local chemical analyses, at the Department of Material Science and Engineering, UGent. SEM analysis provides 3-D particle morphology and local particle surface features generally on a micrometer scale. A beam of electrons is shot to a sample and as a result of their interaction, electrons and photons are released from the sample. These electrons and photons can be captured by detectors, providing valuable information for each point on the sample's surface.

4.1.4 Cation Exchange Capacity

The Cation Exchange Capacity (CEC) of the bentonites analysed was measured following either the ammonium acetate method or the compulsive exchange method (Sumner and Miller, 1996).

In the ammonium acetate method (performed at the Laboratory of Soil Science, UGent), the soil is saturated first with NH_4OAc, this slurry is used to measure the exchangeable cations. Then ethanol is added until no more NH_4^+ is detected in the leachate. Finally the slurry is mixed with KCl and NH_4^+ is determined in the leachate to calculate CEC.

In the compulsive exchange method (performed on the DPH GCL at the Universitá Politecnica delle Marche), the soil is initially saturated with a $BaCl_2$ solution, in order to exchange all the exchangeable cations with Ba^{2+}. From the extract solution the exchangeable cations are measured taking into account that some of them are soluble ions. Then the Ba^{2+} is exchanged by Mg^{2+} by addition of $MgSO_4$, which precipitates $BaSO_4$(s). The quantity of Mg^{2+} absorbed (=CEC) is estimated as the loss of Mg^{2+} from the $MgSO_4$ solution added.

4.1.5 Zeta potential and viscosity

Zeta potential and viscosity measurements were performed to evaluate the impact of the method of preparation on the adsorption ability of the clay and the effect of the polymer on the clay fabric.

The measurements of the parameters were performed at the Laboratory of Applied Physical Chemistry, UGent.

Tests were carried out on 10% (v/v) slurry samples prepared following two procedures:

1. the dry method, that consists on mixing dry clay to a polymeric solution, drying this slurry in the oven at 105° C and mixing it again with deionized water to obtain 10% v/v slurries

2. the wet method, that consists on mixing the clay with polymeric solutions (without drying it in the oven).

The dry method simulates the method of preparation of the HYPER clay, whereas the wet method simulates the method of preparation of a manufactured Dense Prehydrated Geosynthetic Clay Liner (DPH GCL) also studied in this research.

The viscosity of these slurries was measured with a Brookfield DV-II (Fig. 4.5). The sample was put in a cup and the spindle of the viscometer was completely immersed into the sample. The spindle turned at different speeds and the viscosities (at every speed) were recorded.

Zeta-potentials of the slurries were determined in triplicate by electrophoretic light scattering with the Malvern Zetasizer 2c (Fig. 4.6). All emulsions were previously diluted 200 times in the electrolytes. Zeta-potentials were calculated from the experimentally determined electrophoretic mobilities using the Helmholtz – Smoluchowski equation (Hiemenz, 1986).

4.2 Swelling ability determination

4.2.1 Swell index test

Swell Index Tests were performed to study the effect of polymer treatment on the sealing performance of clays. These tests were carried out with deionised water, sea water, KCl and $CaCl_2$ solutions with concentrations varying from 0.001 M to 0.5 M, to study the effect of concentration and valence on the sealing capacity of the untreated and treated clay.

The tests were conducted following the ASTM D5890. The bentonites were oven dried at 105° C. After drying, the bentonites were ground using a mortar and pestle until 100% passed the 200 mesh U.S. standard sieve. 90 ml of the tested

Figure 4.5: Brookfield DV-II Viscometer (Laboratory of Applied Physical Chemistry, UGent)

Figure 4.6: Malvern Zetasizer 2c to measure electrophoretic mobility (Laboratory of Applied Physical Chemistry, UGent)

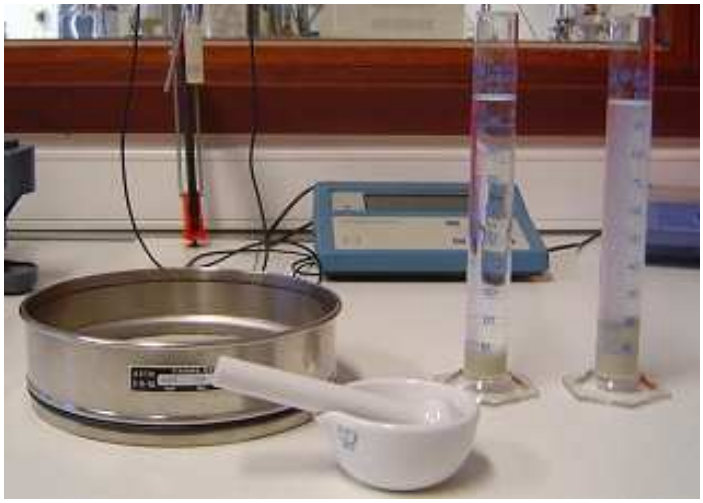

Figure 4.7: 200 mesh U.S. standard sieve, mortar and pestle, graduated 100 ml cylinders for swell index test determination (ASTM D5890)

solutions were poured into a 100 ml graduated cylinder. Two grams of sieved bentonite were placed in the acqueous solutions in the cylinder in 0.1 g increments. After the 2 g were added, additional solution was poured to fill the cylinder to the 100 ml and to rinse any particle of bentonite adhered to the internal sides of the cylinder. After minimum 16 hours of hydration period after the last increment, the final temperature and the volume of swollen bentonite were measured. A picture of the setup used is shown in Fig. 4.7.

4.2.2 Swell Pressure test

Swell pressure tests were performed on the untreated clay, the clay treated with various Na-CMC dosages and on the DPH GCL.

The swelling pressure test apparatus used in this study consists of a stainless steel ring (7.1 cm diameter) accommodated in a standard one-dimensional oedometer cell, located in a frame provided with a load cell connected to a computer (Fig. 4.8).

The specimen for the swell pressure test was prepared by spreading a thin layer of dry clay (0.45 g dry soil/cm^2) into the stainless steel ring placed into the oedometer cell. On the other hand, DPH GCL samples were trimmed from the GCL sheet using the stainless steel cutting ring of the oedometer setup. The ring containing the sample was then placed into the oedometer cell.

After sample assembling the oedometer was inundated with the testing solution. The swelling pressure was measured by the load cell keeping the height of

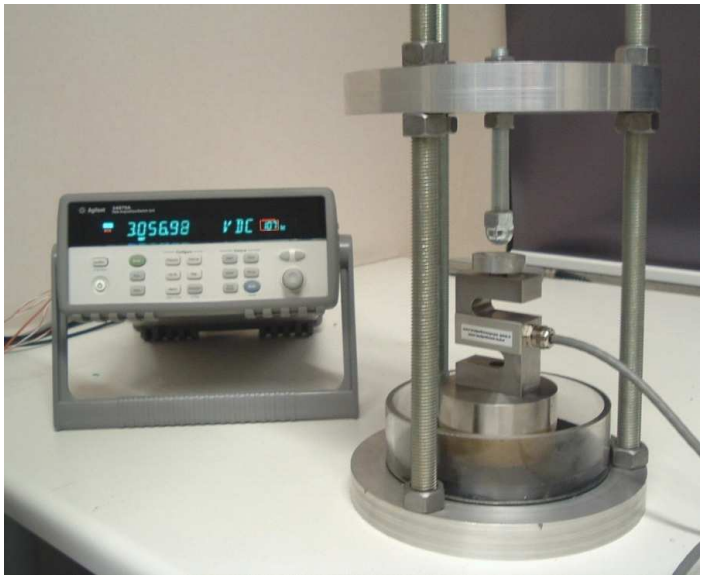

Figure 4.8: Swell pressure setup

the sample constant. For the powder samples a fixed height was chosen to obtain a porosity n = 0.718, whereas the DPH GCL maintained its own initial porosity n = 0.68. The achievement of a steady maximum swelling pressure was chosen as termination criteria.

Figure 4.9 shows the setup designed for the swell pressure test and the sample assembling procedure for the powder clay specimens.

4.3 Hydraulic conductivity test

The hydraulic conductivity tests were performed in conditioned rooms in flexible and rigid wall permeameters connected to Pressure Control Panels by means of bladder-accumulators following suitable ASTM standards (ASTM D5084, D5887, D6766, D5856).

A bladder accumulator is a device used when testing with corrosive or toxic permeants that may attack control panel components. This device allows also sampling of the outlet for chemical analysis. The bladder accumulator is connected in line between the control panel and the test chamber.

4.3.1 Flexible wall permeameters

Falling-head hydraulic conductivity tests were conducted in flexible wall permeameters, in order to investigate the impact of polymer addition, prehydration and

(a)

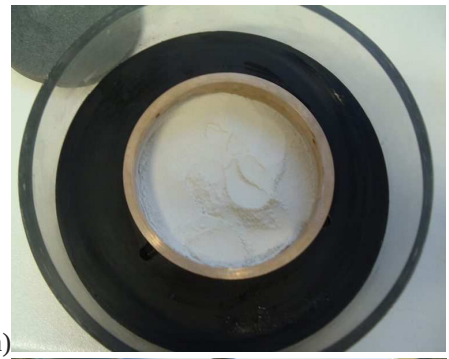

(b)

(c)

Figure 4.9: Sample assembling for the swell pressure test: (a) a thin layer of dry clay was spread into a stainless steel ring between two filter papers and two porous stones; (b) this ring was placed into an oedometer cell; (c) after inundation with the testing solution, the swelling pressure was measured by a load cell keeping the height of the sample constant

Hydraulic conductivity on prehydrated samples			
sample	deionized water	$CaCl_2$	sea water
untreated clay	x	5 mM	x
HYPER clay	x	5 mM	x
MSB	x	5 mM	x
DPH GCL	x	12.5 mM	x
DPH GCL overlap	x	10; 20; 100 mM	x
Hydraulic conductivity of non-prehydrated samples			
untreated clay	x	5 mM	x
HYPER clay	x	5 mM	x
clay+8%Na-CMC		5 mM	
MSB	x	5 mM	x

Table 4.1: Hydraulic conductivity testing program

densification on the hydraulic performance to electrolyte solutions.

The permeant solutions used for these tests were: deionised water, sea water and $CaCl_2$ solutions. Table 4.1 gives an overview of the tests performed. Flexible wall permeameters were used to test the hydraulic conductivity of non-prehydrated samples, whereas, prehydrated samples were tested with rigid wall permeameters at the end of chemico-osmotic test, as described further on in this chapter.

The hydraulic conductivity tests in flexible wall permeameters were performed with an average effective stress of 14 kPa on 7.1 cm diameter samples, with initial porosity n=0.718. Thin clay specimens were prepared, with the purpose of simulating the bentonite core of a standard GCL. To prepare these samples 17.84 g of dry soil were poured in a stainless steel ring between two porous stones and filter papers. Then the ring was inundated with the permeating solution. The aim of this procedure was to obtain samples that represent a standard GCL with dry soil per unit area of 0.45 g/cm^2.

On the other hand, DPH GCL single sheet samples (with initial porosity n=0.68) were obtained from a DPH GCL roll using a cutting stainless steel ring.

4.3.2 Large-scale laboratory setup for overlapped samples

Falling-head hydraulic conductivity tests were conducted in flexible and rigid wall permeameters on the DPH GCL overlapped samples.

A large-scale laboratory permeameter was used to test 30.5 cm diameter samples with 10 cm overlap. these samples were permeated with deionised and sea water (Fig. 4.11).

Figure 4.10: Flexible wall hydraulic conductivity cells connected to a control pressure panel through bladder accumulators. Detail of sample assembling

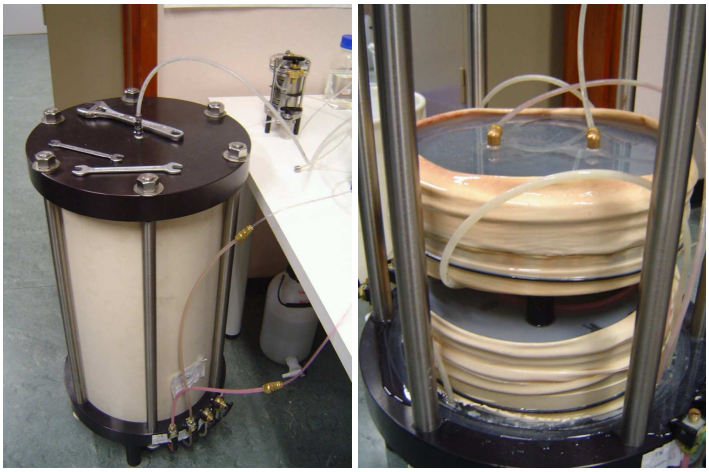

Figure 4.11: Large-scale flexible wall permeameter used for DPH GCL overlaps

A rigid wall stainless-steal permeameter was used to test 14 cm diameter samples with 5 cm overlap seams permeated with $CaCl_2$ solutions (Fig. 4.12).

The hydraulic conductivity tests in the flexible wall permeameter were performed with an average effective stress of 14 kPa and a back pressure of 340 kPa. Effective stresses of 14 kPa, 28 kPa, 55 kPa and 110 kPa were applied in four stages in order to analyze the impact of increasing the effective stress on the hydraulic performance of the overlap. Two samples housed into the large scale setup were permeated with deionized water and with sea water, respectively.

A second series of tests were performed on two overlapped samples with a thin layer of bentonite paste spread in the overlap area to improve the sealing performance. These two samples were also permeated with deionized water and sea water, respectively, with an average effective stress of 14 kPa and a back pressure of 340 kPa.

A third series of hydraulic conductivity tests to 10 mM $CaCl_2$ solutions were performed in the rigid wall medium scale permeameter (14 cm diameter) with an average effective stress of 14 kPa and a back pressure of 14 kPa. After steady state, the $CaCl_2$ was increased from 10 mM to 20 mM and finally up to 100 mM, in order to analyze the impact of increasing the $CaCl_2$ concentration on the hydraulic performance of the overlap.

Although the hydraulic conductivity is traditionally used to represent the hydraulic performance of soils and other porous media, the use of the permittivity is sometimes advantageous for thin compressible geosynthetic specimens such as GCLs because the thickness does not need to be measured or estimated. The permittivity is defined as the ratio between the hydraulic conductivity and the average specimen thickness. The permittivity was evaluated by the unit volume flowing

Figure 4.12: Medium-scale rigid wall oedometer/permeameter used for DPH GCL overlap seams

through the sample per unit time, total area and hydraulic head.

DPH GCL specimens for large-scale tests were prepared by overlapping two half-disks cut from a DPH GCL roll. The overlapped thickness was of 10 cm that represents the actual overlap thickness expected in the site. For every test, two 30.5 cm diameter specimens were cut from DPH GCL sheets (Fig. 4.13). At the overlap, the GCL sheets were laid one on top of the other without removing the geotextile wrapping. No bentonite loss was observed from the edges thanks to the prehydration of the material.

For the second series of tests, a bentonite paste was applied on the overlap contact area to improve sealing performance of the overlap. The bentonite paste, prehydrated with the same polymeric solution as the DPH GCl, was provided by the manufacturer. A thin layer of this paste was spread on every specimen as shown in Fig. 4.14.

As a reference, during the laboratory testing described in this work, 10 cm diameter single sheets from the same roll of DPH GCL were tested in various solutions, in standard flexible-wall permeameters, under 14 kPa effective stress, at the FIMET Department of Universitá Politecnica delle Marche in Italy. One of these samples, permeated with deionized water, was transferred to the Laboratory of Geotechnics, UGent, to remove the soluble salts by permeation with purified water for the chemico-osmotic test on the DPH GCL.

4.3.3 Rigid-wall consolidometer/permeameter: removal of soluble salts for the chemico-osmotic test

As it will be explained in detail in the next paragraph, rigid-wall consolidometers were also used to perform hydraulic conductivity tests on the samples intended for the chemico-osmotic test. In fact, the specimen is first permeated with deionized water to remove soluble salts, improve saturation and measure the reference hydraulic conductivity. Whereas, at the end of the chemico-osmotic/diffusion test the specimen is permeated with a 5 mM $CaCl_2$ solution in the rigid wall consolidometer/permeameter. This hydraulic conductivity test is intended to evaluate the impact of prehydration and permeation to 5 mM $CaCl_2$ solution after solutes diffusion. Figure 4.15 shows a picture of the rigid wall consolidometer/permeameter setup connected to the control pressure panel during the hydraulic conductivity test.

Figure 4.13: DPH GCL overlap sample assembling (without bentonite paste)

Figure 4.14: DPH GCL overlap sample assembling (with bentonite paste)

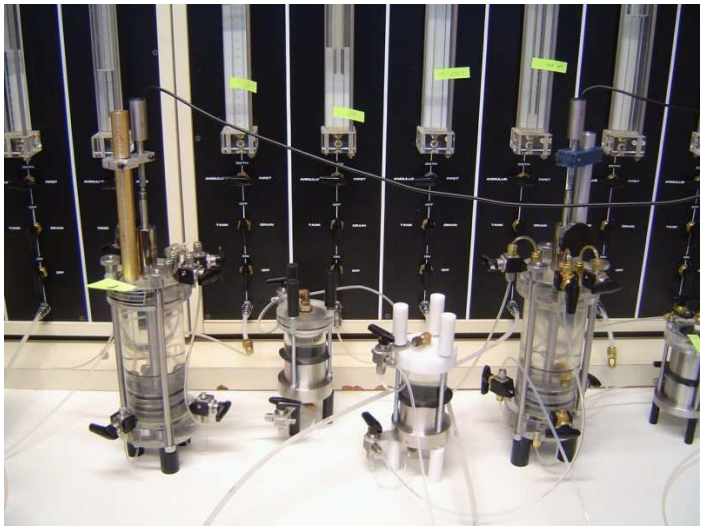

Figure 4.15: Rigid wall consolidometer/permeameters connected to the control pressure panel through bladder accumulators

4.4 Chemico-Osmotic Test

4.4.1 Setup description

To measure chemico-osmotic efficiency and diffusion coefficient of polymer treated clays, a special apparatus was employed following the testing methods of previous studies (Olsen, 1969; Malusis et al., 2001; Mazzieri et al., 2003). A schematic illustration of the testing apparatus is shown in Fig. 4.16. The complete setup consists essentially of two main parts: the pumping system and the rigid-wall consolidometer (testing cell) with pressure transducers (Fig. 4.17).

The testing cell (rigid wall consolidometer/permeameter) consists of a rigid acrylic cylinder containing the soil specimen and a pressure chamber separated by a rigid piston. The soil specimen is confined between two porous stones. Swelling of the soil during the test is prevented by blocking the top piston, maintaining a constant porosity throughout the test (Fig. 4.16).

The pumping system consists of a dual Syringe Pump (Model 33, Harvard Apparatus) equipped with two stainless steel cylinders aimed to circulate separate electrolyte solutions of different concentrations at the top ($C_{t,i}$) and at the base ($C_{b,i}$) of the soil specimen in order to induce and maintain a chemical gradient across the soil. If membrane behavior occurs, a differential pressure (ΔP) between the top and the base of the sample should be measured. Circulation outflow from these boundaries is simultaneously collected through the opposite end of the cylinder actuator at the same rate in order to maintain a constant volume inside the cell

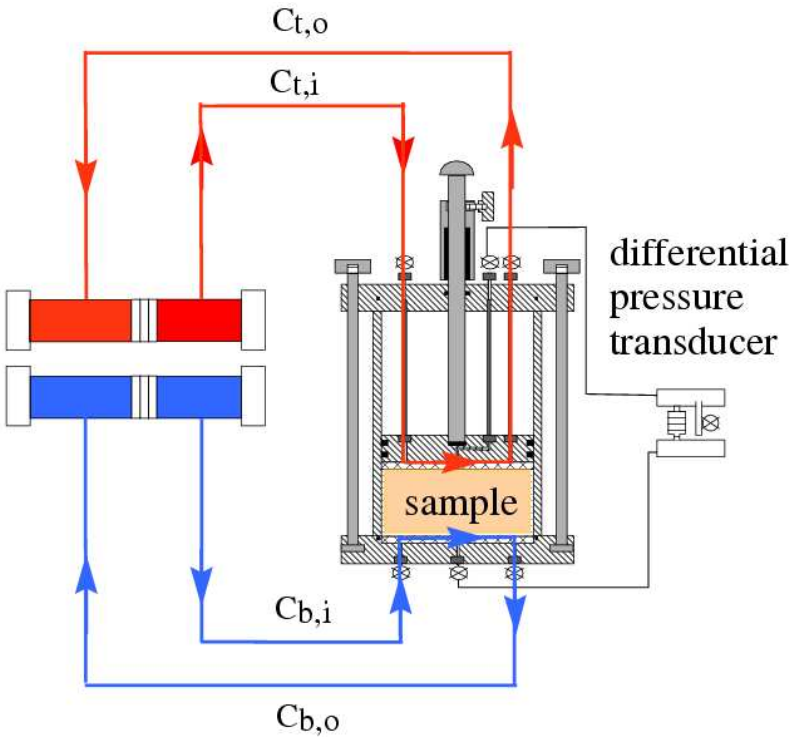

Figure 4.16: Chemico-osmotic test experimental setup

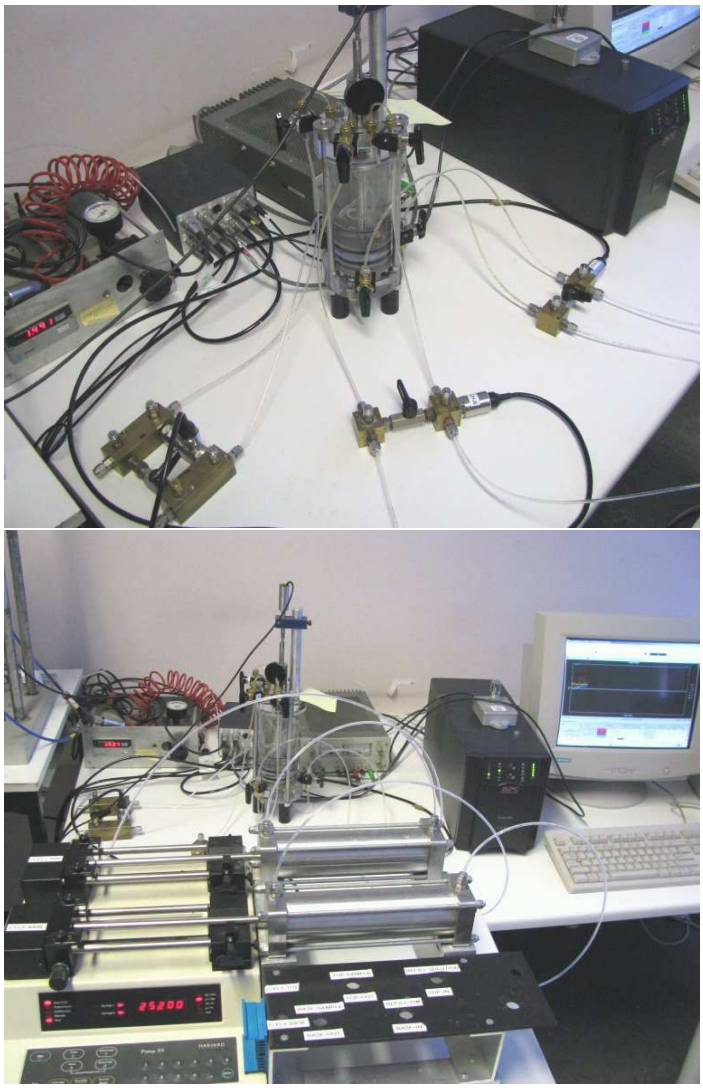

Figure 4.17: Chemico-osmotic setup: (above) rigid-wall consolidometer with pressure transducers and (below) the pumping system

and prevent liquid flux through the specimen (perfect flushing conditions).

The solutions are circulated at either ends of the specimen at the same flow rate to avoid water flow across the sample. Measured solute concentrations in the outlet solutions are used to evaluate the solute mass flux entering the soil from the higher concentration boundary ($C_{t,i} - C_{t,0}$ in Fig. 4.16) and exiting the soil into the lower concentration boundary ($C_{b,0} - C_{b,i}$), due to diffusion. The measured concentrations are used to compute the solute transport parameters (such as Diffusion, D^*, and Retardation Factor, R_d).

Measuring the chemico-osmotic efficiency, an error can occur neglecting the influence of solute diffusion across the sample during the test. This error can be reduced choosing an optimal circulation rate ($4.2xE^{-10}$ m^3/s in this test) sufficiently rapid to minimize changes in the boundary solute concentrations due to diffusion reducing the error in determining the chemico-osmotic efficiency, but sufficiently slow to allow a measurable accumulation of solute mass into the base to determine the transport parameters. In fact, the circulation rate should have an upper boundary limit to avoid dilution of the solute concentrations diffusing from the specimen in order to allow the measurement of the solute mass flux into the base required for determination of the transport parameters.

4.4.2 Chemico-osmotic efficiency determination

Under this perfect flushing conditions, the chemico osmotic efficiency coefficient, ω, is defined as follows (Staverman, 1952; Katchalsky and Curran, 1965):

$$\omega = \frac{\Delta P}{\Delta \pi}|_{q=0} \tag{4.2}$$

where ΔP is the measured pressure difference induced across the specimen as a result of prohibiting chemico-osmotic flux of solution, and $\Delta\pi$ is the theoretical chemico-osmotic pressure difference across an ideal membrane ($\omega = 1$) subjected to an applied difference in solute concentration (Olsen et al., 1990).

The value for ΔP in equation 4.2 is calculated based on the salt concentrations at the specimen boundaries in accordance with the van ′t Hoff expression as follows:

$$\Delta\pi = RT \sum_{N}^{j=1} (C_{b,j} - C_{t,j}) \tag{4.3}$$

where R is the universal gas constant [8.314 J $mol^{-1}K^{-1}$], T is the the absolute temperature [K], $C_{b,j}$ is the initial concentration of solute species j at the bottom (b) of the specimen [mol L^{-3}], $C_{t,j}$ is the initial concentration of solute species j at the top (t) of the specimen [mol L^{-3}], and N = the total number of solute species. For simple salt solutions, such as $CaCl_2$, equation 4.3 may be written more conveniently as:

$$\Delta\pi = \nu RT\Delta C \tag{4.4}$$

where ν is the number of ions per molecule of salt, and $\Delta C = C_{b,i} - C_{t,i}$ is the salt concentration gradient.

The induced pressure difference, ΔP, in equation 4.2 is measured using a differential pressure transducer that is connected to the top and the base of the specimen, as shown in Fig. 4.17.

4.4.3 Transport parameters determination: time-lag method

Diffusion coefficient, D*

The differences in solute (Cl^- and Ca^{2+}) concentrations between the top and bottom boundaries of the specimen also cause solute diffusion from the higher concentration boundary (top) to the lower concentration boundary (bottom), such that a steady-state solute flux through the bottom of the specimen is eventually established and maintained. This scenario is commonly referred to as the steady-state approach for diffusion testing (Shackelford, 1991).

In the steady-state approach, the measured concentrations for a given solute in the circulation outflow (i.e. from the base) are typically converted to cumulative mass per unit area, Q_t, using the following expression (Malusis et al., 2001):

$$Q_t = \frac{1}{A}\sum_{j=1}^{N}\Delta m_j = \frac{1}{A}\sum_{j=1}^{N} C_{b,o,j}\Delta V_j \tag{4.5}$$

where A is the cross-sectional area of the specimen, Δm_j is the incremental mass of the solute species collected (output from the base of the sample) over a time increment (Δt), $C_{b,o,j}$ is the concentration of the solute species in the incremental volume, ΔV_j, of circulation outflow from the base of the sample corresponding to the same Δt, and N is the number of incremental samples corresponding to the total elapsed time, t. The results are plotted in terms of Q_t vs. cumulative time, as shown schematically in Fig. 4.18. The curved portion of the plot represents transient diffusion, whereas the linear portion of the data, corresponding to a constant slope, $\Delta Q_t/\Delta t$, represents steady-state diffusion.

Figure 4.18 shows two characteristic times: the time to steady state, t_{ss}, and the time lag, t_L. The time lag is the time corresponding to the intersection of the extension of the steady-state slope to the x axis (Shackelford, 1991). The value of t_L can be used to determine the retardation factor, R_d, which reflects the adsorption behavior of the solute during transient diffusion, as shown further on in this paragraph (Crank, 1975; Shackelford, 1991).

The time to steady state, t_{ss}, is the time corresponding to the intersection of the initial curved portion of the example plot shown in Fig. 4.18, representing the

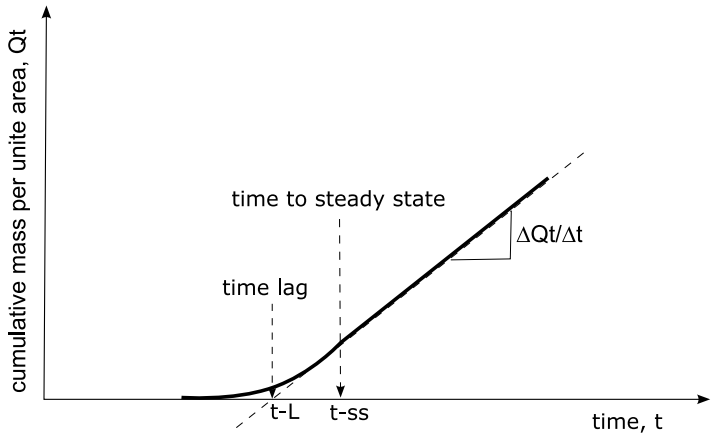

Figure 4.18: Schematic illustration of typical results obtained from combined chemico-osmotic/diffusion experiments: trends in cumulative solute mass through specimen due to diffusion

transient diffusion stage, and the linear portion of the example plot, representing steady-state diffusion.

The effective diffusion coefficient, D^*, of the given solute species is determined from the slope of the steady-state portion of the response, $\frac{\Delta Q_t}{\Delta t}$, in accordance with the following expression:

$$D^* = -\left(\frac{\Delta Q_t}{\Delta t}\right)\left(\frac{L}{n\Delta C}\right) \tag{4.6}$$

where n is the specimen porosity and L is the specimen thickness. The value of D^* determined according to equation 4.6 is a coupled effective diffusion coefficient that includes a coupling term associated with the prevention of solution flow in accordance with the principles of irreversible thermodynamics Malusis and Shackelford (2002a). In the limit, as the membrane efficiency of a clay approaches zero, the coupled effective diffusion coefficient given by equation 4.6 converges to the true effective diffusion coefficient represented by Ficks first law for diffusion in soil as defined by Shackelford and Daniel (1991).

Coupling effect during steady-state solute diffusion: effect of ω on D^*

For the special condition of no net liquid flux, the general expressions for the diffusive flux of the anion (Ja) and the cation (Jc) for a binary salt solution at steady state can be written in a form analogous to Ficks first law for diffusion in soil as follows (Malusis and Shackelford, 2002b):

$$J_a = -nD^*_\omega \frac{\Delta C_a}{\Delta x}; J_c = -nD^*_\omega \frac{\Delta C_c}{\Delta x} \tag{4.7}$$

where n is the specimen porosity, C is the molar concentration, x is the direction of transport, and D^*_ω is a coupled effective salt diffusion coefficient that can be expressed as follows (Groenevelt et al., 1980; Malusis and Shackelford, 2002b):

$$D^*_\omega = D^* - \frac{\omega^2(\overline{C}_a + \overline{C}_c)kRT}{n\rho_w g} \tag{4.8}$$

where D^*_ω is the true (uncoupled) effective salt diffusion coefficient given by the Nernst-Einstein expression (Robinson and Stokes, 1959) modified for the effect of tortuosity as described in Shackelford and Daniel (1991), $\overline{C}_a$ and $\overline{C}_c$ are the arithmetic mean molar concentrations across the membrane, k the hydraulic conductivity of the specimen, R the universal gas constant, T is the absolute temperature, ρ_w is the the density of water, and g is the acceleration due to gravity.

The second term in equation 4.8 represents the explicit diffusive coupling term that arises due to the soil membrane behavior. This explicit diffusive coupling term is called salt sieving, hyperfiltration, or streaming current.

It is possible to define the bulk diffusion coefficient of the considered porous medium as (Manassero and Dominijanni, 2003):

$$D^* = \Theta\tau D_0 \tag{4.9}$$

where D_0 is the diffusivity in free solution; $\Theta = n^*/n$ is the effective solute porosity ratio; n^* is the effective solute porosity that is, the part of the total porosity that allows both the solute and solvent migration; and τ is a tortuosity factor given by the squared ratio of the straight-line macroscopic distance between two points along a solute molecule migration path, to the actual length of the same solute molecule migration path (Porter et al., 1960).

In order to further clarify the definition of the effective solute porosity (n^*) it is useful to define its complementary porosity ($n-n^*$) as the part of total porosity that allows only the water (or solvent) to flow. When $n-n^* = 0$ (that is, $n = n^*$) the semi-permeable membrane effect does not exist. In the case where $n-n^* \neq 0$, the so-called selective filtration or hyper-filtration effect occurs. Moreover, when $n^* = 0$, the ideal semi-permeable membrane behavior takes place and therefore only the solvent flows but not the solute (Staverman, 1952).

It is possible to assume (Ferry, 1936):

$$\Theta = 1 - \omega \tag{4.10}$$

therefore the bulk diffusion coefficient D^* can be defined as follows (Manassero and Dominijanni, 2003):

$$D^* = (1-\omega)\tau D_0 \tag{4.11}$$

Retardation factor, R_d

The analytical solution for Q_t at steady state based on one-dimensional diffusion with a constant source concentration, $C_{t,i}$, in the top piston and a perfectly flushing boundary condition in the base pedestal (i.e., $C_{b,i}$ = 0) can be written as follows (Crank, 1975; Shackelford, 1991):

$$Q_t = \frac{nD^*C_{t,i}}{L}t - \frac{nR_dLC_{t,i}}{6} \tag{4.12}$$

where n is the specimen porosity, D^* is the effective diffusion coefficient, L is the specimen thickness, and R_d is the retardation factor. The retardation factor of the solute, R_d, is evaluated by determining the time tag, t_L, that represents the intercept of the regressed line through the steady-state data on the x axis in Fig. 4.18. The intercept, t_L, is related to R_d by setting Q_t = 0 in equation 4.12 and rearranging the resulting expression for R_d as follows (Shackelford, 1991):

$$R_d = \frac{6D^*t_L}{L^2} \tag{4.13}$$

For the second stage, the transport equation is solved for the case of non-zero initial concentrations at the top and at the bottom of the specimen ($C_{t,1}$ and $C_{b,1}$, final concentrations of the first stage). Assuming a linear initial concentration and an instantaneous increase of the boundary conditions, the analytical solution can be written as follows:

$$R_{d2} = \frac{6D^*t_L}{L^2} \cdot \left(\frac{C_{t,2} - C_{b,2}}{(C_{t,2} - C_{b,2}) - (C_{t,1} - C_{b,1})} \right) \tag{4.14}$$

where $C_{t,1}$ and $C_{b,1}$ are the steady-state concentrations at the top and base as a result of the first diffusion stage; and $C_{t,2}$ and $C_{b,2}$ are the steady-state concentrations at the top and base as a result of the second diffusion stage.

4.4.4 Specimen assembling for the chemico-osmotic test and removal of the soluble salts

Assembling clayey samples

The specimen for the chemico-osmotic test were prepared by spreading a thin layer of dry clay (0.45 g dry soil/cm^2) into the rigid-wall consolidometer described above.

The top plate of the consolidometer can be fixed to a specific height to avoid swelling of the sample during the test. This special feature of the consolidometer allows also to provide the desired sample porosity. Then the consolidometer is inundated with purified water and the soil specimen is allowed to saturate.

Alternatively, the clay is allowed to freely swell and then it is consolidated to the desired porosity. this consolidation is induced by pressurizing the chamber above the top piston.

Due to the considerable salt content of bentonite clays, the specimen is first permeated with purified water to remove soluble salts, improve the saturation and measure the reference hydraulic conductivity.

Assembling DPH GCL samples

A circular specimen of the DPH GCL 7.1 cm diameter was cut from a larger sample (10 cm diameter) previously permeated with deionized for about 1350 days to remove soluble salts. This 7.1 cm diameter specimen was then placed on the base inside the chemico-osmotic testing cell. The cylinder was filled with deionized water to submerge the specimen, and the top piston was lowered into the cylinder to compress the GCL to an initial porosity of n = 0.68.

After compression, the top piston was locked in place to prevent further volume expansion of the specimen during the test due to swelling of the bentonite.

Chemico-osmotic test

After permeation, the testing cell is connected to the cylinders actuators and the pumping system. Then purified water is first circulated for about 7 days at both ends of the specimen to establish a steady baseline differential pressure and remove residual salts from the porous plates.

The chemico-osmotic/diffusion phase of the experiment is then initiated by circulating the first source solution (ΔC_1=1 mM $CaCl_2$) in the top piston while continuing circulation of deionized water in the base, to induce a chemical gradient across the soil.

Multiple-stage chemico-osmotic tests were conducted in this study. These tests consisted of two individual stages for every sample in which differential pressures corresponding to two different source $CaCl_2$ solutions (i.e., ΔC_1=1mM and ΔC_2=5 mM) introduced sequentially through the top piston were measured across the same specimen. Each stage was conducted until steady state conditions were achieved (e.g. steady state differential pressure, Electrical Conductivity and Concentration breakthrough).

Permeation with 5 mM $CaCl_2$ was carried out at the end of the test in order to assess the impact of the electrolyte solution on the hydraulic conductivity of the clay after prehydration.

Figure 4.19: Electrical conductivity meter

4.5 Chemical analysis

4.5.1 Electrical conductivity and salinity

Electrical conductivity (EC) and salinity of water was measured with the conductivity meter inoLab Cond 720. The conductivity meter was connected to a standard conductivity cell TetraCon 325, which has a conductivity measuring range from 1 μS/cm to 2 S/cm (Fig. 4.19). The cell has an integrated temperature sensor and automatically compensates the measured value to an EC referred to a standard room temperature of 25° C.

4.5.2 Redox potential and pH

Redox potential (Eh) and pH values of water were measured with the Microprocessor pH Meters CG 840 (Fig.4.20). The microprocessor was connected to the redox-combination electrode BlueLine 31 Rx, manufactured by SCHOTT, and to the Pt 1000 temperature sensor, to measure the redox voltage from -1000 mV to 1700 mV.

The pH Combination Electrode Type No. N62 was used to measure the pH from 0.00 to 14.00. The measured values were automatic temperature compensated by the Microprocessor.

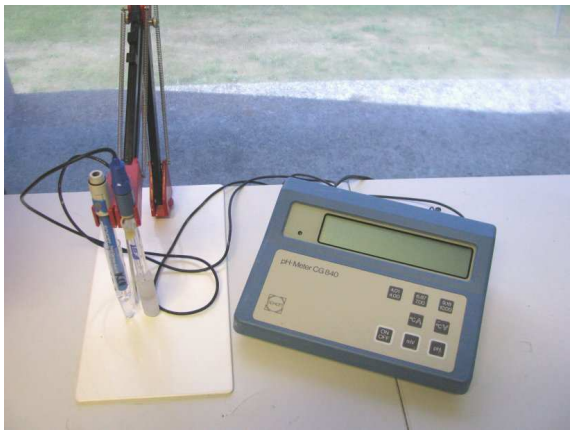

Figure 4.20: Redox potential and pH meter

4.5.3 Chemical analysis

Chemical analysis were performed at the Laboratory of Soil Science, UGent by Atomic Absorption Spectroscopy (AAS) for the cations and Ion Chromatography for the anions.

AAS utilizes the principle that elements in the gas phase absorb light at very specific wavelengths which gives the technique excellent specificity and detection limits. The sample may be an aqueous or organic solution, indeed it may even be solid provided it can be dissolved successfully. The liquid is drawn in to a flame where it is ionized in the gas phase. Light of a specific wavelength appropriate to the element being analyzed is shone through the flame, the absorption is proportional to the concentration of the element. Quantification is achieved by preparing standards of the element.

Ion chromatography performed with a DIONEX ICS-2000 is a process that allows the separation of ions and polar molecules based on their charge. It can be used for almost any kind of charged molecule including large proteins, small nucleotides and amino acids.

Some chemical analysis were also performed at the Laboratory of Geotechnics, UGent, with the Perkin Elmer Spectroquant Analysis System, which includes Photometer Spectroquant NOVA 60 and Spectroquant Test Kits (Fig. 4.21).

The principle of optical measuring of the filter photometer is through reference beam absorption measurement and simultaneous recording of all wavelengths. It is an instrument for measuring light intensity or optical properties of solutions or surfaces. To analyze the light, the photometer measures the light after it has passed through a filter or through a monochromator for determination at defined wavelengths or for analysis of the spectral distribution of the light.

Figure 4.21: Spectroquant NOVA 60 and Spectroquant Test Kits

5

Results and Discussions

5.1 Material Characterization: physical and chemical properties of modified clays

The quality of a bentonite for barrier systems is affected by several factors, including the mineralogical composition (e.g., montmorillonite content), the surface area (e.g., particle-size), the surface charge deficiency (e.g., amount and type of isomorphic substitution), and the composition of the exchange complex (e.g., amount of exchangeable Na^{+} relative to exchangeable Ca^{2+}) (Shackelford et al., 2000; Ashmawy et al., 2002). In general, the quality of the bentonite increases with increasing montmorillonite content, surface area, surface charge deficiency, and/or percentage of sodium Na^{+} on the exchange complex. The effect of these factors on the quality of the bentonite generally is indicated macroscopically by an increase in cation exchange capacity (CEC), an increase in plasticity, an increase in swell capacity in the presence of water, and a decrease in hydraulic conductivity (Lee and Shackelford, 2005). For these reasons a series of physico-chemical analysis were conducted on the clay treated with different polymer dosages, to study the potential benefits of polymers on the clay. Table 5.1 shows an overview of the characterization of the treated and untreated clays analyzed. The physical and chemical properties of the materials are discussed in the following paragraphs.

Property	clay	HYPER clay (2% Na-CMC)	MSB (25 % PC)	DPH GCL
Specific gravity [-]	2.66	2.53	2.15	2.56
Dry clay cont. [kg/m^2]	4.5	4.5	4.5	5.0-6.5
Swell index [ml/2g]	26	37	23	16 (turbid)
Liquid limit [%]	654.63	650.45	554	373.23
pH 1:50 extr.	9		7	8.21 [1:5]
EC 1:50 extr. [mS/cm]	0.15		0.19	3.58 [1:5]
CEC [meq/100g]	44.51	47.29	52.6	51.8
Exchangeable cations				
Na^+ [meq/100g]	26.30	34.15	41.0	77.71
Ca^{2+} [meq/100g]	5.58	11.43	16.9	12.43
Mg^{2+} [meq/100g]	7.89	6.16	6.8	8.57
K^+ [meq/100g]	0.17	0.25	0.8	2.39

Table 5.1: Material characterization

5.1.1 Specific gravity of polymer treated clays

The specific gravity of the clay analyzed decreased with increasing polymer dosage, as shown in Fig. 5.1. These results may depend not only on the lower specific gravity of the polymer alone (about 1.59), but also to a dispersed configuration of the treated clay (McRory and Ashmawy, 2005), corroborating the hypothesis that the presence of the polymer maintain the interlayer between clay platelets open, limiting aggregation and consequently inducing a dispersed structure. The decrease of specific gravity was observed also in organobentonites, which has been attributed to the intercalation of the large organic molecules used in this type of clays (Redding and Burns, 2000; Soule and Burns, 2001).

Assuming that the untreated clay studied here has a similar specific gravity of conventional clays, such as the base clay used to manufacture the DPH GCL, the specific gravity of the DPH GCL (Gs=2.56) was slightly lower than the specific gravity of the untreated clay (Gs=2.66) and comparable with the specific gravity of the HYPER clay (treated with 2% Na-CMC, Gs=2.53). This result is probably due to the presence of the polymers that, maintaining the interlayer between platelets open, induces a dispersed structure with a consequent decrease of the specific gravity.

The specific gravity of the Multiswellable Bentonite (MSB) was 2.15, significantly lower than the untreated clay (Gs = 2.66), which was consistent with the binding of PC molecules in the interlayer of montmorillonite.

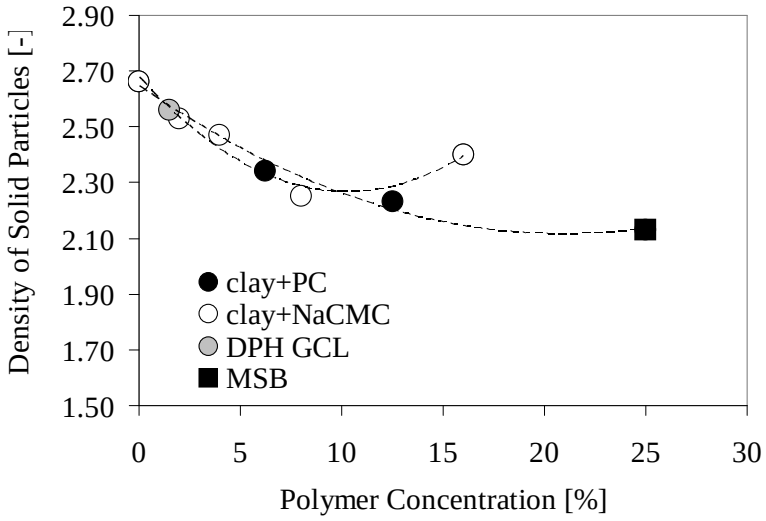

Figure 5.1: The density of solid particles decreased with increasing polymer dosage

5.1.2 X-Ray Diffraction of polymer treated clays

X-ray diffraction (XRD) analyses were performed on samples (oriented on glass slides) of clays treated with different dosages of Na-CMC. As explained in the Methods Section, the XRD patterns allow to determine the basal spacing (see Fig. 5.2) between unit layers, providing an indication of the interlayer thickness of the material.

HYPER clay

The XRD patterns of the clays treated with Na-CMC show the increase of the basal spacing, d, of the platelets with increasing polymer dosage (Fig. 5.3). Figure 5.3b shows that the basal spacing, d, increased with increasing polymer dosage, indicating a gradual increase of the basal spacing with increasing polymer dosage.

The clay modified with 2% of polymer (HYPER clay) was compared with the clay modified with 16% dosage in Fig. 5.4, in order to analyze the impact of the polymer dosage. This figure shows that the characteristic peak of montmorillonite broadened, shifting to the left (that corresponds to higher basal spacings) indicating that the polymer has intercalated in the interlayer region between platelets and that the interplatelets spacing increases with increasing polymer dosage. Figure 5.6 shows schematically the intercalation of the polymer in the interlayer region of the clay platelets.

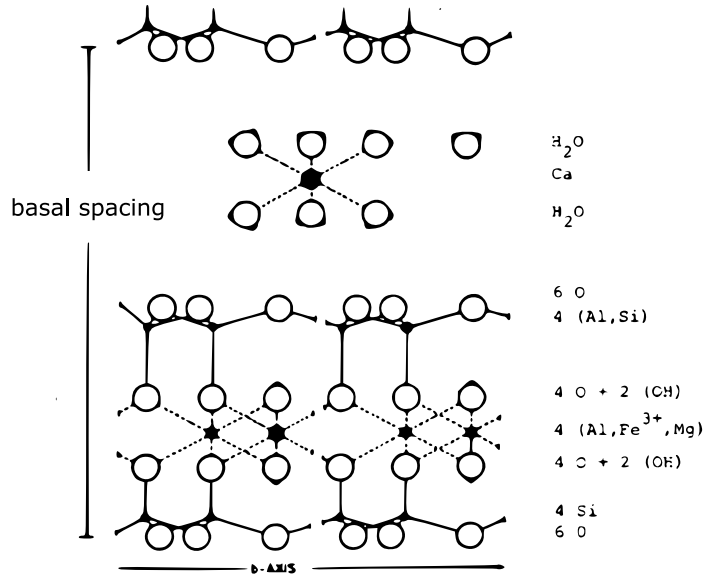

Figure 5.2: Schematic projection of a montmorillonite with indicated the basal spacing, from Van Ranst (2006)

These results suggest the permanence of the polymer in the interlayer region after addition. The presence of this polymer in the interlayer region was also confirmed by additional physical and chemical properties of the materials, as described in the following paragraphs.

DPH GCL and MSB

XRD analysis was also performed on DPH GCL and on the MSB. Assuming that the untreated clay studied here is similar to the base clay used to manufacture the DPH GCL, the spectrum of the DPH GCL was compared to that of the untreated clay. DPH GCL shows a toothed shape broadened and shifted to the left respect to the untreated clay, indicating an increase in the basal spacing as well (Fig. 5.5), which is consistent with the intercalation of polymers into the interlayer.

The X-ray diffraction patterns on the MSB (Fig. 5.7) also show the shift of the basal spacing d of the MSB (d =1.78 nm) compared to the untreated clay (d = 1.23 nm), reflecting the presence of PC molecules coordinated with exchangeable cations in the interlayer between platelets.

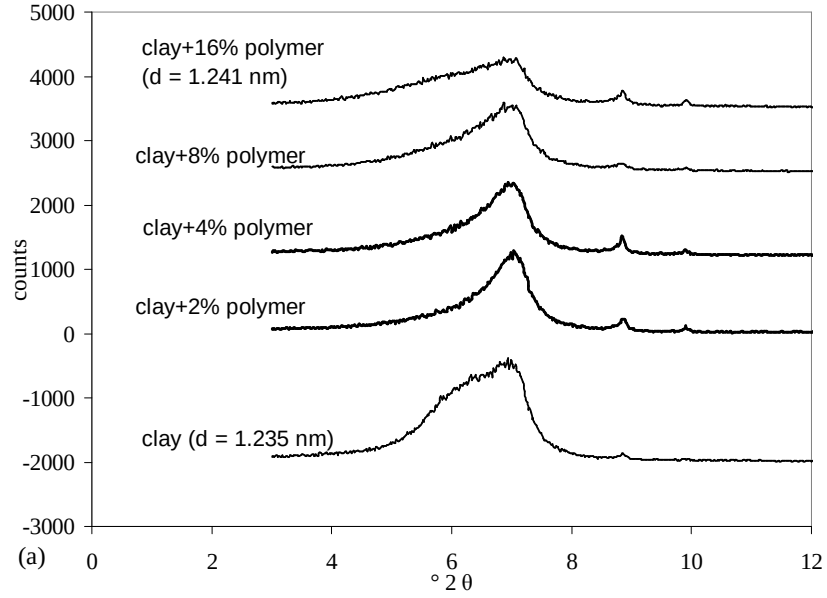

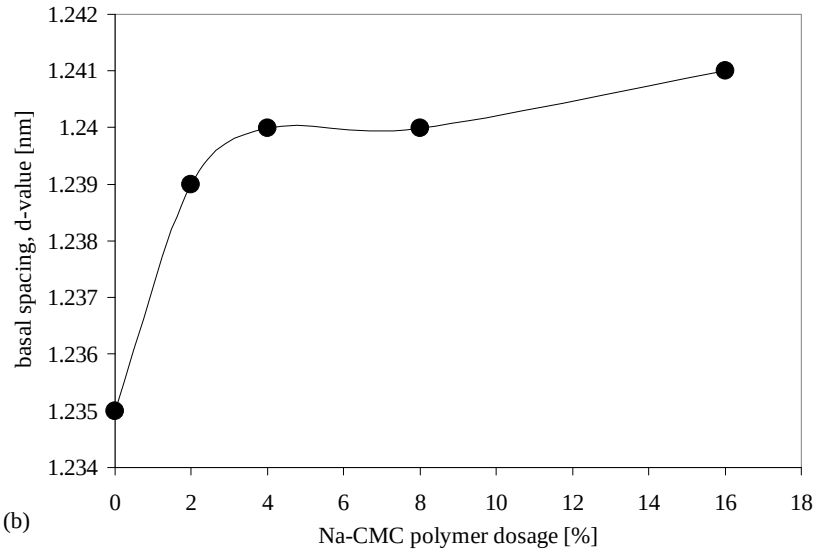

Figure 5.3: (a) Shift of the basal spacing, d, with increasing polymer dosage. (b) Increase of the basal spacing with increasing polymer dosage

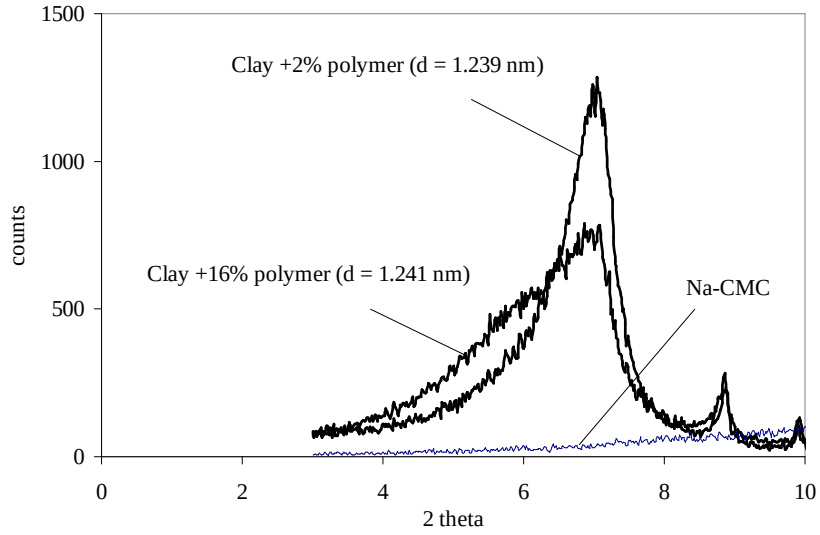

Figure 5.4: Shift of the basal spacing, d, with increasing polymer dosage

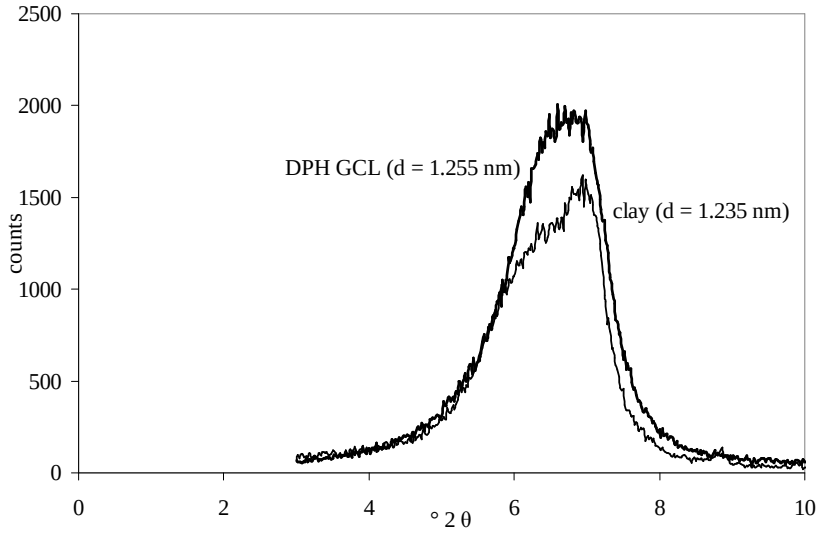

Figure 5.5: Shift of the basal spacing, d, of the DPH GCL compared to untreated clay

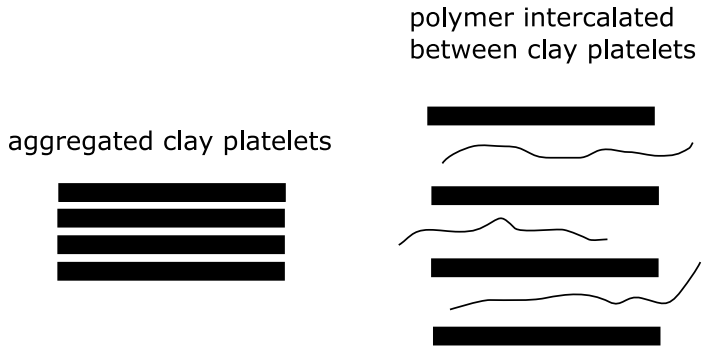

Figure 5.6: Schematic representation of polymers intercalated between clay platelets

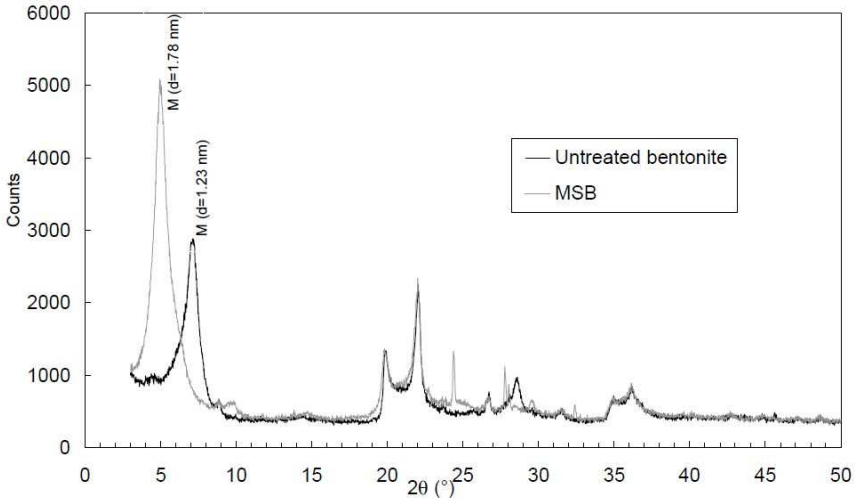

Figure 5.7: Shift of the d basal spacing of the MSB (d =1.78 nm) compared to untreated clay (d = 1.23 nm), (Mazzieri et al., 2010)

5.1.3 Cation Exchange Capacity and exchangeable ions of polymer treated clays

Generally, an increase in cation exchange capacity (CEC) indicates an increase of bentonite quality (Lee and Shackelford, 2005). Kharaka and Berry (1973) noted that the chemico-osmotic efficiency increases with an increase in the exchange capacity of a material. Therefore, in view of potential benefits of the polymer on the quality of the bentonite and on its chemico-osmotic efficiency, it was interesting to analyze the impact of polymer treatment on the CEC.

On the other hand, a decrease of CEC with increasing polymer dosage could indicate that the polymer protects the clay from cation exchange by shielding the clay or by decreasing the exchange sites activity.

HYPER clay

The measured CEC for the untreated bentonite clay tested in this study was around 44.51 meq/100 g. Thus, a higher quality of the polymer treated clay should result in a higher CEC compared to the untreated clay. In contrast, the CEC remained almost constant with increasing polymer dosage (Fig. 5.8). On the other hand, as mentioned above, the quality of a bentonite is indeed affected by CEC but only indirectly. In fact, the parameter to look at is the composition of the exchange complex rather than CEC (e.g., amount of exchangeable Na^+ relative to exchangeable Ca^{2+}). Figure 5.8 shows an increase of exchangeable Na^+ with increasing polymer dosage, indicating a potential enhancement of the quality of the clay by adding the polymer. The increase of the exchangeable Na^+ could be related to the sodium-polymer (Na-CMC) used.

DPH GCL and MSB

The Cation Exchange Capacity and the exchangeable cations of the bentonite obtained from the DPH GCL are reported in Table 5.1. The exchangeable Na^+ alone was higher than CEC. The reason for this discrepancy may be an excess of Na^+ coming from the polymer Na-CMC, as also observed for the HYPER clay treated with 2% Na-CMC (Fig. 5.8). The clay of the DPH GCL is in fact also treated with sodium-polymers, such as CMC and sodium polyacrylate, as indicated in its patent Flynn and Carter (1998).

The exchangeable cations of MSB are also shown in in Table 5.1. Sodium was the dominant cation, with a significant calcium content, in analogy with the untreated clay.

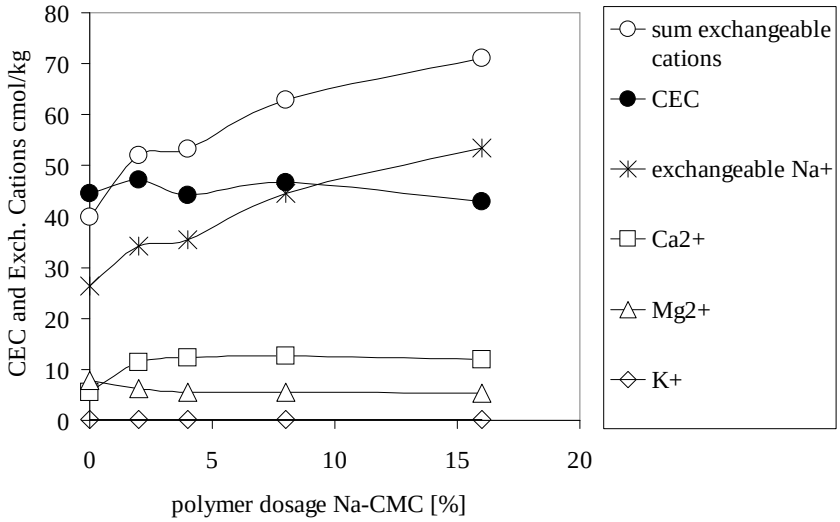

Figure 5.8: Cation Exchange Capacity and Exchangeable Cations vs. polymer dosage

5.1.4 Viscosity and zeta potential of polymer treated clays

To analyze the impact of polymer addition on the viscosity and zeta potential of the clays, 10% (v/v) slurries were analyzed. Two methods of preparation were used: the dry method and the wet method (see the Methods Section). The dry method simulates the method of preparation of the HYPER clay, whereas the wet method simulates the method of preparation of the DPH GCL.

Viscosity

Figure 5.9 shows the viscosity of the bentonite suspensions plotted as a function of increasing polymer dosage. When the polymeric solutions were mixed with bentonite, a higher mechanical resistance against flow was observed. This mechanical resistance against flow was reflected in increase of viscosity with increasing polymer dosage (Fig. 5.9).

A possible explanation of this behavior can be attributed to the interaction between negative charged clay platelets and anionic polymers. Figure 5.10 represents schematically the polymers coating and bridging the clay particles. This structure could have contributed to increase the viscosity with increasing polymer addition.

Zeta potential

Zeta potential (ZP) is the electric potential in the interface double layer at the location of the slipping plane versus a point in the bulk fluid away from the interface, as shown schematically in Fig. 5.11.

The zeta potential was measured for the untreated clay by varying pH of the pore fluid between 3 and 11, as shown in Fig. 5.12 (a). As expected for bentonites, the clay displayed a negative zeta potential for any pH value analyzed reflecting the prevailing negative charge of the bentonite clay surface.

The ZP was also measured for the treated clays by varying the polymer dosage from 0% to 16%. Figure 5.12 (b) shows the ZP values decreased in absolute value with increasing polymer dosage up to 8% followed by a plateau. This unexpected decreasing trend in ZP (and the corresponding increase of viscosity) was also observed by Yalcin et al. (2002) on bentonite clays mixed with anionic surfactants.

The zeta potential indicates the degree of repulsion between adjacent, similarly charged particles in a dispersion (Morris and Zbik, 2009). Therefore, the decrease of zeta potential with increasing polymer dosage suggests that particles tend to aggregate. On the other hand, XRD results indicated an increase of the basal spacing between platelets with increasing polymer dosage. The combination of these two observations may support the hypothesis that the polymers coat and bridge the particles yet maintaining the interlayer between platelets open, as illustrated in Fig. 5.10.

Besides, the polymer intercalation in the interlayer probably increases the amount of immobile water attached to the clay surface, due to the high water absorption capacity of this polymer. The hydraulic conductivity of clays with a large amount of immobile water molecules typically can be very low.

The large net negative charge of montmorillonite combined with the negative charge of the anionic polymers could result in adsorption of a large number of hydrated cations as well as water molecules during hydration. These adsorbed water molecules and cations are essentially immobile. As a result, the portion of the pore space occupied by mobile water is relatively small, and the pathways formed by the bulk water have irregular shapes. Consequently, the hydraulic conductivity of anionic-polymer treated clays with a large amount of immobile water molecules could potentially be very low. Also the diffusion transport in polymer treated clays should be slower because of the reduced cross-sectional area of flow and the more tortuous pathways experienced by solutes diffusing through soil. Besides, cations may be subjected to additional adsorption reactions that will reduce the solute rate of transport.

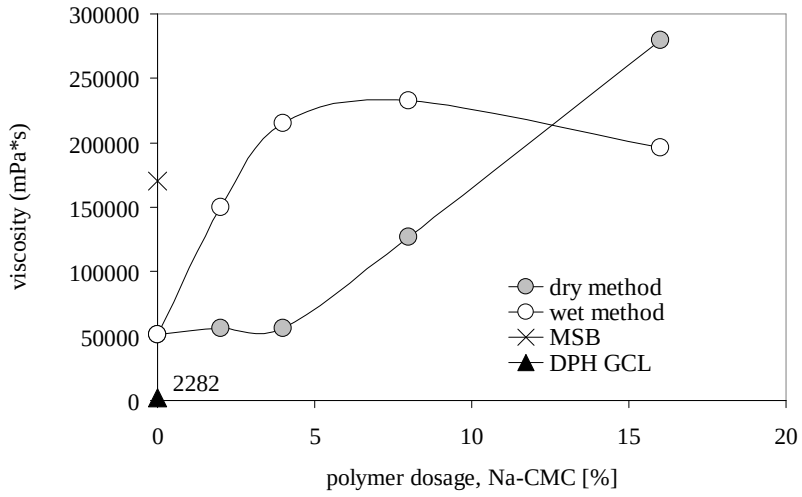

Figure 5.9: Viscosity of the slurries vs. polymer dosage

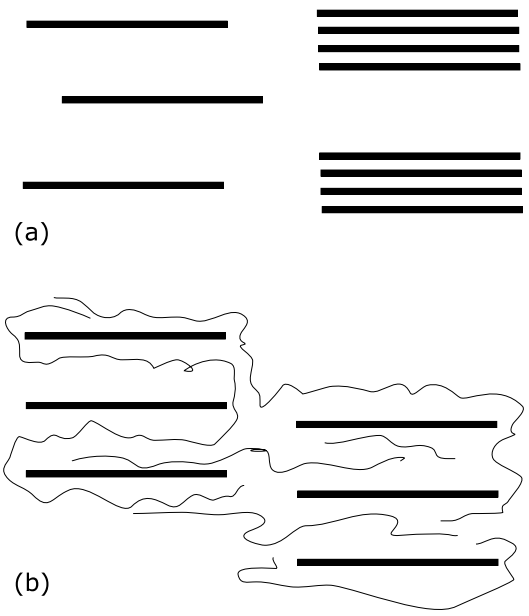

Figure 5.10: Schematic representation of (a) untreated clay (at the left dispersed structure, at the right aggregated structure) and (b) polymer treated clay structures (the polymer maintains the interlayer open). The polymers coating and bridging the clay particles increase the viscosity of the slurries

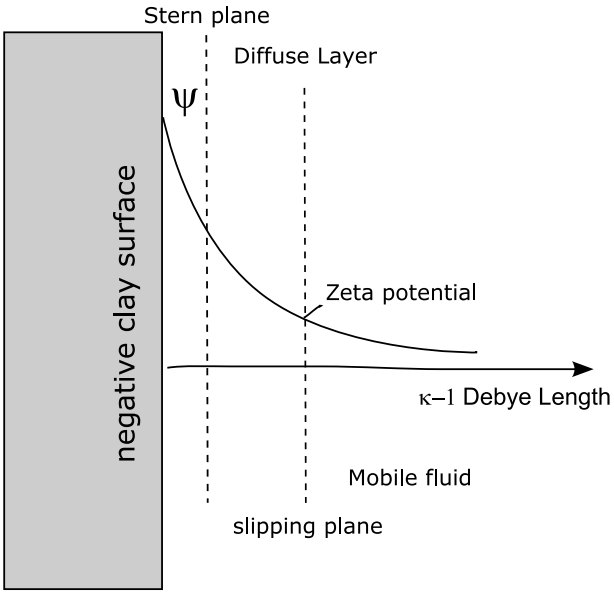

Figure 5.11: Schematic representation of the zeta potential

5.1.5 Atterberg Limits of polymer treated clays

The decrease of liquid limit of a clay corresponds to an increase of its hydraulic conductivity (Lee et al., 2005). Therefore the liquid limit can be used as an index property to evaluate the potential hydraulic performance of a clay. The liquid limit can decrease with increasing $CaCl_2$ concentration, due to the increasing predominance of calcium on the exchange complex of the bentonite particles resulting from cation exchange with sodium that causes stronger net interparticle attractive forces (Lambe and Withman, 1969). The liquid limit decreases with decreasing double layer thickness.

Effect of polymer dosage on the Atterberg limits

Figure 5.13 shows that the liquid limit of the untreated clay increased with increasing Na-CMC polymer dosage. This demonstrates that the polymer addition may improve the water adsorption capacity of the untreated clay, indicating a possible improved barrier performance. This result is in good agreement with results obtained by Qiu and Yu (2007). They modified a bentonite with Na-CMC and demonstrated that treating the clay with Na-CMC increased its water retention ability.

The liquid limit and plasticity index (Fig. 5.13 and 5.14) increased with increasing polymer dosage up to 8%. With further dosage increase up to 16% the

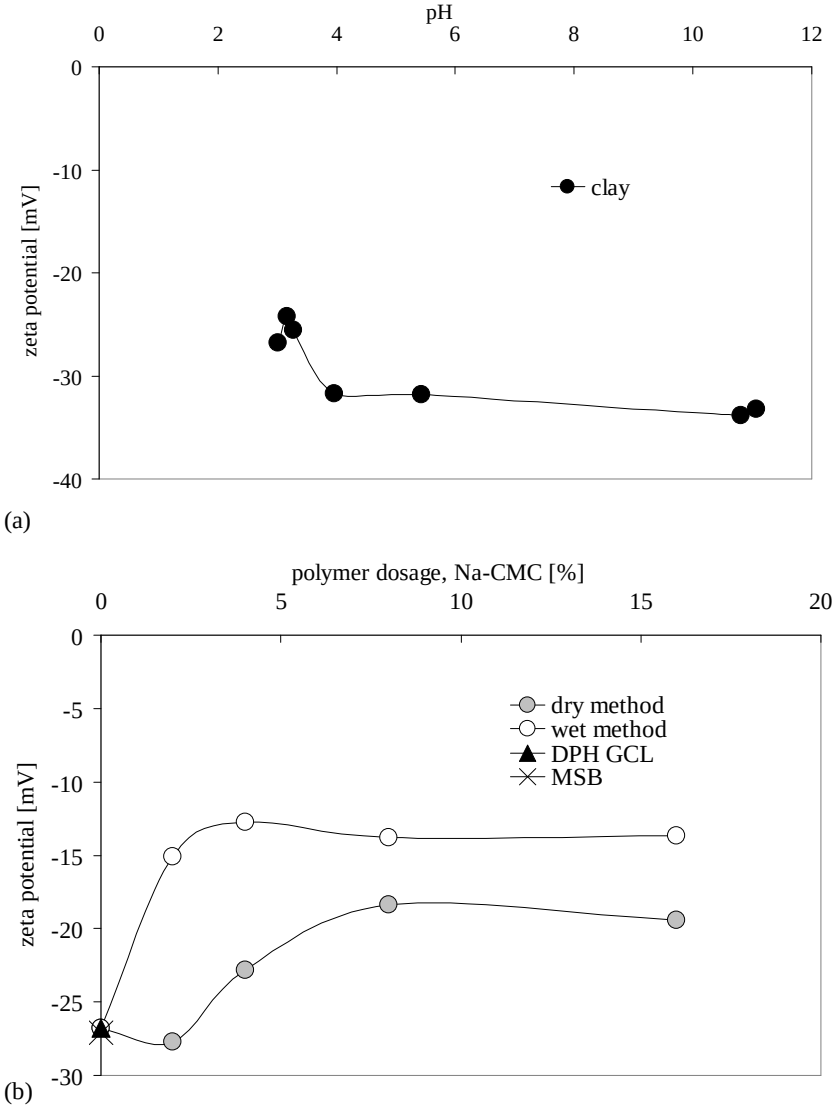

Figure 5.12: (a) Zeta potential vs pH and (b) zeta potential of the slurries vs. polymer dosage

liquid limit remained unchanged, indicating that 8% can be considered as an optimum polymer dosage. This optimum value probably represents the maximum polymer adsorption ability of the clay. This limiting value was observed also for the swell pressure tests, further on in this chapter.

Effect of ionic strength and $CaCl_2$ concentration on the liquid limit

As expected, the liquid limit of the untreated clay saturated with $CaCl_2$ solutions decreased with increasing the ionic strength (see Fig. 5.15 (a)).

It should be stressed out that Fig. 5.13 and 5.15 show that the beneficial effect of the Na-CMC polymer treatment was more pronounced for high concentrated solutions than for diluted solutions. The effect of the polymer for diluted solutions was negligible probably because for diluted solutions the interlayer thickness is already sufficiently open. On the other hand, for concentrated solutions the interlayer thickness is compressed with consequent aggregation between platelets. The effect of the polymer in diluted and concentrated solutions is schematically represented in Fig. 5.16. As shown in this figure, the clay platelets are distant in deionized water or diluted solutions and the interlayer region is sufficiently open in either case, with or without the intercalated polymer. On the other hand, in concentrated solutions the untreated clay particles aggregate, whereas the polymer treated clays maintain the interlayer open.

Liquid limit of DPH GCL and MSB

The liquid limit of MSB and DPH GCL, as shown in Fig. 5.15, increased slightly with increasing $CaCl_2$ concentration up to 5 mM. Beyond that concentration the liquid limit decreased with increasing the ionic strength of the solution, as it occurs for untreated clays. The liquid limit of the MSB was lower than the liquid limit of the clay, except in sea water where it was slightly higher (184.25 for MSB vs. 168.62 for the clay), as shown in Fig. 5.15b.

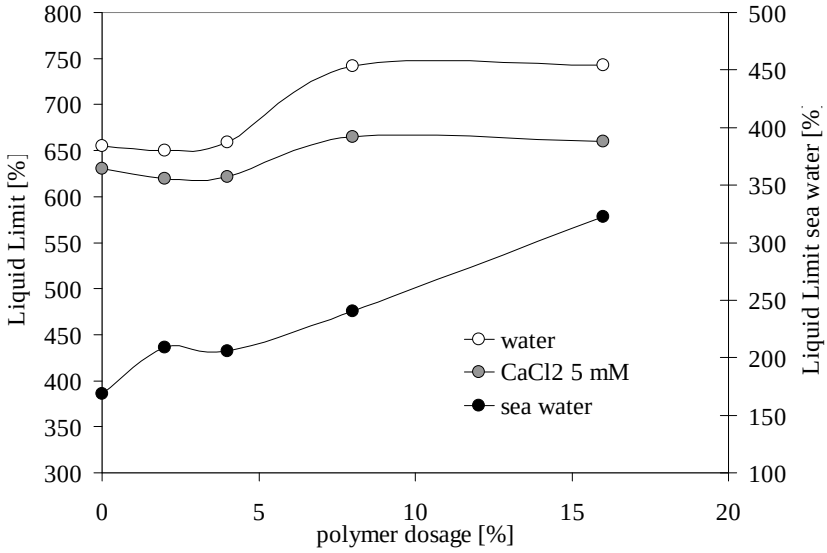

Figure 5.13: Liquid limit increase with increasing Na-CMC polymer dosage.

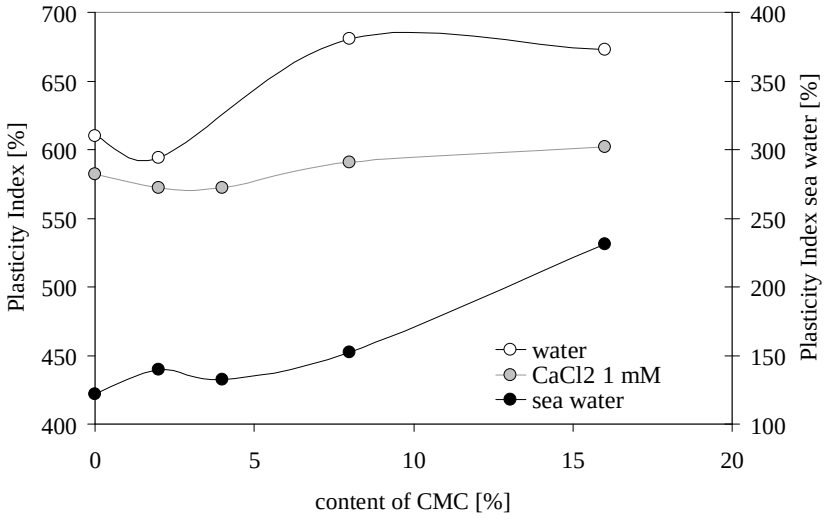

Figure 5.14: Plasticity index increase with increasing polymer dosage

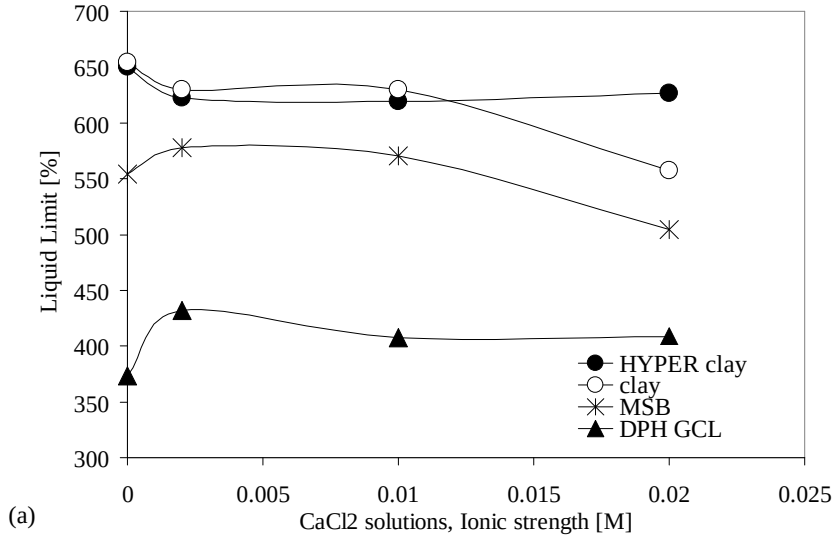

(a)

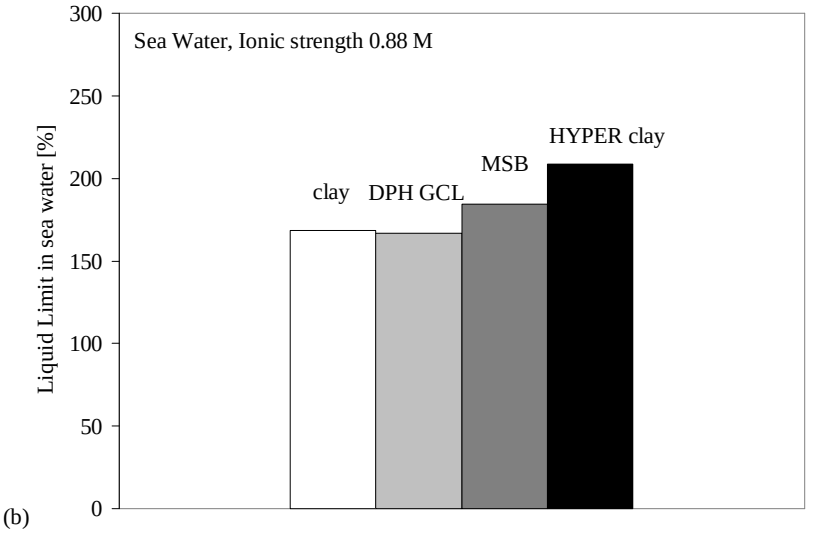

(b)

Figure 5.15: (a) Liquid limit decrease with increasing Ionic Strength for $CaCl_2$ solutions and (b) liquid limit of the specimens analyzed in sea water (high ionic strength)

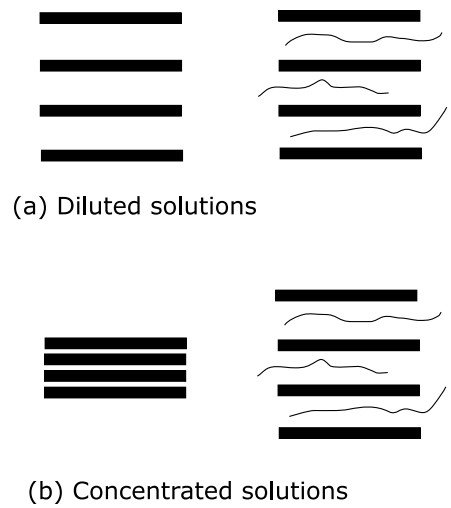

Figure 5.16: (a) The effect of the polymer on the interlayer thickness of the clay particles is negligible in diluted solutions. (b) The beneficial effect of polymer intercalation between clay platelets is more pronounced for concentrated solutions

5.2 Swelling improvement of modified clays

The waterproof mechanism of a Geosynthetic Clay Liner is greatly dependent on the swelling behavior of the bentonites contained in it. The bentonite particles become a water-obstructing layer after they absorb water and swell. When sufficiently confined, hydrated GCLs decrease the mobile water free to flow in the interlayer region, with a consequent decrease in hydraulic conductivity.

Due to the high swelling capacity of Na-bentonite, its hydraulic performance in water is very high. However, strong electrolyte solutions, causing compression of the diffuse double layer, can drastically reduce the swelling ability of bentonites.

Swell index and swell pressure tests were conducted with various electrolyte solutions to investigate the impact of polymer treatment on the swelling ability of clays.

5.2.1 Swell index test

Swell index tests were performed with deionised water, sea water, KCl and $CaCl_2$ solutions with concentrations varying from 0.001 M to 1 M, to investigate the impact of different valences and concentrations on the swelling ability of treated and untreated clays.

Untreated clay and HYPER clay

The swell index (SI) to deionized water of the untreated clay was SI = 26 ml/2g. After treating the clay with Na-CMC, an increased swell index was observed. In fact, the swell index were SI = 37 ml/2g for the HYPER clay (treated with 2% Na-CMC) and SI = 55 ml/2g for the clay treated with 4% Na-CMC. This result suggests that the polymer improves the swelling capacity of the untreated clay.

To corroborate this hypothesis, swell index tests were conducted in electrolyte solutions as well. Figure 5.17 show the swell index of the untreated clay (white columns), the clay treated with 2% Na-CMC (grey) and the clay treated with 4% Na-CMC (black). The figure shows that the addition of the Na-CMC polymer improved the swelling ability of the clay also in presence of electrolyte solutions.

An increase of the swell index was observed in KCl solutions up to a concentration of 0.1 M (Fig. 5.17(a)) and in $CaCl_2$ solutions up to a concentration of 0.1 M (Fig. 5.17(b)). For higher concentrations, the swelling ability remained unaltered or decreased slightly.

Multiswellable Bentonite (MSB)

Results of free swell tests conducted on MSB and its untreated bentonite are shown in Fig. 5.18 (Onikata et al., 1996; Shackelford et al., 2000) and Fig. 5.19 (Katsumi et al., 2008).

The swell tests shown in Fig. 5.18 were conducted by Onikata et al. (1996) with a variety of solutions containing primarily inorganic compounds covering a broad range of electrical conductivity (EC). For all the solutions, the MSB exhibited comparable or greater swell than the natural bentonite, even with aggressive liquids, such as sea water and sulfuric acid.

Figure 5.19 plots the relationship between the free swell of a natural bentonite and the ionic strength of the chemical solutions (Katsumi et al., 2008). The open dots show the swell index of the untreated clay (NB), and the hatched dots show the swell index of MSB. The figure shows that MSB had a greater swelling capacity than the untreated clay (NB) for Ionic Strengths up to 0.5 M.

Dense PreHydrated GCL (DPH GCL)

Swell index tests were performed on the bentonite contained in the DPH GCL with KCl and $CaCl_2$ solutions with concentrations varying from 0.001 M to 1 M. Given that the untreated clay used by the DPH GCL manufacturers was not available, we compare the results to our untreated Na-bentonite. The swell index of the DPH GCL clay was higher that the swell index of the untreated clay for concentrations varying between 0.01 M up to 0.1 M. For higher concentration, the swelling ability were comparable (Fig. 5.20). For concentrations lower that 0.01 M an unusual behavior was observed, as explained in detail below.

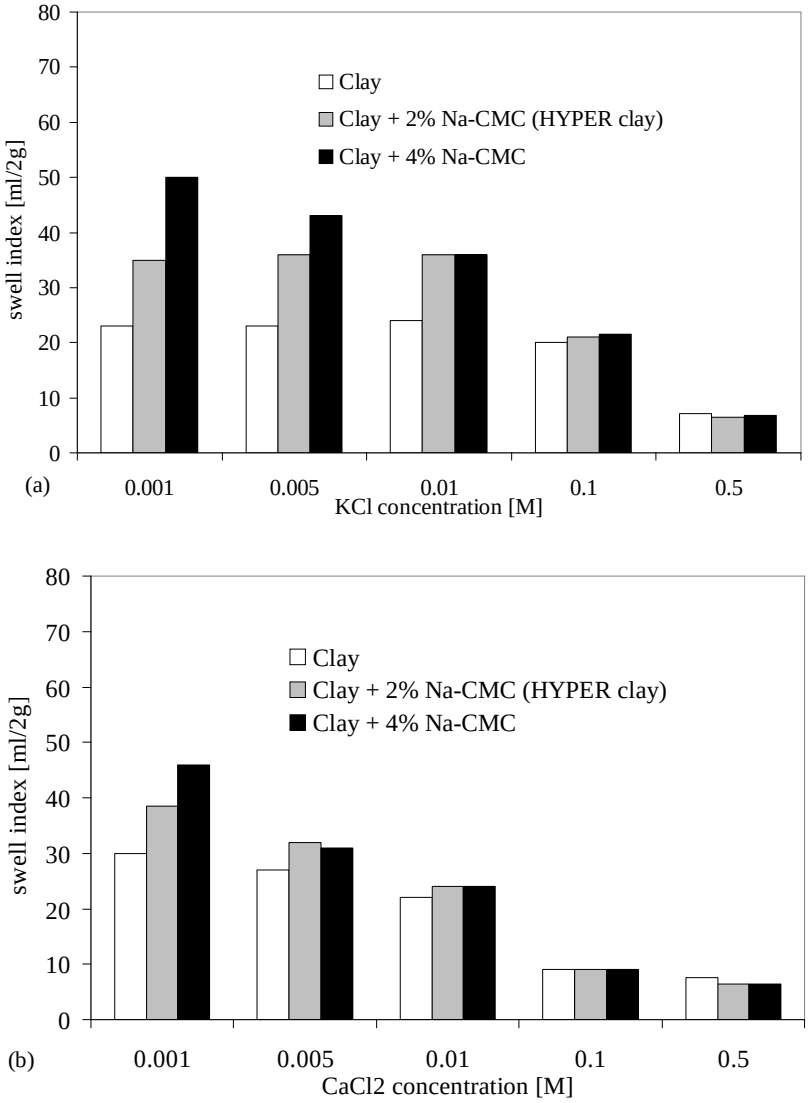

Figure 5.17: The addition of Na-CMC to the clay improved its swelling ability in (a) KCl solutions and (b) $CaCl_2$ solutions

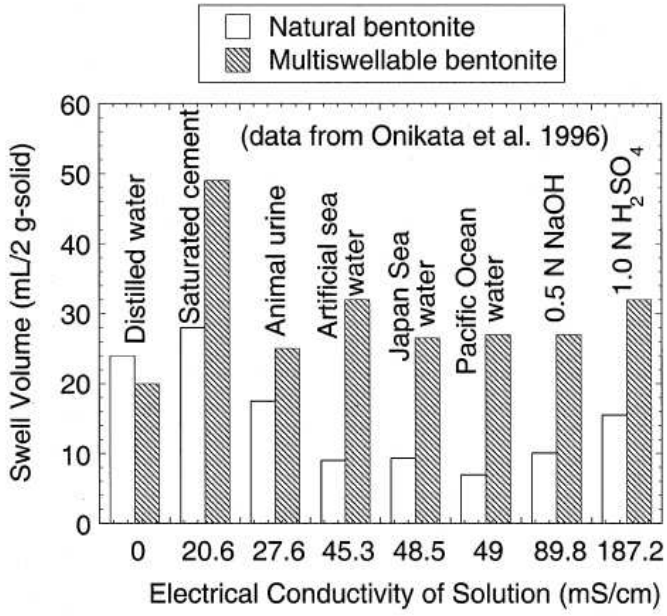

Figure 5.18: Swell test results for Multiswellable Bentonite using various liquids (Shackelford et al., 2000)

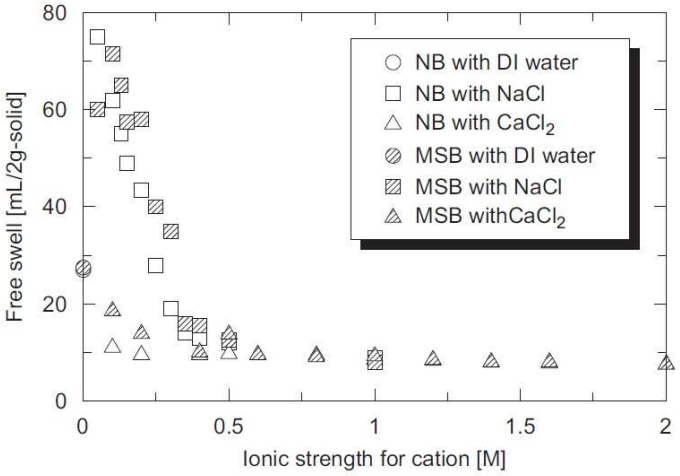

Figure 5.19: Swell index of untreated clay (NB) and MSB in deionized water (DI), NaCl and $CaCl_2$ solutions (Katsumi et al., 2008)

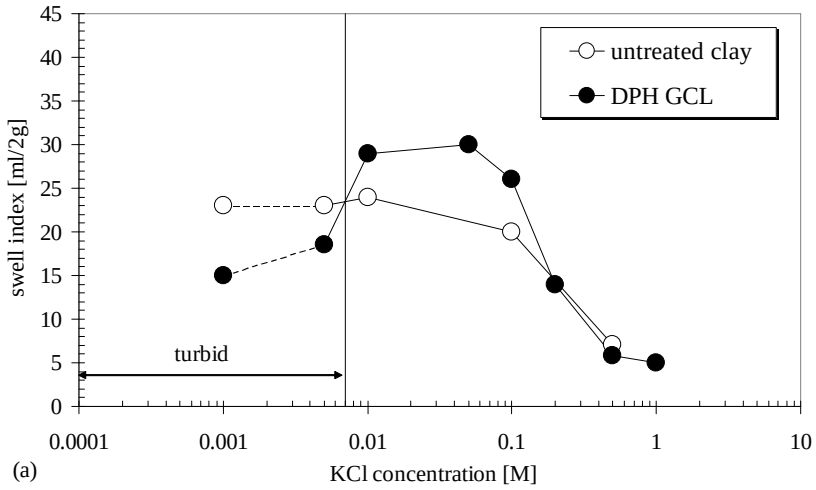

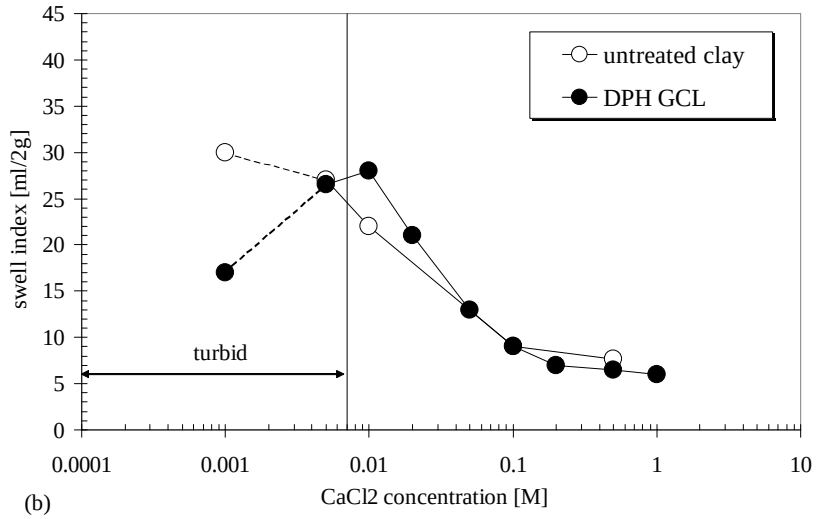

Figure 5.20: Swell index of untreated clay and DPH GCL in (a) KCl solutions and (b) $CaCl_2$ solutions

Overall the swell index decreased with increasing ionic strength of the solution which is consistent with Double Layer Theory. However, the DPH GCL showed an unusual swelling behavior for concentrations lower than 0.01 M. Figure 5.21(a) shows that for concentrations lower than 0.01 M, the trend turned out to be the opposite. The swell index was observed to decrease with decreasing concentrations lower than C=0.01 M. This behavior was probably due to the dispersant properties of the polymers contained in the treated DPH GCL bentonite. The observed surnatant of these solutions were in fact turbid, increasing turbidity with decreasing concentration and valence, as shown in Fig. 5.22. Turbidity of the surnatant implies that part of bentonite remains suspended and does not contribute to the final swelling volume.

Figure 5.21(b) shows the trend of swell index vs. valence on the DPH GCL bentonite. This trend, for concentrations higher than 0.01 M, is consistent with previous findings obtained on untreated bentonites (Jo et al., 2001) . This trend shows a decrease of the swell index with increasing valence. On the other hand, for concentrations lower than 0.01 M the slope of the trend is less evident until it turns opposite due to the dispersant properties of the polymers, as explained above.

These dispersant properties of the polymers, increasing the repulsive forces between platelets, maintain the bentonite in suspension causing a false measurement of the swell index volume. In addition, in presence of $CaCl_2$ solutions the fabric of the clay lead to a card house structure (Fig. 5.22(b), $CaCl_2$ concentration 0.01 M) causing unexpected high swell index results. The large flocs may not remold completely when settled causing also false indication of the swelling ability of clays.

To overcome these limitations and to represent the actual swelling performance of polymer treated bentonites, one-dimensional swell pressure tests were also conducted. This test is proposed as a more suitable method, alternative to the swell index tests, to study the swelling ability of bentonites.

5.2.2 Swell Pressure test

When hydrated, the bentonite clay adsorbs a large amount of water molecules and ions. A swell stress is raised by this water entering the pores among montmorillonite particles and the interstitial layers in individual montmorillonite crystals, leading to an increase in volume and manifested as a stress on the surrounding materials.

Untreated clay

Swell pressure tests were performed on the untreated clay with KCl and $CaCl_2$ solutions with concentrations varying between 0.0001 M and 0.1 M.

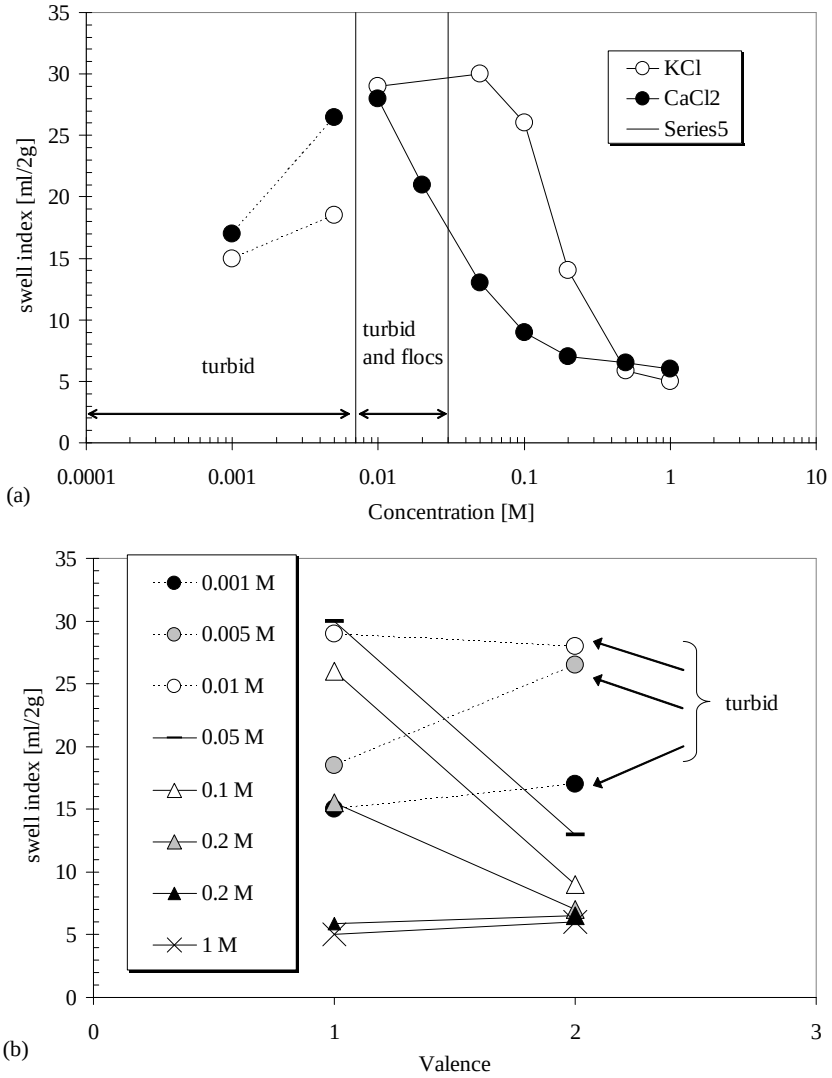

Figure 5.21: Effect of (a) KCl and $CaCl_2$ concentration and (b) valence on the swelling of the bentonite from the DPH GCL

(a)

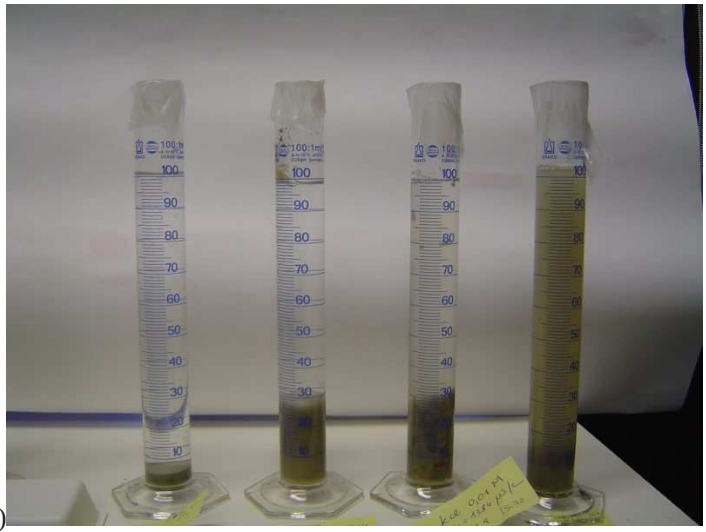

(b)

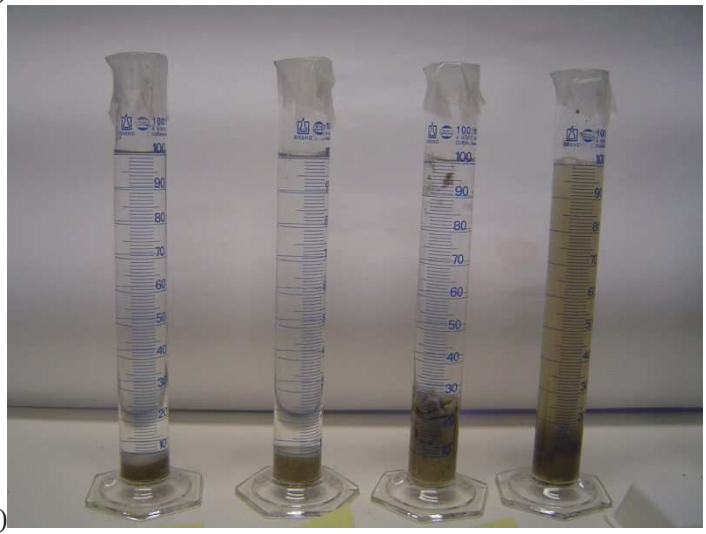

Figure 5.22: Swell index on the DPH GCL bentonite in (a) KCl solutions (1 M; 0.1 M; 0.01 M; 0.001 M) and (b) in $CaCl_2$ solutions (1 M; 0.1 M; 0.01 M; 0.001 M). Turbidity was observed for low concentrated solutions due to the dispersant properties of the polymers

Figure 5.23(b) plots the swell pressure of the untreated clay vs. the ionic strength of the chemical solutions. The ionic strength of a solution is a measure of the concentration of ions in that solution. It represents the sum $\frac{1}{2}\sum_{i=1}^{N} c_i z_i$, where C_i and z_i are the concentration and the valence of the ith ion, respectively. The ionic strength was calculated here using only the cations contained in the chemical solution because the thickness of the double layer, which relates to swelling capacity and barrier performance, is dependent on cationic concentrations according to Stern−Gouy theory (Katsumi et al., 2008).

Figure 5.23(b) also compares the swell pressure with the swell index results. The swell index trend unexpectedly changed for concentrations lower than 0.01 M (5.23(a)). This behavior was explained by the high repulsive forces of the clay particles in low concentrated solutions. These forces were in fact able to maintain the clay in suspension causing a false measurement of the swell index. However, these results do not indicate a loss of swelling ability. In addition, false measurements may also be due to the card-house structure of flocs observed in $CaCl_2$ solutions. In this case, an overestimation of the swelling ability may occur.

Conversely, the swelling pressure results 5.23(b) are not affected by the limits encoutered in the swell index tests. The swell pressure in fact decreases monotonically with increasing concentration and valence of the ions consistently with the Double Layer Theory.

Figure 5.23(b) shows that the swelling pressure remains almost constant for ionic strength lower than 0.01 M. A possible explanation may be the negligible impact of these solutions on the double layer thickness and on the hydration forces between platelets.

HYPER clay

Swell pressure tests were performed on the natural clay treated with various dosages of Na-CMC polymer.

Figure 5.24 shows the increase of the swelling pressure with increasing polymer (Na-CMC) dosage up to 8% Na-CMC in 5 mM $CaCl_2$ solutions. With further dosage increase up to 16% the swelling pressure decreased slighlty, indicating 8% as a possible optimum polymer dosage. This value probably represents the maximum polymer adsorption ability of the clay. This limiting value was observed also out of the impact of polymer dosage on the plasticity of the clay (Section 5.1).

Swell pressure tests were performed also on the HYPER clay (clay treatd with 2% Na-CMC) with KCl and $CaCl_2$ solutions with concentrations varying between 0.0001 M and 0.1 M.

Figure 5.25(b) plots the swell pressure of the HYPER clay vs. the ionic strength of the chemical solutions. The figure shows that, at a given concentration and valence, the swell pressure of the HYPER clay always exceeded the swell pressure of the untreated clay. The polymer, maintaining the interlayer open, probably in-

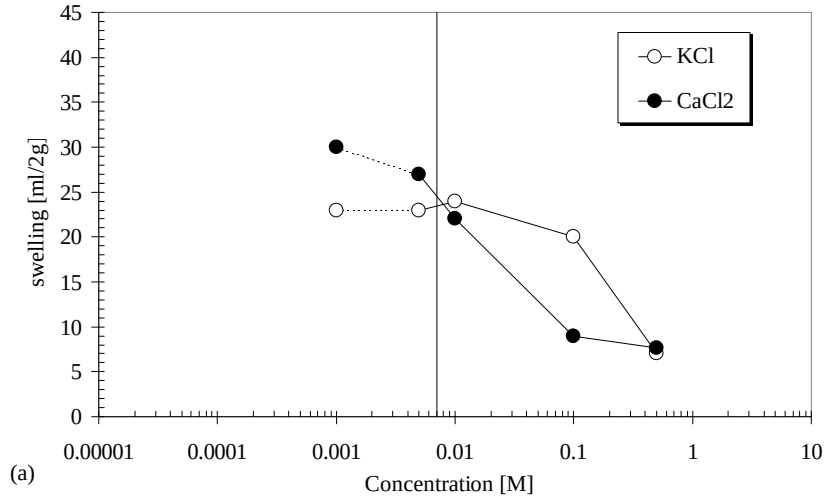

(a)

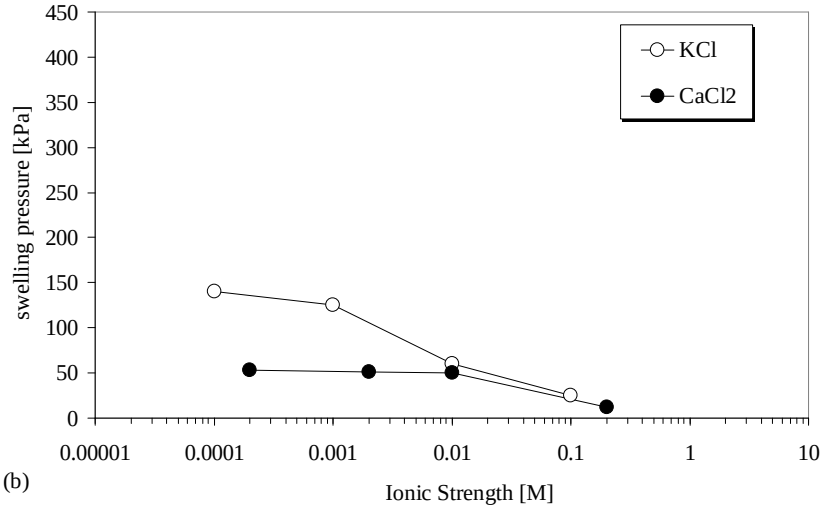

(b)

Figure 5.23: Decrease of swell pressure with increasing ionic strength

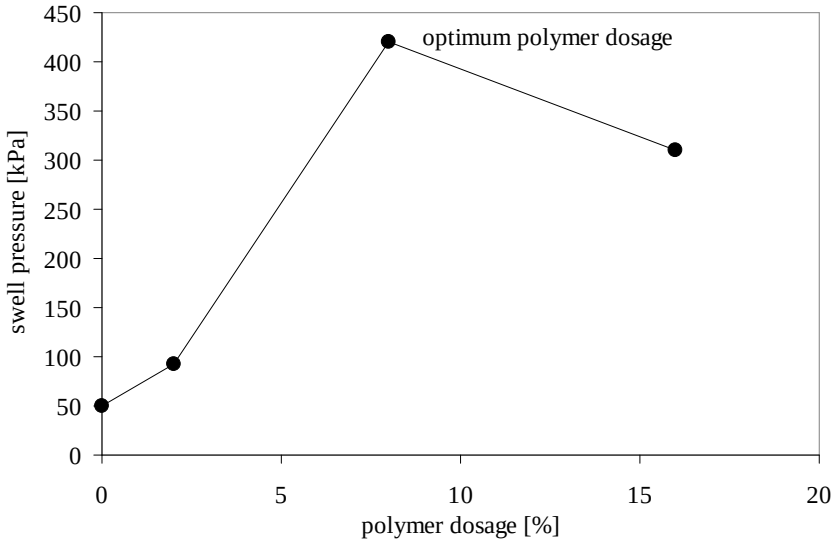

Figure 5.24: Increase of swell pressure with increasing polymer dosage in 5 mM $CaCl_2$ solutions

creased the net repulsive forces between platelets with a consequent increase of the measured swelling pressure.

Figure 5.25 also compares the swell pressure and the swell index of the HYPER clay. As noticed above for the DPH GCL and for the untreated clay, the swell index trend unexpectedly changed for concentrations lower than 0.01 M (5.25(a)).

Conversely, the swelling pressure results 5.25(b) confirmed that the swelling ability at low concentrations is either preserved or improved. The swell pressure decreased in fact monotonically with increasing concentration and valence of the ions consistently with the Double Layer Theory.

Dense Prehydrated GCL

Finally, Fig. 5.26(b) shows the swelling pressure vs. ionic strength of the DPH GCL bentonite in various KCl and $CaCl_2$ solutions (0.001 M up to 1 M).

The figure also shows a comparison with the swell index test. The swell index trend unexpectedly changed for concentrations lower than 0.01 M (5.26(a)). Whereas, the swelling pressure decreased monotonically increasing ionic strength of the solution, giving a better indication of the actual swelling ability of the DPH GCL clay at low concentrations.

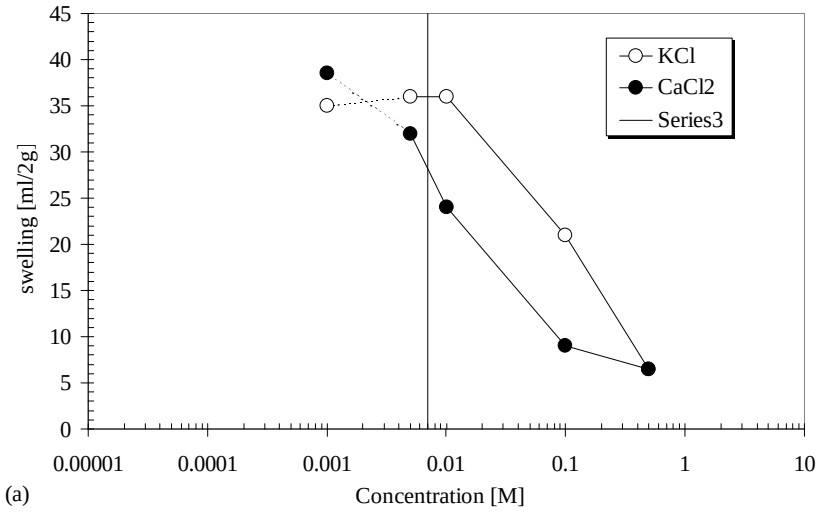

(a)

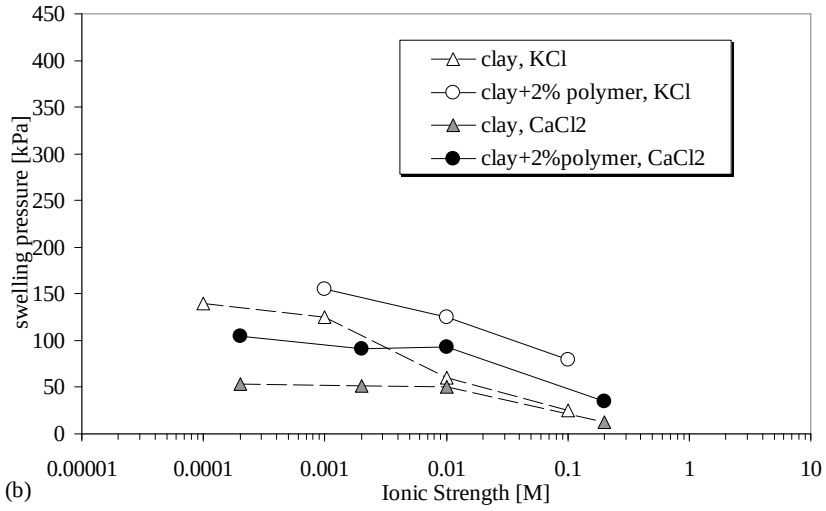

(b)

Figure 5.25: Decrease of swell pressure of HYPER clay with increasing ionic strength

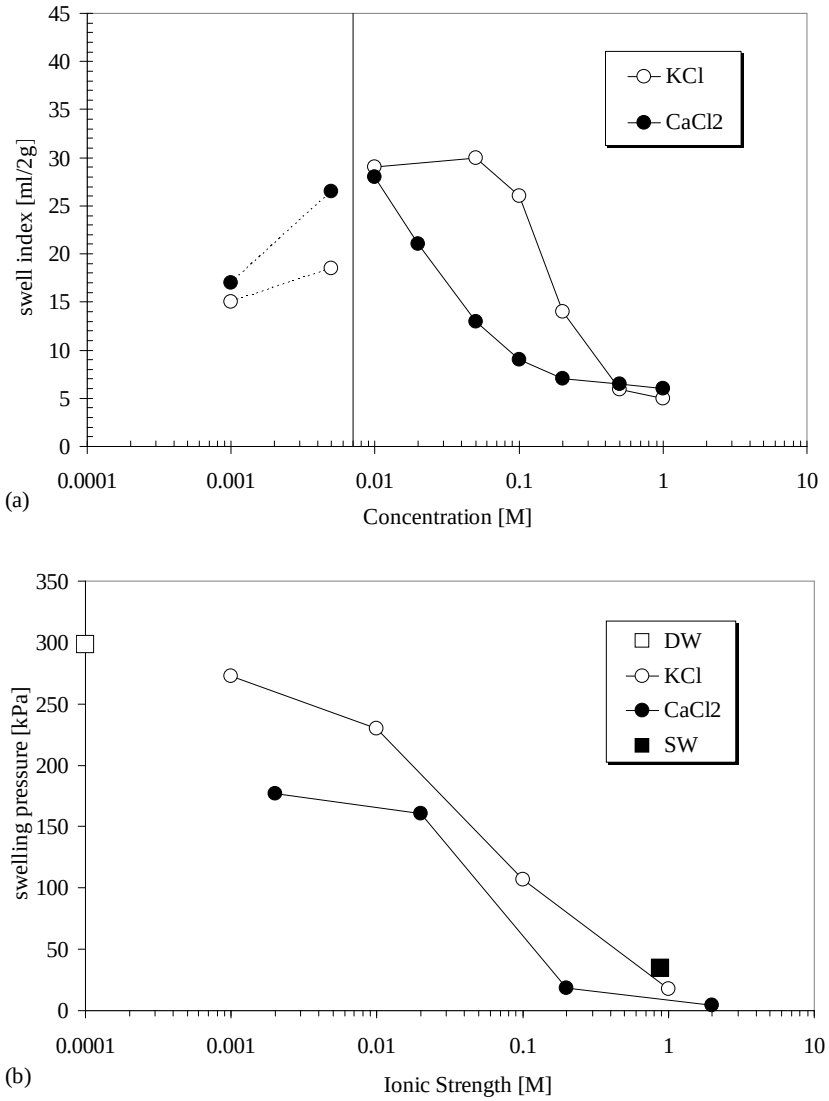

Figure 5.26: Decrease of swell pressure of DPH GCL with increasing ionic strength

5.3 Theoretical interpretation: swelling pressure of bentonites for electrolyte mixtures

The development presented here started from the analysis of the model proposed by Dominijanni (2005) for 2-ion systems. During various stages at Politecnico di Torino, we developed an extension of this model to allow for 3-ion systems. With this extension we back analyzed all experimental data of swelling pressure (shown in the previous section) for natural bentonites and polymer treated bentonites.

Special assumptions for the case of modified clays were introduced. We have demonstrated in the Section 5.1 that the polymer maintains the interlayer open. This property is able to limit the aggregation of platelets. Therefore, we assume that the number of platelets per aggregate of polymer treated clays is constant independently of the ion concentration and valence. Moreover, we expect that the modified bentonites will have a number of platelets, N, per aggregate and a fixed negative charge, C_X, higher than untreated clays.

New equations were derived to calculate partition coefficients starting from Donnan's equations and the electroneutrality condition.

The following paragraphs describe:

- the fixed charge model and the Donnan equations;
- the calculation of the partition coefficients and the swell pressure for single salt solutions (2-ion systems), based on the equations derived by Dominijanni and Manassero (2008);
- the mathematical framework developed here to determine the partition coefficients and the osmotic pressure for electrolyte mixtures in a 3-ion system.

5.3.1 Theoretical background

When a charged membrane separates two solutions of different concentrations, the transfer of ions takes place due to the concentration gradient. If these ions move faster than the ions of opposite charge, separation of the charges takes place. The electrical field created slows down the faster ions and accelerates the slower ones. This mechanism maintains the electroneutrality of the system.

Even though the electroneutrality condition between the ions is respected, an electrical "membrane" potential exists. The models for membrane potentials in a charged membrane are well documented, such as Teorell-Meyer-Sievers (TMS) fixed charge models (Teorell, 1935; Meyer and Sievers, 1936a).

The ability of montmorillonite particles to determine ion partitioning is generally modeled using the diffuse double layer (DDL) theory (Quirk and Marcelja, 1997). However, if the microscopic fluctuations of pressure and concentrations

with respect to their average values are neglected, the DDL theory can be reduced to Donnan's equations (Yaroshchuk, 1995).

The most evident advantage of using Donnan's equations instead of the DDL theory is the possibility to avoid the very difficult mathematical problem of solving the highly non-linear Poisson-Boltzmann equation. Dominijanni et al. (2006) have analyzed in detail the comparison of the two approaches and have shown that the Donnan's equations may be considered as a of first-order approximation of the exact solution of the DDL theory.

The Donnan model, compared to the Poisson-Boltzmann model, is characterized by the tendency to overestimate the swelling pressure, not accounting for the Maxwell stress (Dahnert and Huster, 1999). Also other phenomena are not taken into account in the model such as van der Waals forces, ion specific adsorption and dielectric effects.

Donnan's equations

The Donnan's equations define the equilibrium between the pore solution contained in a charged porous medium and an external bulk solution in thermodynamic equilibrium. These equations establish the equality of the electrochemical-potentials between the pore solution and the external bulk solution.

Using the definition of electro-chemical potential (Katchalsky and Curran, 1965), assuming the same constants of integration in the bulk solution and in the pore water and noticing that the partition mechanism does not act on the water molecules, the Donnan's equations can be expressed as follows (Dominijanni, 2005):

$$\bar{P} - \bar{\Pi} = P - \Pi \tag{5.1}$$

$$\bar{C_i} = C_i exp\left(-z_i \frac{F}{RT}\psi\right) \tag{5.2}$$

where

P and $\bar{P}$ are the fluid pressures in the external (P) and pore ($\bar{P}$) solutions;

z_i is the electro-chemical valence of the i-th ion;

C_i and $\bar{C_i}$ are the concentration of the i-th ion in the external and pore solution;

$\psi = \bar{\Phi} - \Phi$ is the Donnan potential defined as the difference between the electrical potential in the pore solution, $\bar{\Phi}$, and in the external solution, Φ;

R is the universal gas constant (8.314 J mol^{-1} K^{-1});

T is the absolute temperature;

F is the Faraday's constant (96845 C/mol);

Π and $\bar{\Pi}$ are the osmotic pressures in the external and pore solutions, that can be expressed as:

$$\Pi = RT \sum_{i=1}^{N_{ions}} C_i \tag{5.3}$$

$$\bar{\Pi} = RT \sum_{i=1}^{N_{ions}} \bar{C_i} \tag{5.4}$$

The Donnan equation 5.2 can be expressed also as:

$$\bar{C_i} = C_i \Gamma_i \tag{5.5}$$

where Γ_i is defined as the partition coefficient of the i-th ion.

Partition coefficient

Due to the ability of a membrane to generate a partition of the ions, the actual pressure and the ion concentrations are different within the external solution and the pore solution.

If the only partition mechanism considered is that associated to electrostatic repulsion of ions from charged pore walls, the partition coefficients may be related to the macroscopic electric potential of the membrane (or Donnan potential), ψ, as follows:

$$\Gamma_i = \frac{\bar{C_i}}{C_i} = exp\left(-z_i \frac{F}{RT}\psi\right) \tag{5.6}$$

The partition coefficients relate the ion concentrations, $\bar{C_i}$, within the bentonite pores to the external ion concentration, C_i.

Electroneutrality condition

In order to relate the electric potential, ψ, to the physical and chemical properties of the semipermeable porous medium, Teorell (1935) and Meyer and Sievers (1936a) proposed to adopt an electro-neutrality condition, taking into account the concentration of a fixed charge, C_X, uniformly distributed within the porous medium.

The electroneutrality condition within the external solution (eq. 5.7) and within the pore solution (eq. 5.8) can be expressed as follows:

$$\sum_{i=1}^{N_{ions}} z_i C_i = 0 \tag{5.7}$$

$$\sum_{i=1}^{N_{ions}} z_i \bar{C_i} - \bar{C_X} = 0 \tag{5.8}$$

where

z_i is the electro-chemical valence of the i-th ion;

C_i and $\bar{C_i}$ are the concentration of the i-th ion in the external and pore solution;

$\bar{C_X}$ is the concentration of the charge of solid particles per unit volume of the pore solution.

Physical interpretation of the fixed charge concentration

The fixed charge concentration, $\bar{C_X}$, may be assumed proportional to the Cation Exchange Capacity, CEC, and inversely proportional to the void ratio, e (Dominijanni, 2005):

$$\bar{C_X} = \phi_X CEC \rho_s \frac{1}{e} \tag{5.9}$$

where ϕ_X is the fixed charge coefficient and ρ_s is the density of the solid particles. The fixed charge coefficient, ϕ_X, is an adjustable parameter that accounts for all the uncertainties of the fixed charge model.

$\bar{C_X}$ can be related to physical and chemical properties of bentonite as follows (Dominijanni and Manassero, 2008):

$$\bar{C_X} = \bar{C_{X0}} \frac{1}{e'} = \frac{1 - f_{Stern}\sigma}{F} \frac{\rho_S S'}{e'} \tag{5.10}$$

where $\bar{C_{X0}}$ is the fixed charge concentration divided by the void ratio;

f_{Stern} is the fraction of electric charge compensated by cations specifically adsorbed in the Stern layer;

σ is the surface charge, about $0.114\, C/m^2$ (Dominijanni and Manassero, 2008);

N is the number of clay platelets per aggregate;

S'=S/N is the external specific surface around the clay aggregates (Fig. 5.27);

S is the total specific surface when N=1, typically about S=760 m^2/g (Quirk and Marcelja, 1997);

e' is the void ratio referred to the void space between the clay aggregates (Fig. 5.27).

5.3.2 Partition coefficients and swelling pressure for 2-ion systems

Partition Coefficients for a single salt (2-ion system)

A case of special interest is when the pore solution contains a single salt consisting of a cation (e.g. K^+ or Ca^{2+}) and an anion (e.g. Cl^-). Dominijanni and Manassero (2008) derived the partition coefficients for single salts solutions as follows.

The salt in solution is generally supposed completely dissociated:

$$Cation_{z_1}^{\nu_1} Anion_{z_2}^{\nu_2} \rightarrow \nu_1 Cation^{z_1} + \nu_2 Anion^{z_2} \tag{5.11}$$

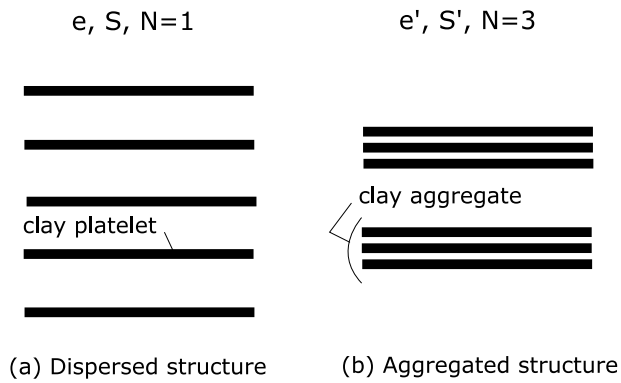

Figure 5.27: Schematic representation of montmorillonite structure

(ν_1, z_1) and (ν_2, z_2) are the stoichiometric coefficient and the electrochemical valence of the cation (index 1) and the anion (index 2). For instance, this equation for the salts KCl and $CaCl_2$ becomes:

$$KCl \rightarrow K^+ + Cl^- \tag{5.12}$$

and

$$CaCl_2 \rightarrow Ca_{2+} + 2Cl^- \tag{5.13}$$

The ionic concentrations, C_i, in external solution are related to the salt concentration, C_s, as follows

$$C_i = \nu_i C_s \tag{5.14}$$

For a single salt, electro-neutrality in the external solution, eq. 5.7, implies that:

$$z_1 C_1 + z_2 C_2 = 0 \tag{5.15}$$

Using equation 5.14, the electro-neutrality condition (eq. 5.15) reduces to:

$$z_1 \nu_1 + z_2 \nu_2 = 0 \tag{5.16}$$

From equation 5.6, a relation between the partition coefficients of the cation, Γ_1, and of the anion, Γ_2, may be derived:

$$\Gamma_1 = \Gamma_2^{-\nu_2/\nu_1} = \Gamma_2^{-z_1/z_2} \tag{5.17}$$

For a single salt, the electro-neutrality condition within the bentonite (eq. 5.8) is given by:

$$z_1\bar{C_1} + z_2\bar{C_2} - \bar{C_X} = 0 \tag{5.18}$$

Using equations 5.14, 5.16 and 5.17, equation 5.18 may be rewritten as follows:

$$\Gamma_2^{-\nu_2/\nu_1} - \Gamma_2 - \frac{\bar{C_X}}{z_1\nu_1 C_s} = 0 \tag{5.19}$$

Equation 5.19 can be solved to relate the partition coefficients to the value of the external salt concentration, C_s, and to the concentration of the charge of the solid particles, $\bar{C_X}$. The partition coefficient for the anion in a 1:1 electrolyte (e.g. NaCl or KCl) is given by:

$$\Gamma_2 = -\frac{\xi}{2} + \sqrt{\left(\frac{\xi}{2}\right)^2 + 1} \tag{5.20}$$

where $\xi = \bar{C_X}/C_s$.

For a 2:1 electrolyte (e.g. $CaCl_2$ or $MgCl_2$) the partition coefficient is given by:

$$\Gamma_2 = \frac{2}{3 \cdot f(\xi/2)} \left(\frac{\xi}{2}\right)^2 - \frac{1}{3}\left(\frac{\xi}{2}\right) + \frac{1}{6} f(\xi/2) \tag{5.21}$$

where

$$f(\xi/2) = [108 - 8 \cdot \left(\frac{\xi}{2}\right)^3 + 12 \cdot (81 - 12\left(\frac{\xi}{2}\right)^3)^{1/2}]^{1/3} \tag{5.22}$$

When the solution contains a (2:1) electrolyte, the partition ability of the bentonite is considerably reduced. This property is reflected on the swell pressure as well.

Theoretical modeling of the swelling pressure (2-ion system)

The partition coefficients derived in the previous section were used here to calculate the swell pressure for single salt solutions (2-ion systems).

The swelling pressure, S_π, can be defined as (Dominijanni, 2005):

$$S_\pi = \bar{\Pi} - \Pi \tag{5.23}$$

substituting equations 5.3 and 5.4 in equation 5.23 we obtain:

$$S_\pi = RT \sum_{i=1}^{N_{ions}} \bar{C_i} - RT \sum_{i=1}^{N_{ions}} C_i \tag{5.24}$$

substituting equations 5.6 in 5.24 we obtain:

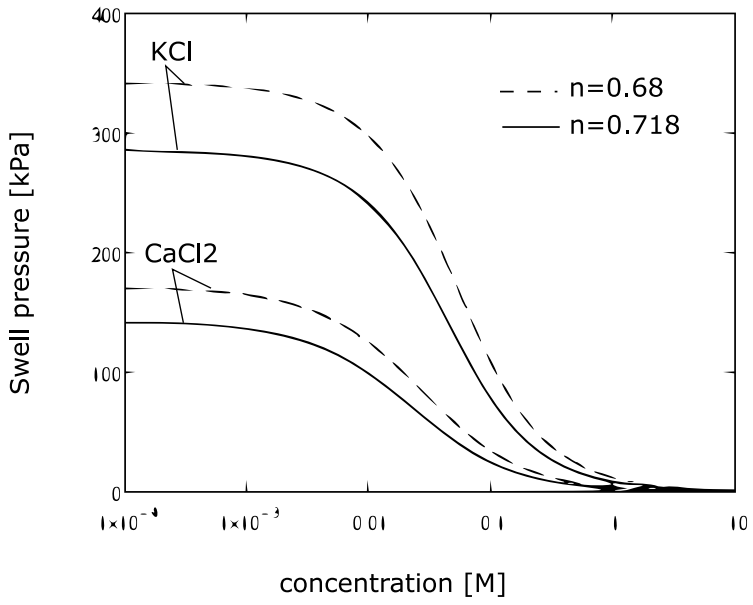

Figure 5.28: Swelling pressure varying salt concentration, valence and porosity, n

$$S_\pi = RT \sum_{i=1}^{N_{ions}} \Gamma_i C_i - RT \sum_{i=1}^{N_{ions}} C_i \tag{5.25}$$

The swelling pressure was plotted in Fig. 5.28 varying salt concentration, valence and porosity. As shown in the figure, the swelling pressure decreases with increasing solute concentration and valence.

In addition, the impact of densification was simulated varying the porosity (n). The two curves in Fig. 5.28 represent the swelling pressure of samples with different porosities. The two porosities evaluated in the figure correspond to a standard GCL (n=0.718, such as the untreated clay samples and the HYPER clay samples) and a denser GCL (n=0.68, such as the DPH GCL). As expected, under equal conditions, the swell pressure decreases with increasing porosity.

5.3.3 Back analysis of the experimental results of swelling pressure

Using equation 5.25, we evaluated the swelling pressure vs. the concentration of the natural clay, the HYPER clay and the DPH GCL by introducing the characteristics of the samples. The results of this simulation are illustrated in Fig. 5.29, 5.30 and 5.31. The figures show the trend of the swelling pressure calculated by varying

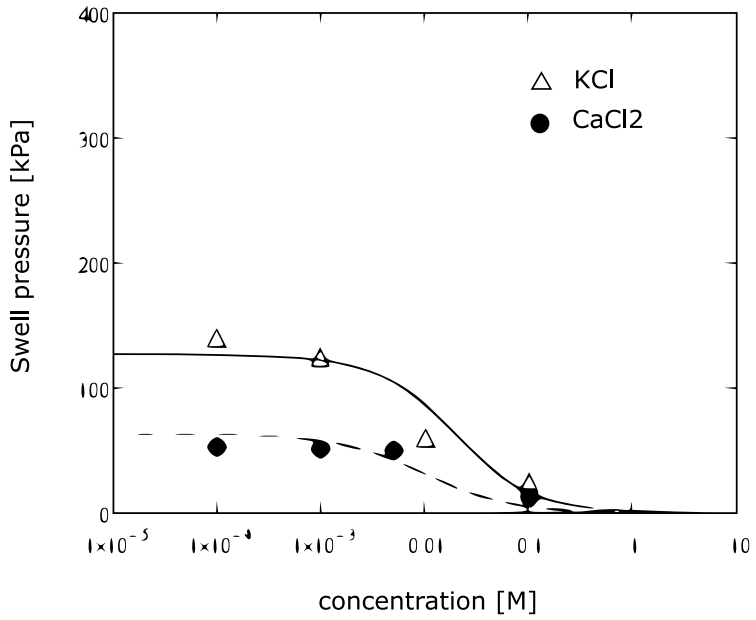

Figure 5.29: Theoretical interpretation of the swell pressure for the untreated clay

the solutes concentrations and valence. Two single salt solutions were considered, a 1:1 solution (such as KCl) and a 2:1 solution (such as $CaCl_2$). The experimental results were also plotted in the figures for comparison.

Untreated clay

Figure 5.32 shows the back analysis of the experimental results of swelling pressure on the untreated clay. As a first approach, we assume the number of platelets per aggregate constant (N = 9, C_{X0} = 0.133), independently of the concentration and the valence of the solutes. Figure 5.32 shows that this assumption was acceptable. In fact, the experimental results were in good agreement with the theoretical simulation, both for KCl and $CaCl_2$ solutions.

HYPER clay

Figure 5.33 shows the back analysis of the experimental results of swelling pressure on the HYPER clay.

The first result was that the swelling pressure of the HYPER clay matches with the experimental results introducing a number of platelets per aggregate (N = 5) lower respect to the untreated clay. This result confirms the findings reported in

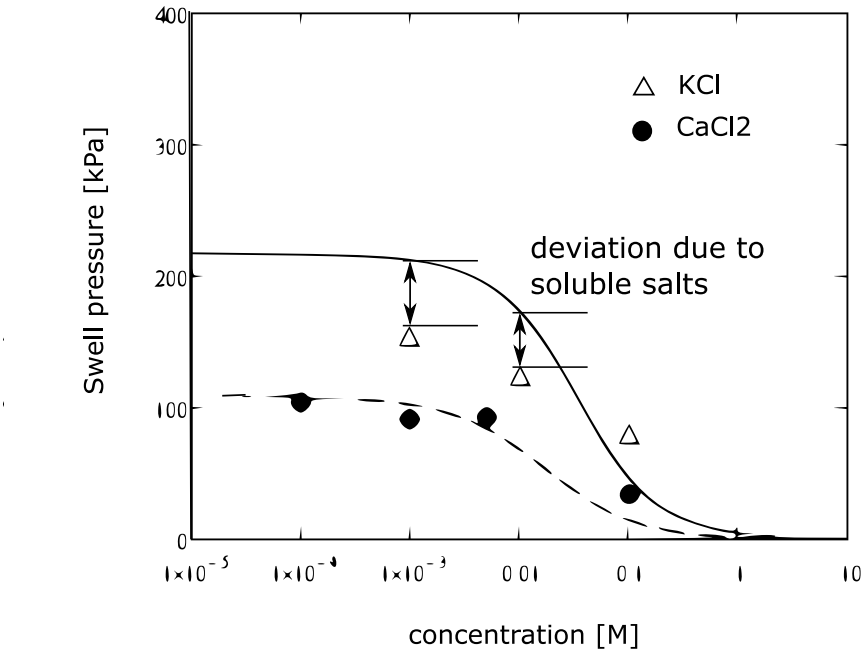

Figure 5.30: Theoretical interpretation of the swell pressure for the HYPER clay

Sections 5.1 and 5.2. In those Sections in fact we demonstrated that a possible impact of the polymer on the clay structure is that maintaining the interlayer open limits the aggregation of the particles maintaining a small number of platelets per aggregate.

Another interesting result is that the HYPER clay was characterized by a fixed charge concentration (C_{X0} = 0.227) larger compared to the untreated clay. This result suggests that the HYPER clay behaves as an untreated clay with a larger negative surface, probably due to the additional negative charge of the anionic polymer chain.

Figure 5.33 shows that the experiments were in good agreement with the theoretical evaluation for $CaCl_2$ solutions and for concentrated of KCl solutions. On the other hand, for diluted monovalent solutions, the theoretical simulation overestimated the experimental results.

The reason of this behavior is probably due to the presence of soluble salts. The impact of the soluble salts is noticeable for high values of the swell pressure associated with diluted monovalent solutions. In this regard, the impact of the presence of three ions (Ca^{2+}, K^{+}, Cl^{-}) on the swell pressure was also studied. The results of this simulation will be described in the Section 5.3.4.

Dense PreHydrated GCL

Figure 5.34 shows the back analysis of the experimental results of swelling pressure on the DPH GCL.

As noticed for the HYPER clay, also the DPH GCL showed a low number of platelets per aggregate (N = 4) and high fixed charge concentration (C_{X0} = 0.287). This results indicated that the polymeric solution used to prehydrate the DPH GCL maintains the interlayer open limiting aggregation.

Moreover, the impact of densification can be noticed comparing the figures 5.30 and 5.31. The swelling pressure of the DPH GCL (with porosity = 0.68) was in fact larger than the swelling pressure of the HYPER clay (n=0.718). Considering that the number of platelets per aggregate and the fixed charge of the two clays were similar, the reason of this behavior can be attributed to the densification of the DPH GCL.

In brief, the high swelling pressures of the DPH GCL represent the enhancement due to polymer addition and densification.

Figure 5.31 shows that, as occurred also for the HYPER clay, the experiments on the DPH GCL were in good agreement with the theoretical evaluation for $CaCl_2$ solutions and for concentrated KCl solutions. On the other hand, for diluted monovalent solutions, the experimental results underestimated the theoretical simulation.

5.3.4 Partition coefficients and swelling pressure for 3-ion systems

As seen in the previous paragraph, the presence of soluble salts has an impact on the actual swell pressure value when the clay is in contact with dilute monovalent solutions (such as low concentrated KCl solutions).

To simulate the actual scenario expected for clay barriers a more general framework of 3-ion systems was studied.

In this Section, first we will describe how we derived the partition coefficients in a 3-ion systems and then how we calculated the swelling pressure.

Determination of the partition coefficients (3-ion system)

The salt solutions are generally supposed completely dissociated:

$$KCl \rightarrow K^{+} + Cl^{-} \tag{5.26}$$

and

$$CaCl_2 \rightarrow Ca^{2+} + 2Cl^{-} \tag{5.27}$$

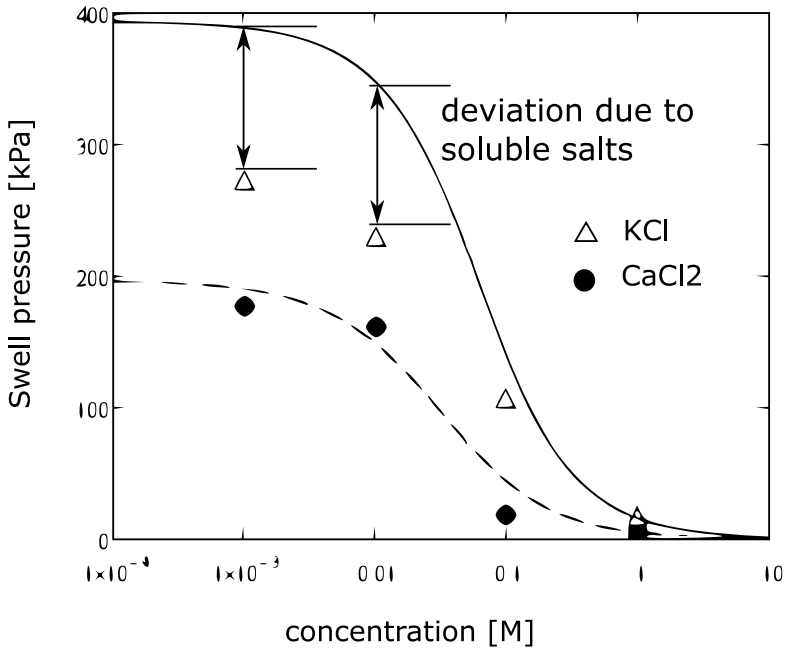

Figure 5.31: Theoretical interpretation of the swell pressure for the DPH GCL

In case of 3-ion systems, the electroneutrality conditions (eqs. 5.7 and 5.8) can be written as follows:

$$C_{Cl} = 2C_{Ca} + C_{Na} \tag{5.28}$$

$$\bar{C}_{Ca} + \bar{C}_{Na} = \bar{C}_{Cl} + \bar{C}_X \tag{5.29}$$

Substituting eq. 5.6 in 5.29 we obtain:

$$2\Gamma_{Ca}C_{Ca} + \Gamma_{Na}C_{Na} - \Gamma_{Cl}C_{Cl} - C_X = 0 \tag{5.30}$$

From equation 5.6 we can obtain the following relations between the partition coefficients:

$$\Gamma_{Na} = \Gamma_{Cl}^{-1} \tag{5.31}$$

and

$$\Gamma_{Ca} = \Gamma_{Cl}^{-2} \tag{5.32}$$

These relations allow us to express equation 5.30 in function of Γ_{Cl} as follows:

$$2\Gamma_{Cl}^{-2}C_{Ca} + \Gamma_{Cl}^{-1}C_{Na} - \Gamma_{Cl}C_{Cl} - C_X = 0 \tag{5.33}$$

Dividing both members of equation 5.33 by $2C_{Ca}$ we obtain:

$$\Gamma_{Cl}^{-2} + \Gamma_{Cl}^{-1}\frac{C_{Na}}{2C_{Ca}} - \Gamma_{Cl}\frac{C_{Cl}}{2C_{Ca}} - \frac{C_X}{2C_{Ca}} = 0 \tag{5.34}$$

Multiplying equation 5.34 by Γ_{Cl}^2 we obtain:

$$-(1+\alpha)\Gamma_{Cl}^3 - \beta\Gamma_{Cl}^2 + \alpha\Gamma_{Cl} + 1 = 0 \tag{5.35}$$

where

$$\alpha = \frac{C_{Na}}{2C_{Ca}} \tag{5.36}$$

$$\beta = \frac{C_X}{2C_{Ca}} \tag{5.37}$$

Knowing α and β, we can solve the third grade polynomial equation (5.35) numerically to obtain Γ_{Cl}.

Consequantly, from equations 5.31 and 5.32 we obtained the remaining partition coefficients, Γ_{Ca} and Γ_{Na}.

$$\Gamma_{Na} = \Gamma_{Cl}^{-1} \tag{5.38}$$

$$\Gamma_{Ca} = \Gamma_{Cl}^{-2} \tag{5.39}$$

Then, using equations 5.6 we obtained the ion concentrations in the pore solution, $\bar{C}_{Ca}$, $\bar{C}_{Na}$ and $\bar{C}_{Cl}$. These concentrations were used to compute the swelling pressure as explained in the next paragraph.

Theoretical modeling of the swelling pressure (3-ion system)

Knowing the partition coefficients and using equations 5.6 we obtained the ion concentrations in the pore solution, $\bar{C}_{Ca}$, $\bar{C}_{Na}$ and $\bar{C}_{Cl}$. Then, substituting the ion concentrations in equation 5.24 we are finally able to calculate the swell pressure for a 3-ion system as follows:

$$S_\pi = RT(\bar{C}_{Ca} + \bar{C}_{Na} + \bar{C}_{Cl} - (C_{Na} + C_{Ca} + C_{Cl})) \tag{5.40}$$

Untreated clay

Figures 5.32 shows the plot of the swelling pressure vs. concentration of the external solutions. The external solutions are 1:1 (e.g. KCl) in Fig. 5.32(a) and 2:1 (e.g. $CaCl_2$) in Fig. 5.32(b).

These figures also show a parametric study of the swelling pressures by varying the concentration of a third ion. The third ion can be represented by a bivalent ion (such as Ca^{2+}) in Fig. 5.32(a) and a monovalent ion (such as K^+) in Fig. 5.32(b).

For a concentration of the 3^{rd} ion C = 0, the curves in Fig. 5.32 correspond to the 2-ion formulation described in the previous Section.

As shown in Fig. 5.32(a), the swelling pressure in KCl decreases with increasing (parametrically) concentration of the 3^{rd} ion (Ca). This behavior can be explained with the Double Layer Theory. The double layer thickness is compressed with increasing concentration and valence of the solutes in the pore solution. Therefore, the presence of a third ion induces the compression of the double layer with a consequent decrease of the swelling pressure.

Moreover, Fig. 5.32(a) shows that for very low concentrations of the third ion (such as C_{Ca}=0.0001 M and C_{Ca}=0.001 M) the swelling pressure increases with increasing KCl concentration. This unusual increase is probably due to the "positive" effect of monovalent ion (K^+) on the double layer thickness. Increasing KCl concentration, the double layer (previously compressed by the third bivalent ion, Ca^{2+}) causes an exchange between K^+ and Ca^{2+} with a consequent increase of the DDL thickness.

Figure 5.32(b) shows that, at low salt concentrations, the swell pressure increases slightly with increasing K^+ concentration up to a K^+ concentration C_K = 0.001 M. This behavior is probably due to the exchange of K^+ with Ca^{2+} as explained above. The opposite behavior is then noticed for a K^+ concentration $C_K >$

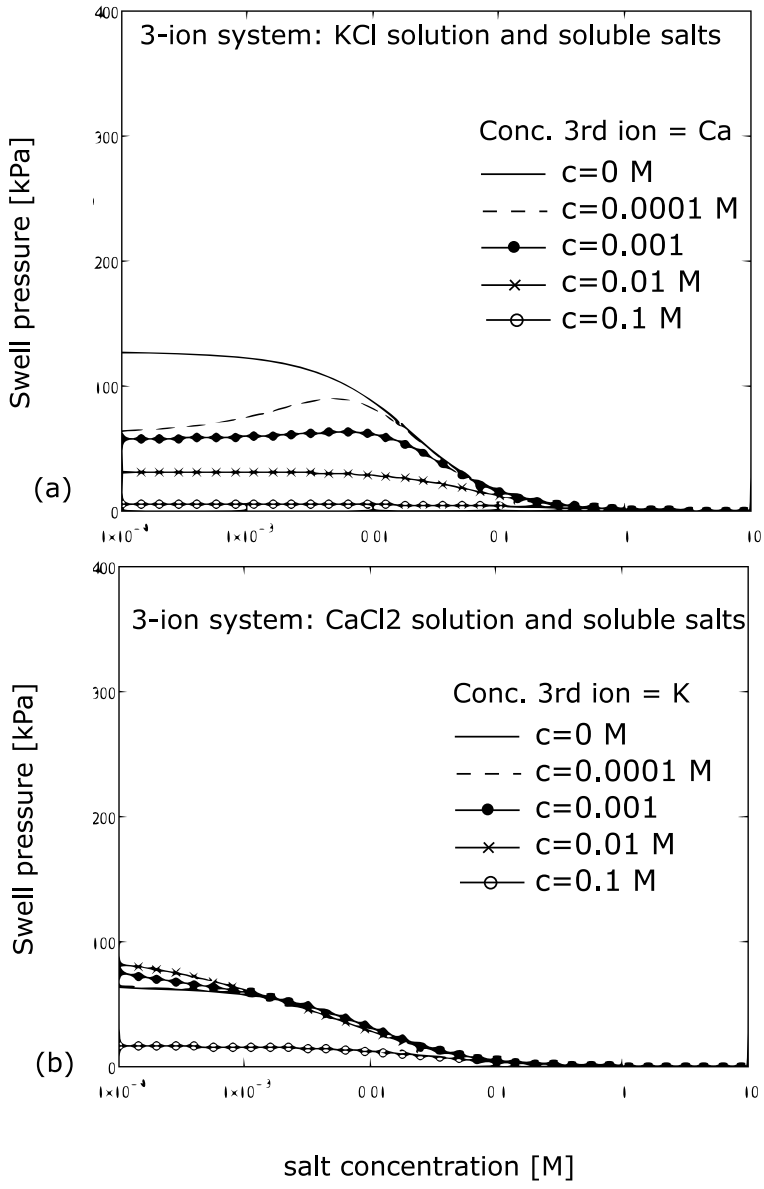

Figure 5.32: Theoretical interpretation of the swell pressure for the untreated clay in a 3-ion system. (a) 1:1 external solution (e.g. KCl) + bivalent ion (Ca^{2+}). (b) 2:1 external solution (e.g. $CaCl_2$) + monovalent ion (K^+.

0.001 M. This behavior is probably due to the compression of the DDL thickness at very high concentrations of K^+.

Nevertheless, the impact of soluble salts may be neglected for untreated clays. In fact, the theoretical interpretation for 2-ion systems showed very good agreement with experimental data on untreated clays (Fig. 5.29).

HYPER clay and DPH GCL

On the other hand, for polymer treated clays the theoretical interpretation for 2-ion systems overestimates the swelling pressures obtained experimentally (Figs. 5.30 and 5.31). This behavior is probably due to two possible reasons:

- the concentration of soluble salts (and exchangeable salts) of the natural clay were lower compared to that of the polymer treated clays. This increased concentration was attributed to the extra soluble and/or exchangeable Na^+ introduced by the sodic polymers (Na-CMC);
- the swelling performance of the polymer treated clays was superior than that of the untreated clay. The impact of the soluble salts is then probably more noticeable for higher values of the swelling pressures, corresponding to thicker DDLs.

Figures 5.33 and 5.34 show the 3-ion system theoretical modeling of the swelling pressure of the HYPER clay and the DPH GCL. The figures show the results of a parametric study performed varying the concentrations of the third ion.

For a concentration of the 3^{rd} ion C = 0, the curves in Figs. 5.33 and 5.34 correspond to the 2-ion formulation described in the previous Section.

Figures 5.33 and 5.34 show that the presence of a third ion produces a deviation of the swelling pressure similar to the deviation noticed between the theoretical and experimental values (Figs. 5.30 and 5.31). The deviation between theoretical and experimental values was attributed to the presence of soluble salts. Therefore, the third ion here may represent the presence of soluble salts.

As expected, the deviation is more noticeable for low concentrated solutions and for high values of the swelling pressure (Figs. 5.33 and 5.34). In fact, the effect of a third ion is negligible if its concentration is considerably lower than the concentration of the external solution.

Moreover, low swelling pressures correspond to compressed double layers. The impact of additional ions in a double layer already compressed is limited compared to thick double layers.

For a clarification of the deviation due to the third ion, Fig. 5.35 shows that the theoretical swell pressure (2-ion model) apparently overestimates the experimental swell pressure because of the presence of soluble salts. The black circle in the figure represents the experimental swelling pressure.

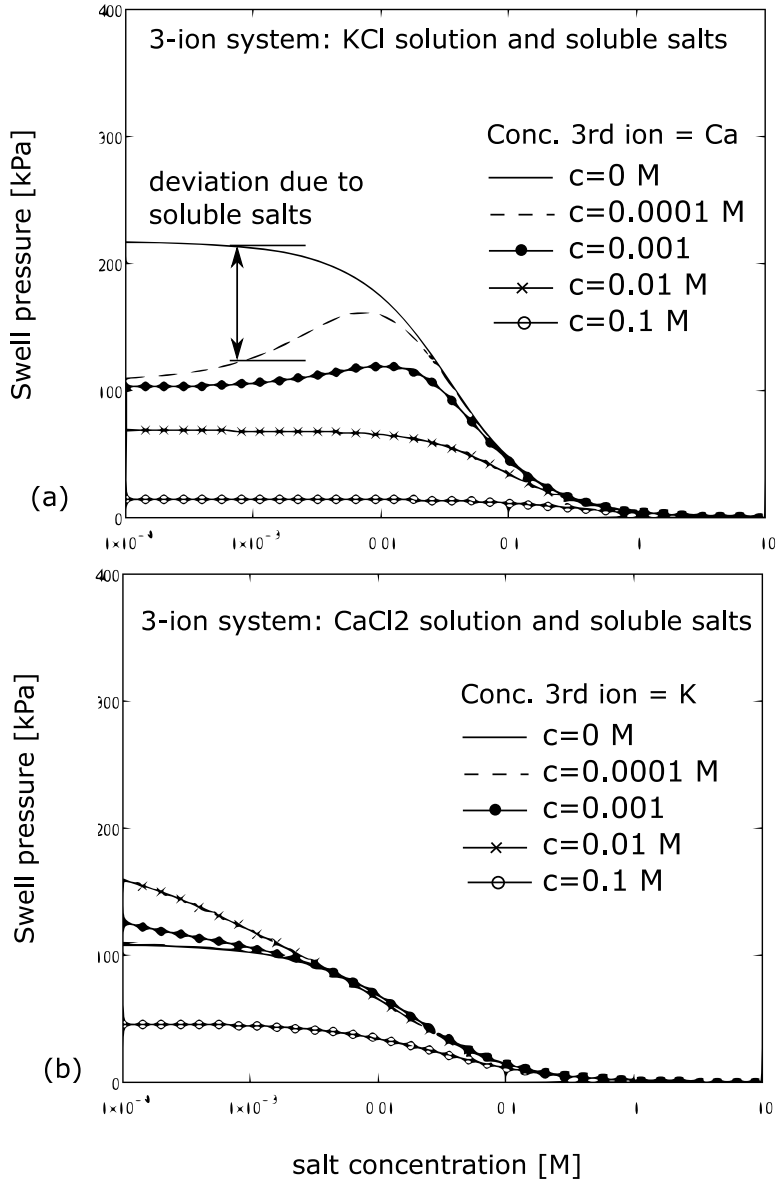

Figure 5.33: Theoretical interpretation of the swell pressure for the HYPER clay in a 3-ion system. (a) 1:1 external solution (e.g. KCl) + bivalent ion (Ca^{2+}). (b) 2:1 external solution (e.g. $CaCl_2$) + monovalent ion (K^+.

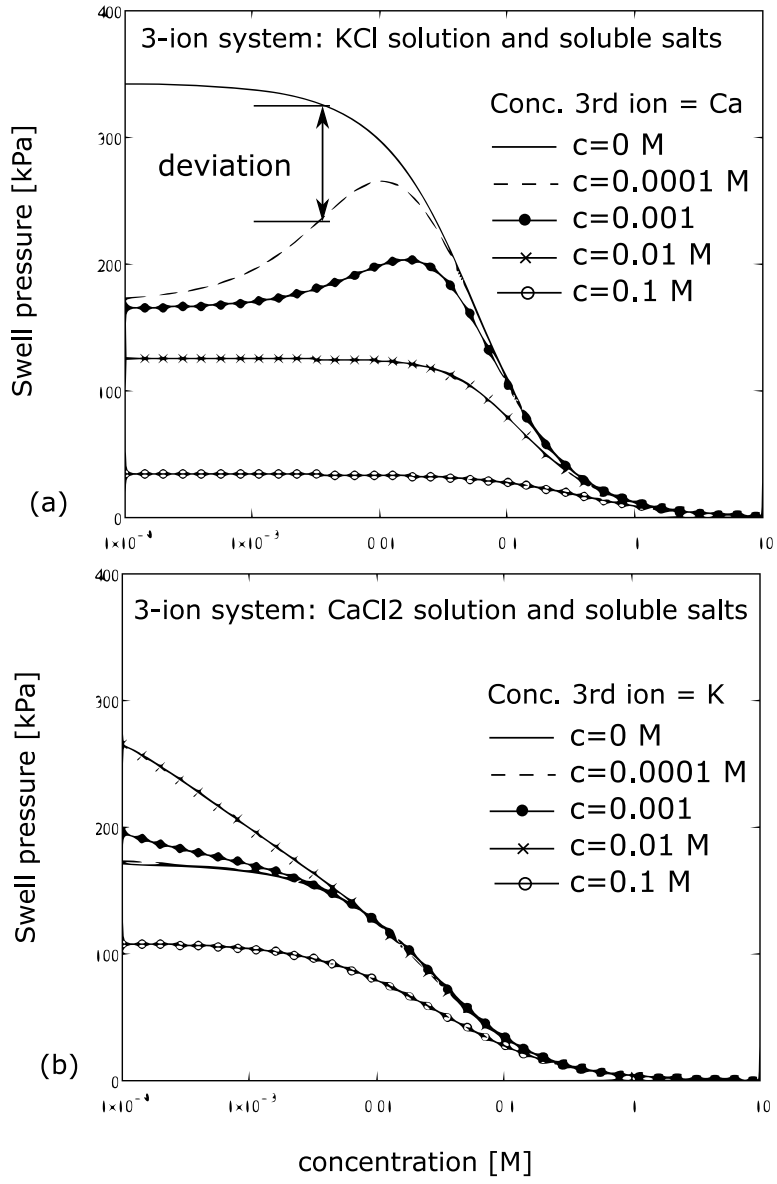

Figure 5.34: Theoretical interpretation of the swell pressure for the DPH GCL in a 3-ion system. (a) 1:1 external solution (e.g. KCl) + bivalent ion (Ca^{2+}). (b) 2:1 external solution (e.g. $CaCl_2$) + monovalent ion (K^+.

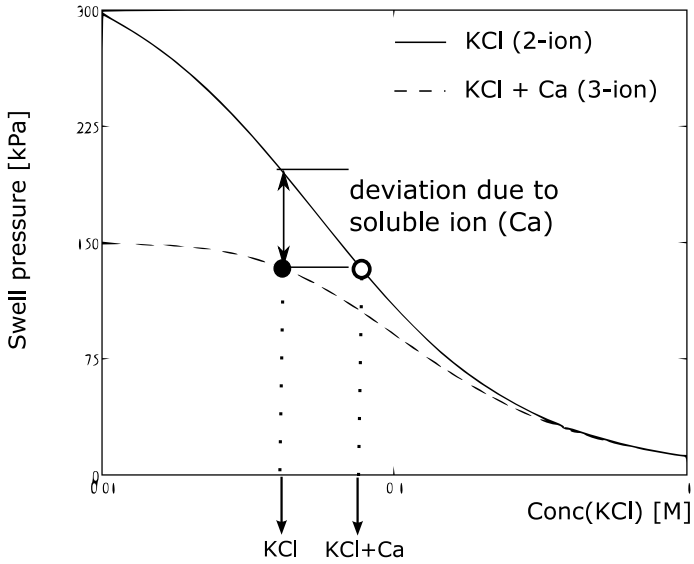

Figure 5.35: Impact of soluble salts: from 2-ion to 3-ion modeling

To obtain reasonable estimations with the 2-ion system, the input concentration to consider (open circle in Fig. 5.35) should be increased to take account of the presence of soluble salts.

Alternatively, the implementation of the 3-ion model is recommended (represented by the dash line in Fig. 5.35).

5.3.5 Summary

In this Section, we have calculated the swelling pressure of bentonites for 3-ion systems based on the Donnan model and the electroneutrality condition.

We assumed that the number of platelets per aggregate were constant independently of the ion concentration and valence. This assumption enables us to obtain acceptable estimations of the experiments performed.

The C_{X0} obtained with the back analysis of the swelling pressure tests overestimated the C_{X0} obtained in the chemico-osmotic test. We attributed this result to the special assumptions used for the theoretical interpretation of the swelling pressure. We neglected, in fact, the interparticle stresses, considering the clay structure as very dispersed. Such assumption has been proposed for instance by Bolt (1956).

Whereas, the theoretical interpretation of the chemico-osmotic experiments provided a better representation of the fixed charge concentration of the clays analyzed.

Nevertheless, we were able to evaluate the effect of polymer addition and densification based on the back analysis of the swelling pressure tests. Out of back analysis of the experimental data with the model, we demonstrated that the polymer treatment increased the net negative charge of the clay (C_{X0}) and limited the aggregation between clay platelets with a consequent improvement of the swelling ability of the clay.

Figure 5.36 shows the impact of the polymer addition and the densification on the swelling pressure in presence of KCl and $CaCl_2$ solutions. The figure shows that the polymer treatment improves the swelling performance of the clay.

Also the densification of a clay increases its swelling pressure. For this reasons, the simultaneous effect of polymer treatment and densification improves considerably the swelling ability of a clay (Fig. 5.36).

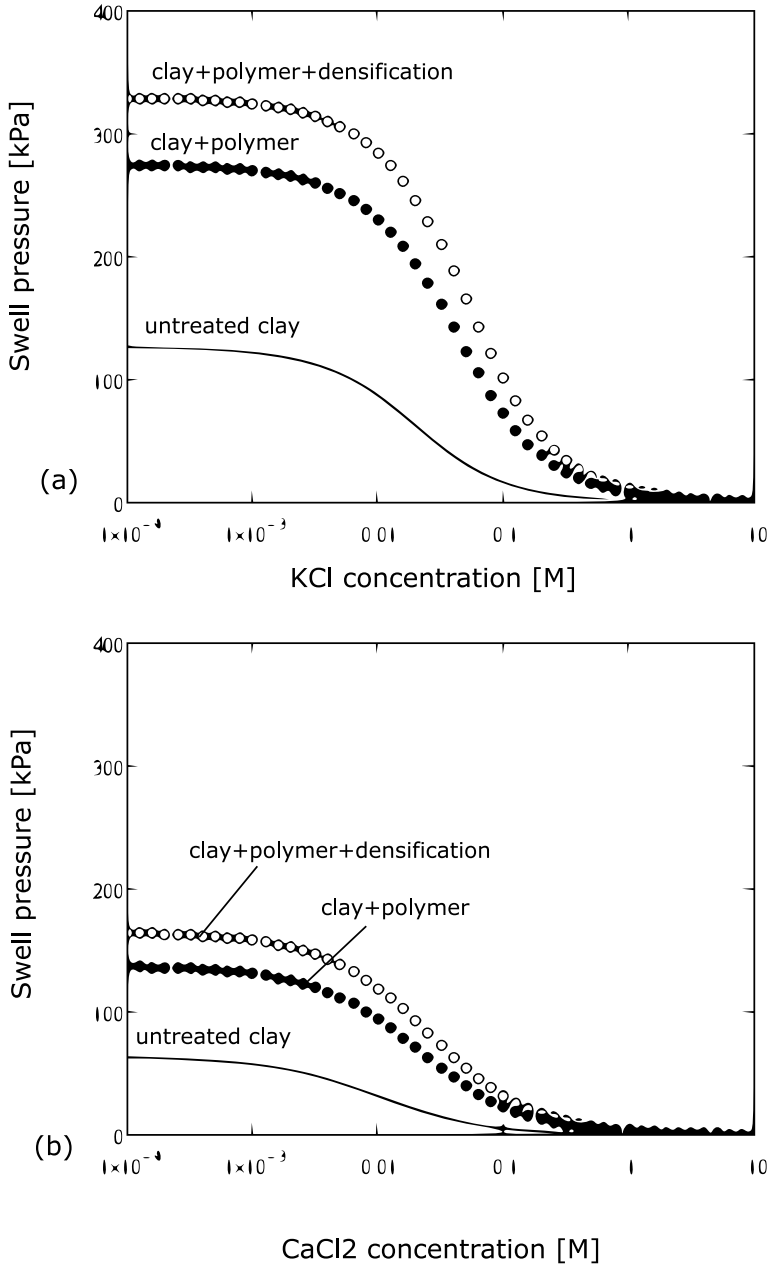

Figure 5.36: Impact of polymer treatment and densification on the swelling pressure of clays (a) in presence of KCl solutions and (b) in presence of $CaCl_2$ solutions

5.4 Effect of polymer treatment on the hydraulic conductivity of clays

5.4.1 Introduction

In the Sections 5.1 and 5.2 we have demonstrated that polymer treated clays show higher water adsorption capacity and higher swelling ability compared to untreated clays. Based on the well known qualitative relationship between these characteristics and the hydraulic performance of clays (Jo et al., 2001; Lee et al., 2005), it is interesting to evaluate the hydraulic conductivity of polymer treated clays in view of its potential benefits. Therefore, a series of hydraulic conductivity tests were performed on untreated clays and clays treated with polymers (HYPER clay, MSB and DPH GCL).

Polymer treatment

The impact of polymer treatment was assessed by means of permeability tests in flexible wall permeameters on samples confined by an effective stress σ'=14 kPa and with initial porosity n=0.718. The permeant solutions used were deionized water, seawater and a 5 mM $CaCl_2$ solution.

Prehydration

The impact of prehydration with deionized water was assessed by means of hydraulic conductivity tests in rigid wall permeameters on samples at a fixed porosity n=0.718. The permeant solutions used after prehydration were seawater and a 5 mM $CaCl_2$ solutions

Polymer treatment, prehydration and densification

Hydraulic conductivity tests on a DPH GCL were conducted to study the impact of the simultaneous effect of polymer treatment, prehydration and densification.

In addition, the hydraulic efficiency of the DPH GCL overlap area was evaluated as well. 30.5 cm diameter overlapped samples were permeated with deionized water and seawater in large scale flexible wall permeameters confined by an effective stress σ'=14 kPa. In parallel, 14 cm diameter overlapped samples were permeated with $CaCl_2$ solutions (0.01 M, 0.02 M and 0.1 M) in a rigid wall stainless steel permeameter.

At the end of the Section, Tables 5.2, 5.3 and 5.4 show an overview of the test results in terms of testing conditions, hydraulic conductivity, Pore Volumes of permeation and duration in days.

5.4.2 Hydraulic conductivity of polymer treated clays after direct permeation with electrolyte solutions

The low hydraulic conductivity of bentonites is primarily due to adsorbed immobile water molecules and hydrated ions in the interlayer region of bentonite clays that restrict the pore space available for the flow and cause tortuous flow pathways. Given that the thickness of the adsorbed layer is inversely related to the ions concentration and valence, bentonites are particularly sensitive to changes in the composition of the pore fluid. In particular, electrolyte solutions with high ion concentration and valence cause the thickness of the diffuse double layer to collapse and therefore the hydraulic conductivity to increase.

In this Section (§ 5.4.2) the impact of polymer treatment on non-prehydrated samples is investigated by means of flexible wall permeameters, using an effective stress of $\sigma' = 14$ kPa and an initial porosity n = 0.718.

Untreated clay

Figure 5.37(a) compares the hydraulic conductivity of the untreated clay to deionized water to the hydraulic conductivity to a 5 mM $CaCl_2$ solution. As expected, the hydraulic conductivity to the $CaCl_2$ solution was higher than to deionized water. This increase was caused by the replacement of Na^+ of the bentonite with the Ca^{2+} of the solution and the consequent compression of the double layer thickness. The hydraulic conductivity to deionized water was in fact k = 6.42E^{-12} m/s (after 19.46 Pore Volumes, PV, of flow and 276 days of permeation), whereas the hydraulic conductivity to $CaCl_2$ was k = 3.53E^{-11} m/s (after 2.2 PV of flow and 149 days of permeation).

Figure 5.37(b) compares the hydraulic conductivity of the untreated clay to deionized water to the hydraulic conductivity to sea water. Also for the sea water the hydraulic conductivity was higher than to deionized water due to the high concentrated ions contained in the sea water that, entering the interlayer region between bentonite platelets, compress the double layer thickness. The hydraulic conductivity to seawater was in fact k = 6.00E^{-10} m/s (after 19 PV of flow), almost two order of magnitude higher than that to deionized water (k = 6.42E^{-12} m/s).

In brief, high ions concentration (such as in seawater) and high ions valence (Ca^{2+}) increased the hydraulic conductivity of the untreated clay.

HYPER clay

The impact of Na-CMC polymer addition on the hydraulic performance of clays was investigated.

Figure 5.38(a) shows the hydraulic conductivity of the HYPER clay to the $CaCl_2$ 5 mM solution. The results suggest taht polymer addition decreases the

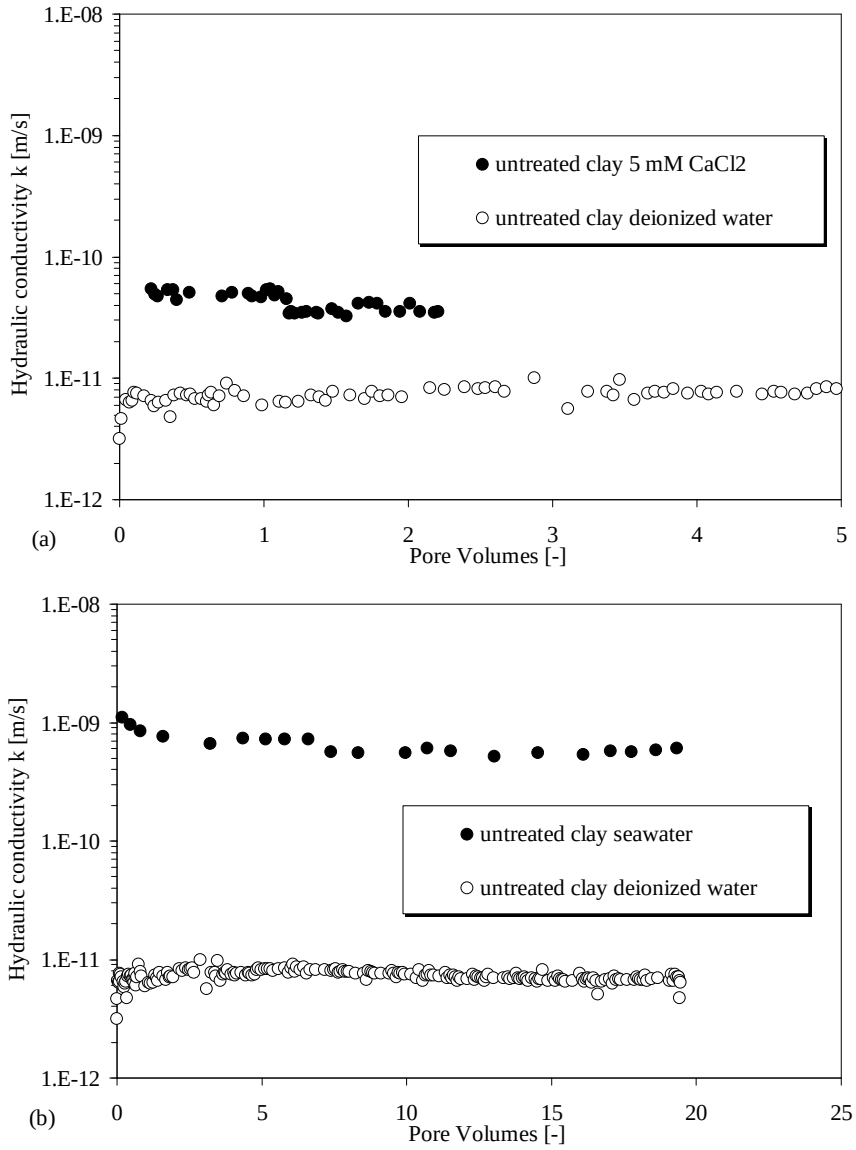

Figure 5.37: Increase of the hydraulic conductivity of the untreated clay to $CaCl_2$ 5 mM and sea water compared to deionized water

hydraulic conductivity of the clay. The hydraulic conductivity of the untreated clay was in fact k=3.53E^{-11} m/s (after 2.2 PV and 148.8 days of permeation), whereas the hydraulic conductivity of the HYPER clay (clay+2% Na-CMC) was k=1.37E^{-11} m/s (after 1.37 PV and 156.9 days).

Figure 5.38(a) shows also that the hydraulic conductivity to a $CaCl_2$ solutions (5 mM) decreased with increasing polymer dosage up to 8% Na-CMC. The hydraulic conductivity of the clay treated with 8% Na-CMC was in fact k=7.03E^{-12} m/s, after 1.25 PV and 156.9 days, which is comparable in magnitude to the hydraulic conductivity of the untreated clay to deionized water (k=6.42 E^{-12} m/s).

These results were in good agreement with swell index results. In fact the swell index in presence of the 5 mM $CaCl_2$ solution increased with increasing polymer dosage (SI = 23 ml/2g, SI = 36 ml/2g and SI = 43ml/2g, for Na-CMC dosages 0%, 2% and 8%, respectively). As expected, the higher the swell index the lower the hydraulic conductivity of the materials tested.

Figure 5.39(a) compares the hydraulic conductivity to sea water of the untreated clay to that of the HYPER clay. As shown in the figure, the hydraulic conductivity of the HYPER clay to sea water (k=4.17E^{-11} m/s) was about one order of magnitude lower than the hydraulic conductivity of the untreated clay (k = 6.00E^{-10} m/s), after 25.5 PV of flow and 545 days of permeation.

The HYPER clay showed lower hydraulic conductivity to sea water even though the swell index in presence of sea water of the HYPER clay and the untreated clay are of the same magnitude (about SI=9 ml/2g). This result indicates that the low hydraulic conductivity in presence of the polymer is probably due to other factors as well not revealed by the the swell index test, for example, the higher water adsorption capacity of the HYPER clay compared to the untreated clay. The liquid limit can give an indication of the water adsorption capacity of a clay. The liquid limit of the HYPER clay was in fact higher in sea water compared to the untreated clay (208.7% vs. 168.6%), as seen in Section 5.1.

This difference between the two index properties (SI and liquid limit) that are qualitatively related to permeability (Jo et al., 2001; Lee et al., 2005), is probably due to the different exposure of the bentonite particles and the solution. For example, the liquid to solid ratio for the swell index test is higher than that for the liquid limit. The greater the exposure the stronger the attraction between the interlayers, which could lead to a lower swell index. However, such low swell index value, related to high exposure, may not be representative of the actual situation.

In Sections 5.1 and 5.2 we have demonstrated that the treatment with Na-CMC polymer results in:

- larger interlayer separation during hydration,
- limited aggregation between particles,
- adsorption of a large number of hydrated cations and water molecules,

- tortuous structure with long flow pathways.

These characteristics of the HYPER clay may explain its low hydraulic conductivity to electrolyte solutions, such as sea water and the 5 mM $CaCl_2$ solution.

Multiswellable Bentonite

Figure 5.40(a) compares the hydraulic conductivity to a 5 mM $CaCl_2$ solution of the non-prehydrated MSB to the hydraulic conductivity of the untreated clay. As shown in the figure, the two hydraulic conductivities were comparable. The hydraulic conductivities were in fact k = $4.59E^{-11}$ m/s for the MSB and k=$3.53E^{-11}$ m/s for the untreated clay.

Likewise, Katsumi et al. (2008) found a hydraulic conductivity of the MSB to deionized water comparable to the hydraulic conductivity of the untreated clay (k = $1.0E^{-11}$ m/s and k = $5.84E^{-12}$ m/s, respectively). However, they observed a hydraulic conductivity of the MSB about one order of magnitude lower than that of the untreated clay permeated with $CaCl_2$ solutions with concentrations varying between 0.1 M and 0.5 M.

These results could be explained based on Fig. 5.16 in Section 5.1. There, we stated that polymer treated clays behavior is similar to that of untreated clays for low concentrated solutions (such as 5 mM $CaCl_2$) because the diffuse double layer is considerably open with or without the polymer. Whereas, the beneficial effect of the polymer can be observed for higher concentrations corresponding to thinner DDL thicknesses.

Termination criteria

Typical termination criteria that should be met to consider a hydraulic conductivity test complete are (ASTM D5084):

1) the ratio of the rate of inflow to the rate of outflow shall be between 0.75 and 1.25 for the last three consecutive flow measurements;

2) there shall be no significant upward or downward trend in the hydraulic conductivity for the last three consecutive measurements;

3) the hydraulic conductivity should be steady, four or more consecutive hydraulic conductivity determinations should fall within 25% or better of the mean value;

4) and, for compatibility testing with aggressive solutions (ASTM D6766), the test shall continue until at least two pore volumes of flow passed through the specimen and chemical equilibrium is established between the effluent and influent. Equilibrium is established when the ratio of outflow-to-inflow pH and the ratio of outflow-to-inflow electrical conductivity differ less than 0.1.

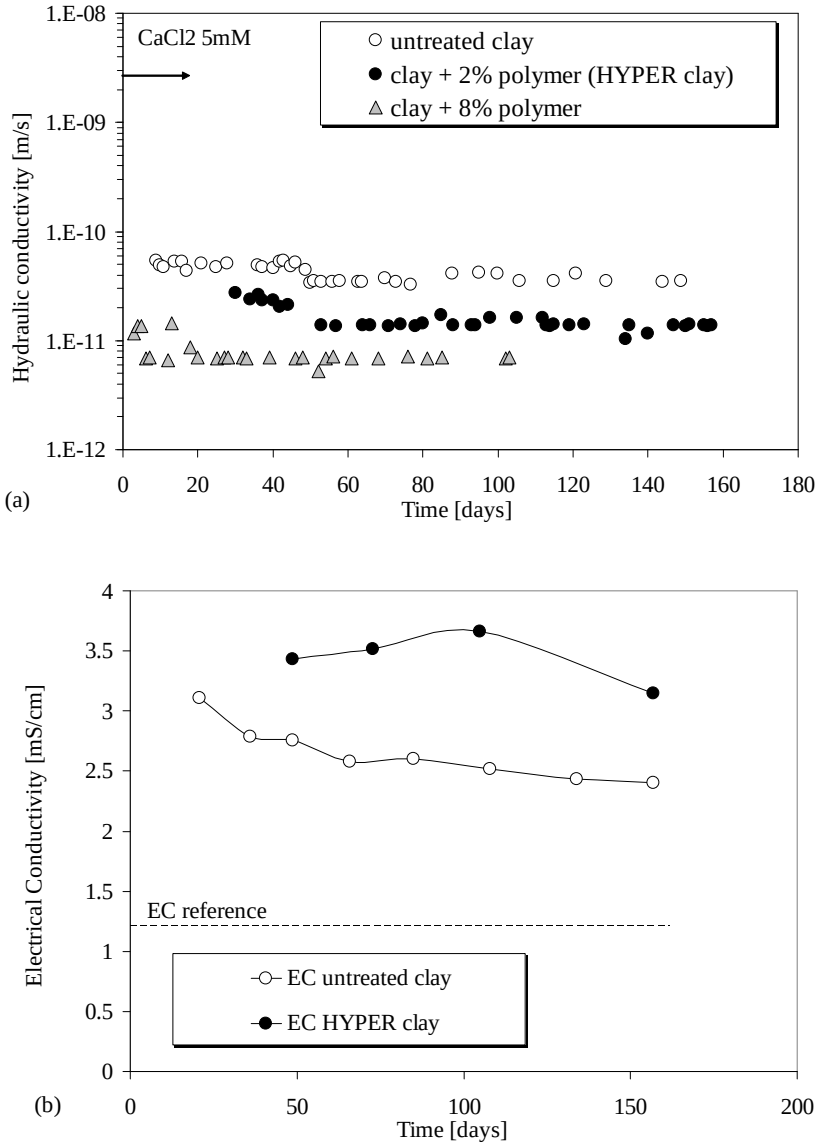

Figure 5.38: Hydraulic conductivity decreased with increasing polymer (Na-CMC) dosage

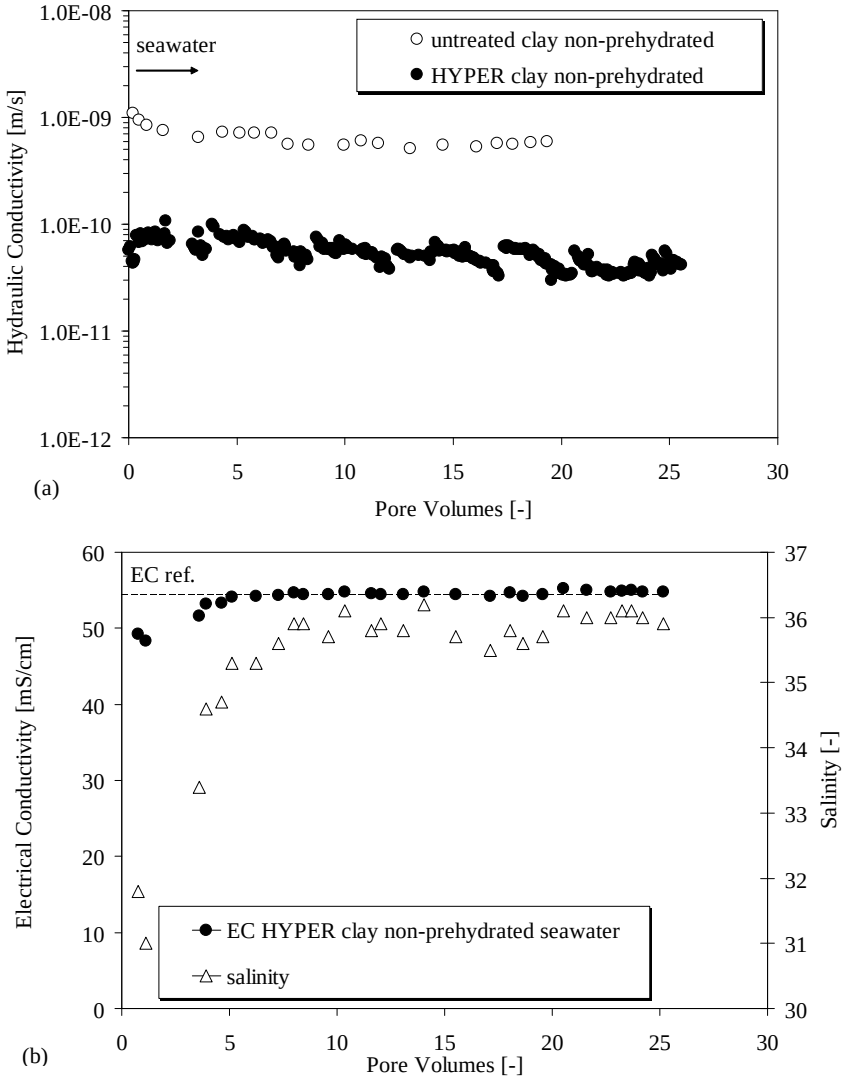

Figure 5.39: Hydraulic conductivity to seawater of the untreated and the HYPER clay. The hydraulic conductivity decreased by adding 2% Na-CMC

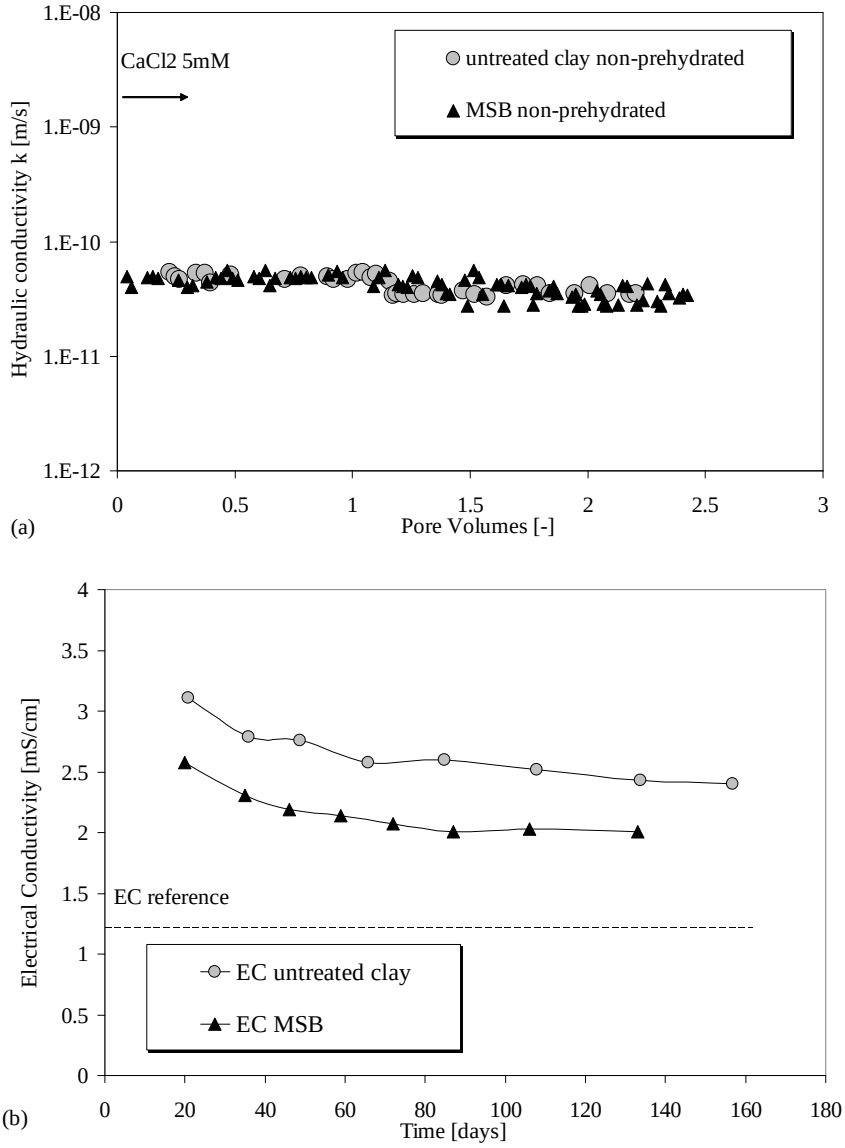

Figure 5.40: Hydraulic conductivity of non-prehydrated MSB to $CaCl_2$ compared to the hydraulic conductivity of the untreated clay

The termination criteria 1 to 3 were fulfilled for all the tests. Whereas the chemical equilibrium (point 4) was fulfilled for the tests on the non-prehydrated samples permeated with seawater (Fig. 5.39(b)).

Chemical equilibrium for the non-prehydrated samples permeated with the 5 mM $CaCl_2$ solution was not established (Figs. 5.38(b) and 5.40(b)). The very low hydraulic conductivity and ion diffusion in diluted solutions (such as 5 mM $CaCl_2$) delay considerably the establishment of chemical equilibrium even after years of permeation. Therefore, these tests are continued to investigate the long term barrier performance.

5.4.3 Hydraulic conductivity of polymer treated clays after prehydration with deionized water

In this Section the impact of polymer treatment and prehydration on samples is investigated by means of rigid wall permeameters, with fixed height and porosity n = 0.718.

Untreated clay and Hyper clay

Figure 5.41 shows that the hydraulic conductivity to deionized water of hte natural clay and the HYPER clay were comparable (k = $6.4E^{-12}$ m/s vs. k = $6.5E^{-12}$ m/s, respectively). The hydraulic conductivity to water was not influenced by the presence of the polymer, probably because the diffuse double layer of the untreated clay and the HYPER clay hydrated with water were both sufficiently thick independently of the presence of the polymer.

After about 300 days of prehydration with deionized water, the samples were permeated with a 5 mM $CaCl_2$ solution, as shown in Fig. 5.41. The hydraulic conductivity of the untreated clay after prehydration increased from k = $6.4E^{-12}$ to k = $4.0E^{-11}$ m/s (Fig. 5.41(a)). Whereas, the hydraulic conductivity of the HYPER clay to $CaCl_2$ after prehydration w decreased slightly, from k = $6.5E^{12}$ m/s to k = $3.1E^{-12}$ (Fig. 5.41(b)).

The chemical equilibrium for the prehydrated untreated clay permeated with the 5 mM $CaCl_2$ solution was initally established and then the EC unexpectedly decreased (Figs. 5.42(b)). A possible explanation is that the pH values observed for the $CaCl_2$ solutions indicate equilibrium with $CaCO_3$ (pH = 8.15 8.8, see Appendix B). It is likely that $CaCO_3$ precipitation occurred which may explain the low electric conductivity values observed on the outlet in this test.

The chemical equilibrium of the prehydrated HYPER clay permeated with the 5 mM $CaCl_2$ solution was not established (Fig. 5.43(b)) even after 200 days of permeation. Which is an indication that exchange reactions were still occurring. Hence, this test will also be continued to investigate the long-term barrier performance.

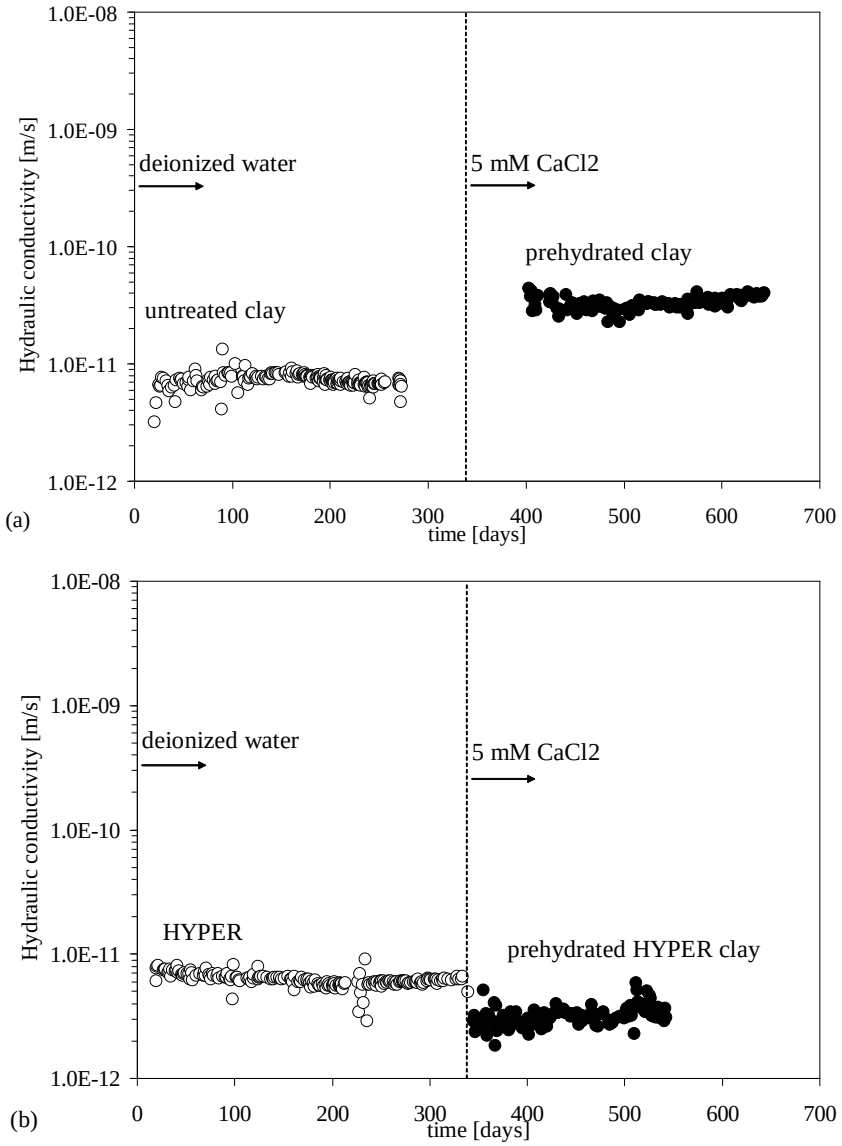

Figure 5.41: Hydraulic conductivity to 5 mM $CaCl_2$ solution of the (a) untreated clay and (b) of the HYPER clay after prehydration with water

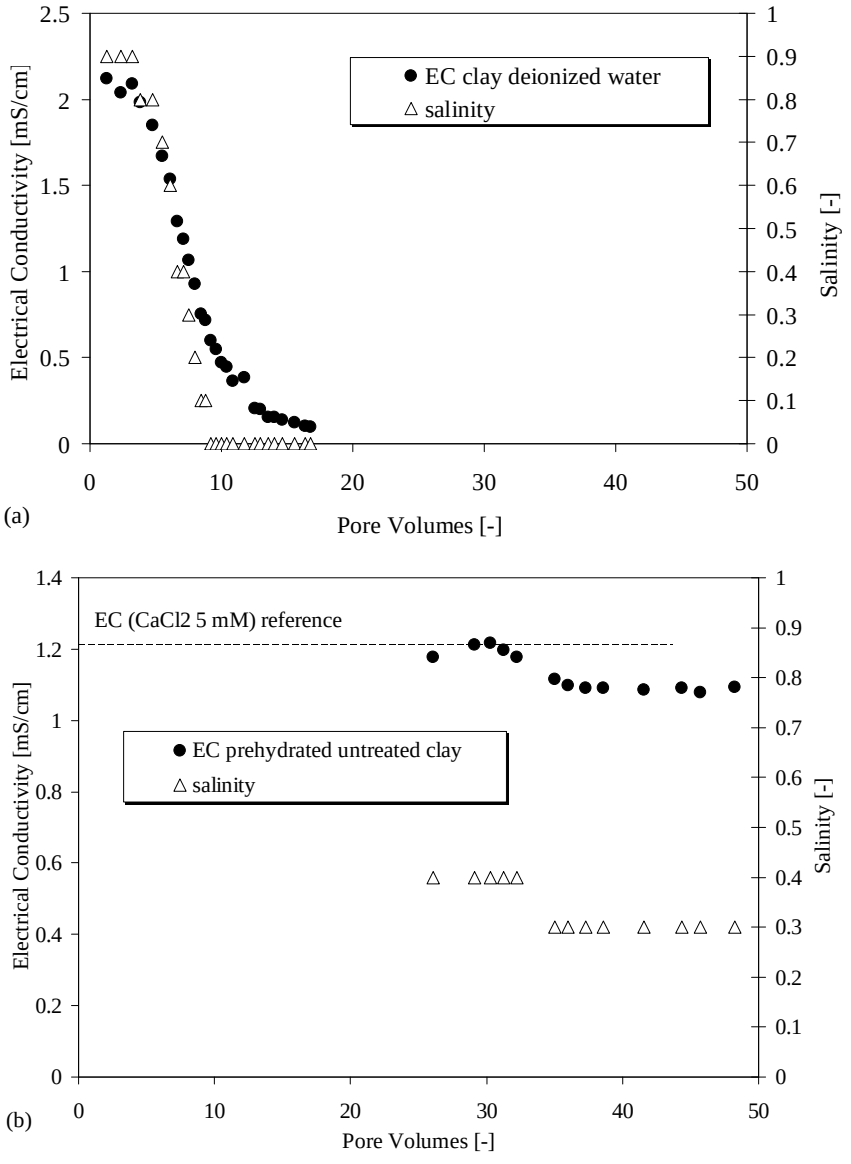

Figure 5.42: Electrical conductivity of the untreated clay during permeation with (a) deionized water and (b) $CaCl_2$ 5 mM

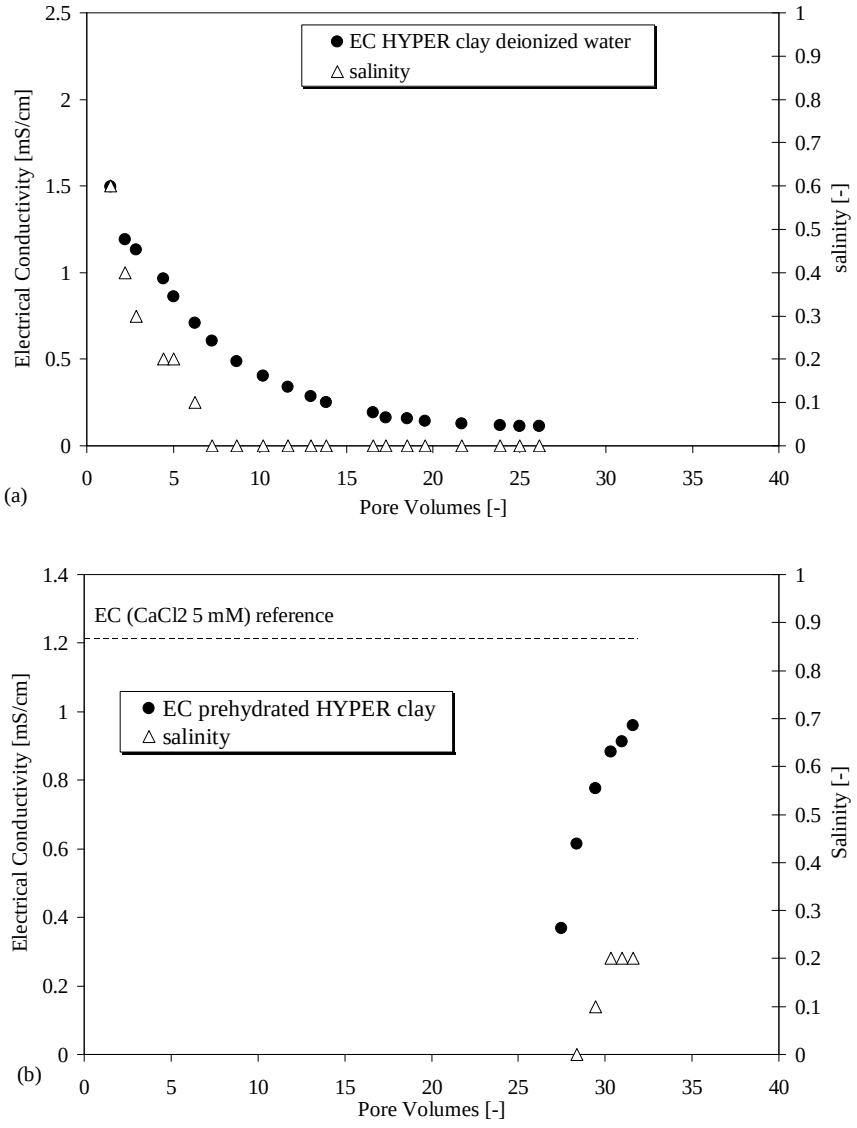

Figure 5.43: Electrical conductivity of the HYPER clay during permeation with (a) deionized water and (b) $CaCl_2$ 5 mM

MSB

Figure 5.44(b) shows the hydraulic conductivity of the MSB to a 5 mM $CaCl_2$ solution after 12.5 PV and 90.6 days of prehydration. The hydraulic conductivity to $CaCl_2$ of MSB was about one order of magnitude higher than to deionized water (k = 6 E−11 m/s vs. k = $1.53E^{-11}$ m/s). This hydraulic conductivity was unexpectedly slightly higher than that of the untreated clay to the 5 mM $CaCl_2$ solution after prehydration (k = $4.0\ E^{-11}$ m/s).

A possible explanation of this behavior may be that swelling of MSB occurs as water molecules are attracted inside the PC clouds that surround the interlayer cations (Onikata et al., 1999). During the initial hydration phase, the MSB specimen was allowed to swell freely with deionized water. Several molecular layers of water were attracted around the interlayer cations, which could have weakened the intermolecular bond between PC and interlayer cations, so that the PC could eventually have been released. Permeation with deionized water to prehydrate the sample may also have facilitated elution of PC from the soil.

The termination criteria for this test were fulfilled and the chemical equilibrium was established (Fig. 5.45).

5.4.4 Hydraulic conductivity of DPH GCL: impact of polymer treatment, prehydration and densification

This Section illustrates the hydraulic conductivity tests on the Dense Prehydrated GCL to study the impact of the simultaneous effect of polymer treatment, prehydration and densification.

In Section 5.2 we showed that the bentonite of the DPH GCL exhibited higher swelling capacity (both in terms of swell index and swell pressure) than conventional bentonites and even than the HYPER clay. Given the excellent hydraulic performance noticed for the HYPER clay, it is of great value to evaluate also the hydraulic performance of this DPH GCL.

A few studies available in literature (Schroeder et al., 2001; Kolstad et al., 2004; Katsumi et al., 2008) deal with compatibility tests on DPH GCLs. They showed that the nature of the tested permeating fluids had no major impact on the hydraulic performance of single sheet samples.

Moreover, the hydraulic conductivity of seams is crucial to the overall performance of GCLs as hydraulic barrier. To test correctly the efficiency of DPH GCL seams, large-scale laboratory hydraulic conductivity tests were conducted on full-scale overlap widths. The permeating fluids were deionized water, seawater and a series of $CaCl_2$ solutions.

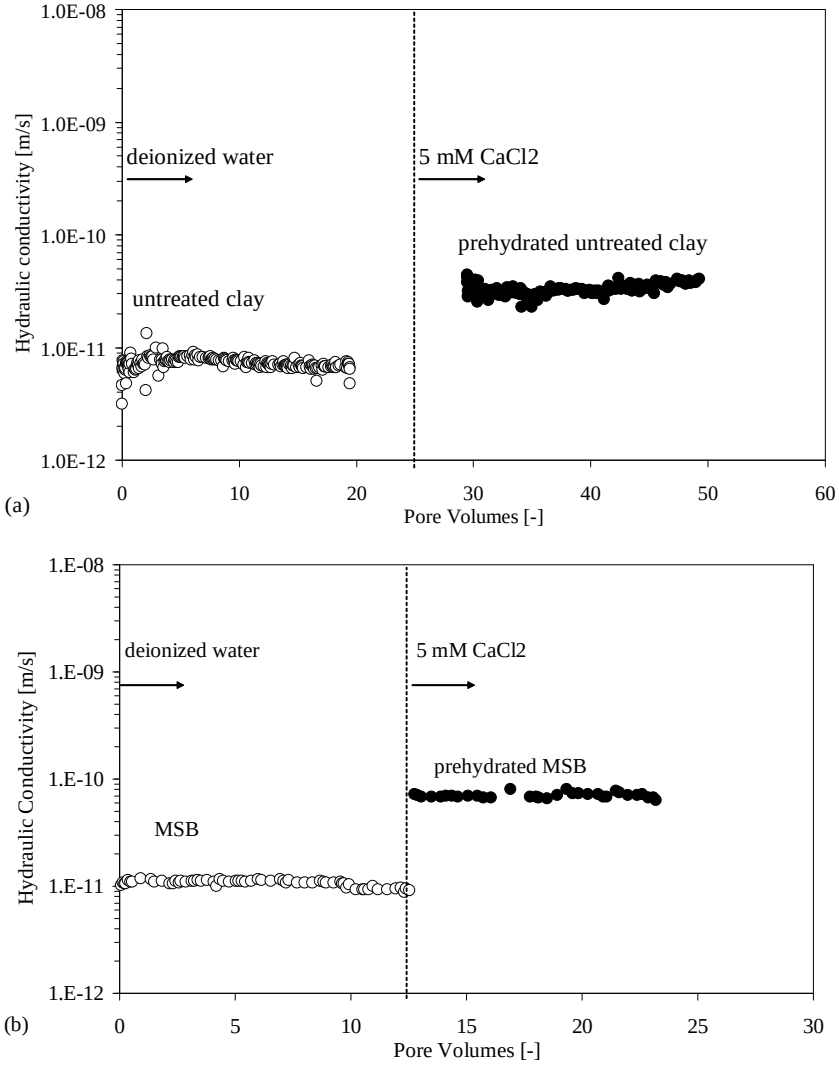

Figure 5.44: Hydraulic conductivity to 5 mM $CaCl_2$ solution of the (a) untreated clay and (b) of the MSB after prehydration with water

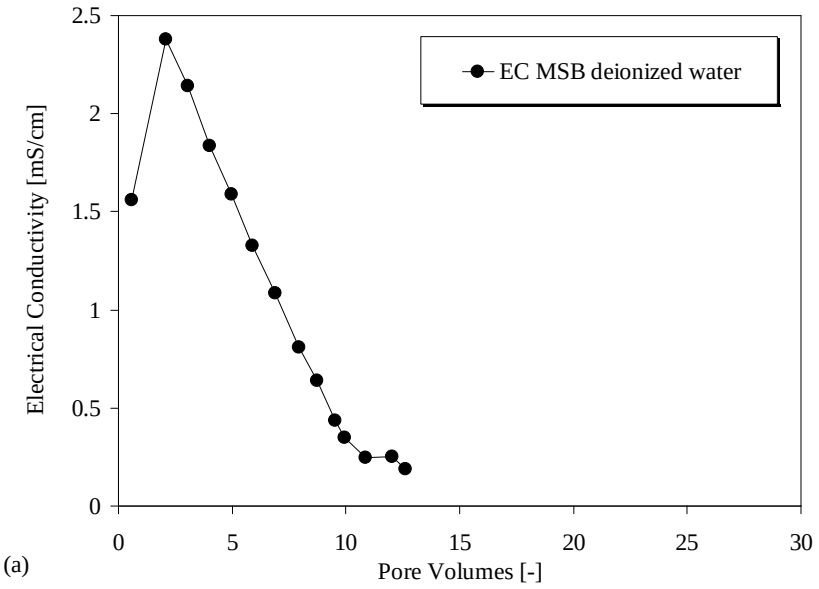

(a)

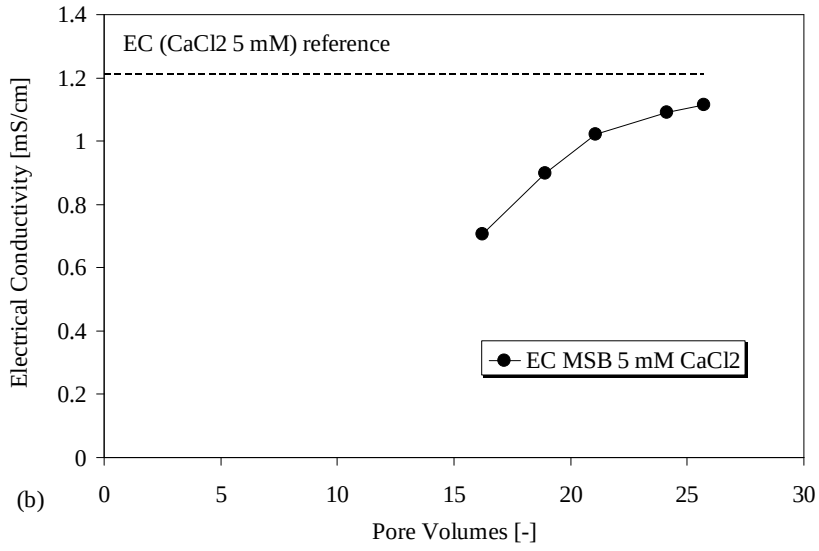

(b)

Figure 5.45: Electrical conductivity of the MSB during permeation with (a) deionized water and (b) $CaCl_2$ 5 mM

5.4.5 Hydraulic conductivity of DPH GCL single layer samples

Hydraulic conductivity tests on single sheet DPH GCL samples were conducted as a reference at the FIMET Department of the Universitá Politecnica delle Marche. These tests were performed in standard permeameters on 10 cm diameter samples with initial porosity $n_{initial}$=0.68. Deionized water, seawater and a $CaCl_2$ 0.0125 mM solution were used as permeants.

Figure 5.46(a) shows the hydraulic conductivity of the DPH GCL to the various permeant solutions. As shown in the figure, the hydraulic conductivity to sea water and $CaCl_2$ were very low. The hydraulic conductivity to deionized water was k = 2.02 E^{-11} m/s, to sea water was k = 1.39 E^{-12} m/s and to $CaCl_2$ was 5.86 E^{-12} m/s. The permeation with deionized water was continued here to finalize the removal of the soluble salts to prepare the sample for the chemico-osmotic test (as described further on in Section 5.5). The removal of soluble salts went on for 17 PV of flow corresponding to 1379 days of permeation (Fig. 5.46(b)). Whereas, the permeability test to sea water lasted 175.8 days (1.45 PV) and to $CaCl_2$ 533.1 days (4.32 PV).

These results indicate that the simultaneous effect of prehydration, polymer treatment and densification was able to maintain low hydraulic conductivities even in presence of aggressive solutions (such as the sea water and the $CaCl_2$ used in this experiment). These aggressive solutions are typically able to compress the DDL thickness of untreated clays increasing their permeability (as illustrated in Fig. 5.37, § 5.4.2).

The hydraulic conductivity of the DPH GCL to sea water was unexpectedly lower than that to deionized water. This result is probably due to high swelling capacity in deionized water compared to sea water. In other words, the final porosity of the sample (n_{final}) was higher in deionized water than in sea water. This difference was in fact evident by comparing the final porosity of the samples after the test, which was about n_{final}=0.77 in deionized water and n_{final}=0.45 in sea water (Fig. 5.46(a)).

The chemical equilibrium was not reached for the samples permeated with electrolyte solutions even after such extended testing period. These results may depend not only on the typical delay due to very low hydraulic conductivity and ion diffusion, but also on suspected microbial activity inside this samples. This aspect will be discussed in detail in Sections 5.4.7.

5.4.6 Large scale hydraulic conductivity tests on overlapped DPH GCL samples

The efficiency of the overlapped area of the DPH GCL was studied by means flexible wall hydraulic conductivity tests in large-scale laboratory permeameters. 30.5 cm diameter samples with 10 cm overlap seam (actual width expected in the

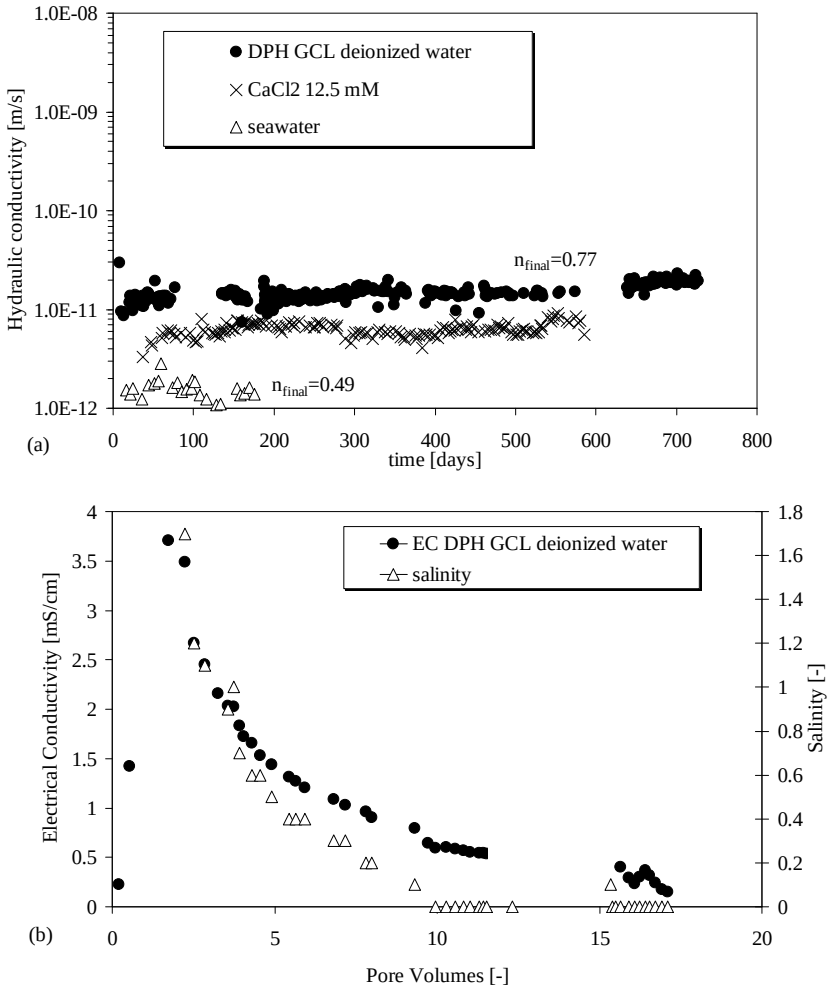

Figure 5.46: The hydraulic conductivity of single sheet DPH GCL to deionized water, $CaCl_2$ and seawater. The polymer treatment, prehydration and densification maintained the permeability to electrolyte solutions and deionized water comparable

site) were tested at a confining effective stress σ'=14 kPa. The permeant solutions used were deionised water and and sea water.

The performance of the overlap was studied in two scenarios: (1) with an added bentonite paste at the contact zone in the overlap and (2) without bentonite paste.

To test the impact of the effective stress on the mechanical seal of the overlap, the hydraulic conductivity was evaluated increasing the effective stress in 4 steps (14 kPa, 28 kPa, 55 kPa, 110 kPa).

In parallel, medium-scale hydraulic conductivity tests were also conducted. 14 cm diameter samples with 5 cm overlap were tested in a rigid wall oedometer/permeameter with an effective stress σ'=14 kPa. The permeant solutions used were a series of $CaCl_2$ solutions (0.01 M, 0.02 M and 0.1 M).

Table 5.4 shows an overview of the tests performed and the results in terms of hydraulic permittivity, Pore Volumes of flow and test duration. The permittivity is defined as the ratio between the hydraulic conductivity and the average specimen thickness. The use of the permittivity was advantageous to assess the hydraulic performance of DPH GCL overlaps because the thickness, that is not constant, does not need to be measured or estimated.

Large-scale DPH GCL overlap

Figure 5.47 shows the hydraulic permittivity of the DPH GCL overlap samples permeated with deionized water and sea water compared to the permittivity to deionized water of a single sheet sample. The permittivity of the overlap to deionized water (Ψ=8.85 E^{-10} s^{-1}) was comparable to that of the single sheet sample (Ψ=2.58 E^{-9} s^{-1}), whereas the permittivity to sea water of the overlap (Ψ=3.68 E^{-6} s^{-1}) after few days of permeation was about 3 orders of magnitude higher than that of the single sheet sample.

The swell index of the bentonite from the DPH GCL in sea water was very low (SI = 8.3 ml/2g) with respect to that observed in deionized water (SI = 16 ml/2g). However, prehydration with addition of polymers and densification during manufacturing of the DPH GCL maintained low hydraulic conductivities on the single sheet samples even in presence of sea water.

The key factor to assure low hydraulic permittivity of the overlapped samples is the self-sealing capacity at the interface between the two GCL layers. In deionized water the DPH GCL bentonte showed a high swell potential, enough to pass through the supporting geotextile net and to effectively adhere both DPH GCL overlapped layers.

Conversely, in sea water the DPH GCL bentonite showed a reduced swell potential which was not sufficient to ensure good sealing. As a result, a preferential flow path through the overlap may have occurred.

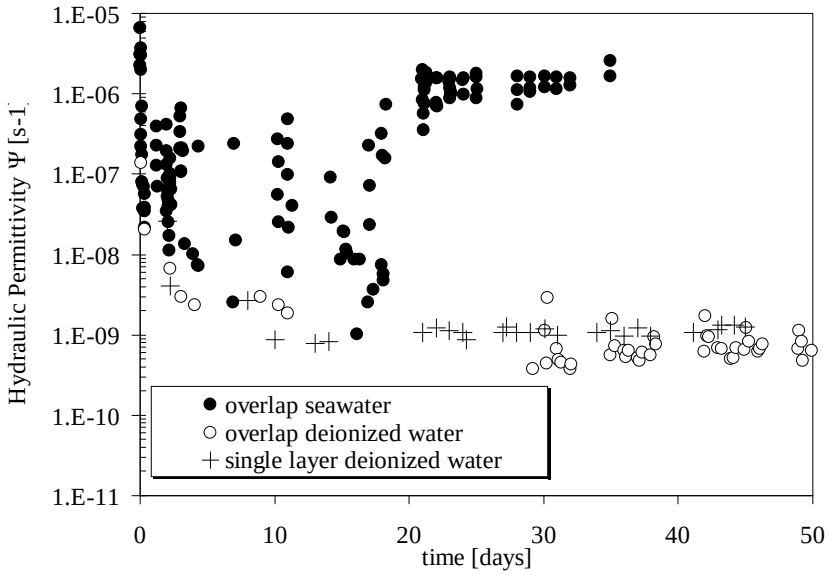

Figure 5.47: Hydraulic permittivity of the DPH GCL overlap compared to the single sheet sample

Impact of the effective stress on the hydraulic performance of the DPH GCL overlap

The impact of the effective stress on the mechanical seal of the overlap was evaluated by increasing the effective stress in 4 steps (σ'=14 kPa; 28 kPa; 55 kPa; and 110 kPa).

Figure 5.48 shows the impact of the effective stress on the hydraulic performance of the overlap samples. As expected, a decrease of the hydraulic conductivity was noticed (for both deionized water and sea water) with increasing effective stress from 14 kPa up to 110 kPa. The permittivity to deionized water decreased from $\Psi = 8.85\ E^{-10}\ s^{-1}$ to $\Psi = 1.67\ E^{-10}\ s^{-1}$, whereas that to sea water decreased from $\Psi = 3.68\ E^{-6}\ s^{-1}$ to $2.51\ E^{-7}\ s^{-1}$. The permittivity obtained are shown in detail in Table 5.4.

Even though the permittivity of the overlap decreased with increasing effective stress, the hydraulic efficiency to sea water did not achieve the efficiency of a single sheet.

At the end of these series of tests, a colored dye was added to the influent solution to stain the flow paths of the overlapped sample permeated with sea water. Inspection of the GCL during disassembly showed that the colored dye, at the outlet of the sample, was present only at the overlapped area, indicating that the flow

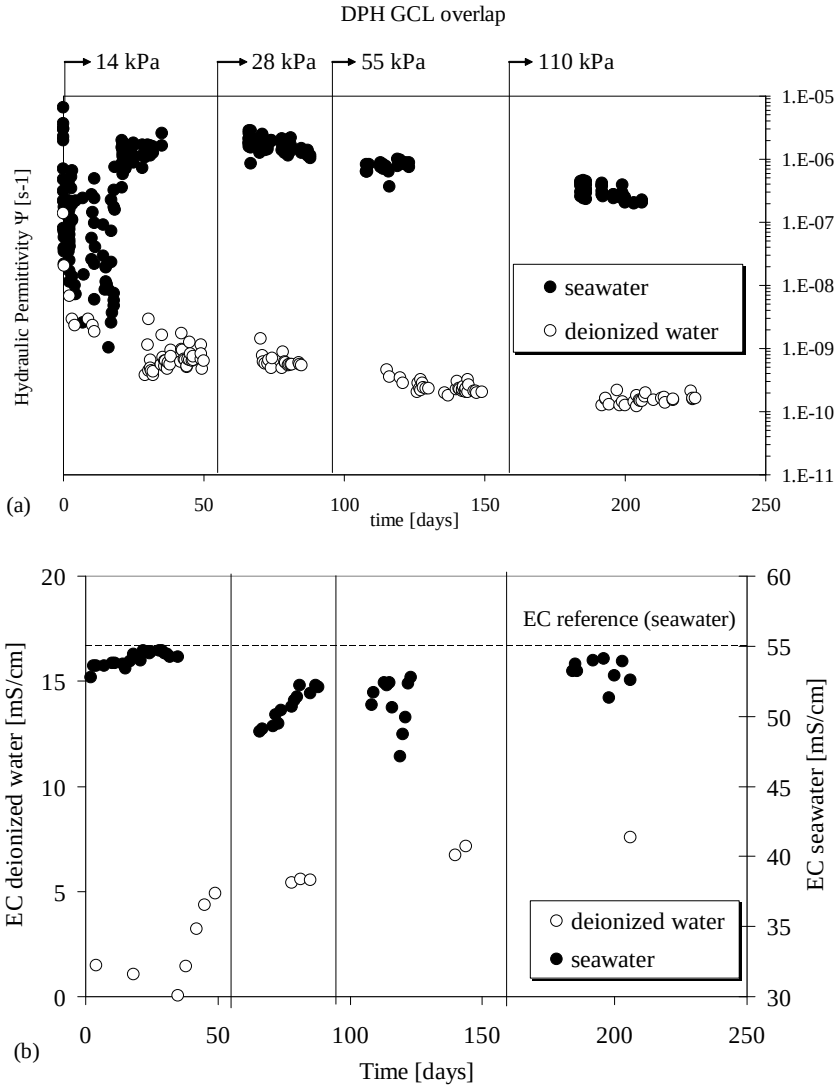

Figure 5.48: (a) Hydraulic permittivity of the DPH GCL overlap without bentonite paste in 4 effective stress steps and (b) Electrical conductivity of the outlet

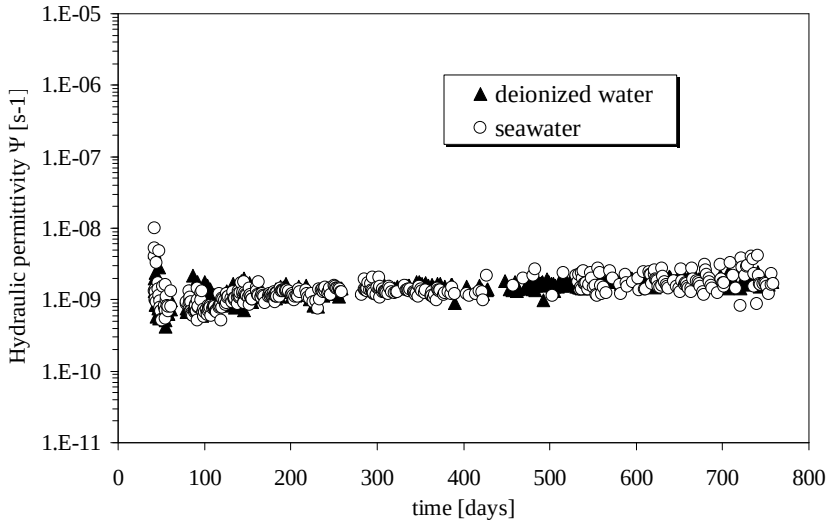

Figure 5.49: Hydraulic permittivity of the DPH GCL overlap with bentonite paste

was primarily passing through the overlap causing the high permittivity detected.

DPH GCL overlap with bentonite paste

To improve the overlap sealing in presence of sea water, the impact of the addition of bentonite paste was evaluated.

Figure 5.49 shows the hydraulic conductivity to deionized water and sea water of the DPH GCL overlap samples. The addition of the bentonite paste improved considerably the overlap efficiency to sea water. The permittivity to sea water was in fact Ψ=1.46 E^{-9} s^{-1} comparable to that to deionized water, which was Ψ=1.44 E^{-9} s^{-1}.

This result was maintained after 12.85 Pore volumes of flow corresponding to a test duration of 758.3 days.

DPH GCL overlap to $CaCl_2$ solutions (without bentonite paste)

Figure 5.50 shows the hydraulic permittivity of the DPH GCL overlap samples permeated with a series of $CaCl_2$ solutions. The permittivity of the overlap to $CaCl_2$ 0.01 M was Ψ = 6.7 E^{-10} s^{-1} (after 9.64 PV and 291 days), that to $CaCl_2$ 0.02 M was Ψ = 7.7 E^{-10} s^{-1} (after 1.05 PV and 111 days) and that to $CaCl_2$ 0.1 M was Ψ = 9.4 E^{-10} s^{-1} (after 8.24 PV and 427). These permittivities were all comparable to that of the single sheet samples (Ψ = 2.58 E^{-9} s^{-1}).

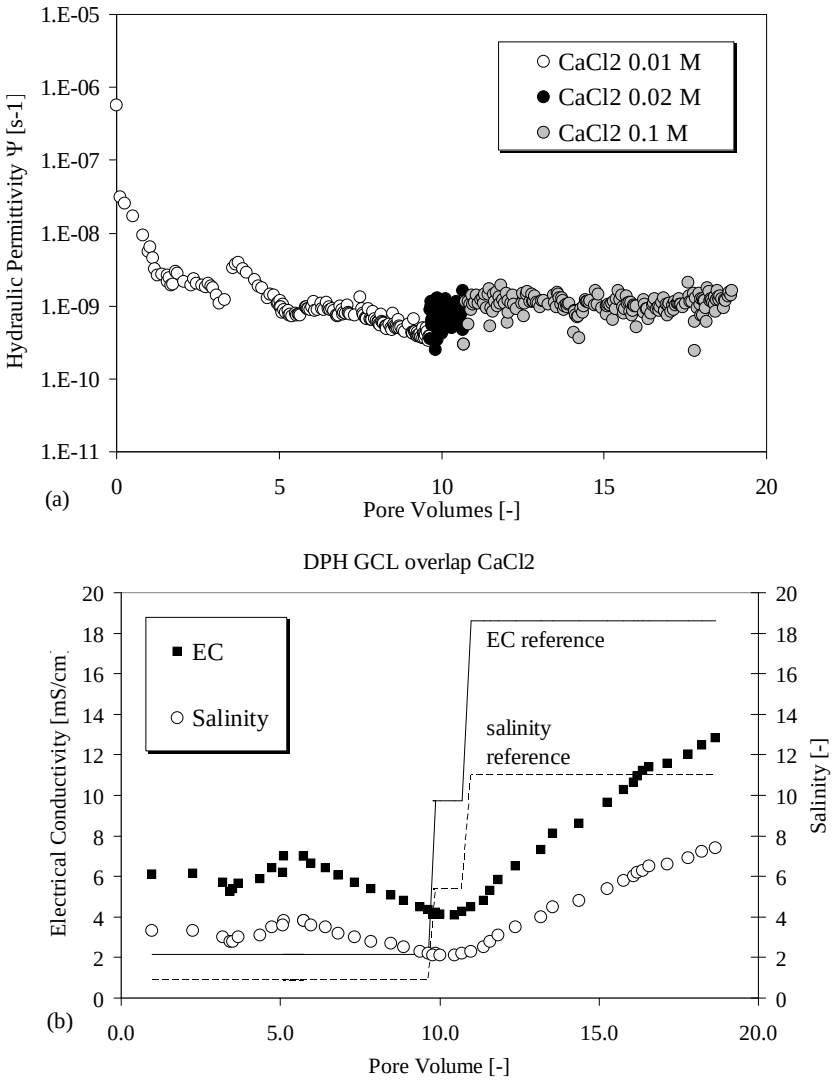

Figure 5.50: (a) Hydraulic permittivity of the DPH GCL overlap without bentonite paste to $CaCl_2$ solutions and (b) Electrical conductivity of the outlet

The swell index of the bentonite obtained from the DPH GCL in the 0.1 M $CaCl_2$ solution was very low (SI = 9 ml/2g) similar to that obtained in sea water (8.3 ml/2g). Even though, the permittivity of the overlapped sample permeated with 0.1 M $CaCl_2$ showed a good sealing behaviour, indicating that the overlap sealed well even without bentonite paste. This ovelap sealing was probably improved by the previous prehydration with $CaCl_2$ 0.01 M. In fact, the swelling ability of the DPH GCL in 0.01 $CaCl_2$ was sufficiently high (SI = 28 ml/2g) with a consequent beneficial effect on the sealing of the overlap in presence of 0.1 M $CaCl_2$.

5.4.7 Chemical equilibrium

DPH GCL overlap

Up to the end of the test on the overlap to deionized water (without bentonite paste), the chemical equilibrium was not reached even after 225 days of permeation corresponding to almost 2 Pore Volumes of flow (open dots in Fig. 5.48(b)). The pH was in fact acidic (pH=4.93) compared to the deionized water (pH = 8.21), the electrical conductivity was 7.56 mS/cm higher than that to deionized water (EC lower than 10 μS/cm), the salinity was about 3 which was higher than that of deionized water that (with the accuracy of the instrument) was zero.

The concentrations of ions at the end of the third stage (55 kPa) was measures. These concentrations were: Na^+ = 150 mg/l, Ca^{2+} = 410 mg/l, SO_4^{2-} = 465 mg/l. Such high electrical conductivity was probably due not only to the presence of a large amount of soluble ions and other compounds in the pore water of this GCL, but also to bacterial reactions in anaerobic conditions. Gas bubbles were in fact observed in the lines, probably as a result of microbial activity.

Neither the chemical equilibrium of the overlap permeated with sea water was achieved, even after more than 200 days of permeation. Although the chemical equilibrium was reached for the electrical conductivity (black dots in Fig. 5.48(b)), the pH was acidic (pH = 5.79) compared to the inlet solution (pH = 7.94). After about 15 pore volumes of flow, the concentration of SO_4^{2-} ions was analyzed and was $C_{SO_4^{2-}}$=2300 mg/L lower than $C_{SO_4^{2-}}$=2420 mg/l of the inlet solution (sea water). The acidic pH and the low $C_{SO_4^{2-}}$ at the outlet compared to the inlet solution, may be due to redox reactions inside the sample during permeation.

To analyze these phenomena, the redox-potential (Eh) and the pH of the outlet were plotted on the redox stability diagram for sulfur. Following the arrow in the stability diagram (Fig. 5.51), reducing conditions were observed in the outlet. The outlet (represented by black dots in Fig. 5.51) moved in fact in the diagram from the area of pH and Eh values typical of solutions containing SO_4^{2-} to the area of solutions containing H_2S.

This reducing conditions are consistent with the decrease of the concentration

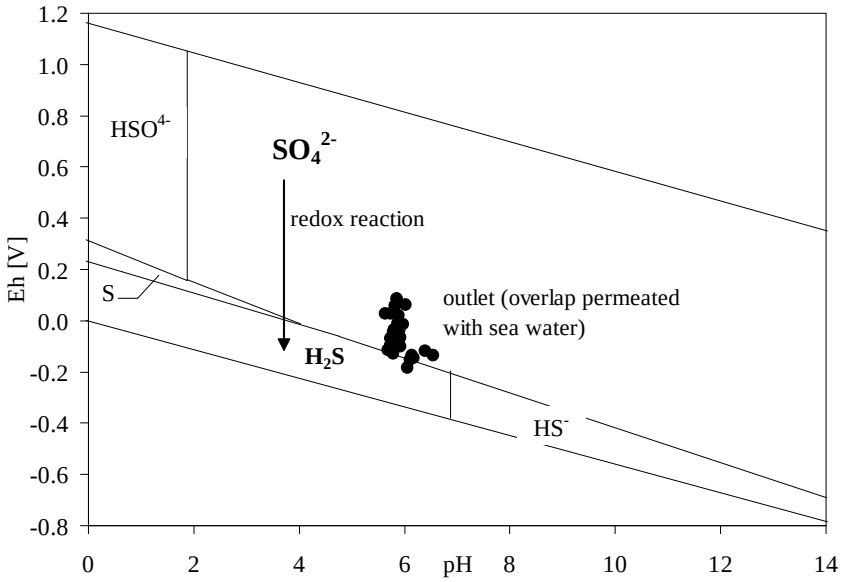

Figure 5.51: Stability diagram for Sulfur: bacterial redox reactions

of sulfate (SO_4^{2-}) inside the sample. Moreover, typical odor of hydrogen sulfide was indeed noticed during sampling of the outlet. Therefore, the reduction of SO_4^{2-} to hydrogen sulfide (H_2S) probably occurred inside the sample. Given that the sample was in anaerobic conditions, H_2S may have resulted from the bacterial breakdown of organic matter in the absence of oxygen. Gas bubbles were in fact observed in the lines, probably due to microbial activity.

Bacterial activity may indeed reduce SO_4^{2-} to S^{2-} (and as a consequence to H_2S) according to the following chemical reaction:

$$2CH_2O + SO_4^{2-} \rightarrow 2HCO_3^- + H_2S \tag{5.41}$$

DPH GCL overlap with bentonite paste

The tests on the overlap with bentonite paste and permeated with deionized water did not achieve either the chemical equilibrium even after 758.3 days of permeation, corresponding to 12.6 Pore Volumes of flow (Fig. 5.52(a)). The electrical conductivity of the outlet was in fact EC = 2.33 mS/cm higher than that of the inlet (deionized water) that was lower than 10 μS/cm.

Whereas, the sample permeated with sea water did achieve the chemical equilibrium for the electrical conductivity after 758.3 days of permeation corresponding to 12.85 Pore Volumes of flow (Fig. 5.52(b)). But the pH was still acidic

(pH = 6.04, see also Appendix B), probably as a result of microbial reactions in anaerobic conditions.

DPH GCL overlap permeated with $CaCl_2$ solutions

The sample permeated with $CaCl_2$ did not achieve chemical equilibrium at the time of the thesis publication (Fig. 5.50(b)). The electrical conductivity was in fact EC_{outlet} = 4.35 mS/cm after about 10 Pore Volumes of permeation with $CaCl_2$ 0.01 M (which has an EC_{inlet} = 2.14 mS/cm) and was EC_{outlet} = 12.84 mS/cm after about 10 Pore Volumes of permeation with $CaCl_2$ 0.1 M (which has an EC_{inlet} = 18.62 mS/cm) that is still ongoing. For this reason the test will be continued to study the long term performance in $CaCl_2$ 0.1 M solution.

Whereas the chemical equilibrium for the pH was achieved after 5 Pore volumes of flow (see Appendix B).

Gas control

Gas bubbles arose from the inlet and the effluent lines during the permeability tests on the DPH GCL. This phenomenon was probably due to microbial reactions. Permeant solutions spiked with 500 ppm of biocide were suggested by Nelson (2000) and Jo et al. (2005) to eliminate biological activity during hydraulic conductivity testing without inducing alteration of their results.

We attempted five different methods to eliminate gas bubbles:

1. increasing the back pressure,
2. increasing the hydraulic head,
3. flushing the inlet and effluent lines,
4. using a 500 ppm solution of biocide,
5. cooling the samples at 4°C.

As a first approach, to eliminate the gas bubbles, the back pressure was increased from 70 kPa to 340 kPa but the problem was not solved.

Then, daily flushing of the inlet and effluent lines was necessary to eliminate the bubbles temporarily.

The hydraulic head was then increased from 70 cm to 200 cm. But the problem was completely solved only after adding 500 ppm antimicrobial biocide to the inlet solution.

The use of biocide did not alter the permittivity measured. On single sheet samples, the permittivity to deionized water was in fact Ψ= 7.61 E^{-10} s^{-1} and to 500 ppm biocide was Ψ= 7.72 E^{-10} s^{-1}.

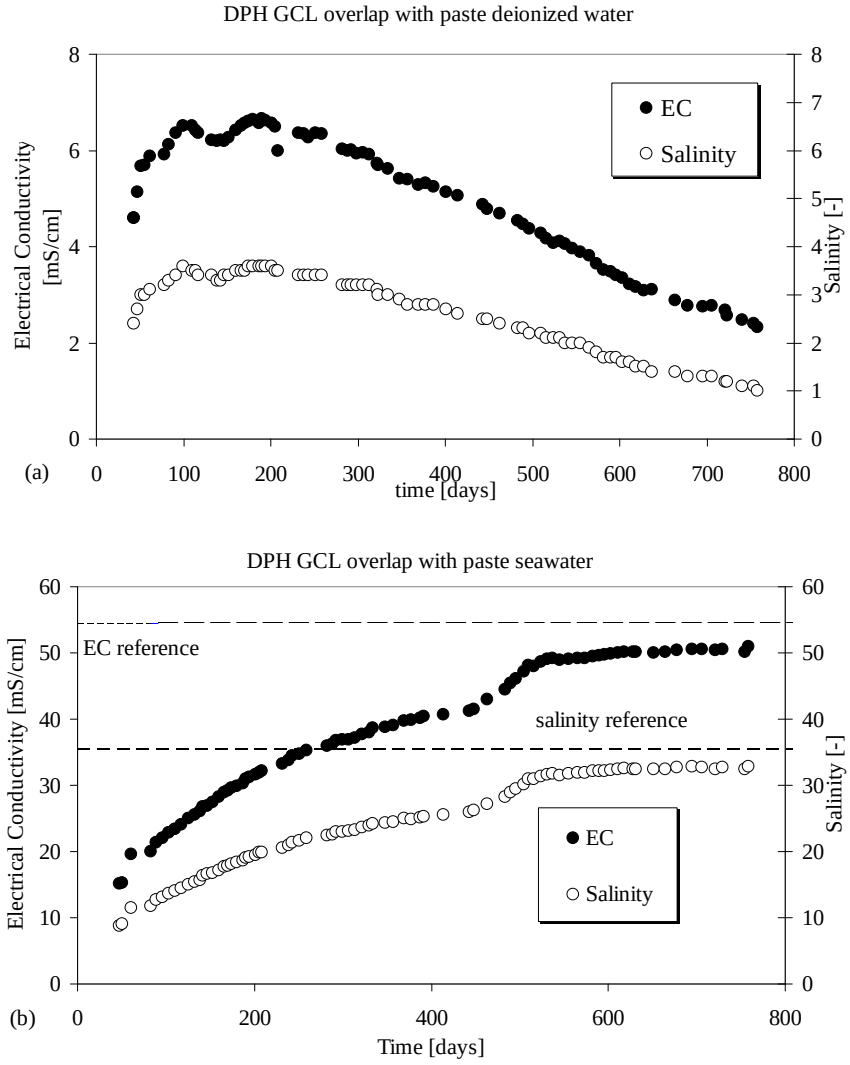

Figure 5.52: Electrical permittivity of the outlet of the hydraulic conductivity test on the DPH GCL overlap with bentonite paste permeated with (a) deionized water and (b) seawater

Benson and Wang (2000) eliminated the fluctuations caused by gas formation by performing hydraulic conductivity tests in a refrigerator at 4°C. We followed the same principle on the 10 cm diameter sample permeated with deionized water. The test was stopped and the sample was stored at 4°C for some months. Later, the test was restarted showing no problems of gas formation any more but with a slight increase of the hydraulic conductivity.

Increasing the back pressure, increasing the hydraulic head and the daily flushing appeared to remove temporarily the gas bubbles; however, these methods did not remove the gas formation source. Whereas, the use of the biocide or the refrigeration proved to be more successful allowing the outflow-to-inflow ratio became steady with no fluctuations caused by the gas.

5.4.8 Summary of the hydraulic conductivity test results

Figure 5.53 shows a summary of the hydraulic conductivity test results on the DPH GCL samples. The figure compares the hydraulic conductivity of the DPH GCL single sheet samples, the overlap and the overlap with paste.

As shown in the figure, the permittivity for the single sheet samples were very low even in presence of sea water and a $CaCl_2$ solution 0.0125 M. The permittivity of the overlap to deionized water and $CaCl_2$ 0.1 M were comparable to that of the single sheet, whereas the permittivity to sea water was about three orders of magnitude higher. Conversely, the hydraulic performance in sea water of the overlap sealing was considerably improved by the use of bentonite paste (Fig. 5.53).

The swell volume observed in sea water was very low compared to that observed in deionized water. Even though the prehydration with addition of polymers and the densification of the DPH GCL preserved low hydraulic conductivities for single sheet samples, the swell mechanisms was of fundamental importance to guarantee a good sealing of the overlap area in sea water. For these reasons it is strongly recommended the use of bentonite paste to seal the overlap.

5.4.9 Long term hydraulic efficiency of modified clays and prospectives for chemico-osmotic efficiency

At constant total porosity, compression of the double layers thickness results in an increase of the fraction of pore space available to water transport (high hydraulic conductivity) and a reduction of the pore space restricted to ions (low chemico-osmotic efficiency). Conversely, the decrease in permeability may suggest a potential increase in chemico-osmotic efficiency.

The effect of invading salts has also important implications in terms of the long-term hydraulic performance of GCLs. For example, in Fig. 5.54 hydraulic conductivity test results of GCLs permeated with $CaCl_2$ solutions are shown. The graph on top shows the hydraulic conductivity of non prehydrated samples, whereas

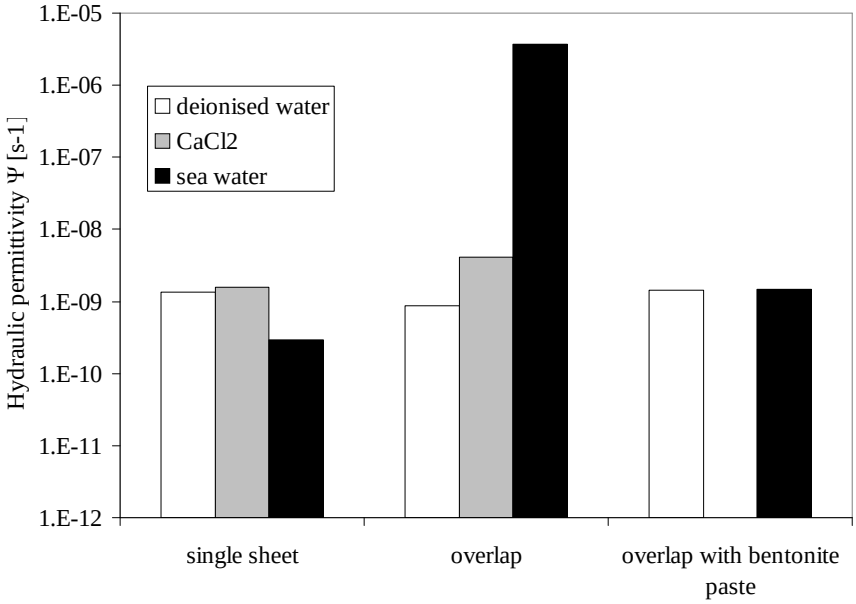

Figure 5.53: Overview of the hydraulic conductivity test results of the DPH GCL

Hydraulic conductivity on non-prehydrated samples [m/s]		
sample	5 mM $CaCl_2$	sea water
untreated clay	$3.53E^{-11}$	$6.0E^{-10}$ *
PV	2.2	19
time [days]	148.8	290
HYPER clay	$1.37E^{-11}$	$4.17E^{-11}$
PV	1.25	25.5
time [days]	156.9	544.7
clay+8%Na-CMC	$7.03E^{-12}$	
PV	0.17	
time [days]	103	
MSB	$4.59E^{-11}$	
PV	2.46	
time [days]	143	

Table 5.2: Hydraulic conductivity test results. Flexible wall permeameter, effective stress $\sigma' = 14$ kPa, initial porosity n=0.718.
**n=0.69 and $\sigma' = 15$ kPa (Mazzieri and Pasqualini, 2006)*

Hydraulic conductivity on samples prehydrated with deionized water [m/s]

sample	deionized water	5 mM $CaCl_2$
untreated clay	6.42 E^{-12}	4.02E^{-11}
PV	19.46	28
time [days]	276	359.58
HYPER clay	6.5 E^{-12}	3.1E^{-12}
PV	26.7	5.3
time [days]	334	200
MSB	1.53E^{-11}	6E^{-11}
PV	12.55	10.14
time [days]	90.65	160.36

Table 5.3: Hydraulic conductivity test results. Rigid wall permeameter, fixed height, porosity n=0.718

the graph below shows the hydraulic conductivity to $CaCl_2$ solutions of samples prehydrated for more than one year with deionized water.

The time required for the hydraulic conductivity of prehydrated samples to loose their improved performance ranged between 1 to 1.7 yrs (Fig. 5.54, graph below). This result means that the beneficial effect of prehydration can be lost.

The effect of partial or complete destruction of membrane behavior due to diffusion of invading cations illustrated in Fig. 5.55 is similar to the effect of permeation with salt solutions on the hydraulic conductivity of GCLs as shown in Fig. 5.54.

Thus, an important issue that warrants further attention is how to alter or otherwise modify the composition or structure of bentonite such that the adsorbed layer of cations associated with the bentonite particles can resist collapse and also the existence of any membrane behavior can be sustained.

The hydraulic conductivity of the HYPER clay to sea water remained constant after 545 days of permeation (Fig. 5.39 in §5.4.2), as that of the DPH GCL overlap with paste, that was preserved after 758 days of permeation with sea water (Fig. 5.49 in §5.4.6) and after 427 days with $CaCl_2$ (Fig. 5.50 in §5.4.6).

Therefore, a low permeability protracted in the long term, may suggest that also the chemico-osmotic efficiency of the HYPER clay and of the DPH GCL will be maintained with time even in presence of aggressive solutions (e.g. exchanging Ca^{2+} with the Na^{+} of the clay).

Hydraulic Permittivity (Ψ) on DPH GCL samples

	single sheet	overlap	overlap with paste
deionized water			
$\Psi_{(\sigma'=14kPa)}$ [s^{-1}]	2.58 E^{-9}	8.85 E^{-10}	1.44 E^{-9}
Pore Volumes	17	1	12.59
time [days]	1379	50	758.3
$\Psi_{(\sigma'=28kPa)}$ [s^{-1}]		4.92 E^{-10}	
$\Psi_{(\sigma'=55kPa)}$ [s^{-1}]		1.95 E^{-10}	
$\Psi_{(\sigma'=110kPa)}$ [s^{-1}]		1.67 E^{-10}	
sea water			
$\Psi_{(\sigma'=14kPa)}$ [s^{-1}]	2.63E^{-10}	3.68 E^{-6}	1.46 E^{-9}
Pore Volumes	1.45	17.73	12.85
time [days]	175.8	35	758.3
$\Psi_{(\sigma'=28kPa)}$ [s^{-1}]		1.45 E^{-6}	
$\Psi_{(\sigma'=55kPa)}$ [s^{-1}]		1.06 E^{-6}	
$\Psi_{(\sigma'=110kPa)}$ [s^{-1}]		2.51 E^{-7}	
0.0125 M $CaCl_2$			
$\Psi_{(\sigma'=14kPa)}$ [s^{-1}]	1.09E^{-9}		
Pore Volumes	4.32		
time [days]	533.1		
0.01 M $CaCl_2$			
$\Psi_{(\sigma'=14kPa)}$ [s^{-1}]		6.7 E^{-10}	
Pore Volumes		9.64	
time [days]		291	
0.02 M $CaCl_2$			
$\Psi_{(\sigma'=14kPa)}$ [s^{-1}]		7.7 E^{-10}	
Pore Volumes		1.05	
time [days]		111	
0.1 M $CaCl_2$			
$\Psi_{(\sigma'=14kPa)}$ [s^{-1}]		9.4 E^{-10}	
Pore Volumes		8.24	
time [days]		427	

Table 5.4: Hydraulic conductivity test results on DPH GCL samples. Flexible wall permeameter, initial porosity n=0.64

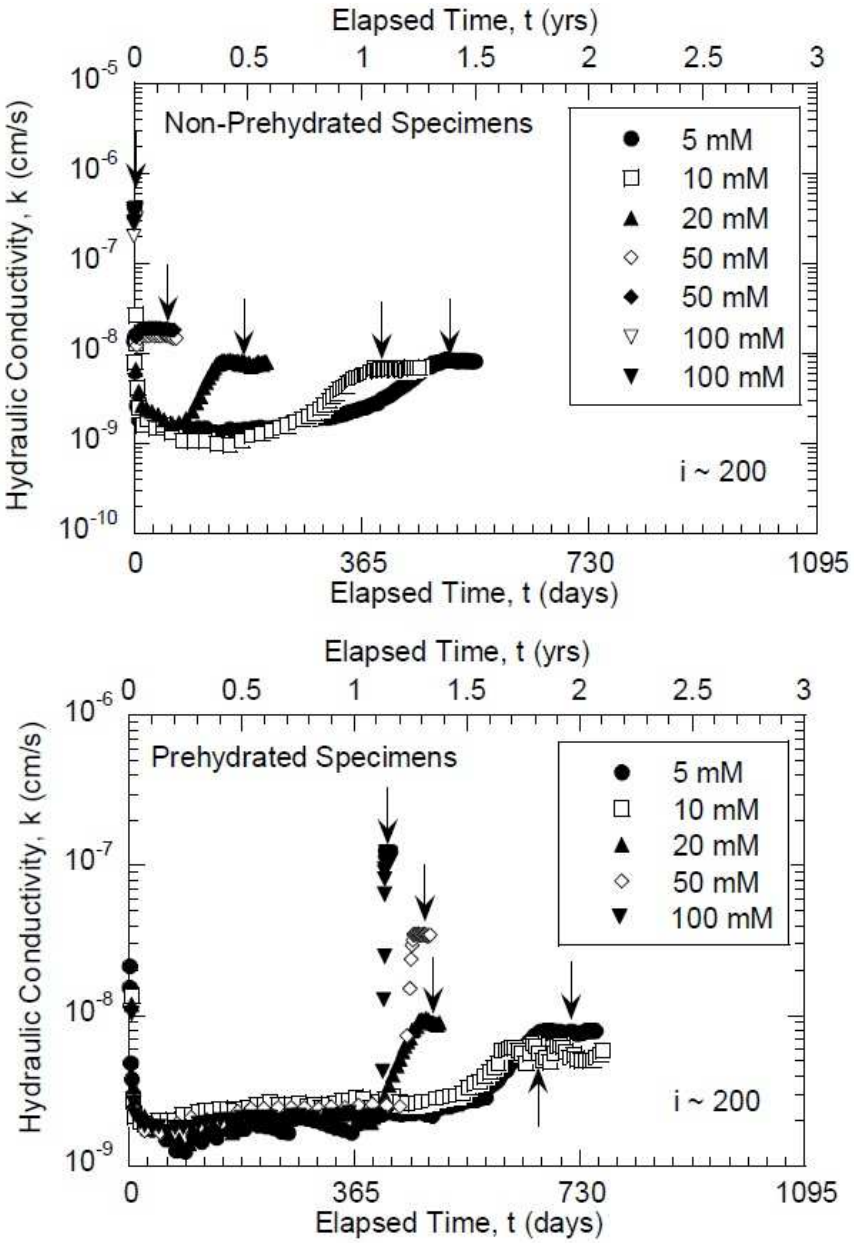

Figure 5.54: Long term hydraulic conductivity of non-prehydrated and prehydrated GCLs permeated with calcium chloride ($CaCl_2$) solutions, data from Lee (2004); time corresponding to establishment of chemical equilibrium designated by arrows (Shackelford, 2005)

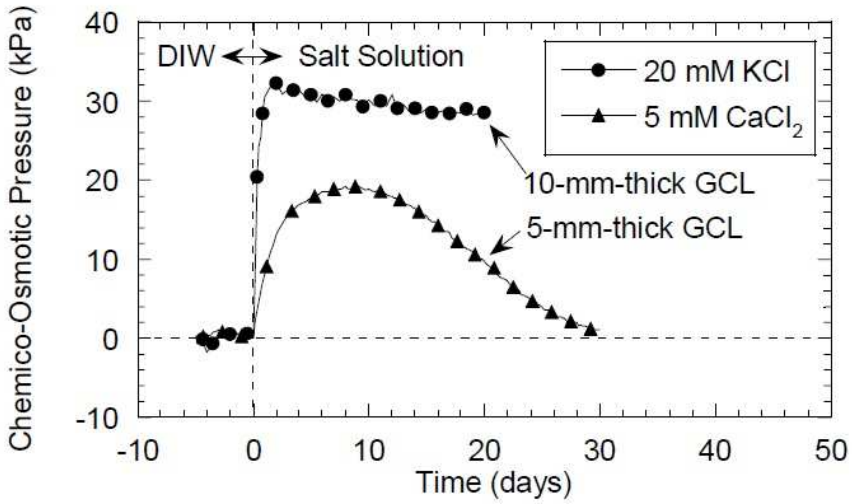

Figure 5.55: Temporal trends in chemico-osmotic pressure difference for monovalent (K+) and divalent (Ca^{2+}) cations invading the bentonite contained in two GCLs during chemico-osmotic membrane tests (Malusis and Shackelford, 2002a; Shackelford and Lee, 2003; Shackelford, 2005)

5.5 Chemico-osmotic performance of polymer treated clays

As mentioned in the Methods Section, a series of multiple-stage chemico-osmotic tests were conducted in this study to analyze the effect of polymer addition on the chemico-osmotic efficiency. Multiple-stage chemico-osmotic tests were conducted on the following samples:

- untreated clay
- HYPER clay, clay treated with 2% of anionic polymer (Na-CMC)
- MSB, clay treated with 25% Propylene Carbonate (PC), Hojun corp. Japan
- DPH GCL, manufactured GCL prehydrated with polymeric solution and densified

In every test the initial porosity of the sample was equal (n=0.718), except for the DPH GCL with a lower porosity (n=0.68). The lower porosity allowed to analyze the impact not only of polymer treatment but also of densification on the chemico-osmotic efficiency.

Multiple-stage tests were chosen to investigate the impact of the solute concentration gradient (ΔC_1=1 mM and ΔC_2 = 5 mM) of the $CaCl_2$ solution across the specimen on the chemico-osmotic efficiency and on the transport parameters

5.5.1 Chemico-osmotic efficiency of a non-treated bentonite clay: impact of ion concentration

Induced differential pressures and chemico-osmotic efficiency

The initial stage of every test consists of circulation of purified water through both porous stones at the opposite ends of the specimen in order to measure a reference differential pressure and to remove residual soluble salts. Although a concentration gradient was not applied across the specimen during this stage, a slight induced pressure difference was observed. In this study the baseline pressure difference was of the order of $-\Delta P_{ref}$=1 kPa to 5 kPa. These values were similar to those observed by Olsen (1969); Malusis et al. (2001). This non-zero baseline pressure difference has been attributed not only to possible residual salt content in the porous stones but also, as stated also by Malusis et al. (2001), to different hydraulic resistances of the two porous stones and/or small deviation from the no-flow condition assumed, due to slight differences in the dimensions of the cylinder actuators. The head losses in each stone are not exactly the same, typically resulting in a slight recorded pressure difference across the specimen. In either case, this non-zero baseline pressure difference was not included when evaluating the chemico-osmotic efficiency.

The measured differential pressures induced across the non-treated clay sample in the multiple-stage test are presented in Fig. 5.56(a). The corresponding chemico-osmotic efficiencies are plotted vs. time in Fig. 5.56(b). After replacing the purified water circulating across the top of the specimen with the first 1 mM $CaCl_2$ electrolyte solution (at t=0 in Fig. 5.56), the induced pressure difference increased immediately and continued to increase gradually to a maximum value, $-\Delta P_{max}$=4.1 kPa, corresponding to a maximum chemico-osmotic efficiency coefficient, ω_{max}=0.56. Subsequently, the induced pressure difference and corresponding chemico-osmotic efficiency gradually decreased to steady-state values, $-\Delta P_{ss}$ = 2.1 kPa and ω_{ss} = 0.29, that remained constant up to 60 days when the next stage started.

As expected, the maximum differential pressure value increased from $-\Delta P_{max1}$ = 4.1 kPa to $-\Delta P_{max2}$ = 4.4 kPa as the $CaCl_2$ concentration source solutions circulated on the top of the specimen increased from ΔC_1=1 mM to ΔC_2=5 mM $CaCl_2$. An increase of the maximum differential pressure occurs also for monovalent electrolyte source solutions, such as KCl, studied in a similar test by Malusis and Shackelford (2002a).

On the other hand, both the maximum and steady-state chemico-osmotic effi-

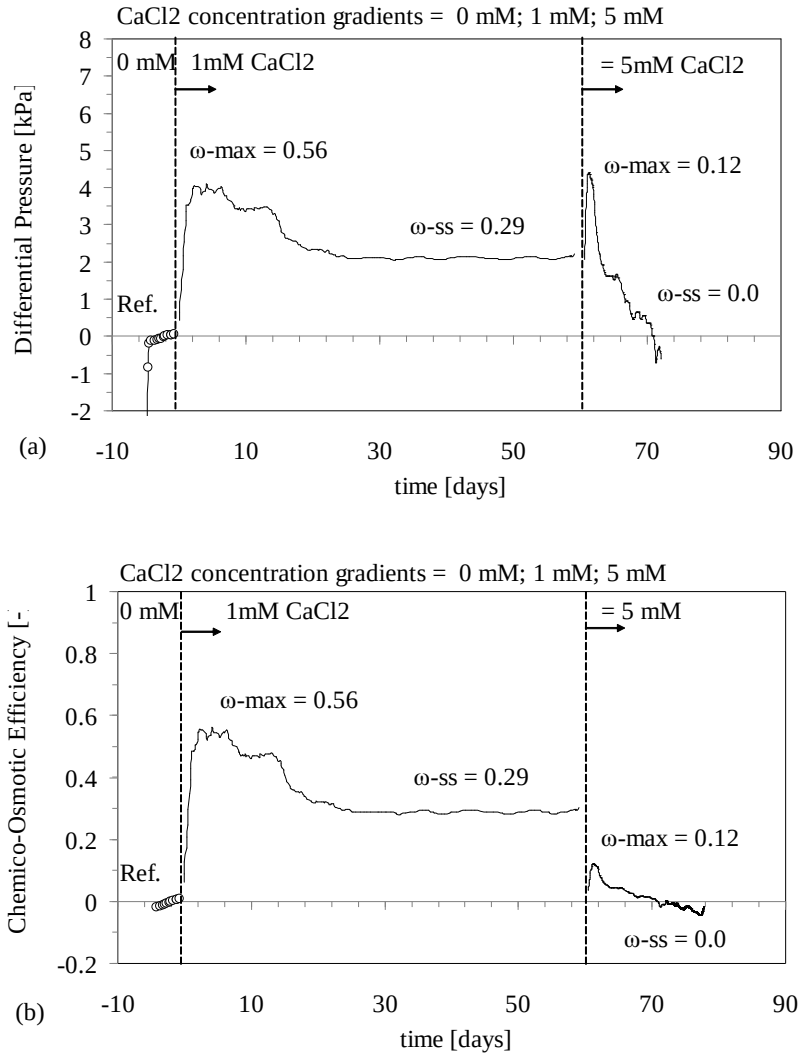

Figure 5.56: (a) Chemico-osmotic induced differential pressures and (b) chemico-osmotic efficiency of the specimen for multiple-stage test (concentration gradients ΔC_1=1 mM $CaCl_2$ and ΔC_2=5 mM $CaCl_2$) on the untreated clay

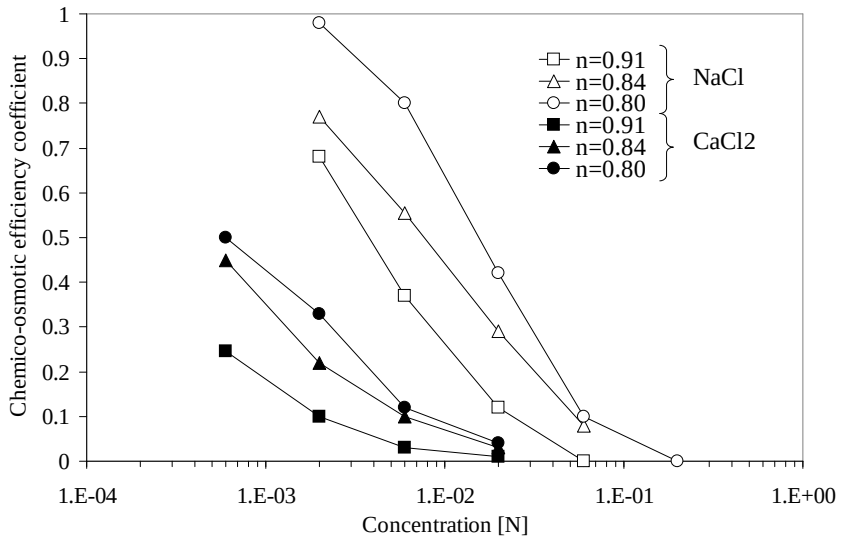

Figure 5.57: Factors affecting the chemico-osmotic efficiency of a GCL: ion concentration, valence and porosity of the clay. Data from Kemper and Rollins (1966)

ciency decreased with increasing the $CaCl_2$ concentration source (Fig. 5.56(b)), which is consistent with previous findings (Malusis and Shackelford, 2002a; Kemper and Rollins, 1966), as shown in Fig. 5.57. This figure shows the factors that tend to decrease the membrane efficiency, such as an increase of ion concentration or valence, and an increase of porosity.

In the multiple-stage test conducted on the untreated clay, the maximum chemico-osmotic efficiency, ω_{max}, decreased from 0.56 to 0.12 increasing the concentration of the solution circulated on the top solution, whereas the chemico-osmotic efficiency at the steady state, ω_{ss}, decreased from 0.29 to 0.0. The gradual destruction of the ω_{max} to the ω_{ss} with time, was also observed by Shackelford and Lee (2003) on a Bentofix GCL (Terrafix) after 35 days of circulation of a 5 mM $CaCl_2$ (in that study the first stage with ΔC_1 = 1 mM $CaCl_2$ conducted here, was not performed).

The salt concentration of 1 mM $CaCl_2$ circulated on the top of the specimen, resulted in only a partial reduction in the chemico-osmotic efficiency with time. On the other hand, a higher divalent calcium concentration (5 mM $CaCl_2$) was sufficient to completely destroy the chemico-osmotic efficiency of the untreated clay, this last observation confirms Shackelford and Lee (2003) results.

As observed also by Shackelford and Lee (2003), side-wall leakage is not likely the reason of the decrease of chemico-osmotic efficiency in this experiment for the following reasons: (1) solution flow, that is one of the main reasons for side-wall leakage, was prevented during these chemico-osmotic experiments; (2) the solu-

tions used here are diluted compared to the majority of solutions that cause sidewall leakage; (3) the swelling pressure of the specimen was 50 kPa, sufficiently high to prevent shrinkage and no evidence of shrinkage was observed after disassembling; (4) a gradual decrease of differential pressure was observed here in contrast with a sudden decrease expected after specimen shrinkage.

Instead, the gradual decrease of the membrane efficiency with time is probably due to a compression of the diffuse double layer of the clay due to diffusion of the Ca^{2+} source through the specimen, which is consistent with previous conclusions (Barbour and Fredlund, 1989; Shackelford and Lee, 2003).

Transport parameters for the untreated clay

The impact of solute diffusion on the gradual destruction of the membrane efficiency can be assessed by measuring Chloride (Cl^-) and Calcium (Ca^{2+}) concentrations in the circulating liquid exiting the base of the specimen vs. time, as reported in Fig. 5.58. As shown in this figure, the breakthrough of Cl^- occurred earlier than Ca^{2+}, probably due to cation exchange between Na^+ of the clay and the diffusing Ca^{2+}. Concentrations were expressed in meq/L in order to visualize the balance between positive and negative charges.

The sum of Na^+ and Ca^{2+} concentrations analyzed in the base outflow approaches the Cl^- concentration, in accordance to electroneutrality requirements. However, the sum of cations exceeded the Cl^- concentration values (by about 0.5 meq/L), probably due to the limited sensitivity of the instrument used for analysis with respect to the very low concentrations used as concentration gradient here (1 mM $CaCl_2$). This excess could be due to soluble/exchanged Na^+ from the clay, in fact similar sodium concentration excess was noticed also in the top outflow. Similar excess of sodium, on the top and on the base, were also noticed in the second stage, when 5 mM $CaCl_2$ (10 meq/L Ca^{2+}) of concentration gradient was circulated. During the transient phase of the test, both Na^+ ions (from the soil), Ca^{2+} and Cl^- ions (from the source solution) diffused downwards in order to satisfy the electrical balance. Exchanged Na^+ also diffused upwards into the top source solution. Release of Na^+ into the soil pore fluid as a result of exchange with Ca^{2+} created a local Na^+ concentration gradient between the soil close to the top boundary and the source solution (which was free from Na^+) so that counter-diffusion of Na^+ occurred in the direction opposite to that of the main chemical gradient (Jungnickel et al., 2004; Mazzieri et al., 2010).

The measured Cl^- and Ca^{2+} concentrations from the top specimen boundary are shown in Fig. 5.59. These concentrations imply that the applied circulation rate used in this study ($4.2xE^{-10}$ m^3/s) was not sufficient to mimic perfect flushing boundary conditions.

The time required to reach steady-state diffusion was evaluated in a systematic manner (Shackelford and Lee, 2003) by performing sequential linear regression

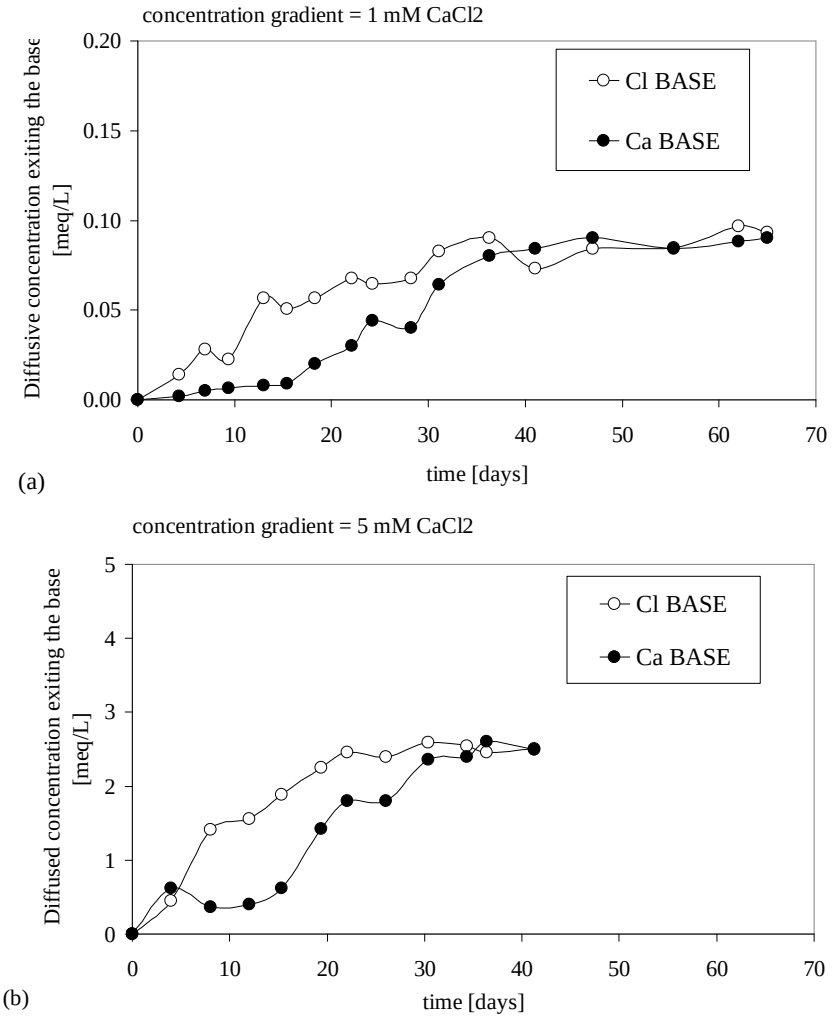

Figure 5.58: Measured chloride and calcium concentrations exiting the base of the untreated clays due to diffusion, corresponding to concentration gradients (a) ΔC_1=1 mM $CaCl_2$ and (b) ΔC_2=5 mM $CaCl_2$

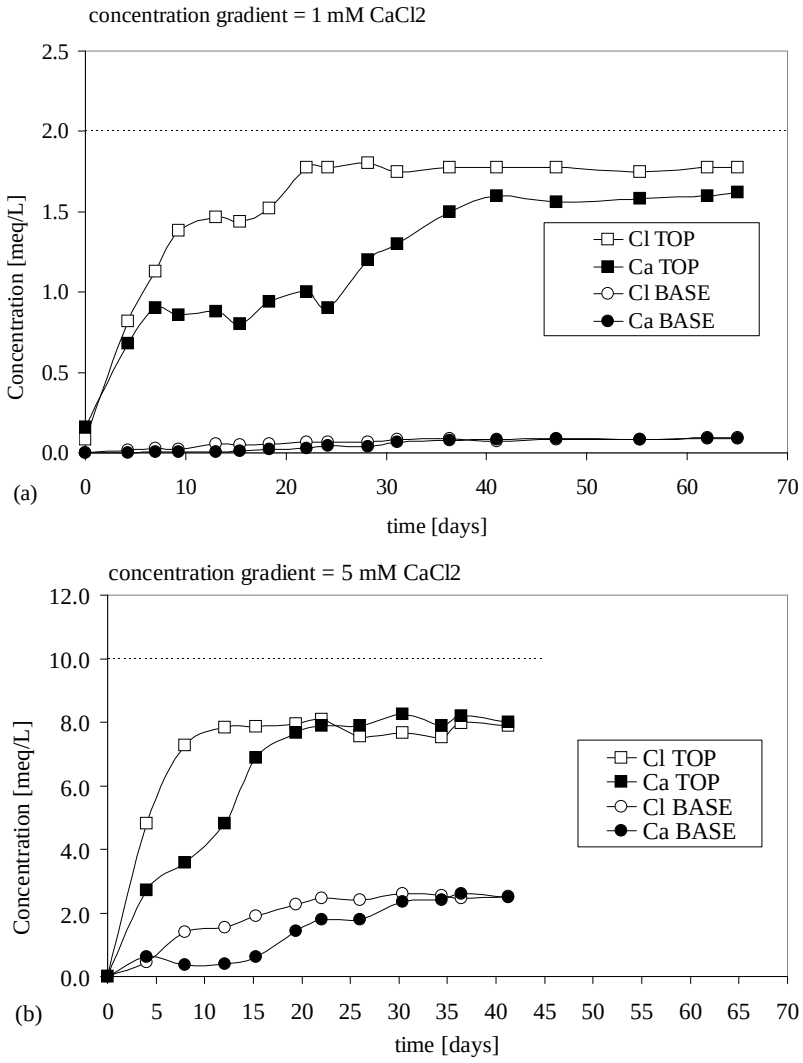

Figure 5.59: Measured chloride and calcium concentrations exiting the base and the top of the untreated clays, corresponding to concentration gradients (a) ΔC_1=1 mM $CaCl_2$ and (b) ΔC_2=5 mM $CaCl_2$

analyses on an increasing number of cumulative mass per unit area Qt vs. time (Fig. 5.60 and 5.61), starting from an analysis performed using only the last two data points, followed by subsequent linear regression analyses on an increasing number of data (i.e. adding one additional datum for each subsequent analysis) until all of the data were used in an analysis.

The coefficient of determination, r^2, resulted from each regression analysis, is plotted as a function of the number of data used in the regression for ΔC_1 in Fig. 5.62 and for ΔC_2 in Fig. 5.63 . The number of data corresponding to the location where r^2 starts to deviate significantly from unity is taken as the transition from a non-linear to linear slope in the Qt vs. time data, corresponding to the steady-state condition.

Fig. 5.62 and 5.63 show the number of data at which steady-state diffusion of Cl^- and Ca^{2+} was established. For the stage where a concentration gradient ΔC_1 = 1 mM $CaCl_2$ was imposed, the time at the steady state for Cl^- was t_{ss} = 28.21 days and t_{ss}=36.29 for Ca^{2+}. For the successive stage with a concentration gradient ΔC_2 = 5 mM $CaCl_2$, the time at the steady state for Cl^- was t_{ss} = 19.38 days and t_{ss} = 26.02 days for Ca^{2+} (Fig. 5.60 and 5.61).

The time lag, t_L, based on the results of the linear regression analyses, and the slope of the steady-state portion of the data for each solute are shown in Fig. 5.60 and 5.61. To evaluate the solute transport parameters D^* (effective diffusion coefficient) and Rd (retardation factor), the trends in cumulative mass per unit area versus time were analyzed by the time-lag method (Fig. 5.60 and 5.61). As shown in these figures, the higher t_L for Ca^{2+} relative to the t_L for Cl^- is attributed to the tendency for cation exchange associated with the divalent calcium cation.

At steady state, electroneutrality requires that the charge flux $J(Cl^-)$ of the Cl^- has the same magnitude as the charge flux $J(Ca^{2+})$ of the Ca^{2+}. This requirement may be written as in equation 5.42.

$$J(Cl^-)\,|z_{Cl^-}| = J(Ca^{2+})\,|z_{Ca^{2+}}| \tag{5.42}$$

where $J(Cl^-)$ and $J(Ca^{2+})$ are the steady-state diffusive molar fluxes of Cl^- and Ca^{2+}, and z_{Cl^-} and $z_{Ca^{2+}}$ are the charges of Cl^- and Ca^{2+} (i.e. -1 and +2, respectively). Therefore, the steady-state diffusive molar flux of Cl^- theoretically should be twice the magnitude of the steady-state diffusive molar flux of Ca^{2+}. Based on the results shown in Fig. 5.64, the observed ratio of the steady-state diffusive mass flux of Cl^- to the steady-state diffusive mass flux of Ca^{2+} in both tests were sufficiently close to this theoretical value suggesting that steady-state diffusion was essentially established.

Finally, the effective diffusion coefficients, D^*, for Cl^- and Ca^{2+} were, respectively, $0.40E^{-10}$ m^2/s and $0.41E^{-10}$ m^2/s, for a concentration gradient ΔC_1 = 1 mM $CaCl_2$. The D^* of the solutes (Cl^- and Ca^{2+}) were similar, which is consistent with the electroneutrality requirement at steady-state diffusion. Also the

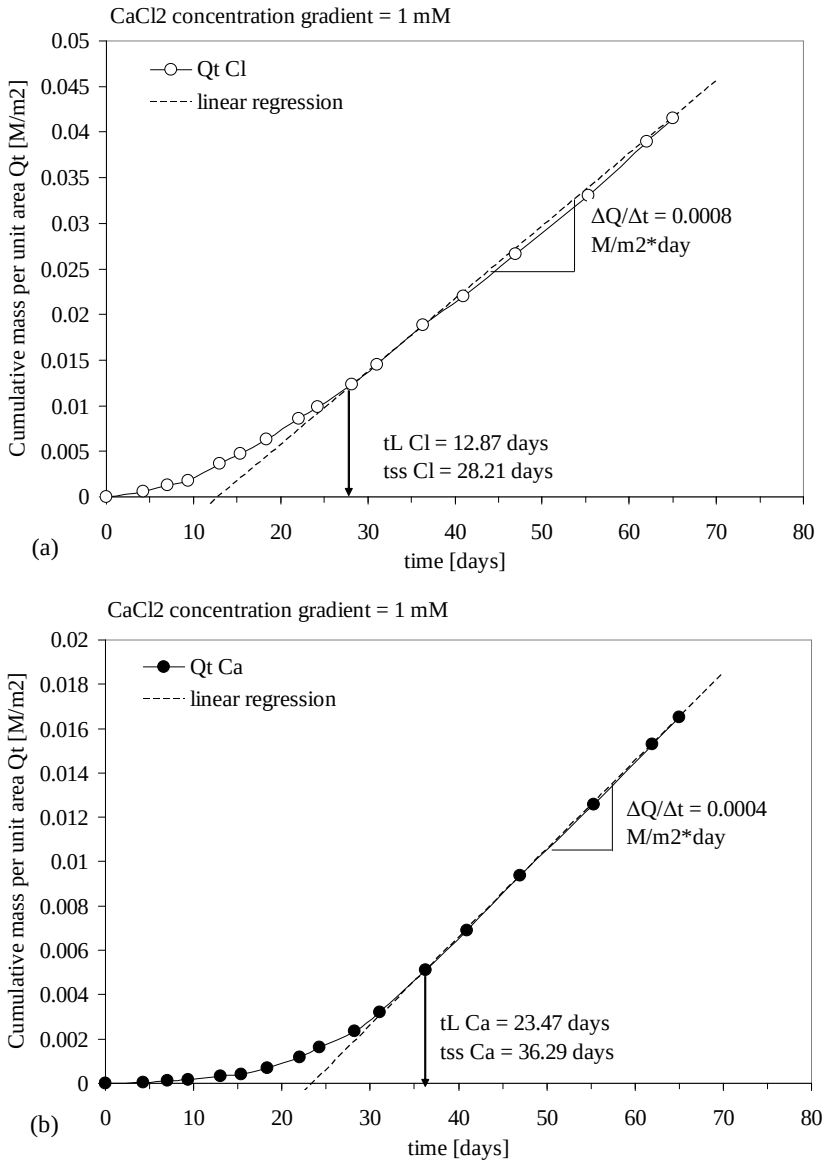

Figure 5.60: Untreated clay, ΔC_1 = 1 m M $CaCl_2$: cumulative mass per unit area based on the measured concentrations at the base, with t_L = time lag; t_{ss} =time to steady-state diffusion

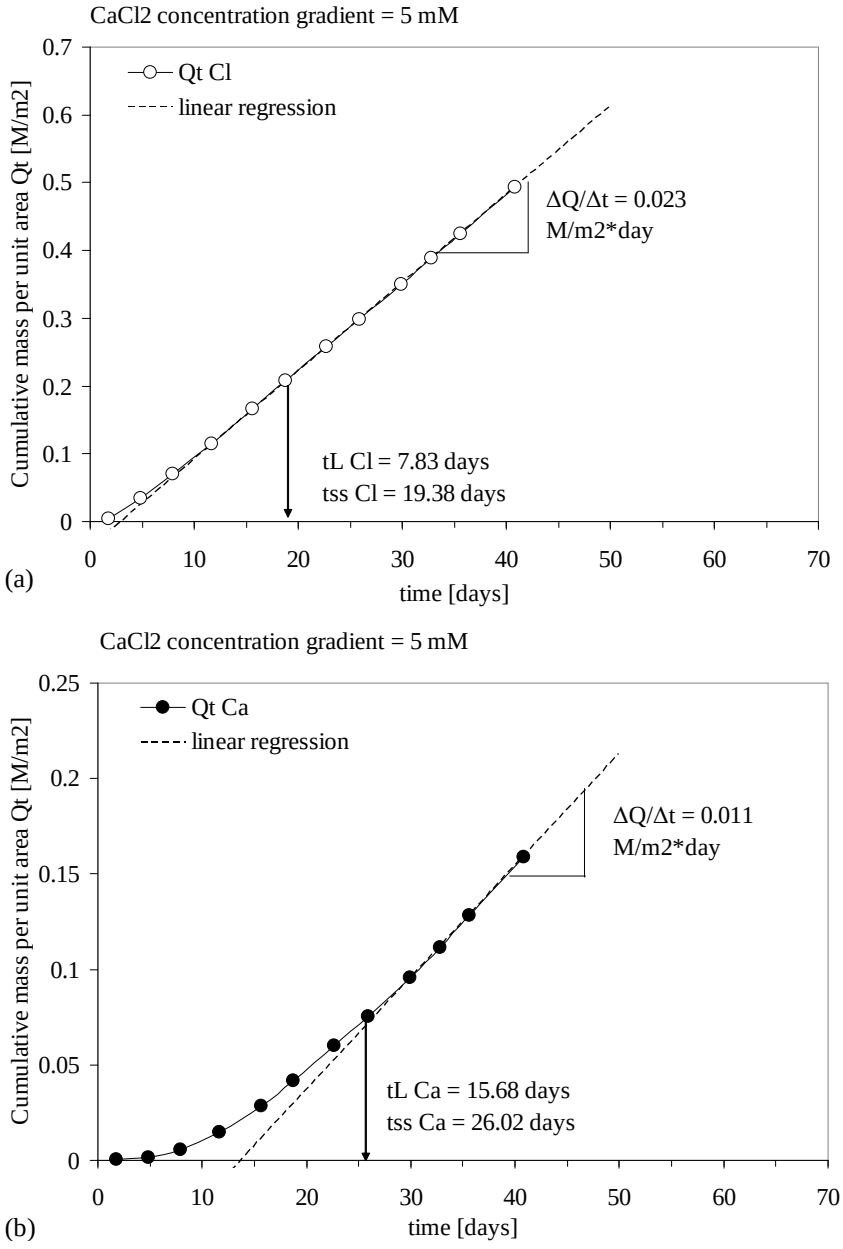

Figure 5.61: Untreated clay, ΔC_2 = 5 m M $CaCl_2$: cumulative mass per unit area based on the measured concentrations at the base, with t_L = time lag; t_{ss} =time to steady-state diffusion

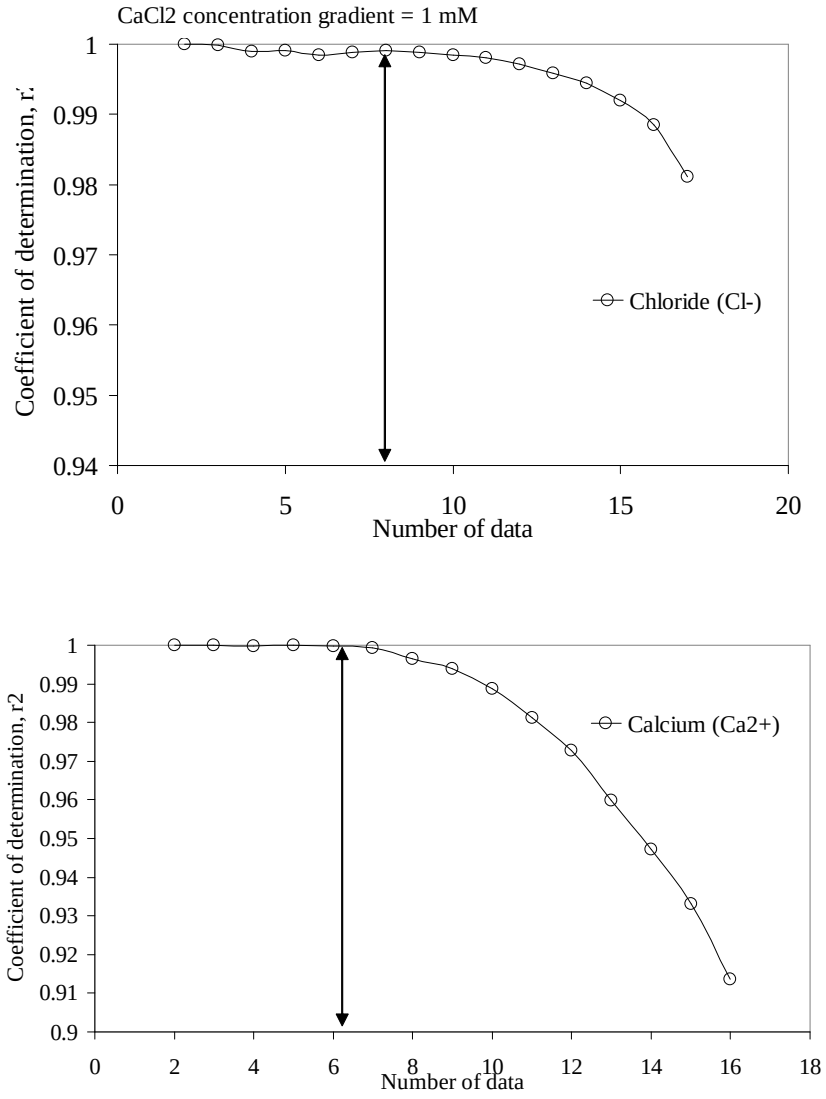

Figure 5.62: Untreated clay, ΔC_1 = 1 m M $CaCl_2$: coefficients of determination from multiple linear regression analyses performed on measured cumulative mass data as a function of the number of data used for linear regression

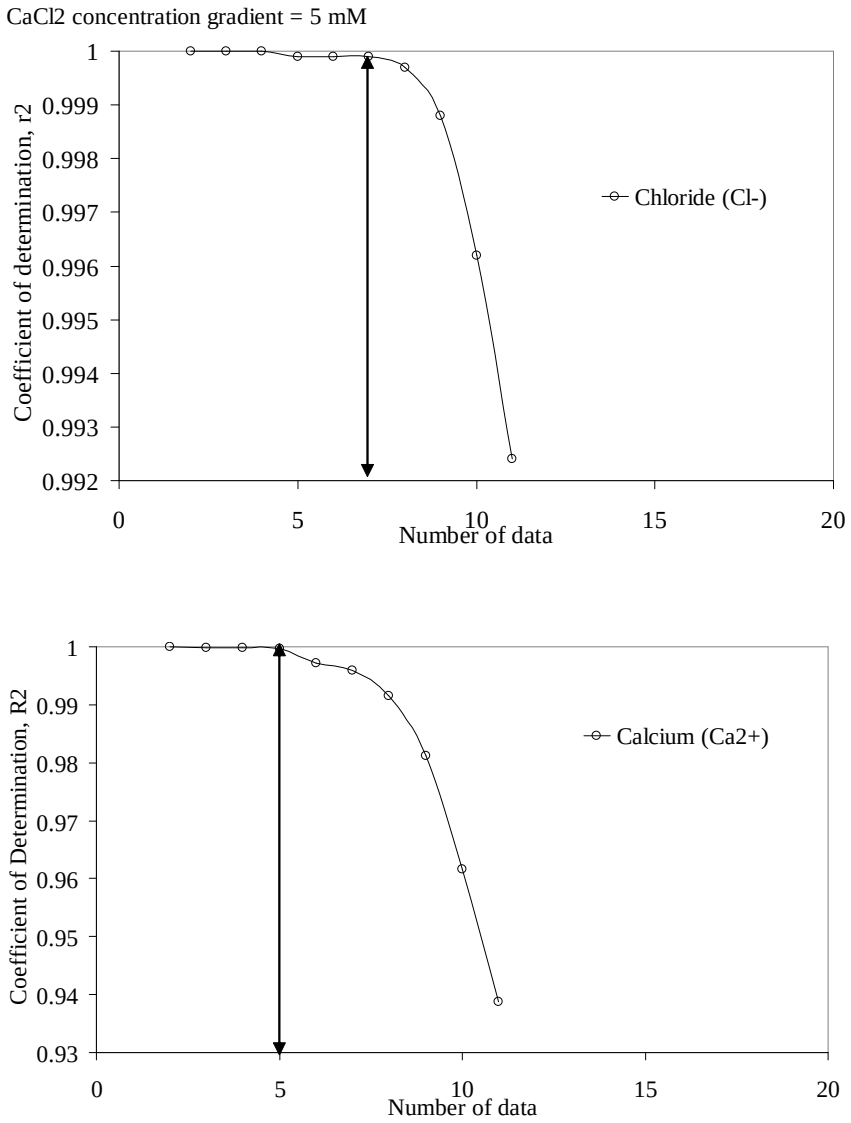

Figure 5.63: Untreated clay, ΔC_2 = 5 m M $CaCl_2$: coefficients of determination from multiple linear regression analyses performed on measured cumulative mass data as a function of the number of data used for linear regression

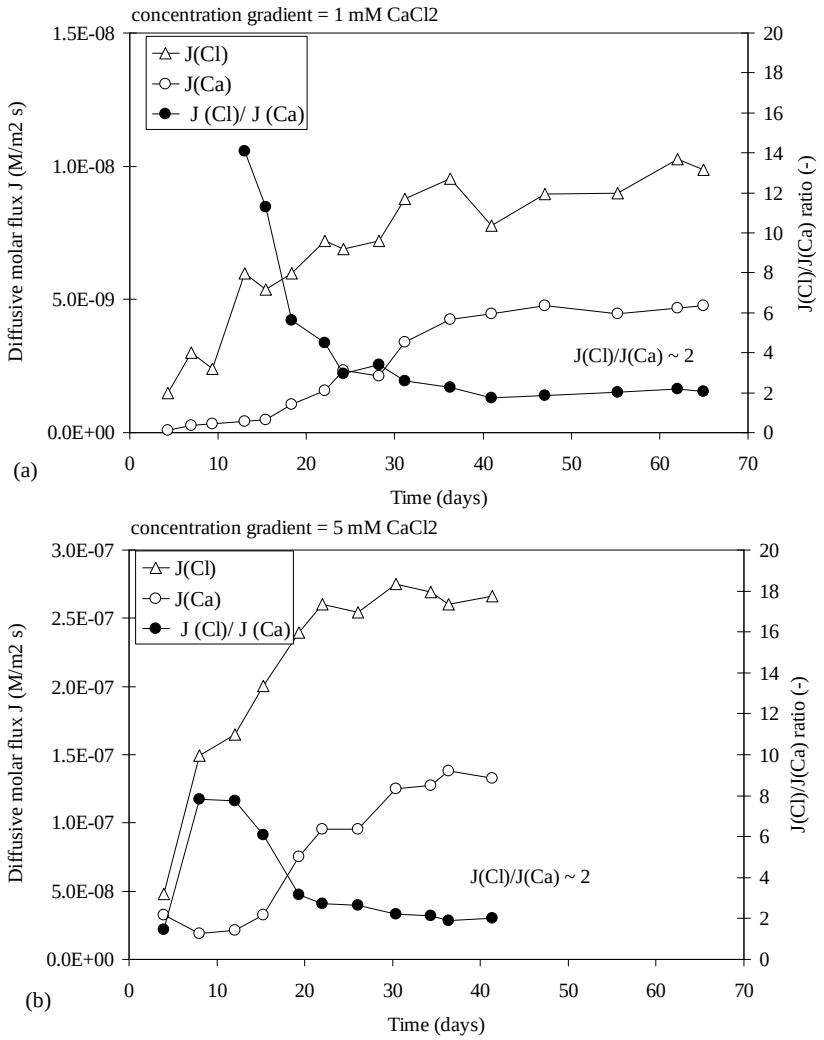

Figure 5.64: Diffusive molar flux vs. time of the multiple-stage osmotic test on the untreated clay

effective diffusion coefficients for a concentration gradient ΔC_2 = 5 mM were similar, D^* = 2.22E^{-10} m^2/s for both solutes. D^* was calculated in accordance with equation 4.6 using a measured porosity n = 0.718 and thickness L = 5.99 mm.

Not only the Diffusion coefficient, but also the retardation factor (Rd) was determined with the time-lag method, using equations 4.13 and 4.14. Based on the calculated R_d values, both Cl^- and Ca^{2+} were retarded in both stages of the chemico-osmotic test. The main retarding process for Ca^{2+} was the cation exchange with Na^+ onto the soil surface. The chemico-osmotic effect and the electrostatic interaction among the diffusing ions also influence the transport of Ca^{2+}. Cl^- is usually considered a conservative tracer in soil diffusion studies since it tends to be repelled from negatively charged surfaces. Theoretically, a conservative tracer should have Rd=1. Besides solute restriction ($\omega > 0$), the retardation of Cl^- could be partly explained by the counter-diffusion of Na^+ into the top solution, which may have delayed the downward diffusion of Cl^- due to electroneutrality requirements.

For an overview of the transport parameters of the clays analyzed, refer to table 5.5 further on in this Chapter.

Destructive role of diffusion on the membrane behavior of the untreated clay

Membrane behavior in clays generally is attributed to electrostatic repulsion of the ions by electric fields associated with the diffuse double layers (DDLs) of adjacent clay particles. Therefore, the factors that tend to decrease the DDL thickness, such as an increase of ion concentration and/or valence, may result in a reduction of membrane efficiency. The multi-stage test on the untreated clay showed, for every concentration gradient, a similar trend of the chemico-osmotic efficiency with time. As shown in Fig. 5.56, the chemico-osmotic efficiency showed a maximum value, (ω_{max}), after few hours of testing and a gradual decrease to a lower constant value, (ω_{ss}), at steady-state diffusion conditions. This gradual decrease of chemico-osmotic behaviour can be attributed to the compression of DDL thickness caused by increasing concentrations of bivalent Ca^{2+} in the pore fluid due to diffusion. This conclusion was also stated by Shackelford and Lee (2003). The results obtained here with a $CaCl_2$ concentration gradient ΔC_2 = 5 mM qualitatively resemble their findings. Shackelford and Lee (2003) also observed a variable osmotic efficiency, with a peak value followed by a gradual decrease to zero. Their conceptual explanation for the correlation between Ca^{2+} diffusion and the destruction of the membrane behavior can be formulated on the basis of the clay structure models described by Pusch and Schomburg (1999). In these models, bentonite clay consists of an intermingled structure of both unit particles and particle clusters, with the primary pores located between the unit particles and the clusters. At the measured porosity of the specimen n = 0.718, interlayer spacing of the particles will be controlled by surface hydration rather than by the diffuse double layer

interactions, such that the interlayer spacing of the unit particles will probably not have been affected much by the exchangeable cation (van Olphen, 1977). However, DDLs will probably have extended into the voids between both unit particles and particle clusters, thereby restricting the diffusive migration of the ions (Shackelford and Lee, 2003).

In brief, the destruction of the membrane behavior can be explained in terms of decreasing diffuse double layer thickness between unit particles and particle clusters with increasing pore concentration due to ion diffusion. In addition, the decrease of DDL thickness causes also particles aggregation, with a consequent decrease of the specific surface area of the clay contributing to surface hydration forces. As a consequence, not only the thickness of the DDL, but also the hydration forces of the water molecules on the clay surface decrease with a consequent decrease in chemico-osmotic efficiency.

5.5.2 Impact of polymer treatment with 25% Propylene Carbonate on the chemico-osmotic efficiency of a Multiswellable Bentonite

Induced differential pressures and chemico-osmotic efficiency

A chemico-osmotic efficiency test has been performed also on the modified MultiSwellable bentonite (MSB, Hojun corp. Japan) obtained by treating natural sodium bentonite with 25 % Propylene Carbonate (PC). Based on the results of this thesis and of Katsumi (2010), we have shown that the MSB exhibited higher swelling capacity and lower hydraulic conductivity than untreated bentonites for $CaCl_2$ solutions up to 0.5 mol/L. Therefore, in view of pollutant containment applications, it was interesting to evaluate the potential for chemico-osmotic behaviour of MSB.

During the chemico-osmotic/diffusion test on the MSB, as occurred for the untreated clay, replacement of deionized water with the solution source on the top boundary, caused an immediate increase in the differential pressure to a peak value that gradually decreased (Fig. 5.65). In this test, a concentration gradient of ΔC_2= 5 mM $CaCl_2$ was directly used (no previous stage with ΔC_1 = 1 mM was conducted on MSB). The peak value was $-\Delta P_{max}$= 6.1 kPa and occurred after about 16 hours of circulation with the solution source. Then, the differential pressure gradually decreased to values fluctuating around $-\Delta P_{max}$ = 0 kPa. Considering the scatter of the measurements, the steady state was assumed after about 22 days of circulation with the solution (Fig. 5.65).

As a result, also the MSB specimen exhibited initial membrane behavior, as occurred for the untreated clay. However, it was gradually destroyed during the test. The peak chemico-osmotic efficiency, was ω_{max}= 0.17, slightly higher than for the untreated clay as shown in Fig. 5.65. The steady-state osmotic efficiency

was ω_{ss}=0, as occurred for the untreated clay. Therefore, the treatment of the clay with Propylene Carbonate (PC) was not able to maintain a chemico-osmotic efficiency at the steady state.

However, it is plausible that the PC was flushed out during the phase of soluble salts removal before the test started. This phase lasted 12.55 Pore Volumes of flow, about 90 days. Then, the MSB behaved as the untreated clay. So the gradual decrease of the membrane efficiency with time was probably due to a compression of the diffuse double layer due to diffusion of the Ca^{2+} source through the specimen.

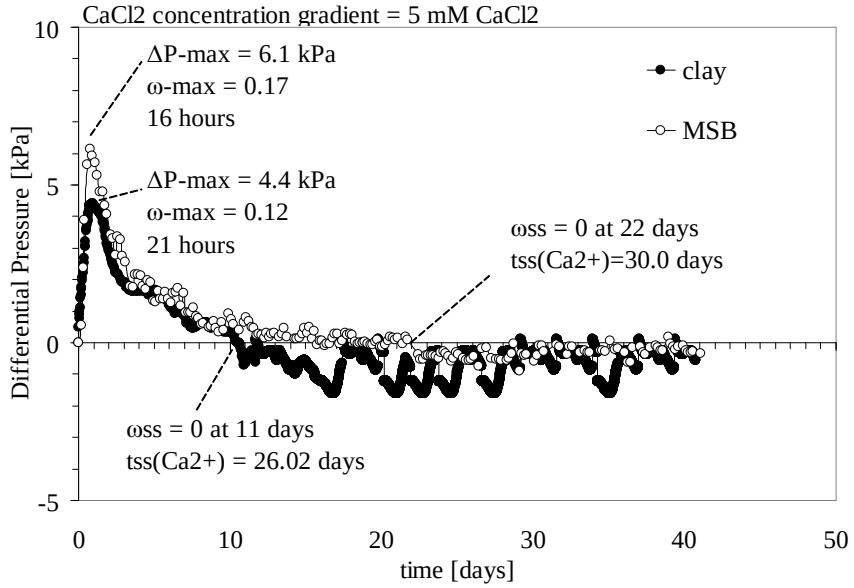

Figure 5.65: Impact of the Propylene Carbonate (PC) on the chemico-osmotic efficiency of the MSB (clay+25%PC) with a concentration gradient of 5 mM $CaCl_2$

Transport parameters for the Multiswellable Bentonite

Also for the MSB, the impact of solute diffusion on the gradual destruction of the chemico-osmotic efficiency was assessed by measuring chloride (Cl^-) and calcium (Ca^{2+}) concentrations in the circulating liquid exiting the base of the specimen vs. time, as reported in Fig. 5.66. The breakthrough of Cl^- occurs earlier than Ca^{2+}, indicating that also for the MSB cation exchange occurred between Na^+ of the clay and the diffusing Ca^{2+} from the solution source.

Both Na^+ and Ca^{2+} ions diffused downwards along with Cl^- for electrical balance. The sum of Na^+ and Ca^{2+} concentration analyzed in the base outflow approaches the Cl^- concentration, in accordance to electroneutrality requirements.

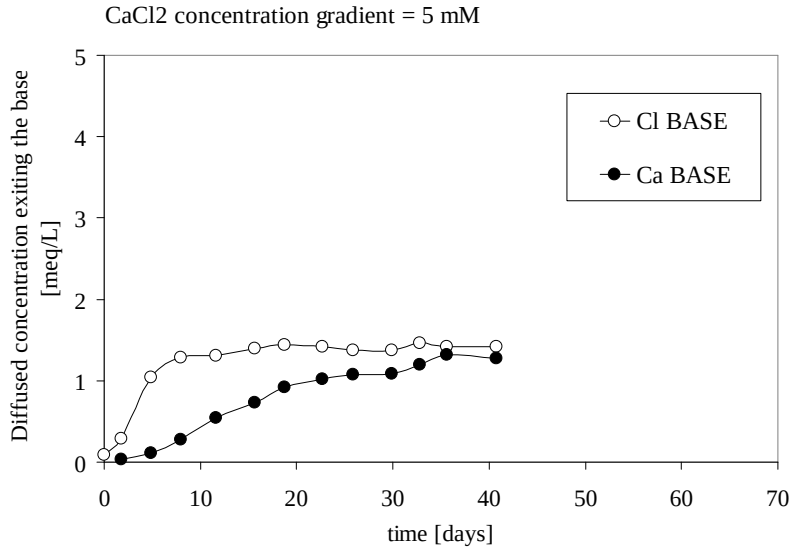

Figure 5.66: Measured chloride and calcium concentrations exiting the base of the MSB due to diffusion, corresponding to a concentration gradient of ΔC = 5 m M $CaCl_2$

As mentioned above for the untreated clay, counter-ion diffusion of Na^+ was observed also here.

The measured Cl^- and Ca^{2+} concentrations from the top specimen boundary are shown in Fig. 5.67. These concentrations imply that also for the MSB, as for the untreated clay, the applied circulation rate used ($4.2xE^{-10}$ m^3/s) was not sufficient to mimic perfectly flushing boundary conditions.

The time required to reach steady-state diffusion was evaluated by performing sequential linear regression analyses on an increasing number of cumulative mass per unit area Qt vs. time (Fig. 5.68).

To evaluate the solute transport parameters D^* (effective diffusion coefficient) and Rd (retardation factor), the trends in cumulative mass per unit area versus time were analyzed by the time-lag method, as shown in Fig. 5.68. As shown in this figure and in Table 5.5, for a concentration gradient ΔC = 5 mM $CaCl_2$, the time to reach the steady state was t_{ss} = 11.5 days for Cl^- and t_{ss} = 30 days for Ca^{2+}. The time lag, t_L, based on the results of the linear regression analyses, and the slope of the steady-state portion of the data for each solute are also shown in Fig. 5.68. The higher t_L for Ca^{2+} (t_L=13.7 days) with respect to the t_L for Cl^- (t_L=2.8 days) is attributed to the tendency for cation exchange associated with the divalent calcium cation.

At steady state, electroneutrality requires that the charge flux J(Cl^-) of the Cl^- has the same magnitude as the charge flux J(Ca^{2+}) of the Ca^{2+}. Therefore,

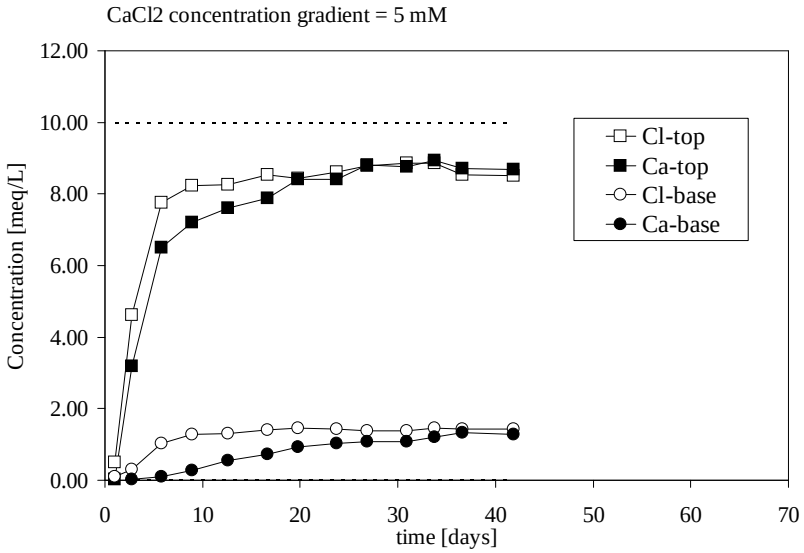

Figure 5.67: Measured chloride and calcium concentrations exiting the base and the top of the MSB, corresponding to a concentration gradient of ΔC = 5 m M $CaCl_2$

the steady-state diffusive molar flux of Cl^- theoretically should be twice the magnitude of the steady-state diffusive molar flux of Ca^{2+}. Based on the results shown in Fig. 5.69, the observed ratio of the steady-state diffusive mass flux of Cl^- to the steady-state diffusive mass flux of Ca^{2+} in both tests were sufficiently close to this theoretical value suggesting that steady-state diffusion had essentially been established.

Finally, the effective diffusion coefficients, D^*, for Cl^- and Ca^{2+} were, respectively, 1.79E^{-10} m^2/s and 1.60E^{-10} m^2/s, for a concentration gradient ΔC = 5 mM $CaCl_2$. The D^* of the solutes (Cl^- and Ca^{2+}) were similar, which is consistent with the electroneutrality requirement at steady-state diffusion. D^* was calculated in accordance with equation 4.6 using a measured porosity n = 0.718 and thickness L = 7.4 mm. As observed for the untreated clay, both Cl^- and Ca^{2+} were retarded in the chemico-osmotic test (R_d(Cl) = 4.6, R_d(Ca)=17.5). As mentioned above, release of Na^+ cations during diffusion of Ca^{2+} suggested that cation exchange onto the soil surface was the main retarding process for Ca^{2+}. The chemico-osmotic effect and the electrostatic interaction among the diffusing ions also had a role in the retardation of Ca^{2+} and Cl^-. The retardation of Cl^- could be partly explained by electroneutrality requirements due to the counter-diffusion of Na^+ into the top solution. The boundary concentrations vary during the test as a result of diffusion (Fig. 5.67), with a consequent influence in the transport parameters.

For an overview of the transport parameters of the clays analyzed, refer to table

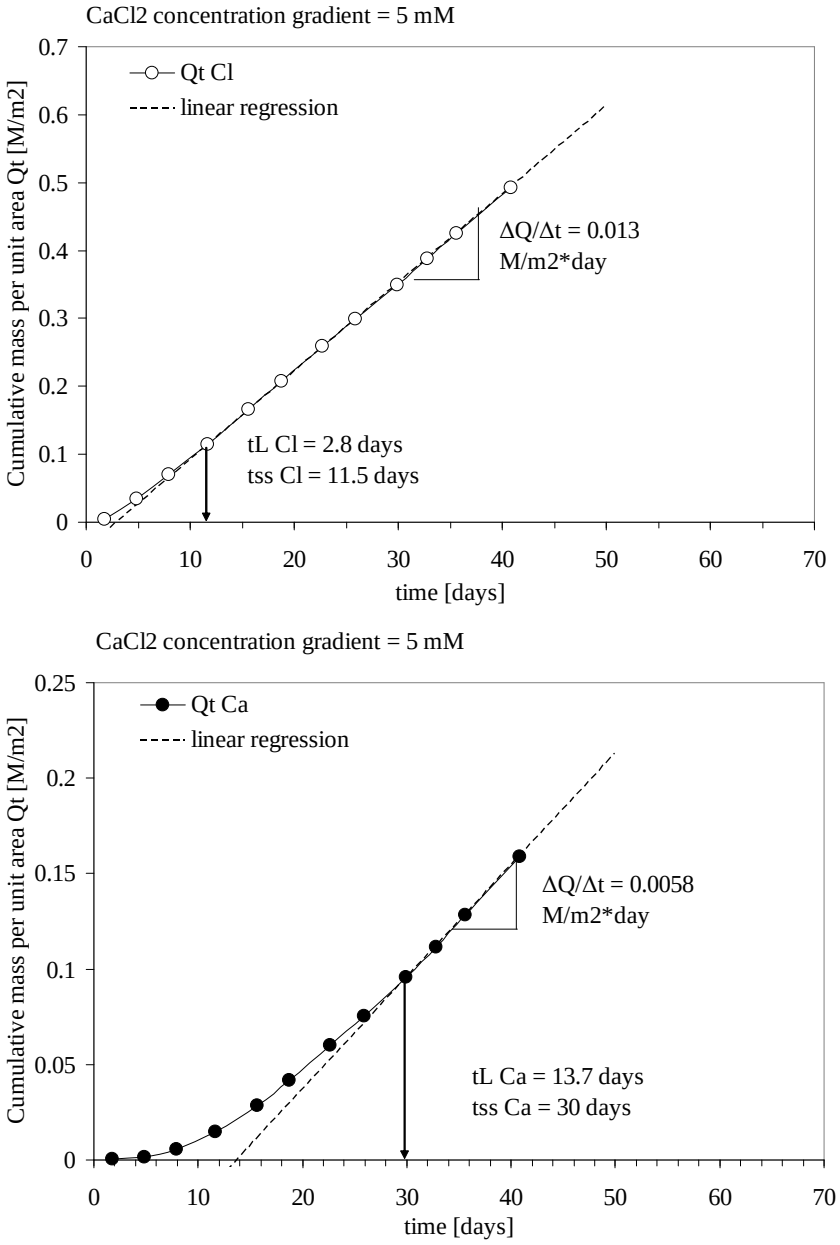

Figure 5.68: MSB, ΔC = 5 m M $CaCl_2$: cumulative mass per unit area based on the measured concentrations at the base, with t_L = time lag; t_{ss}=time to steady-state diffusion

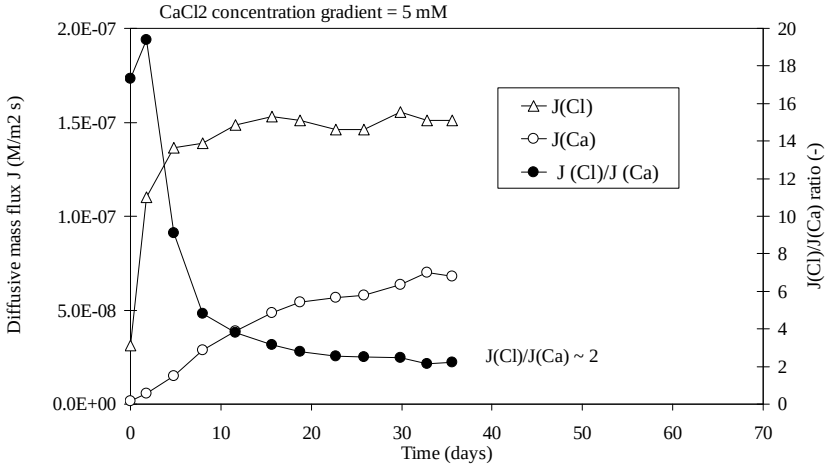

Figure 5.69: Diffusive molar flux vs. time of the chemico-osmotic test with ΔC = 5 m M $CaCl_2$ on the MSB

5.5 further on in this Chapter.

Destructive role of diffusion on the membrane behavior of the MSB

The chemico-osmotic test on the untreated clay showed a gradual decreasing trend of the chemico-osmotic efficiency with time. As shown in Fig. 5.65, the chemico-osmotic efficiency showed a maximum value (ω_{max}=0.12) after few hours of testing and a gradual decrease to a lower constant value (ω_{ss}=0.0) at steady-state diffusion conditions.

The results obtained here on the MSB, with a $CaCl_2$ concentration gradient ΔC_2 = 5 mM, qualitatively resemble the findings on the untreated clay. In fact, MSB did exhibit initial membrane behavior (ω_{max}=0.17) gradually destroyed to ω_{ss}=zero as a result of salt migration into the MSB and the consequent compression of the diffuse double layer (Fig. 5.65).

The conceptual explanation for the correlation between Ca^{2+} diffusion and the destruction of the membrane behavior can be explained in terms of decreasing diffuse double layer thickness between unit particles and particle clusters with increasing pore concentration due to ion diffusion, resulting in a gradual destruction of the observed membrane behavior.

The decrease of DDL thickness causes also particles aggregation, with a consequent decrease of the specific surface area of the clay contributing to surface hydration forces. As a consequence, not only the thickness of the DDL, but also the hydration forces of the water molecules onto the clay surface decrease with a consequent decrease in chemico-osmotic efficiency.

Based on improved swelling and hydraulic performance of MSB compared to the untreated clay, it was expected to observe also an improved chemico-osmotic behavior of the MSB. Conversely, the PC treatment did not provide any improvement on the chemico osmotic efficiency of the MSB. This plain performance of the MSB may be attributed to a variation of the initial properties conferred by PC treatment. According to Onikata et al. (1999), PC is bound to the bentonite by coordination with the adsorbed cations in the interlayer of montmorillonite. Since the exchange of Ca^{2+} for Na^{+} cations was demonstrated, the question arises as to whether the exchangeable Na^{+} were removed together with the coordinated PC clouds.

Comparison of the dry mass of the specimen before and after the test revealed a mass loss of about 2.00 g. This loss can be partially attributed to the solids which remained attached to the cell and to the removal of PC during permeation (with deionized water to remove soluble salts before the test) and/or oven-drying of the clay after the test. Considering the initial nominal content of PC in MSB (25%), it can be calculated that 3.56 g of PC were initially bound in the specimen. Even if the mass loss of 2.00 g were entirely attributed to PC, 1.56 g of PC would remain bound to the soil.

Swell index tests were performed on the MSB specimen at the end of the test: the free swell was 11 ml/2g in deionized water and 10 ml/2g in 5 mM $CaCl_2$. These values were significantly different from the results obtained on unused MSB (23 ml/2g in deionized water and 50 ml/2g in 5 mM $CaCl_2$) and were close to values commonly obtained with Ca-bentonites (Egloffstein, 2001). These results suggest that at the end of the test the MSB converted into a Ca-exchanged bentonite partially or totally deprived of PC and of the swelling properties initially conferred by PC. Conversion into a Ca-bentonite occurred probably during the diffusion stage and partly during permeation with 5 mM $CaCl_2$.

5.5.3 Impact of polymer treatment and ion concentration on the chemico-osmotic efficiency of a HYPER clay

Induced differential pressures and chemico-osmotic efficiency

To study the impact of polymer treatment on the membrane behavior of the clay analyzed, a multi-stage chemico-osmotic test was also performed on the HYPER clay obtained by treating bentonite clay with 2 % Sodium-Carboxymethyl Cellulose (Na-CMC). The HYPER clay was tested at the same porosity used for the untreated clay and the MSB (n = 0.718). We have shown that the HYPER clay exhibited higher swelling capacity and lower hydraulic conductivity than the untreated bentonite in presence of electrolyte solutions such as $CaCl_2$ 5 mM and sea water. Therefore, in view of pollutant containment applications, it was interesting to evaluate the potential for chemico-osmotic behaviour for the HYPER clay as

well.

The measured differential pressures induced across the HYPER clay sample and the chemico-osmotic efficiency in the multiple-stage test are presented in Fig. 5.70. As for the untreated clay, in this multiple-stage test two concentration gradients were used sequentially, ΔC_1= 1 mM $CaCl_2$ and ΔC_2= 5 mM $CaCl_2$. After replacing the purified water circulating across the top of the specimen with the first solution (1 mM $CaCl_2$), at t = 0 days, as shown in Fig. 5.70, the induced pressure difference increased immediately and continued to increase gradually to a maximum value of $-\Delta P$ = 4.74 kPa corresponding to a maximum chemico-osmotic efficiency coefficient ω_{max}=0.65. Subsequently, the second concentration gradient was applied circulating a 5 mM $CaCl_2$ solution through the top boundary. After replacing the solution, the induced pressure difference due to ΔC_2 = 5 mM $CaCl_2$, increased and continued to increase gradually to a maximum value of $-\Delta P$ = 4.81 kPa corresponding to a maximum chemico-osmotic efficiency coefficient ω_{max}=0.13.

The chemico-osmotic efficiency of the HYPER clay was maintained at the steady state, in contrast to the gradual decrease observed for the untreated clay and the MSB. Figure 5.71 and 5.72 show a comparison between the gradual destruction of the membrane behavior of the untreated clay due to diffusion and, on the contrary, the preservation of the membrane behavior with time for the HYPER clay due to the shielding role of this polymer.

Transport Parameters for the HYPER clay

The solutes diffusion through the HYPER clay was assessed by the chemico-osmotic test, by measuring Chloride (Cl^-) and Calcium (Ca^{2+}) concentrations in the circulating liquid exiting the base of the specimen vs. time, as reported in Fig. 5.73. As shown in Fig. 5.73(a) with a concentration gradient ΔC_1=1 mM $CaCl_2$, the breakthrough of Cl^- occurred earlier than Ca^{2+}, indicating that also for the HYPER clay some cation exchange occurred between Na^+ of the clay and the diffusing Ca^{2+} from the solution source. This behavior, confirms also the hypothesis that the clay and the HYPER clay behave similarly in contact with dilute solutions such as ΔC_1=1 mM $CaCl_2$, whereas the effect of the polymer became evident for higher concentrations. In fact, for a concentration gradient ΔC_2=5 mM $CaCl_2$, the HYPER clay breakthrough of Ca^{2+} and Cl^- were similar (Fig. 5.73(b)), suggesting that the exchange of Ca^{2+} with Na^+ was shielded due to the presence of the polymer. The polymer blocks the compression of the DDL when the concentration increases, whereas for diluted concentrations the DDL is already sufficiently thick and the effect of the polymer is negligible.

Likewise, the time at the steady-state, t_{ss}, and the retardation factor, R_d, of Cl^- and Ca^{2+} were comparable. These results could in fact indicate that the exchange was restricted during this second phase of testing with ΔC_2=5mM $CaCl_2$. Also the

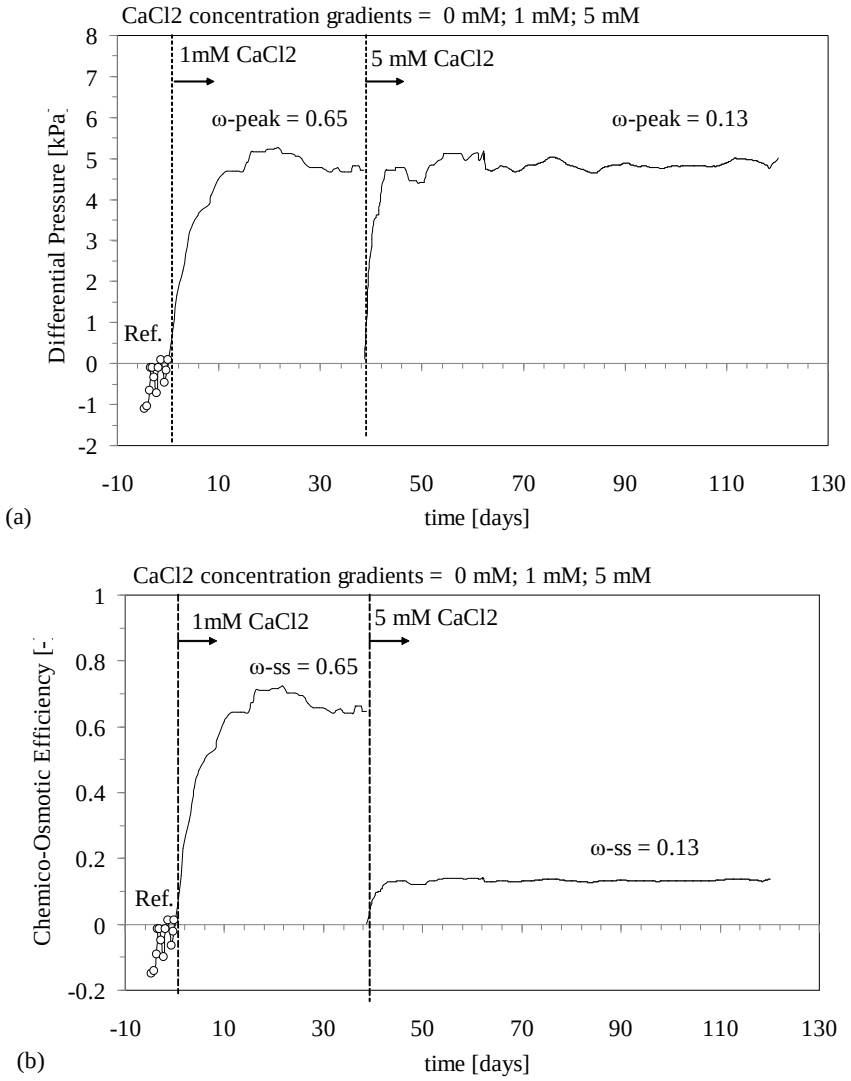

Figure 5.70: (a) Chemico-osmotic induced differential pressures and (b) chemico-osmotic efficiency of the HYPER clay for multiple-stage test (concentration gradients ΔC_1=1 mM $CaCl_2$ and ΔC_2=5 mM $CaCl_2$)

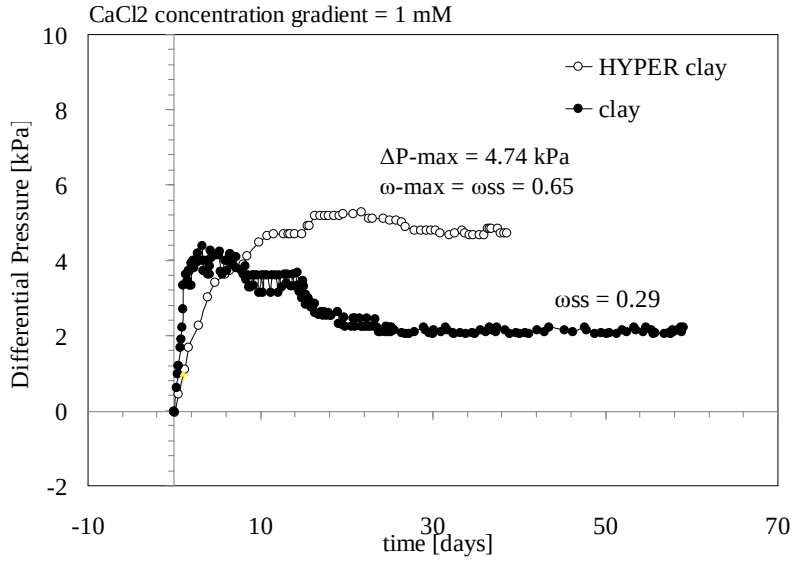

Figure 5.71: Enhancement due to the anionic polymer (Na-CMC) on the chemico-osmotic efficiency of the HYPER clay with a concentration gradient ΔC1=1 mM $CaCl_2$

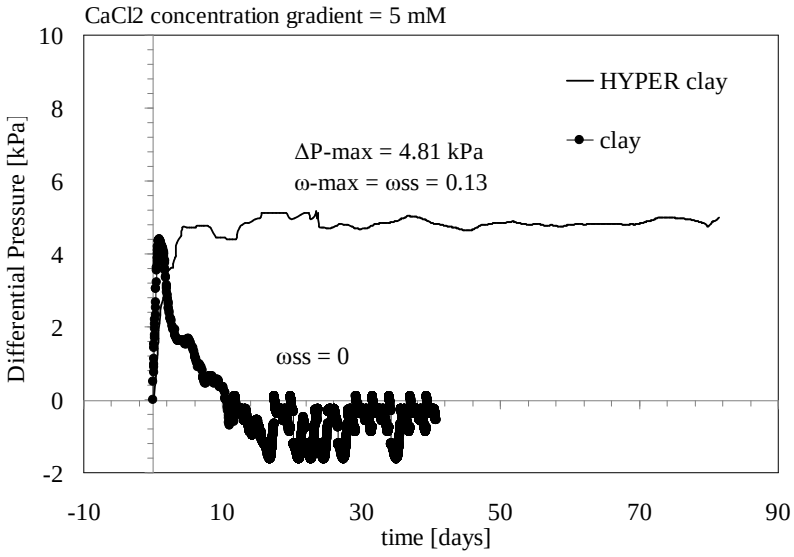

Figure 5.72: The anionic polymer (Na-CMC) protects the HYPER clay against destruction of the chemico-osmotic efficiency induced by diffusion (concentration gradient ΔC2=5 mM $CaCl_2$)

diffusive molar flux ratio of Cl^- and Ca^{2+} (J(Cl)/J(Ca)) was nearly constant from the start of the stage with ΔC_2=5mM $CaCl_2$, indicating that the two solutes moved together, as a result of limited exchange between Ca^{2+} and Na^+ in the transient phase of the test.

Figure 5.74 shows the measured Chloride and Calcium exit concentrations of the HYPER clay compared to the untreated clay. These exiting concentrations were similar for a concentration gradient ΔC_1 = 1 m M $CaCl_2$, confirming the hypothesis that the HYPER clay behaves alike the untreated clay for diluted solutions. Conversely, for the higher concentration gradient (ΔC_2 = 5 mM $CaCl_2$), the HYPER clay breakthrough showed some delay with respect to the untreated clay, confirming that the impact of the polymer is emphasized for concentrated solutions with respect to diluted solutions.

To further corroborate this hypothesis, it should be stressed that the retardation factor, R_d, of the HYPER clay was comparable to the untreated clay for ΔC_1= 1 mM $CaCl_2$, but it was higher for the higher concentration gradient (ΔC_2 = 5 mM $CaCl_2$) (table 5.5). In addition, the comparison of the effective diffusion, D^*, confirms that for the diluted solution (ΔC_1) the HYPER clay showed a D^* comparable to the untreated clay, whereas for the concentrated solution (ΔC_2) the HYPER clay showed a lower D^* compared to the untreated clay. Figure 5.75 shows that for the untreated clay, as expected, the diffusion coefficient increases with increasing the Ionic Strength and decreasing the chemico-osmotic efficiency (as also found by Malusis and Shackelford (2002b) for monovalent KCl solutions). In contrast, Fig. 5.75 (a) shows that for the HYPER clay a lower increase of the diffusion coefficient was observed, suggesting that the increase of Diffusion with the Ionic Strength was softened by the presence of the polymer.

In fact, the higher solute concentrations in the pore space associated with an increase in the concentration of the source solution, causes contraction of the diffuse double layers that results in a decrease in chemico-osmotic efficiency and a corresponding increase in D^* as more pores become available for solute transport. On the other hand, the polymer, maintaining the DDL open, restricts the availability of pores for solute transport with a consequent decrease of D^*. In fact, the degree of solute restriction is greatest when the double layers of adjacent clay particles overlap in the pore space, leaving no free solution for solute transport (Marine and Fritz, 1981).

In brief, for a concentration gradient ΔC_2 = 5 mM $CaCl_2$ the solutes breakthrough, the constant ratio between the diffusive molar fluxes, the effective diffusion and the retardation factor of the HYPER clay compared to the untreated clay, validate the statement that the polymer on the HYPER clay, compared to the untreated clay, maintains the interlayer open and protects the clay from cation exchange, restricting to a greater extent the solute flux through the specimen and preserving its chemico-osmotic efficiency with time.

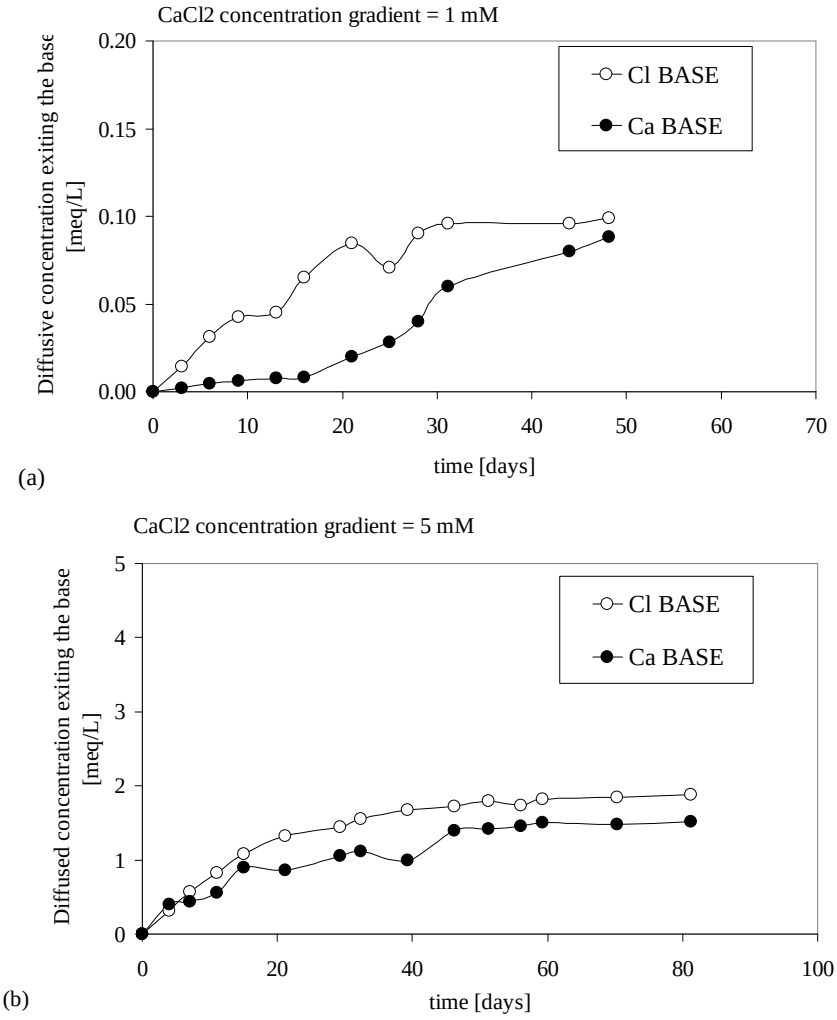

Figure 5.73: Measured chloride and calcium concentrations exiting the base of the HYPER clay due to diffusion, corresponding to a concentration gradient of (a) ΔC_1 = 1 m M $CaCl_2$ and (b) ΔC_2 = 5 m M $CaCl_2$

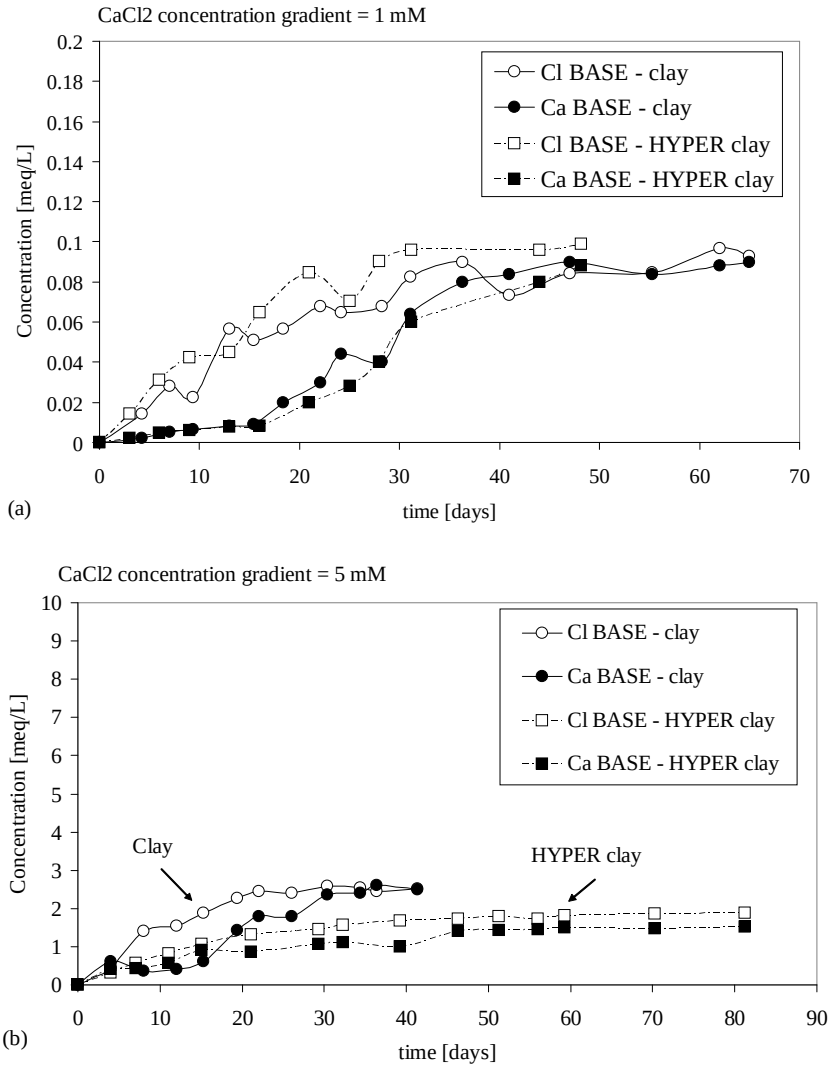

Figure 5.74: Measured chloride and calcium exit concentrations of the HYPER clay compared to the untreated clay. For a concentration gradient of ΔC_1 = 1 m M $CaCl_2$ the curves are similar. For a ΔC_2 = 5 m M $CaCl_2$, the HYPER clay diffusion shows some delay respect to the untreated clay

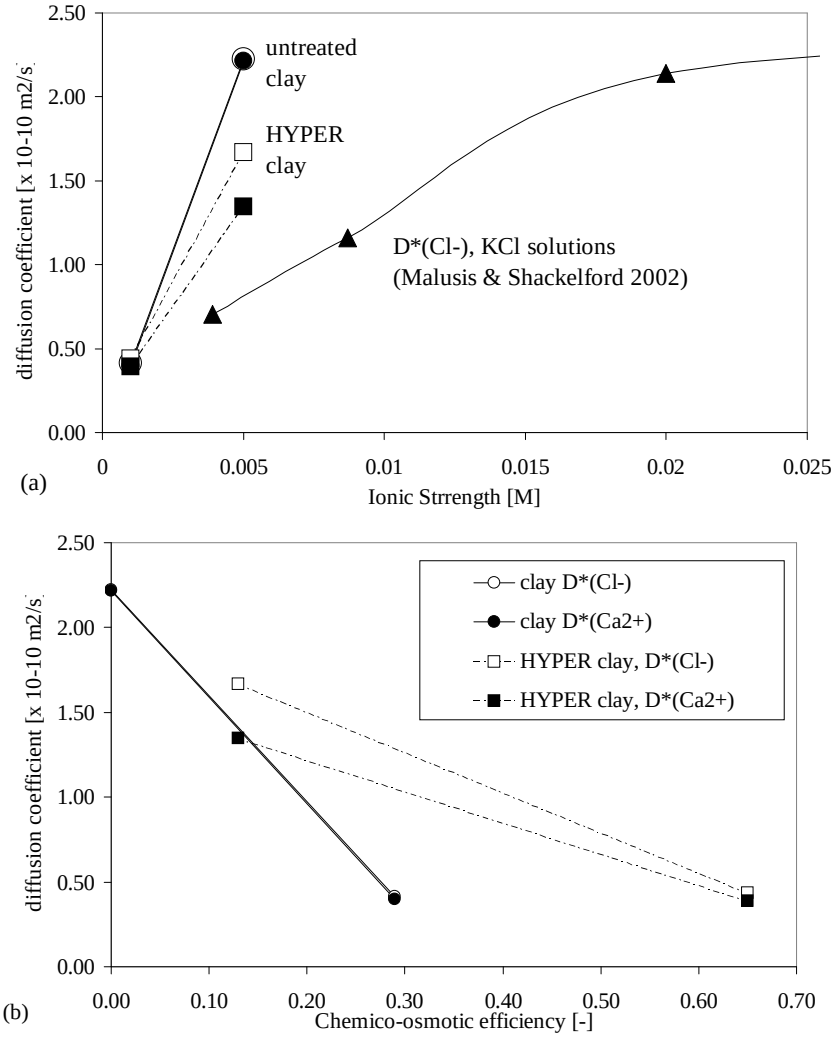

Figure 5.75: Effective solute diffusion coefficients vs. (a) Ionic Strength and (b) chemico-osmotic efficiency

Both Na^+ and Ca^{2+} ions diffused downwards along with Cl^- for electrical balance. The sum between Na^+ and Ca^{2+} concentration analyzed in the base outflow approaches the Cl^- concentration, in accordance to electroneutrality requirements. Counter-ion diffusion of Na^+ was also observed for the HYPER clay, likewise for the untreated clay and MSB, as mentioned above. For the HYPER clay, concentrations of Na^+ (both on the top and on the base of the specimen) were higher compared to the untreated clay, probably due to excess soluble/exchanged Na^+ coming not only from the clay, but also from the sodium-polymer, Na-CMC.

The measured Cl^- and Ca^{2+} concentrations from the top specimen boundary are shown in Fig. 5.76. As for the untreated clay, also for the HYPER clay, the time required for each steady-state diffusion was evaluated by performing sequential linear regression analyses on an increasing number of cumulative mass per unit area Qt vs. time (Fig. 5.77 and 5.78).

To evaluate the solute transport parameters D^* (effective diffusion coefficient) and R_d (retardation factor), the trends in cumulative mass per unit area versus time were analyzed by the time-lag method, as shown in Fig. 5.77 and 5.78. The effective diffusion coefficients, D^*, of the HYPER clay for Cl^- and Ca^{2+} were, respectively, $0.44E^{-10}$ m^2/s and $0.39E^{-10}$ m^2/s, for a concentration gradient ΔC_1 = 1 mM $CaCl_2$. The D^* of the solutes (Cl^- and Ca^{2+}) were similar, which is consistent with the electroneutrality requirement at steady-state diffusion. D^* was calculated in accordance with equation 4.6 using a measured porosity n = 0.718 and thickness L = 6.3 mm.

As observed for the untreated clay and for the MSB, also for the HYPER clay both Cl^- and Ca^{2+} were retarded in the chemico-osmotic test for a concentration gradient ΔC_1=1 mM $CaCl_2$ (R_d(Cl) = 6.9, R_d(Ca)=11.5). For ΔC_1 = 1 mM $CaCl_2$, release of Na^+ cations during diffusion of Ca^{2+} suggested that cation exchange onto the soil surface was the main retarding process for Ca^{2+}. The chemico-osmotic effect and the electrostatic interaction among the diffusing ions also had a role in the retardation of Ca^{2+} and Cl^-. The retardation of Cl^- could be partly explained by electroneutrality requirements due to the counter-diffusion of Na^+ into the top solution. The boundary concentrations vary during the test as a result of diffusion, with a consequent influence in the transport parameters.

For a concentration gradient ΔC_2 = 5 mM $CaCl_2$, the effective diffusion coefficients, D^*, of the HYPER clay for Cl^- and Ca^{2+} were, respectively, $1.67E^{-10}$ m^2/s and $1.35E^{-10}$ m^2/s. The D^* of the solutes (Cl^- and Ca^{2+}) were similar, which is consistent with the electroneutrality requirement at steady-state diffusion.

Also for a concentration gradient ΔC_2=5 mM $CaCl_2$, both Cl^- and Ca^{2+} were delayed (R_d(Cl) = 43.76, R_d(Ca)=43.28). Given that the cation exchange onto the soil surface was restricted, the retardation of Ca^{2+} and Cl^- are mainly due to the chemico-osmotic effect and the electrostatic interaction among the diffusing ions. The retardation of Cl^- could be partly explained by electroneutrality

requirements due to the counter-diffusion of Na^+ measured into the top solution. Also the boundary concentrations vary during the test as a result of diffusion, with a consequent influence in the transport parameters.

As explained above, the steady-state diffusive molar flux of Cl^- theoretically should be twice the magnitude of the steady-state diffusive molar flux of Ca^{2+}. Based on the results shown in Fig. 5.79, the observed ratio of the steady-state diffusive mass flux of Cl^- to the steady-state diffusive mass flux of Ca^{2+} in both stages approached sufficiently this theoretical value suggesting that steady-state diffusion had essentially been established. Moreover, for the concentration gradient ΔC_2, this ratio J(Cl)/J(Ca) was approximately around 2.5 from the start of the test (Fig. 5.79), suggesting that the adsorption of Ca^{2+} onto the clay due to cation exchange was restricted by the polymer, with a steady-state diffusive molar flux ratio from the start of the second stage.

Shielding role of the polymer, Na-CMC, on the membrane behavior of the HYPER clay with time

The multi-stage test on the untreated clay showed, for every concentration gradient, a similar trend of the chemico-osmotic efficiency with time. As shown in Fig. 5.65, the chemico-osmotic efficiency showed a maximum value after few hours of testing and a gradual decrease to a lower constant value at steady-state diffusion conditions. This gradual decrease of chemico-osmotic behaviour was attributed to the compression of DDL thickness caused by increasing concentrations of bivalent Ca^{2+} in the pore fluid due to diffusion.

In contrast, the HYPER clay preserved its membrane efficiency with time, probably due to the presence of the polymer that maintained the interlayer between particles open (Fig. 5.71 and 5.72). Ruehrwein and Ward (1952) stated that the adsorption of anionic polymers on to clays occurs through ionic exchange, Michaels and Morelos (1955) suggested that adsorption is mainly conditioned by hydrogen bonding, a third possibility would originate from the interaction between polyvalent cations (such as Ca^{2+}), acting as crosslinking agents between the clay negative surface and the anionic polymer (Stutzmann and Siffert, 1977). In the presence of salts and cations naturally present at the clay surface, the negative charges of the clay and the anionic polymer are shielded from one another allowing the polymer to coil and collapse on the clay surface (Breen, 1999). The polymer and the adsorbed cation coat the clay surface, potentially forming a protective layer. The adsorption of polymer chains (such as Na-CMC) in clay can be irreversible and entropy-driven because a polymer chain displaces many water molecules and attracts thousands of cations which would need to be displaced simultaneously (Theng, 1982; Ashmawy et al., 2002). For these reasons polymers can protect the clay from cation exchange that is the main reason for the compression of the double layer and for the consequent decrease of chemico-osmotic

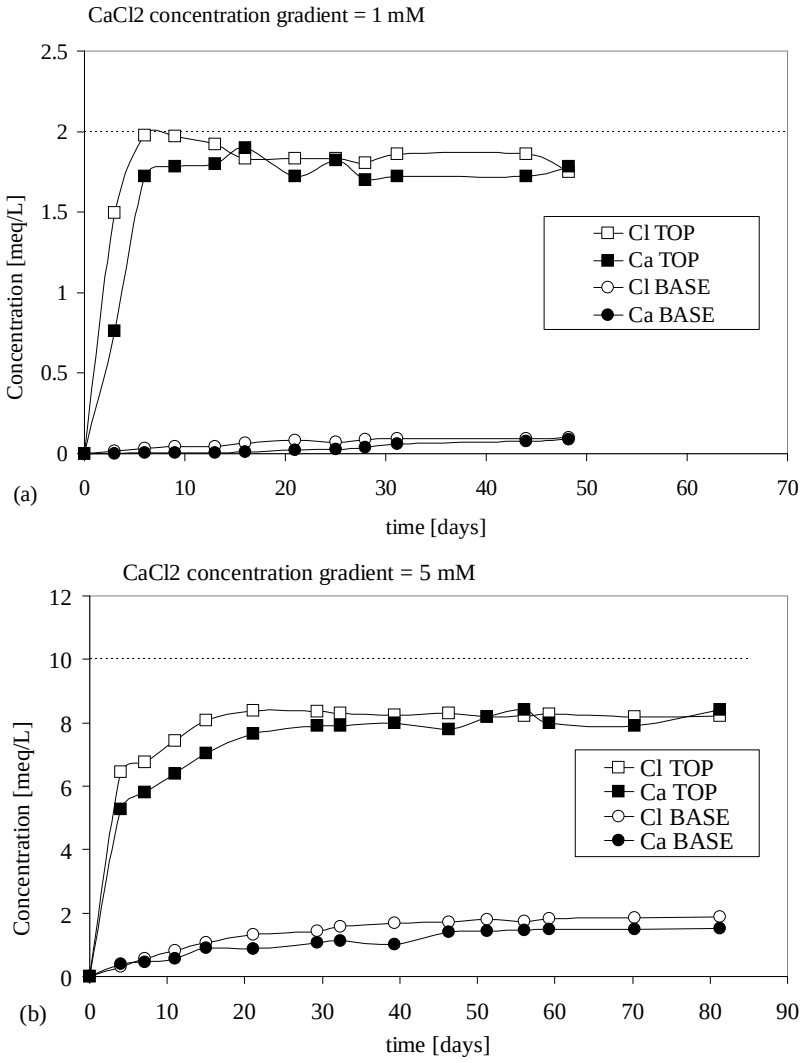

Figure 5.76: Measured chloride and calcium concentrations exiting the base and the top of the HYPER clay, corresponding to a concentration gradient of ΔC_1 = 1 m M $CaCl_2$ and ΔC_2 = 5 m M $CaCl_2$

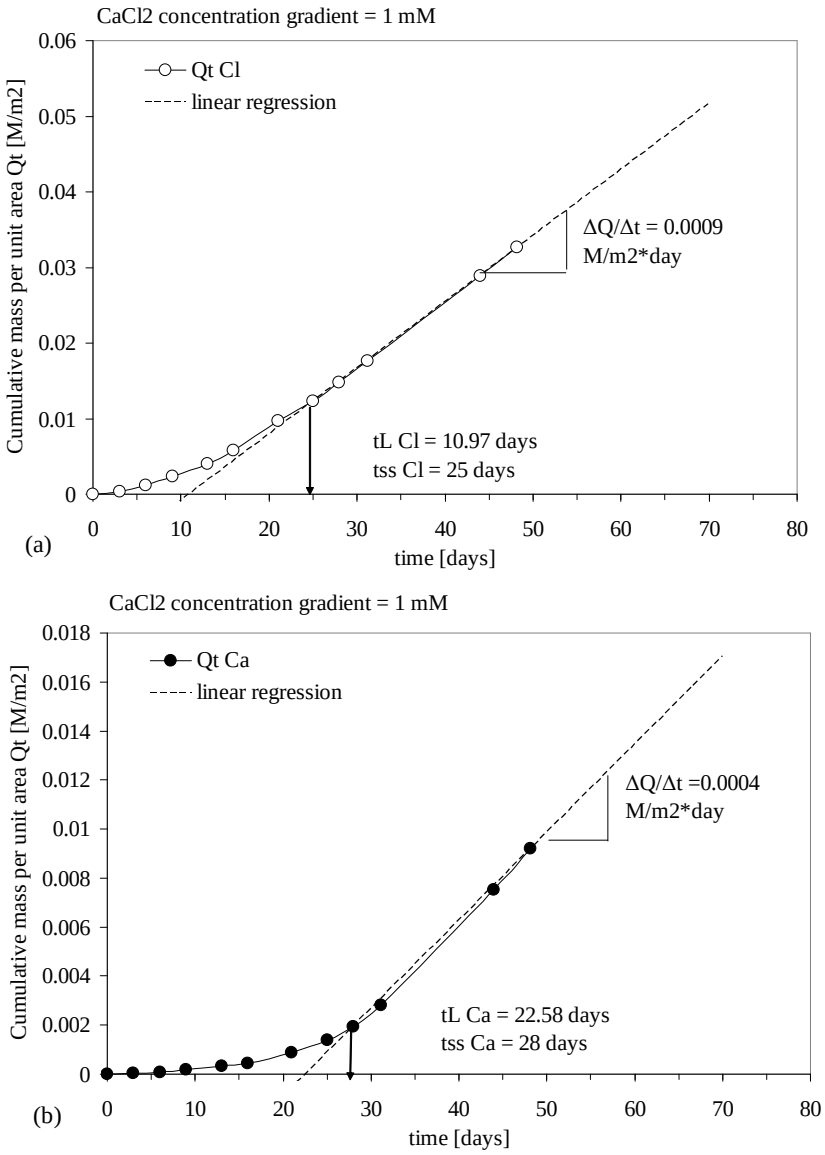

Figure 5.77: HYPER clay, ΔC_1 = 1 m M $CaCl_2$: cumulative mass per unit area based on the measured concentrations at the base, with t_L = time lag; t_{ss}=time to steady-state diffusion

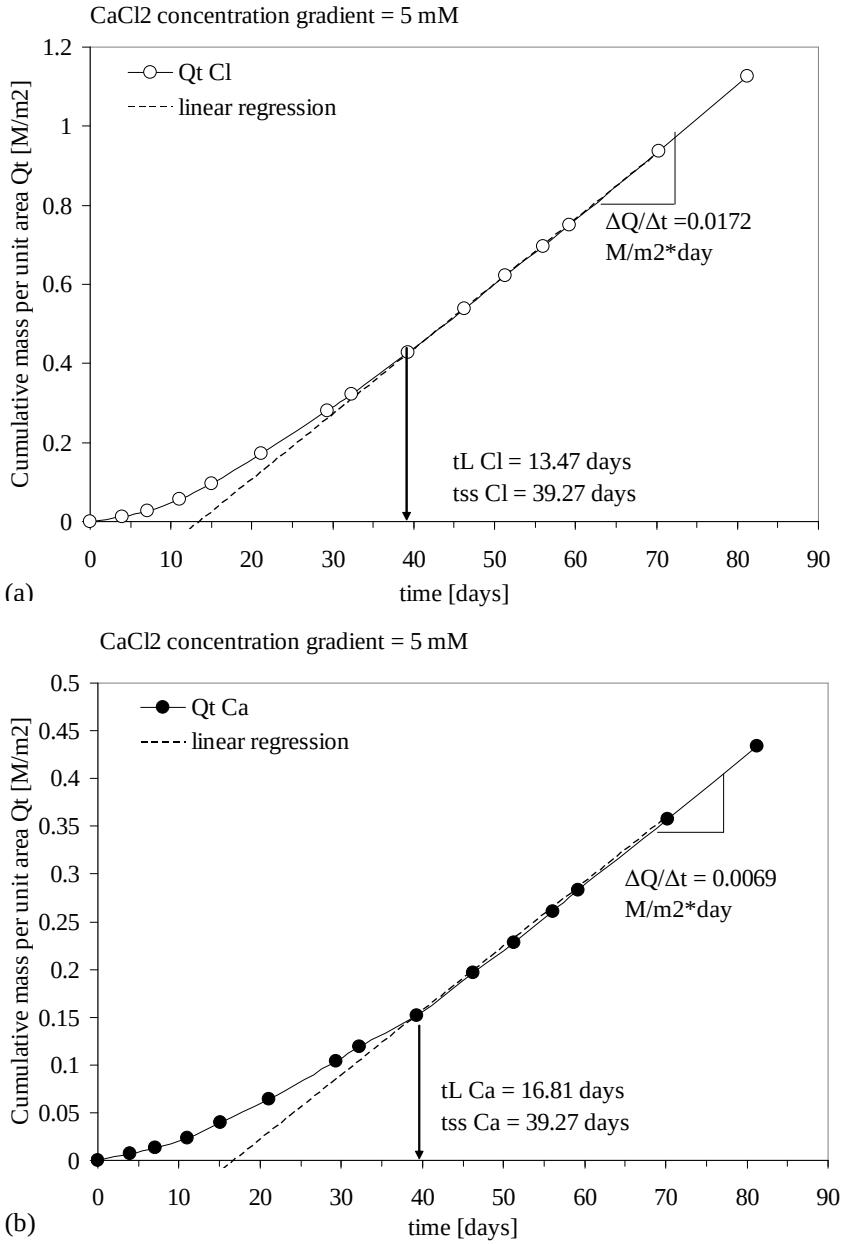

Figure 5.78: HYPER clay, ΔC_2 = 5 m M $CaCl_2$: cumulative mass per unit area based on the measured concentrations at the base, with t_L = time lag; t_{ss} =time to steady-state diffusion

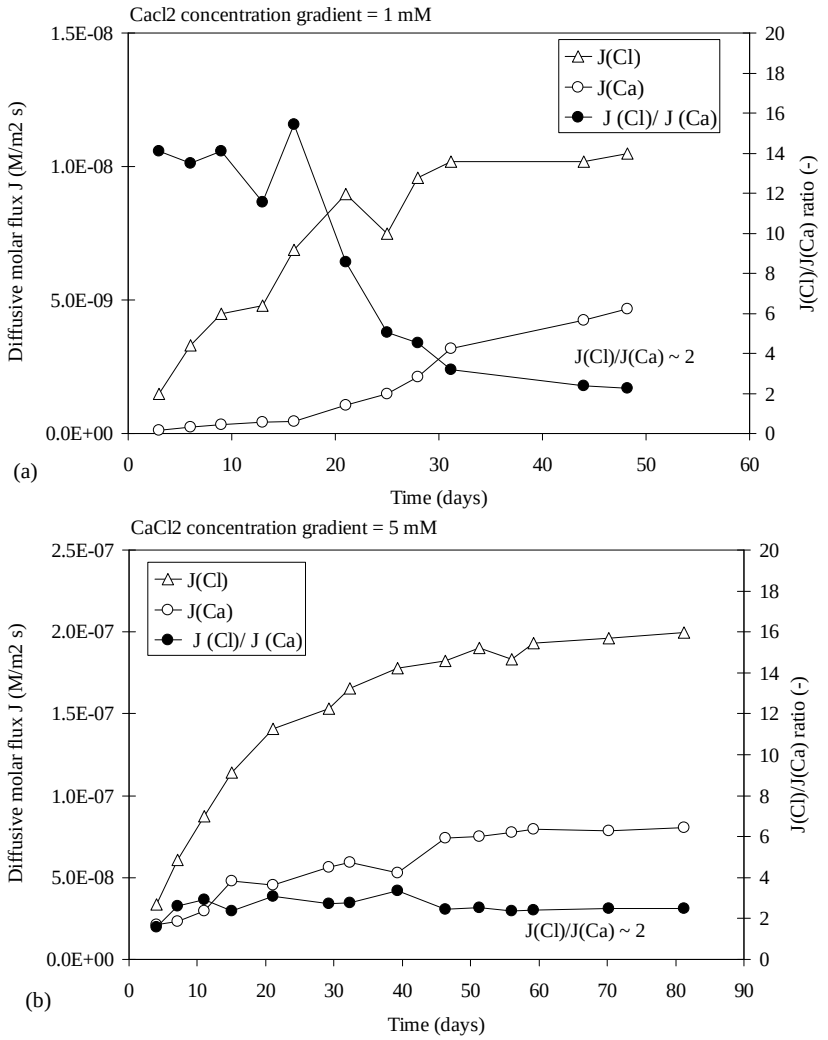

Figure 5.79: Diffusive molar flux vs. time of the multiple-stage osmotic test on the HYPER clay

efficiency.

The peak value -ΔP_{max} of the HYPER clay and the untreated clay were comparable. Then, the Ca^{2+} ions diffused through the samples and the -ΔP of the untreated clay gradually decreased, whereas the -ΔP of the HYPER clay maintained constant, as a result of polymer protection against cation exchange. Therefore, the Na-CMC polymer enhanced the membrane behavior of the HYPER clay compared to the untreated clay in presence of Ca^{2+} in the pore solution.

In conclusion, the treatment of the clay with Sodium-Carboxymethyl Cellulose (Na-CMC) was able to maintain a chemico-osmotic efficiency of the HYPER clay even at the steady state. Test results showed that the MSB looses its Propylene Carbonate during the test, behaving as an untreated clay. In contrast, the preservation of the chemico-osmotic efficiency of the HYPER clay with time suggests that the Na-CMC was not flushed out during the long period of permeation with deionized water which lasted 26 Pore Volumes of flow (334 days).

Swell index tests were performed on a HYPER clay specimen before and after submersion in a 100 mM $CaCl_2$ solution for about 30 days. The swell index before submersion was 37 ml/2g, whereas the swell index after such prolonged contact with the 100mM $CaCl_2$ solution was 24 ml/2g. This value is are lower than the result obtained on fresh HYPER clay but was nevertheless considerably higher than typical values of calcium bentonites (e.g. of the order of 10 ml/2g). These results suggest that the polymer was still present in the HYPER clay after contact with the high concentrated $CaCl_2$ solution and that the polymer treatment with Na-CMC protected the clay from cation exchange.

5.5.4 Chemico-osmotic efficiency of a Dense PreHydrated GCL

Induced differential pressures and chemico-osmotic efficiency

Based on the results in Section 5.2 and 5.4, we have shown that the DPH GCL exhibits higher swelling capacity and lower hydraulic conductivity than standard GCLs. Furthermore, a chemico-osmotic efficiency test was performed also on the polymer treated and densified Dense Prehydrated GCL (DPH GCL). In this test, a concentration gradient of ΔC_1= 1 mM $CaCl_2$ was used.

During the chemico-osmotic/diffusion test on the DPH GCL, replacement of deionized water with the solution source on the top boundary, caused an immediate increase in the differential pressure to a peak value that gradually decreased (Fig. 5.80). The peak value was $-\Delta P_{max}$= 6.62 kPa, corresponding to a peak chemico-osmotic efficiency value ω_{ss}=0.91. Then, the differential pressure gradually decreased to values of about $-\Delta P_{ss}$ = 2 kPa.

These results show that the DPH GCL specimen exhibited initial membrane behavior, as for the other clays analyzed here. However, the chemico-osmotic efficiency gradually decreased to the steady-state ω_{ss}= 0.27, comparable to the ω_{ss}

obtained for the untreated clay (Fig. 5.81).

Transport Parameters for the DPH GCL

The solutes diffusion through the DPH GCL is currently being assessed by measuring Chloride (Cl^-) and Calcium (Ca^{2+}) concentrations in the circulating liquid exiting the base of the specimen vs. time.

Preliminary results showed that, as for the other clays analyzed, also for the DPH GCL the breakthrough of Cl^- occurred earlier than Ca^{2+}. This result indicates that the diffusion of the Ca^{2+} was delayed. This delay could be due to the adsorption of the Ca^{2+} onto the clay surface due to cation exchange of the Ca^{2+} from the source solution with Na^+ from the clay. The chemico-osmotic effect and the electrostatic interaction among the diffusing ions also can have a role in the retardation of Ca^{2+}.

After 30 days of testing, the concentration of Ca^{2+} from the base outlet were still very low (of the order of 0.02 meq/L) compared to the concentrations obtained for the other chemico-osmotic tests discussed above. In fact, the Ca^{2+} concentration at the base outlet (at 30 days) was: $C_{Ca^{2+}}$ = 0.08 meq/L for the untreated clay and $C_{Ca^{2+}}$ = 0.06 meq/L for the HYPER clay.

Based on the results after 30 days of testing, the diffusive molar flux ratio was about J(Cl)/J(Ca)=10. This result is still considerably far from the expected steady-state value of 2. Therefore, a longer period will be required to reach the steady-state.

Given these preliminary results, we expect for the DPH GCL a low diffusion coefficient and a high Retardation factor (for Calcium).

Preliminary considerations on the chemico-osmotic efficiency of a Dense Prehydrated GCL

The chemico-osmotic efficiency results obtained on the DPH GCL, with a $CaCl_2$ concentration gradient ΔC_1 = 1 mM, qualitatively resemble the findings on the untreated clay (Fig. 5.81). In fact, DPH GCL did exhibit initial membrane behavior (ω_{max}=0.91) gradually reduced to ω_{ss}=0.27 as a result of salt migration and the consequent compression of the diffuse double layer. The peak vlaue of the chemico-osmotic efficiency, ω_{max}, was significantly high probably as a result of polymer treatment and low porosity (n=0.68).

On the other hand, the polymer treatment and the low porosity were unexpectedly not able to maintain the chemico-osmotic efficiency with time as occurred for the HYPER clay (Fig. 5.82).

This result was unexpected as the DPH GCL shows a good hydraulic performance that remained constant for almost 3 years (see results in the Section 5.4).

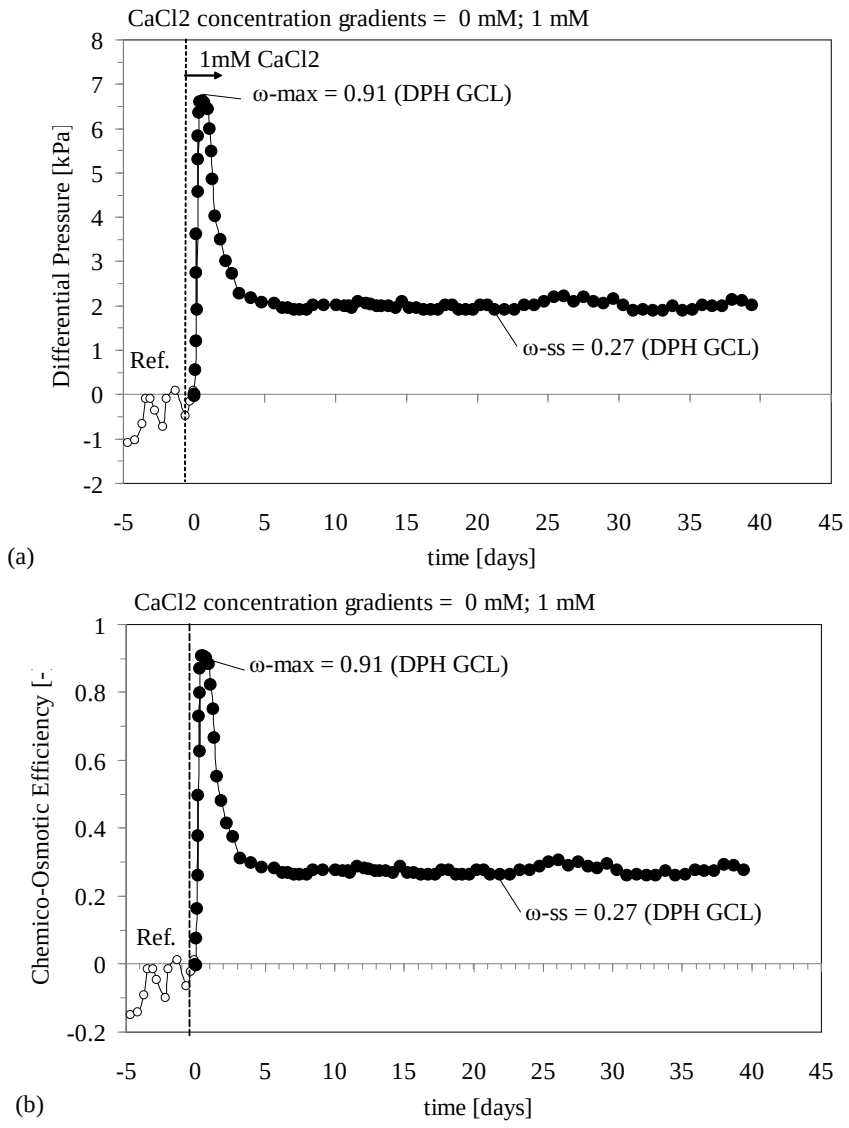

Figure 5.80: Chemico-osmotic efficiency of the Dense Prehydrated GCL with a concentration gradient of 1 mM $CaCl_2$

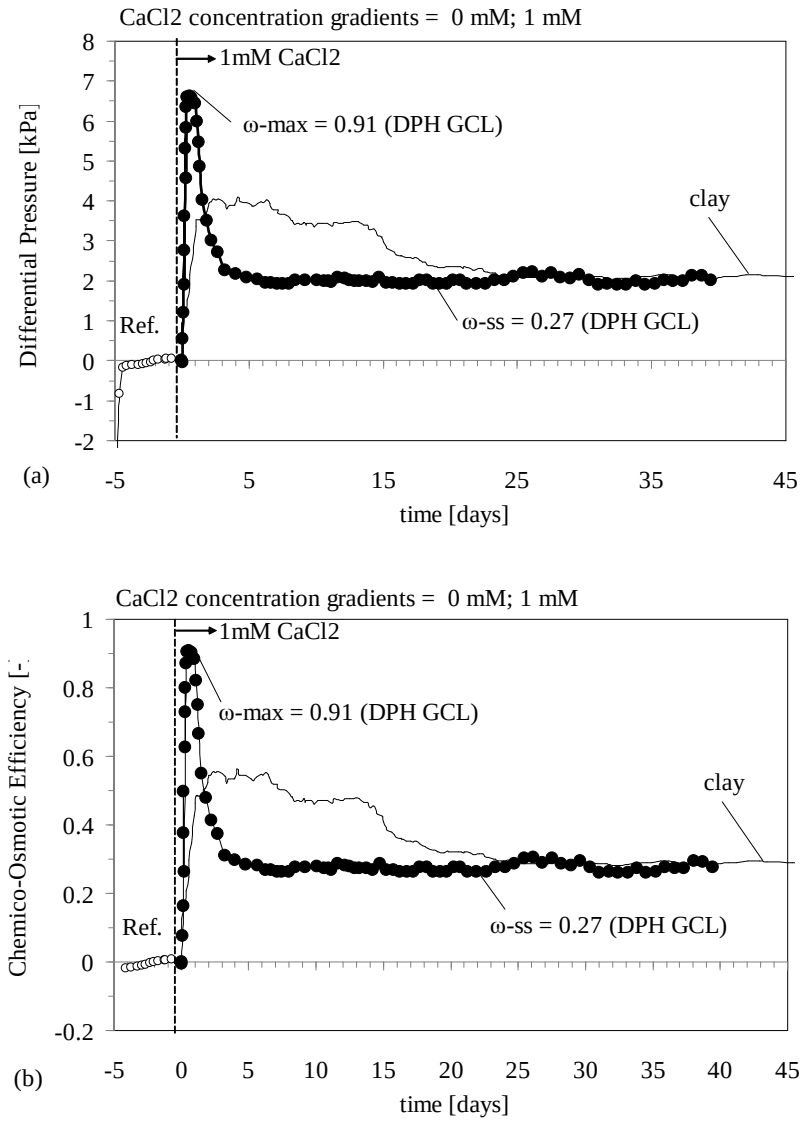

Figure 5.81: (a) Differential pressure and (b) chemico-osmotic efficiency of the DPH GCL compared to an untreated clay (ΔC_1 = 1 mM $CaCl_2$)

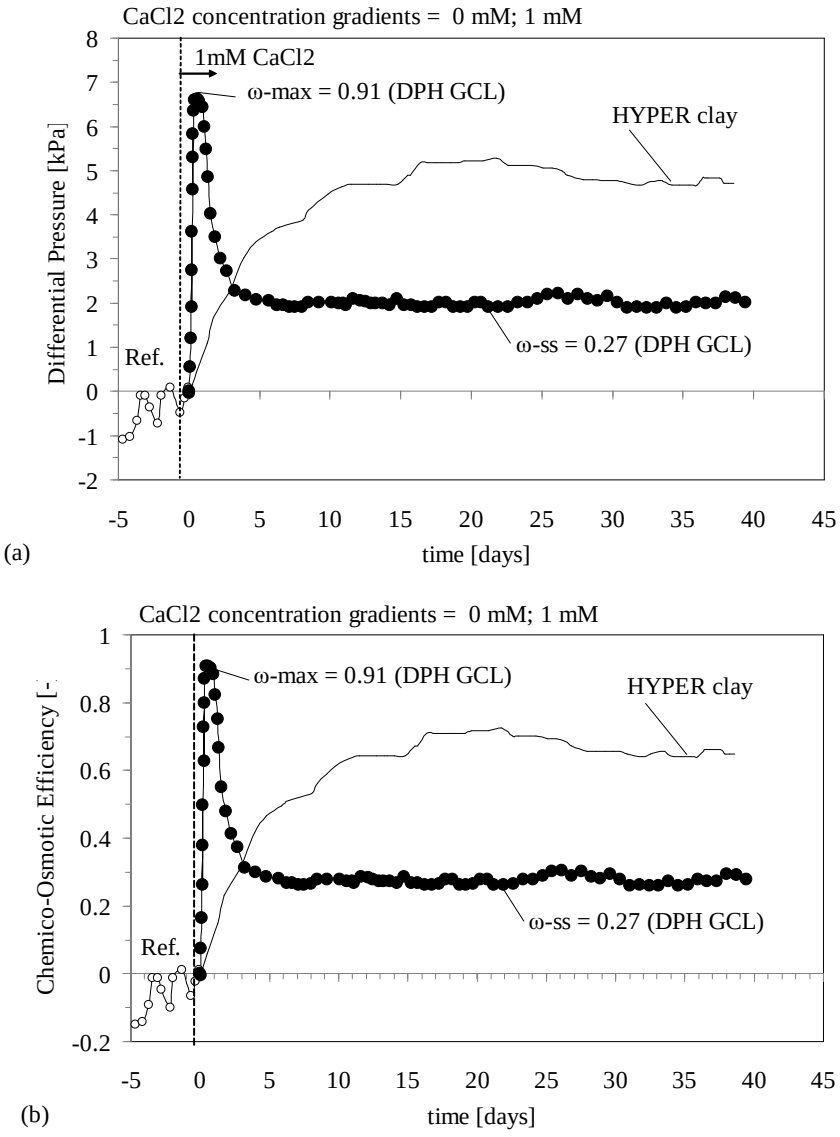

Figure 5.82: (a) Differential pressure and (b) Chemico-osmotic efficiency of the DPH GCL compared to the HYPER clay (ΔC_1 = 1 mM $CaCl_2$)

In contrast, the HYPER clay did maintain its chemico-osmotic efficiency with time. The difference on the behavior of these two polymer treated clays could be due (1) to differences in the duration of the flushing phase of the osmotic test and (2) to differences in the method of preparation used for the two clays.

Firstly, a very long flushing phase was required to decrease the outlet Electrical Conductivity (EC) of the DPH GCL in order to remove soluble salts before the chemico-osmotic test started (1379 days to remove soluble salts as much as possible and decrease the EC to about 1/2 EC of the source solution). On the other hand, the flushing phase required for the HYPER clay was considerably shorter (344 days), with a consequent probable influence on the results. In fact, longer time of flushing of soluble salts could have induced removal of the soluble polymer from the DPH GCL.

Secondly, the method of preparation of the HYPER clay consist of oven drying (at 105° C) a slurry of clay mixed with the polymeric solution containing 2% Na-CMC. On the other hand, the method of preparation of the DPH GCL consist of drying at 20° C (room temperature) under vacuum the slurry of clay mixed with various additives included polymers.

Stutzmann and Siffert (1977) compared the quality of the adsorption of anionic polymers on to montmorillonite surface for two scenarios: (a) drying the treated clay either at 60° C and (b) drying under vacuum at 20° C. They found that the adsorption of the polymer on the montmorillonite after drying at 60° C can be considered as intense, irreversible fixation, corresponding to chemisorption. On the other hand, the adsorption observed with vacuum drying corresponds rather to an unstable adsorption equilibrium, such as a reversible physisorptive adsorption (Stutzmann and Siffert, 1977). The quality of polymer adsorption depends on the residual water retained by the montmorillonite at different drying temperatures. At low temperatures more water is retained by the bentonite. Due to their repulsive forces and solubility, the anionic polymers can remain suspended winding through this retained water and prone to be removed.

Moreover, the polymer adsorption can be irreversible at high temperatures because a polymer chain displaces many water molecules, attracting thousands of cations which would need to be displaced simultaneously (Theng, 1982; Ashmawy et al., 2002).

Mazzieri and Pasqualini (2008) studied the permeability of the same DPH GCL subjected to dry/wet cycles and using a 12.5 mM $CaCl_2$ solution as hydrating liquid. They observed that the hydraulic conductivity to $CaCl_2$ increased to 8E-11 m/s after the 1st drying cycle and to 5E-08 m/s after the 2nd. After completion of the test, a small portion of the bentonite was dried and used for a swell index test into the $CaCl_2$ solution. The result was 9 ml/2g against about 21 ml/2g of as-received DPH GCL. The bentonite settling pattern showed less turbidity compared to the as-received DPH GCL, indicating that the polymer was probably removed

sample	$CaCl_2$ $[mM]$	solute	t_L [days]	t_{ss} [days]	$D^* \cdot 10^{-10}$ [m^2/s]	R_d [-]	ω_{max} [-]	ω_{ss}
clay	ΔC_1=1	Cl^-	12.87	28.21	0.40	7.65	0.56	0.29
		Ca^{2+}	23.47	36.29	0.41	13.49	0.56	0.29
	ΔC_2=5	Cl^-	7.83	19.38	2.22	36.21	0.12	0.0
		Ca^{2+}	15.68	26.02	2.22	68.60	0.12	0.0
MSB	ΔC_2=5	Cl^-	2.8	11.5	1.79	4.6	0.17	0.0
		Ca^{2+}	13.7	30.0	1.60	17.5	0.17	0.0
Hyper clay	ΔC_1=1	Cl^-	10.97	25	0.44	6.91	0.65	0.65
		Ca^{2+}	22.58	28	0.39	11.54	0.65	0.65
	ΔC_2=5	Cl^-	13.47	39.27	1.67	43.76	0.13	0.13
		Ca^{2+}	16.81	39.27	1.35	43.28	0.13	0.13
DPH GCL	ΔC_1=1	Cl^-					0.91	0.27
		Ca^{2+}					0.91	0.27

Table 5.5: Chemico-osmotic/diffusion test results

during the test. Also the value of the swell index at the end of the test (typical value for calcium bentonites) confirms this hypothesis, suggesting that the DPH GCL converted into a calcium exchanged form as a result of cation exchange.

5.5.5 Summary of the results

The transport parameters of the clays analyzed are summarized in table 5.5. As shown in the table, the time lag, t_L, the time at steady-state, t_{ss}, and the retardation factor, R_d, of Ca^{2+} are higher than the corresponding parameters of Cl^-. The delay of the Ca^{2+} is due to its adsorption onto the clay surface, mainly due to cation exchange with sodium Na^+.

As shown in table 5.5, the Diffusion, D^*, of the MSB was slightly lower than the Diffusion of the natural clay. This result was probably influenced also by the first stage performed on the natural clay, and not on the MSB, with a concentration gradient ΔC_1 = 1 mM $CaCl_2$.

As shown in table 5.5, the Diffusion, D^*, of the HYPER clay, with a concentration gradient ΔC_1 = 1 mM $CaCl_2$, was comparable to the Diffusion of the natural clay. This result confirms the statement that for diluted solutions the effect of the polymer is limited because the double layer is already sufficiently thick and the transport parameters are similar to the untreated clay. On the other hand, the Diffusion of the HYPER clay, with a higher concentration gradient (ΔC_2 = 5 mM $CaCl_2$) was lower than the Diffusion of the natural clay. This result suggests that the polymer protected the exchangeable sodium of the HYPER clay from cation exchange with Ca^{2+}. In fact, the time at steady state (t_{ss}) and the retardation factor

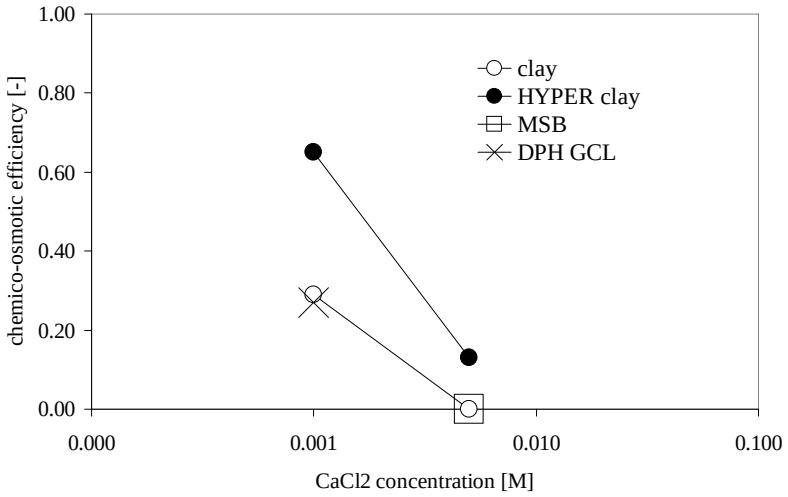

Figure 5.83: Chemico-osmotic efficiency overview

(R_d) of Ca^{2+} was not delayed compared to t_{ss} and R_d of the Cl^-, as expected after cation exchange occurs (see table 5.5).

Diffusion of Ca^{2+} and of Cl^- are similar for electroneutrality restraint, as mentioned above, for the natural clay, MSB, HYPER clay (see table 5.5). On the other hand, D^* of Ca^{2+} for the HYPER clay (ΔC_2=5 mM $CaCl_2$) was slightly lower than D^* of Cl^-. A possible explanation of this is probably the presence of excess Na^+ from the polymer (Na-CMC), that diffused downwards with Cl^- and Ca^{2+}.

Based on improved swelling and hydraulic performance of MSB, it was expected to observe also an improved chemico-osmotic behavior compared to the untreated clay. Conversely, Fig. 5.83 shows that the PC treatment did not provide any improvement on the chemico-osmotic behavior of the MSB. This plain performance of the MSB may be attributed to the elimination of the PC during the test.

Likewise, based on the excellent hydraulic performance of DPH GCL in the long term, it was expected to observe also an improved chemico-osmotic behavior. Conversely, the chemico-osmotic efficiency gradually decreased with time to a ω_{ss} value typical of standard bentonites (Fig. 5.83). These results probably indicates that the initial superior properties of the DPH GCL changed with time under the chemico-osmotic testing conditions.

On the other hand, Fig. 5.83 shows that the addition of the Na-CMC polymer increased the chemico-osmotic efficiency of the HYPER clay compared to the untreated clay, both for ΔC_1 and ΔC_2. These results suggest that the use of the

HYPER clay in containment application may be very promising.

5.6 Theoretical interpretation of the chemico-osmotic behavior in 3-ion systems

5.6.1 Introduction

Problem statement

The analytical solutions of most of the existent models that represent chemico-osmotic properties of clays, are restricted to simple geometries and limited boundary conditions. For instance, they apply only to 2-ion systems, such as sodium clays (Na-clays) in contact with NaCl solutions or calcium clays (Ca-clays) in contact with $CaCl_2$ solutions.

On the other hand, we should represent the actual conditions expected in practice. For example, clayey barriers are typically a Na-clay barrier in contact with bivalent electrolyte solutions (such as $CaCl_2$ solutions). This scenario represents an example of a 3-ion system (Na^+, Ca^{2+}, Cl^-) which is closer to actual conditions. In the framework of this research, a new approach has been proposed to provide an essential alternative to the current solutions for 2-ion systems.

New 3-ion System Model: numerical solution of the transport equations

The transport equations for a semipermeable porous media derived in Dominijanni (2005) are the starting equations for the new mathematical approach developed here. These equations were so far solved analytically by Manassero and Dominijanni (2003) for the case of a 2-ion system. To overcome this restriction, we wanted to extend this solution to allow for 3-ions.

For the analysis of the data, a particular development of the general model proposed by Dominijanni (2005) was necessary. During various stages at Politecnico di Torino, we developed together the interpretation of the laboratory tests carried out to measure the chemico-osmotic efficiency coefficient (in function of time) of natural and modified bentonites.

Specific boundary conditions were defined to model the chemico-osmotic properties of clays in a 3-ion system. The definition of correct boundary conditions was necessary to represent actual conditions expected in the transient phase.

The Transport Equations for a 3-ion system were solved by means of a finite difference method: the control volume approach. This model was able to represent the exchange of Na^+ with Ca^{2+} in time in good agreement with the experiments, both on treated and untreated clays.

The following paragraphs, first show the theoretical background based on the general model of Dominijanni (2005). Consequently, it illustrates the mathemati-

cal development for the improvement of this model for the case of a 3-ion system. Finally, a parametric study and the interpretation of the results based on the new model are presented.

The parametric study was intended to analyze the impact of the fixed charge concentration of the clay and the impact of the number of clay particles per aggregate on the chemico-osmotic efficiency coefficient vs. time. Whereas, the interpretation (back analysis) of the experimental data allowed to define the fixed charge concentration for both the untreated and polymer treated clays.

5.6.2 Theoretical background

A complete outline of the theoretical background for the theoretical interpretation is illustrated in Chapter 2. However, a short overview of the most important features are also given below for a better understanding of the mathematical development executed here.

From Microscopic to Macroscopic scale

Dominijanni (2005) performed the derivation of a macroscopic model from microscopic equations. At the microscopic scale, the transport equations are

1. the Poisson-Boltzmann equation for the microscopic distribution of the electric potential and of the ion concentrations;
2. the Nernst-Planck equations for the ion transport;
3. the modified Navier-Stokes equation for the volumetric flux.

The macroscopic model was derived as a first-order approximation of the transport equations at the microscopic scale.

Dominijanni's Model

Dominijanni (2005) performed a review of the coupled flow theory by Yeung and Mitchell (1993) and proposed a new set of equations. The main purpose was to take into account the osmotic phenomenon for the evaluation of solute and solvent flows through porous media under concentration and pressure gradients.

The model was developed in three stages:

- First, the postulates of irreversible thermodynamics (Katchalsky and Curran, 1965) were used to develop equations describing the simultaneous flows of solute and solvent.
- Second, the equations of continuity were derived for the coupled movement of solvent and solute.

- Finally, the solute flow equation and the solution continuity equation were combined and solved depending on the specific boundary value problem.

Dominijanni's mechanical model was developed using the Continuum Theory of Mixtures and the Donnan equilibrium of electrolyte solutions.

The model equations were derived from the mass and the momentum balances of all components of the system.

The boundary conditions were evaluated using Donnan equilibrium and the condition of electro-neutrality within the porous medium, accounting for the presence of a fixed charge of the solid skeleton.

An analytical solution was given for the evaluation of the chemico-osmotic efficiency coefficient of 1:1 electrolytes (2-ion system).

5.6.3 Mathematical Development of the solutions for a 3-ion system

Momentum Balance Equations

The ionic molar fluxes, J_i, can be obtained from the momentum balance equations, neglecting inertial effects and assuming the solution as ideal (e.g. very dilute):

$$J_i = q\bar{C_i} - nD_i^* \frac{d\bar{C_i}}{dx} - nz_i\bar{C_i}D_i^* \frac{F}{RT}\frac{d\Phi}{dx} \tag{5.43}$$

where q=volumetric flux;
$\bar{C_i}$=ion concentration;
n=porosity;
D_i^*=effective diffusion coefficient;
z_i=electro-chemical valence;
F=Faraday constant;
R=universal gas constant;
T=absolute Temperature;
Φ=electric potential within the clay.

Equation 5.43 is the Nernst-Planck equation that accounts for the presence of the electrochemical forces.

The volumetric flux of the solution, q, can be obtained from the momentum balance equation as follows:

$$q = -nd_h\left(\frac{d\bar{P_t}}{dx} - \varpi C_x F\frac{d\Phi}{dx}\right) \tag{5.44}$$

where d_h = mechanical permeability at zero electric gradient;
$\bar{P_t}$=total pressure of the solution within the pores;
ϖ=sign of the fixed charge.

Equation 5.44 accounts for the linear composition of two driving forces: (1) the pressure, that corresponds to the internal force associated to the thermal motion of the molecules composing the solution, and (2) the electro-chemical force, representing the net drag exerted by the ions during their migration under the electric gradient.

Equations 5.43 and 5.44 may be considered as the generalization of the transport equations commonly used to the case of soils having a charged soil skeleton.

Transport equations for a semipermeable porous medium

The transport equations (5.45 and 5.46) were derived by Dominijanni (2005) for a semipermeable porous medium, taking into account the osmotic phenomenon for the evaluation of solute and solvent flow under concentration and pressure gradients.

$$q = \frac{n d_h}{1 + d_h C_x^2 F^2 / \bar{\kappa}} \left(\frac{d\bar{P}_t}{dx} + \varpi C_x \frac{F^2}{\bar{\kappa}} \sum_{i=1}^{N} z_i D_i^* \frac{d\bar{C}_i}{dx} \right) \tag{5.45}$$

where

$$\bar{\kappa} = \sum_{i=1}^{N} \kappa_i = \frac{F^2}{RT} \sum_{i=1}^{N} z_i^2 \bar{C}_i D^* i;$$

is the equivalent electrical conductivity of the solution within the membrane; and

$$\bar{t}_i = \frac{\bar{\kappa}_i}{\bar{\kappa}}$$

is the transference (or transport) number of the i-th ion within the membrane.

The ion fluxes can be expressed as follows:

$$J_i = q\bar{C}_i \left(1 + \frac{\bar{t}_i}{z_i} \frac{\varpi C_x}{\bar{C}_i} \right) - n D_i^* \frac{d\bar{C}_i}{dx} + n \frac{\bar{t}_i}{z_i} \sum_{j=1}^{N} z_j D_j^* \frac{d\bar{C}_j}{dx} \tag{5.46}$$

Equations 5.45 and 5.46 have been solved analytically by Dominijanni (2005) for the case in which the pore solution contains a single salt (2-ion system). In the following paragraphs, we propose numerical solution for the more general case of a 3-ion system, which more closely models actual experimental and practical situations.

Assumptions

The mathematical model is considered to be an open system consisting of a solute and solvent flowing in the pores of a soil, in which the following assumptions are made:

(a) one-dimensional flow;

(b) solid skeleton incompressibility;

(c) isothermal conditions;

(d) no electric currents

$$I_e = F \sum_{i=1}^{N} z_i J_i = 0 \tag{5.47}$$

(e) electroneutrality condition

$$\sum_{i=1}^{N} z_i C_i^{'} = 0 \tag{5.48}$$

$$\sum_{i=1}^{N} z_i \overline{C_i^{'}} + \varpi C_x = 0 \tag{5.49}$$

(f) sufficiently diluted solution so that ideal solution relationships are valid;

(g) applicability of the postulates of irreversible thermodynamics.

In addition to that, the solution of the model for the case of a 3-ion system considers the following additional assumptions:

(a*) one-dimentional flow only due to the compressibility of the fluid (given that a closed system is considered here).

(b*) solvent compressibility

$$\frac{V_1}{k_w}\frac{dP_1}{dt} = Sq_1 \tag{5.50}$$

$$\frac{V_2}{k_w}\frac{dP_2}{dt} = -Sq_2 \tag{5.51}$$

Boundary conditions

As boundary conditions we assume the validity of the Donnan's Equations. For these boundary conditions (equations 5.52 and 5.53) it may be convenient to introduce a "virtual" solution, that, at any point x within the porous medium, is in thermodynamic equilibrium with the real solution, in analogy with the external bulk solutions. So we can pass from the real variables, $\overline{P_t}$ and $\overline{C_i}$, to the virtual variables, P and C_i, that are the pressure and the ion concentration of a fictive bulk solution.

In correspondence of the boundaries (x = 0 and x = L), the virtual solution coincides with the real external solution in contact with the porous medium. As a result, at the boundaries the pressure and the ion concentration are continuous with respect to the external bulk solutions. The relations that allow for the change of variables are similar to the boundary conditions, with the important difference that are valid not only at the boundaries, but at any point x within the porous medium.

To solve the transport equations, the following boundary conditions have to be imposed (Donnan's equation):

$$\vec{C_i} = C_i' exp\left(-z_i \frac{F}{RT}\psi_m'\right) i = 1,2,...N \tag{5.52}$$

$$\vec{P_{tot}} = P' - RT\sum_{i=1}^{N} C_i' + RT\sum_{i=1}^{N}\vec{C_i} \tag{5.53}$$

where ψ_m' is the macroscopic electric potential of the charged porous medium, or Donnan's potential, and P' is the external hydraulic pressure. In equations 5.52 and 5.53, all the variables (pressures and concentrations) are referred to the generic boundary ($'$). The Donnan's potential is given by the difference between the electric potential within the pores,Φ', and the electric potential in the external bulk solution, φ'. The Donnan's potential may be evaluated with the help of the electro-neutrality conditions in the external bulk solution and within the pores of the medium using the electroneutrality condition (equations 5.48 and 5.49).

Knowing the values of the pressure and of the ion concentrations in the bulk solutions in contact with the porous medium, equations 5.52 and 5.53 allow for the determination of the boundaries conditions for the transport equations (Dominijanni, 2005).

Diffusion

Fick$'$s first law for one-dimensional conditions can be expressed as:

$$J_d = -nD^* \frac{\partial C}{\partial x} \tag{5.54}$$

where J_d is the diffusive mass flux per unit area per unit time, D^* the effective diffusion coefficient, and $\partial C/\partial x$ the concentration gradient.

From Fick$'$s law and the equation of continuity, the rate at which a contaminant can diffuse in soils can be given by the Fick's second law as:

$$-n\frac{\partial C}{\partial t} = -\frac{\partial J}{\partial x} \Rightarrow -n\frac{\partial C}{\partial t} = nD^*\frac{\partial^2 C}{\partial^2 x} \tag{5.55}$$

which is the equation for diffusion in one-dimensional conditions when D^* is constant (Crank, 1975).

In many systems Diffusion may depend on the concentration, C, of diffusing substance. Therefore the equation to consider when the diffusion coefficient is not constant is:

$$\left\{\frac{\partial C}{\partial t}\right\} = \frac{\partial}{\partial x}\left([D]\left\{\frac{\partial C}{\partial x}\right\}\right) \tag{5.56}$$

that becomes:

$$\left\{\frac{\partial C}{\partial t}\right\} = [D]\left\{\frac{\partial^2 C}{\partial x^2}\right\} + \left\{\frac{\partial [D]}{\partial C}\right\}\left\{\left(\frac{\partial C}{\partial x}\right)^2\right\} \tag{5.57}$$

Diffusion in a plane sheet

We consider the case of one-dimensional diffusion in a medium bounded by two parallel planes, e.g. the planes at x = 0, x = L. This will apply in practice to diffusion into a plane sheet of material where all the diffusing substance enters through the plane faces.

Consider the case of diffusion through a plane sheet or membrane of thickness L and diffusion coefficient D, whose surfaces, x = 0, x = L, are maintained at constant concentrations C_1, C_2 respectively. After a time, a steady state is reached in which the concentration remains constant at all points of the sheet. The diffusion equation in one dimension then reduces to

$$d^2C/dx^2 = 0 \tag{5.58}$$

provided the diffusion coefficient D is constant. On integrating with respect to x we have

$$dC/dx = constant \tag{5.59}$$

and by a further integration we have, on introducing the conditions at x = 0, x = L,

$$\frac{C - C_1}{C_2 - C_1} = \frac{x}{L} \tag{5.60}$$

Both 5.59 and 5.60 show that the concentration changes linearly from C_1 to C_2 through the sheet. Also, the rate of transfer of diffusing substance is the same across all sections of the membrane and is given by

$$J = -D^* dC/dx = D^*(C_1 - C_2)/L \tag{5.61}$$

If the thickness L and the surface concentrations C_1 C_2 are known, D can be deduced from an observed value of J by using 5.61 (Crank, 1975).

Non-dimensional variables

Solving the problem of Diffusion, the group of variables D^*t/L^2 occurs frequently. The diffusion coefficient D is measured in $[length]^2/[time]$. Thus if we write the group D^*t/L^2 = T, we see that T is a dimensionless variable representing the time.

For the problem of diffusion, convenient non-dimensional variables are

$$X = \frac{x}{L},\ \ T = D^* \frac{t}{L^2},\ \ u = \frac{C}{C_0} \tag{5.62}$$

Then

$$\frac{\partial C}{\partial x} = \frac{\partial C}{\partial X}\frac{\partial X}{\partial x} = \frac{\partial C}{\partial X}\frac{1}{L} \tag{5.63}$$

$$\frac{\partial^2 C}{\partial x^2} = \frac{\partial^2 C}{\partial X^2}\frac{1}{L^2} \tag{5.64}$$

and

$$\frac{\partial C}{\partial t} = \frac{\partial C}{\partial T}\frac{\partial T}{\partial t} = \frac{\partial C}{\partial T}\frac{D}{L^2} \tag{5.65}$$

Thus, the simple diffusion equation becomes

$$\frac{\partial C}{\partial t} = D^* \frac{\partial^2 C}{\partial x^2} \tag{5.66}$$

$$\frac{\partial u}{\partial T} = \frac{\partial^2 u}{\partial X^2} \tag{5.67}$$

For the numerical solution developed in this research we propose as non-dimentional T=t/t_0 with $t_0 = L^2/D$ and D=$D^*_{Ca^{2+}}$. Substituting the non-dimensional variables in equation 5.57 we obtain:

$$\left\{\frac{\partial u}{\partial T}\right\} = \frac{[D]}{D^*_{Ca^{2+}}}\left\{\frac{\partial^2 u}{\partial X^2}\right\} + \frac{1}{D^*_{Ca^{2+}}}\left\{\frac{\partial [D]}{\partial u}\right\}\left\{\left(\frac{\partial u}{\partial X}\right)^2\right\} \tag{5.68}$$

Physical derivation of a numerical solution

Consider a plane sheet in which a solute concentration gradient exists initially. We wish to calculate how the distribution of solute changes with time. We divide the sheet into layers each of thickness h as in Fig. 5.84 and denote by C_0, C_1, C_2 the concentrations at three neighboring interfaces.

The dotted lines at R and S (Fig. 5.84) denote the mid sections of the two adjacent layers.

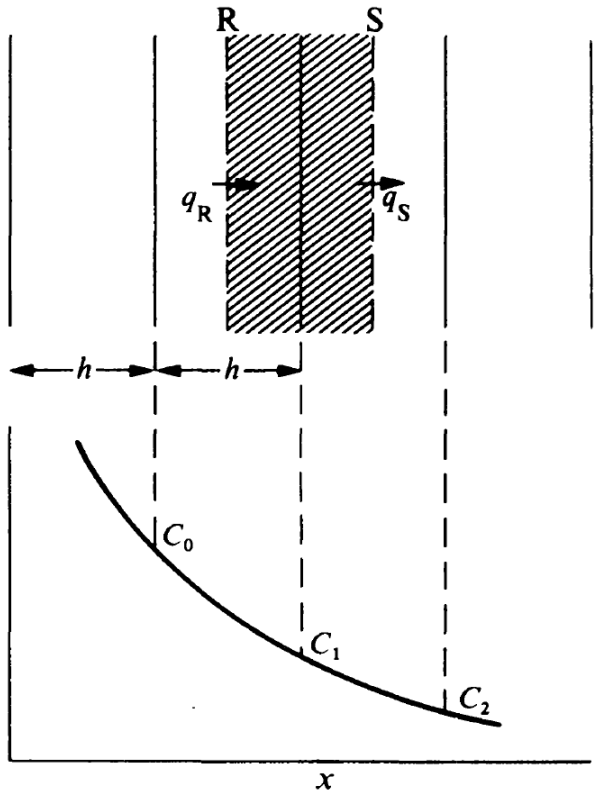

Figure 5.84: Physical derivation of a numerical solution (Crank, 1975)

We recall Fick's first law of diffusion: rate of transfer of solute through unit area is proportional to gradient of concentration and the constant of proportionality is the diffusion coefficient D^*.

Thus in a short time τ the amount of solute which has entered the shaded layer through unit area of the surface R is given approximately by

$$q_R = D^*\tau(C_1 - C_0)/h \tag{5.69}$$

At the same time, the amount flowing out through the face at S is approximately

$$q_s = D^*\tau(C_2 - C_1)/h \tag{5.70}$$

The net amount of solute accumulated in the shaded element in time τ is

$$q_R - q_S = -\frac{D^*\tau}{h}(C_1 - C_0 - C_2 + C_1) = \frac{D^*\tau}{h}(C_0 - 2C_1 + C_2) \tag{5.71}$$

If we now take C_1 to represent the average concentration in the narrow shaded element, the net gain of solute by the element can be written approximately as

$$(C_1^{'} - C_1)/h \tag{5.72}$$

where $C_1^{'}$ is the concentration at the end of the interval τ. Equating this with 5.71 we have

$$C_1^{'} - C_1 = \frac{D^*\tau}{h^2}(C_0 - 2C_1 + C_2) \tag{5.73}$$

By choosing for example $D^*\tau/h^2$ = 1/2 we find

$$C_1^{'} = \frac{1}{2}(C_0 + C_2) \tag{5.74}$$

This relationship enables us to calculate the concentration at a point at time t + τ if we know the concentrations C_0, C_2 at the two neighboring points at time t. We can apply 5.74 successively at each point of the sheet and advance the calculation in time steps τ (Crank, 1975).

5.6.4 Numerical solution of the problem of diffusion with a finite difference method: the Control Volume Approach

Transport equations for a 3-ion system

As mentioned above, the purpose of the mathematical development illustrated here is to solve the transport equations for a 3-ion system by means of a finite difference method.

First we will define the transport equations to solve and the unknown variables that we would like to find in function of time; then, we will describe the finite difference method used and the mathematical steps followed; and finally we will show how we solved the transport equations.

In order to solve the transport equations (equations 5.45 and 5.46) we should obtain the concentration C of the 3 ions (Na^+, Ca^{2+}, and Cl^-) in function of time from a system of three differential equations in 3 variables (C_{Na^+}, $C_{Ca^{2+}}$ and C_{Cl^-}).

$$\begin{cases} J_{Na^+} = f(C_{Na^+}) \\ J_{Ca^{2+}} = f(C_{Ca^{2+}}) \\ J_{Cl^-} = f(C_{Cl^-}) \end{cases} \tag{5.75}$$

Considering the electroneutrality condition for the three ions (i = Na^+, Cl^-, Ca^{2+}) we can reduce the number of variables. The electroneutrality condition can be expressed as:

$$2\bar{C}_{Ca^{2+}} + \bar{C}_{Na^+} + \bar{C}_{Cl^-} = \bar{C}_x \tag{5.76}$$

$$\bar{C}_{Na^+} = \bar{C}_{Cl^-} + \bar{C}_x - 2\bar{C}_{Ca^{2+}} \tag{5.77}$$

Supposed $\bar{C}_x$ constant, we can obtain:

$$\frac{\partial \bar{C}_{Na^+}}{\partial x} = \frac{\partial \bar{C}_{Cl^-}}{\partial x} - 2\frac{\partial \bar{C}_{Ca^{2+}}}{\partial x} \tag{5.78}$$

Substituting the three ions (i = Ca^{2+}, Na^+, Cl^-) in equations 5.46 we obtain the fluxes $J_{Ca^{2+}}$, J_{Na^+} and J_{Cl^-}. Then, considering the electroneutrality condition as expressed in equation 5.78, we obtain:

$$\{J\} = \begin{pmatrix} D_{11} & D_{12} \\ D_{21} & D_{22} \end{pmatrix} \left\{ \frac{\partial C}{\partial x} \right\} \tag{5.79}$$

where

$$\{J\} = \begin{pmatrix} J_{Ca^{2+}} \\ \\ J_{Cl^-} \end{pmatrix}$$

$$\left\{ \frac{\partial C}{\partial x} \right\} = \begin{pmatrix} \partial C_{Ca^{2+}}/\partial x \\ \\ \partial C_{Cl^-}/\partial x \end{pmatrix}$$

$$D_{11} = -nD^*_{Ca_{2+}} + n\bar{t}_{Ca^{2+}} D^*_{Ca^{2+}} - n\bar{t}_{Ca^{2+}} D^*_{Na^+}$$

$$D_{12} = n\bar{t}_{Ca^{2+}} D^*_{Na^+}/2 - \bar{t}_{Ca^{2+}} D^*_{Cl^-}/2$$

$$D_{21} = -n\bar{t}_{Cl^-} 2D^*_{Ca^{2+}} + n\bar{t}_{Cl^-} 2D^*_{Na^+}$$

$$D_{22} = -nD^*_{Cl^-} - n\bar{t}_{Cl^-} D^*_{Na^+} + n\bar{t}_{Cl^-} D^*_{Cl^-}$$

Numerical solution of the problem of diffusion

The differential equations were numerically solved by the finite difference method described above extended to a more general case.

Figure 5.85(a) shows the schematic sketch of the boundary conditions we consider here. As shown in the figure, there is an elementary volume of membrane surrounded by two solutions at the boundaries 1 and 3. Figure 5.85(b) illustrates the initial conditions of the ions distribution inside the elementary volume.

Boundary conditions

We consider as boundary conditions for t>0:

for x=0 (solution 1 = $CaCl_2$ with concentration C_0)

$C_{Ca^{2+}}(x=0,t) = C_0$;

$C_{Cl^-}(x=0,t) = 2C_0$;

$\bar{C}_{Na^+,1} = 0$;

$\bar{C}_{Na^+,1} = 0$;

$\bar{C}_{Ca^{2+},1}$ and $\bar{C}_{Cl^-,1}$ can be obtained from Donnan's equations.

for x=L (solution 3 = water)

$C_{Ca^{2+}}(x=L,t) = 0$;

$C_{Cl^-}(x=L,t) = 0$;

$C_{Na^+}(x=L,t) = 0$;

$\bar{C}_{Na^+,3} = 0$;

$\bar{C}_{Ca^{2+},3} = 0$;

$\bar{C}_{Cl^-,3} = 0$.

Initial conditions

We consider as initial conditions for t=0 (as shown in Fig. 5.85(b)):

$\bar{C}_{Na^+}(x,t=0) = C_x$, all the exchangeable cations are ions of Na^+;

$\bar{C}_{Ca^{2+}}(x,t=0) = 0$, there are no exchangeable nor soluble ions of Ca^{2+};

$\bar{C}_{Cl^-}(x,t=0) = 0$, there are no exchangeable nor soluble ions of Cl^-.

The net amount of solute accumulated in the shaded layer (shown in Fig. 5.85 (a)) in a short time δt should be equal to the mass of solute which has entered the shaded layer minus the mass of solute flowed out, as indicated in equation 5.80.

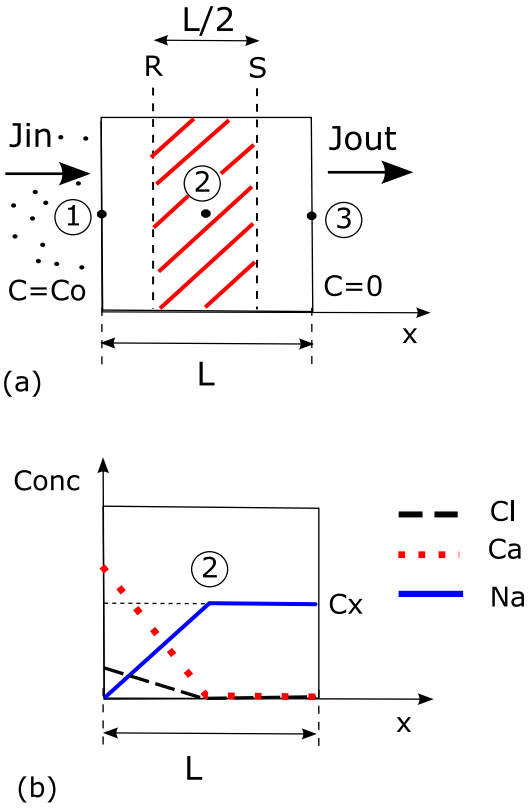

Figure 5.85: Schematic sketch of the (a) boundary conditions for the control volume approach and (b) initial conditions inside the elementary volume

$$M_{final} - M_{initial} = M_{in} - M_{out} \tag{5.80}$$

where

$$M_{in} = J_{in} \cdot S \cdot \delta t \tag{5.81}$$

$$M_{out} = J_{out} \cdot S \cdot \delta t \tag{5.82}$$

$$M_{initial} = n \cdot C_{initial} \cdot S \cdot L/2 \tag{5.83}$$

$$M_{final} = n \cdot C_{final} \cdot S \cdot L/2 \tag{5.84}$$

Therefore, equation 5.80 becomes:

$$n \cdot \delta C \cdot S \cdot L/2 = (J_{in} - J_{out}) \cdot S \cdot \delta t \tag{5.85}$$

$$\frac{\delta C_i}{\delta t} = (J_{in,i} - J_{out,i}) \frac{1}{L/2} \tag{5.86}$$

We can now calculate the ionic fluxes $J_{in,i}$ and $J_{out,i}$ for every ion, i, from equations 5.46, linearizing the derivatives in J_{in} calculated from point 1 to the point 2 in Fig. 5.85, and J_{out} from point 2 to point 3.

We solved numerically equations 5.86 with the finite-difference method described above advancing the calculation in time steps. For a detailed description of the iteration used please refer to the Appendix Sections.

Figure 5.86 shows a simulation of the diffusion process. The concentrations of Ca^{2+} and Na+ are plotted vs. time for the specific boundary conditions assumed. The trend of the two solutes in the figure clearly shows the cation exchange between the Ca^{2+} from the source solution 1 and the Na^{+} present in the exchangeable sites of the clay. The calculated cation exchange shows good agreement with the expected trend.

5.6.5 Chemico-osmotic efficiency in function of time for a three-ion system

The numerical solution of the transport equations for a 3-ion system described above provided the variables $\overline{C_i}$. Using Donnan's equations we can calculate C_i. The following paragraphs will describe the calculation of the chemico-osmotic efficiency as a function of time, ω(t), based (for definition) on the calculation of the differential pressure, ΔP(t). This differential pressure will be calculated out of the

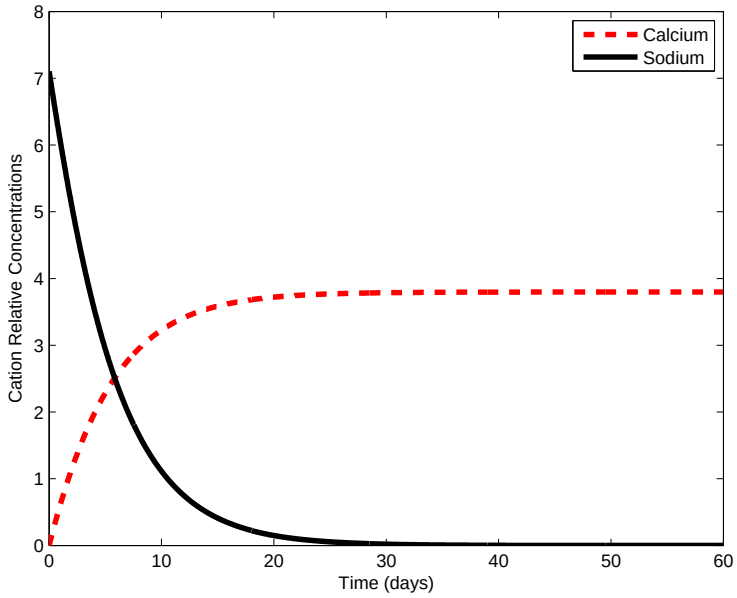

Figure 5.86: The gradual decrease of Na^{+} with time is due to the exchange with Ca^{2+} of the source solution

ion concentrations obtained above and assuming that the solvent is compressible, as explained in detail further on.

Under perfect flushing conditions, the chemico-osmotic efficiency coefficient is defined as follows:

$$\omega = \frac{\Delta P}{\Delta \pi} \tag{5.87}$$

where ΔP is the measured pressure difference induced across the membrane as a result of prohibiting chemico-osmotic flux of solution (closed system), and $\Delta\pi$ is the theoretical chemico-osmotic pressure difference across an ideal membrane subjected to an applied difference in solute concentration.

The value for $\Delta\pi$ is calculated based on the salt concentrations at the specimen boundaries in accordance with the van $'$t Hoff expression as follows:

$$\Delta \pi = RT \sum_{i=1}^{N} \bar{C}_i \tag{5.88}$$

that for a source concentration C_0 of a $CaCl_2$ solution becomes

$$\Delta \pi = RT(\bar{C}_{Ca^{2+}} + 2\bar{C}_{Cl^-}) = 3RTC_0 \tag{5.89}$$

To obtain the chemico-osmotic efficiency, ω(t), in function of time, we should calculate

$$\omega(t) = \frac{\sum dP(t)}{\Delta \pi} \tag{5.90}$$

We solved $\omega(t)$ by the finite difference method. We first obtained dP from Donnan's equations as

$$dP = d\bar{P} - d\bar{\Pi} + d\Pi \tag{5.91}$$

where

$$d\bar{P}(t) = \bar{C}_x \frac{F^2}{\bar{\kappa}} (2D^*_{Ca^{2+}} d\bar{C}_{Ca^{2+}} + D^*_{Na^+} d\bar{C}_{Na^+} - D^*_{Cl^-}) \tag{5.92}$$

and

$$d\bar{\Pi} = RT(d\bar{C}_{Ca^{2+}} + d\bar{C}_{Na^+} + d\bar{C}_{Cl^-}) \tag{5.93}$$

$$d\Pi = RT\, dC_i \tag{5.94}$$

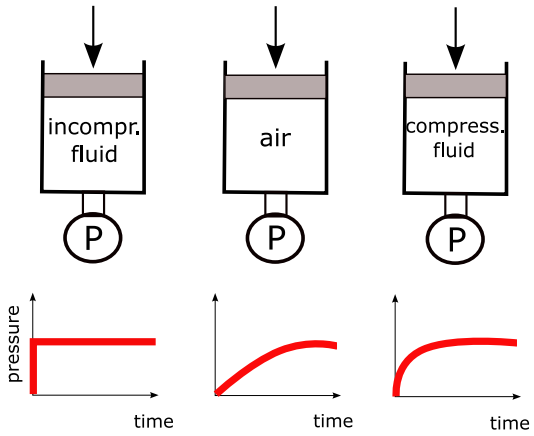

Figure 5.87: Effect of the fluid compressibility on the propagation of the pressure in the porous medium

Fluid compressibility

So far we neglected the compressibility of the fluid. However, the compressibility of the fluid is important for the solution of this problem, because it affects the mobilization rate of the differential pressure in time.

The fluid compressibility can be seen as intermediate between the thermodynamic properties of an ideal fluid (incompressible) and an ideal gas (compressible). In this regard, Fig. 5.87 shows the impact of the compressibility of a fluid on the pressure mobilization with time. Assuming the fluid incompressible, the mobilization of pressure should give and immediate raise of the pressure change. Conversely, an ideal gas (compressible) will show a gradual increase of the pressure. A compressible fluid can be seen between these two extreme situations, with a gradual increase of the pressure change, as shown in Fig. 5.87.

In thermodynamics and fluid mechanics, compressibility is a measure of the relative volume change of a fluid as a response to a pressure change. The compressibility law can be expressed as:

$$\frac{1}{K_w} = -\frac{1}{V}\frac{\partial V}{\partial P} \tag{5.95}$$

where

K_w is the bulk modulus of water;

V is the fluid volume;

P is the pressure.

Figure 5.88 represents a schematic representation of the closed system we would like to simulate here. In case of incompressible fluids, no water flow is

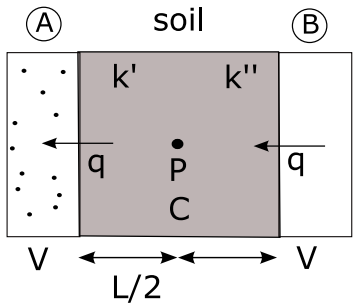

Figure 5.88: Schematic representation of volumetric flow, q, through the soil due to the concentration gradient between the two reservoirs (A and B) of volume V. Even if in a closed system, the flow is allowed due to the fluid compressibility

allowed through the soil. On the other hand, considering the compressibility of the fluid, a small volumetric flow, q, different than zero is allowed.

The two reservoirs (A and B) in contact with the soil in Fig. 5.88 represents the porous stones in the experiments. Every reservoirs has the same volume V.

$$V_A = V_B = V \tag{5.96}$$

The volumetric flows, q, entering and exiting the reservoirs are defined as:

$$q_A = \frac{dV_A}{dtS} \tag{5.97}$$

$$q_B = -\frac{dV_B}{dtS} \tag{5.98}$$

where S is the surface of the soil crossed by the volumetric flow.

The volumetric flow, q_B, entering the soil from the reservoir with lower concentration, B, is assumed to be equal in absolute value to the volumetric flow, q_A, exiting the soil into the reservoir with higher concentration, B.

$$q_A = q_B = q \tag{5.99}$$

Substituting equations 5.97, 5.98 and 5.99 into 5.95 we obtain:

$$\frac{dP_A}{dt} = \frac{SK_w}{V} \cdot q \tag{5.100}$$

$$\frac{dP_B}{dt} = -\frac{SK_w}{V} \cdot q \tag{5.101}$$

We can express q_A and q_B in function of the ion concentrations solved above as:

$$q_A = \frac{k'}{L/2}\left[(P_A - P) - RT\sum_{i=1}^{3}(C_i^A - C_i) + RT\sum_{i=1}^{3}(\bar{C}_i^A - \bar{C}_i) - \bar{C}_x\frac{F^2}{\bar{\kappa}'}\sum_{i=1}^{3} z_i D_i^* \left(\bar{C}_i^A - \bar{C}_i\right)\right] \tag{5.102}$$

and similarly

$$q_B = \frac{k''}{L/2}\left[(P - P_B) - RT\sum_{i=1}^{3}(C_i - C_i^B) + RT\sum_{i=1}^{3}(\bar{C}_i - \bar{C}_i^B) - \bar{C}_x\frac{F^2}{\bar{\kappa}'}\sum_{i=1}^{3} z_i D_i^* \left(\bar{C}_i - \bar{C}_i^B\right)\right] \tag{5.103}$$

Introducing the variables α, β, γ and δ known from the solution of the transport equations, we can rewrite equations 5.102 and 5.103 as

$$\begin{cases} q_A = \alpha \cdot (P_A - P + \beta) \\ \\ q_B = \gamma \cdot (P - P_B + \delta) \end{cases} \tag{5.104}$$

Dividing q_A by α and q_B by γ and by summation of the two equations, we obtain

$$q = a \cdot (P_A - P_B + b) \tag{5.105}$$

where
$a = \alpha\gamma/(\alpha+\gamma)$;
$b = \beta + \delta$.
Equations 5.100 and 5.101 become

$$\begin{cases} dP_A/dt = SK_w/V \cdot a(P_A - P_B + b) \\ \\ dP_B/dt = -SK_w/V \cdot a(P_A - P_B + b) \end{cases} \tag{5.106}$$

Solving numerically equation 5.106, advancing by time steps, we can calculate

$$\Delta P(t) = \sum (P_A(t) - P_B(t)) \tag{5.107}$$

Finally we can evaluate the chemico-osmotic efficiency in time:

$$\omega(t) = \frac{\Delta P(t)}{\Delta\pi} \tag{5.108}$$

Figure 5.90 shows the outcome of a numerical calculation. The figure shows that the chemico-osmotic efficiency decreases with time as a result of diffusion. The diffusion causes in fact the exchange of the Ca^{2+} in the source solution with the Na^+ of the clay (as shown in Fig. 5.86), with a consequent compression of the double layer thickness. This DDL collapse destroys gradually the chemico-osmotic efficiency.

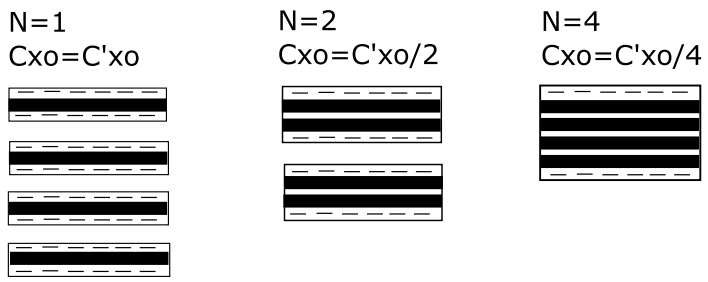

Figure 5.89: Schematical representation of the relation between the fixed solid negative charge (Cxo) and the number (N) of clay platelets

Figure 5.91 shows the parametric study of the chemico-osmotic efficiency varying the concentration of the charge of solid particles, C_{X0}. The concentration of the charge of solid particles represent in fact the negative charge of the clay surface. The higher the negative charge the larger the diffuse double layer thickness and therefore the higher the chemico-osmotic efficiency of a clay. As expected the chemico-osmotic peak and steady state values increased with increasing C_{X0} of the bentonite.

In this parametric study we assumed the number of clay platelets per aggregate constant equal to 3. On the other hand, we also analyzed the impact of the number of unit particles per aggregate, N, on the chemico-osmotic efficiency vs. time. Figure 5.92 shows the parametric study of the chemico-osmotic efficiency varying not only the concentration of the negative charge of the solid particles, C_{X0}, but also the number of platelets per aggregate, N.

For this simulation we assume

$$C_{X0} = \frac{C'_{X0}}{N} \tag{5.109}$$

where

C'_{X0} is a reference fixed charge concentration for the clay analyzed. This charge concentration could indicatively be considered as the fixed charge of the clay in case of complete dispersion of the platelets (N=1), as shown schematically in Fig. 5.89.

The concentration of the charge of solid particles depends, in fact, not only on the surface charge of the clay unit particles but also on the clay structure. In fact, increasing the number of platelets per aggregate the fixed charge decreases. When the number, N, of clay platelets per aggregate increases, the external specific surface decreases and the double layer thickness decreases as well.

The simulation results show that not only the chemico-osmotic efficiency increases with decreasing N, but also the trend of ω vs. time changes. As shown in Fig. 5.92, decreasing N the peak of the chemico-osmotic efficiency and its gradual

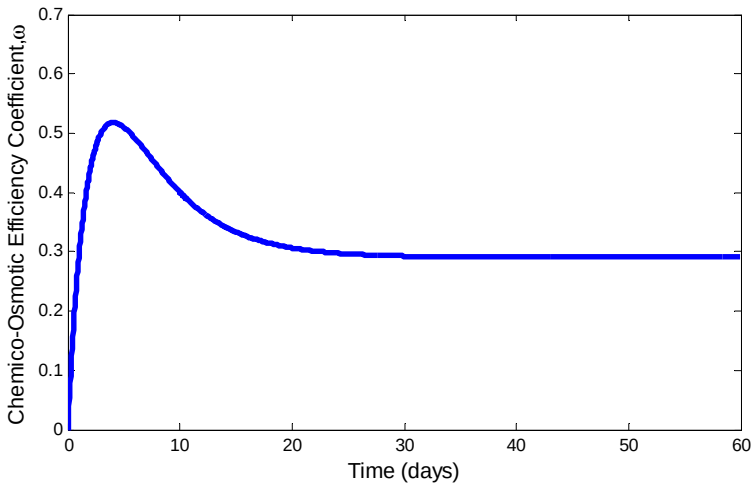

Figure 5.90: Chemico-osmotic efficiency decrease in function of time obtained solving numerically the Transport Equations in a 3-ion system

decrease with time tends to disappear. This result is intuitively acceptable, since the decrease of the number of platelets per aggregate to N=1 means that the structure of the clay tends to be dispersed with thicker double layers and a consequent improved chemico-osmotic performance.

5.6.6 Interpretation of the chemico-osmotic experiments

The chemico-osmotic efficiency of non-treated and polymer treated clays was evaluated by means of the experimental tests described in section 5.5. Conversely, this section is dedicated to the theoretical interpretation of the experimental results by means of the modeling approach proposed.

Untreated clay

Experimental test results on untreated clay showed that the chemico-osmotic efficiency, for a given porosity and a given concentration gradient, decreases with time due to diffusion. The diffusion of Ca^{2+} into the Na-clay causes in fact the exchange between the cations with a consequent compression of the double layer thickness.

Figure 5.93 shows the theoretical interpretation of the experiment on the natural clay. Among the parametric curves shown in Fig. 5.91, one particular one represents very well the experimental result (N = 3, C_{X0} = 0.018). Figure 5.93 illustrates the good agreement between the experiments and the theoretical results.

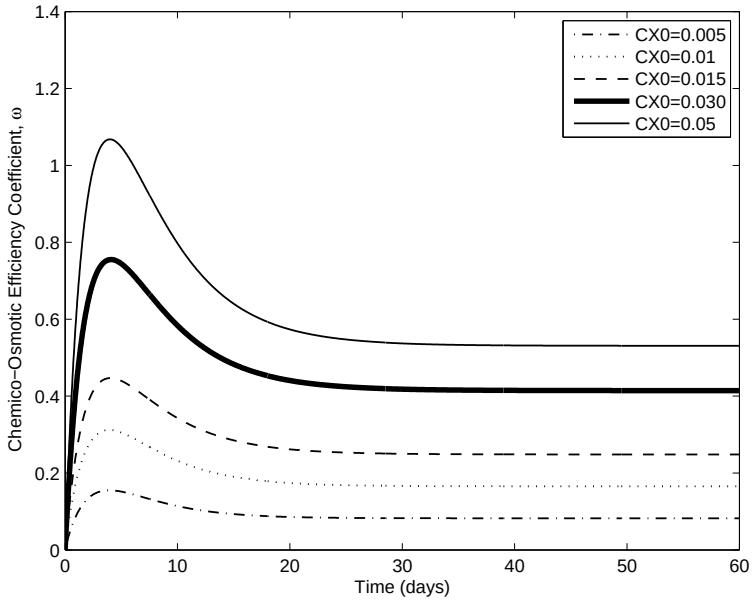

Figure 5.91: Parametric study of the chemico-osmotic efficiency vs. time varying the fixed charge concentration C_{x0}

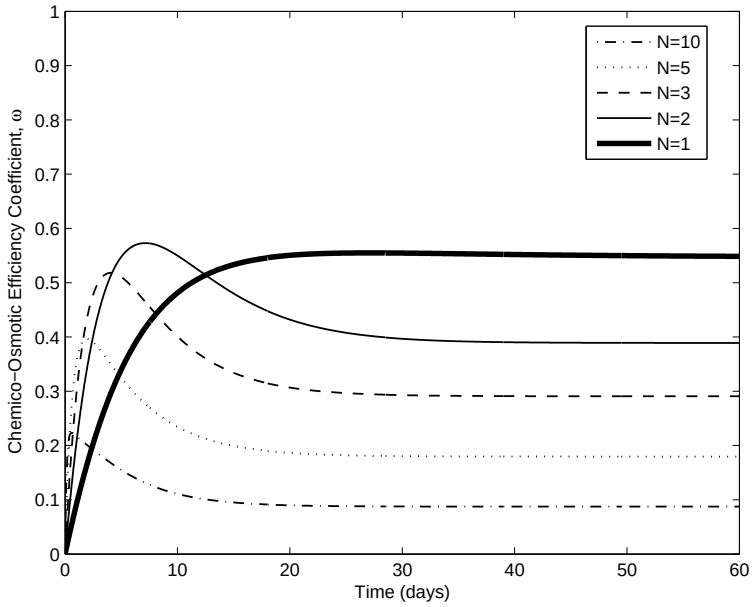

Figure 5.92: Parametric study of the chemico-osmotic efficiency vs. time varying the fixed charge concentration C_{x0} and the number of platelets per aggregate

Both the peak and the gradual decrease of ω with time due to diffusion are well represented by the modeling approach. Therefore, the interpretation of the results, in terms of osmotic efficiency vs. time, seems to be consistent.

HYPER clay

Figure 5.94 shows the theoretical interpretation of the experiments on the clay treated with the anionic polymer Na-CMC (HYPER clay). Experimental results demonstrated that, in contrast to natural clays, the HYPER clay maintained its chemico-osmotic efficiency with time. This improved performance is probably due to the polymer that maintains the double layer open.

Figure 5.94 shows that also for the HYPER clay a theoretical curve represents well the experimental results. Figure 5.95 compares the theoretical curves representing the natural and the polymer treated clay. The trend of ω of the HYPER clay is characterized by a higher C_{X0} and a lower N compared to the untreated clay (C_{X0} = 0.084, N = 1). The lower N suggests that the polymer, maintaining the interlayer open, prevented the double layer collapse preserving a dispersed structure. The higher C_{X0} depends on the clay structure and on the surface negative charge. This theoretical interpretation probably indicates that not only the anionic polymer maintains the interlayer open but also it increases the negative charge concentration of the clay.

Moreover, comparing the two curves in Fig. 5.95, we can probably deduce that for the HYPER clay a delay on the solute diffusion (demonstrated in the experiments) is reflected on a delay in reaching the ω-peak.

This preliminary interpretation of experimental data from laboratory tests provides a first validation of the proposed model. Nevertheless, further laboratory tests and theoretical considerations are necessary to obtain additional insights into the specific aspects that govern osmotic phenomena in modified clays.

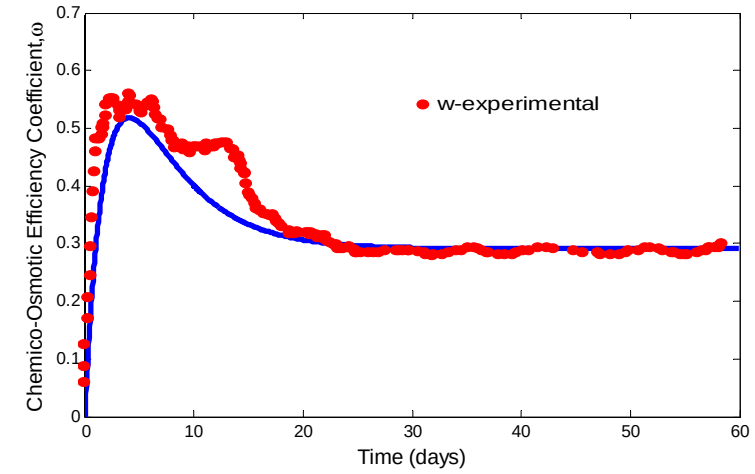

Figure 5.93: Theoretical interpretation of the chemico-osmotic experiments on the untreated clay

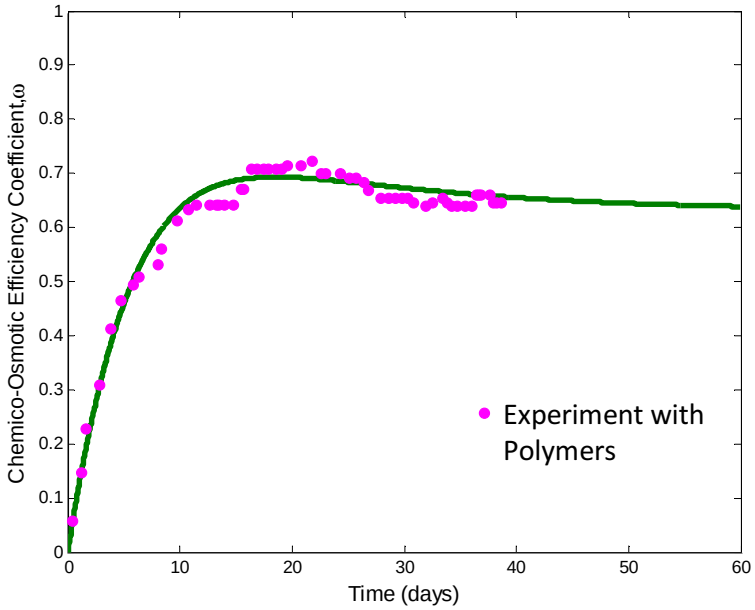

Figure 5.94: Theoretical interpretation of the chemico-osmotic experiments on the HYPER clay

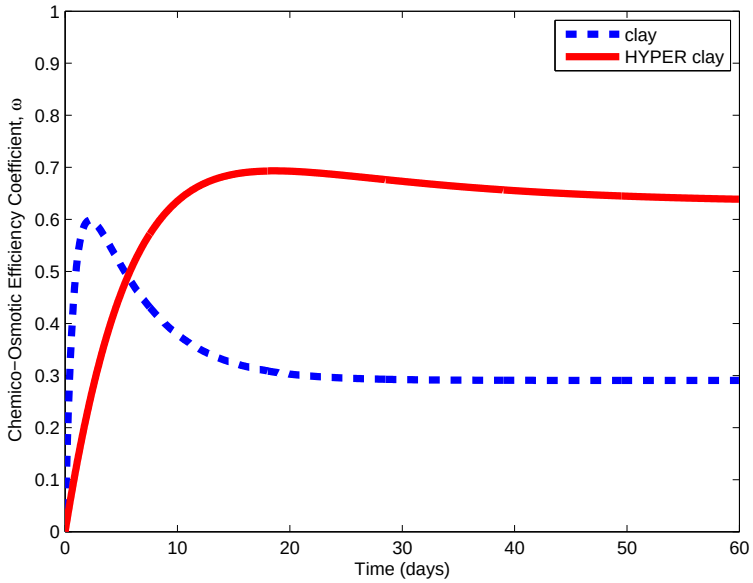

Figure 5.95: Theoretical interpretation of the chemico-osmotic experiments on polymer treated clays. The polymer treatment causes: an increase of C_{X0}, a decrease of number of platelets per aggregate, a delay on the pressure wave transmission

6

Conclusions and Recommendations for Future Work

6.1 Conclusions

The aim of hydraulic clayey barriers is to isolate waste liquids from the environment. Bentonite clay is widely used in hydraulic barriers because of its elevated sealing capacity in presence of water. However, exposure to high concentrations of inorganic solutions can change the clay fabric increasing its hydraulic conductivity, with a consequent enormous harm to the environment.

The main purpose of this research was to develop a superior clay with enhanced Hydraulic Performance.

An engineered clay (HYPER clay) was developed for this purpose by adsorbing an anionic polymer to the surface of an untreated bentonite. Furthermore, two commercially available polymer treated clays were studied: a Multiswellable Bentonite (MSB) and a Dense Prehydrated GCL (DPH GCL). To demonstrate the potential benefits of polymer treatment, index properties and swelling ability were evaluated. Subsequently, hydraulic and chemico-osmotic tests were executed on untreated and polymer treated clays to evaluate their resistance to chemical attack. Finally a theoretical interpretation of the experimental results was conducted with a newly developed multi-ion system approach.

6.1.1 Experimental Results

All experimental and theoretical goals of this PhD thesis were completed. The main conclusions can be summarized as follows.

Material Characterization

The effect of polymers adsorption on clays was studied by physical and chemical analysis that demonstrated the potential benefits of polymers on the sealing, hydraulic and membrane properties of clays. XRD analysis of the clay demonstrated the intercalation of the anionic polymer in the interlayer region of the clay inducing a dispersed clay structure with a consequent potential decrease of the hydraulic conductivity. The increase of the viscosity and the decrease of the zeta potential with increasing polymer dosage, revealed that the polymer interaction occurred not only in the interlayer region between platelets but also at the particle surface inducing bridging between particles.

Moreover, the liquid limit (water adsorption capacity) of the clay in deionized water and electrolyte solutions increased with increasing polymer dosage suggesting a potential benefit of the polymer on preserving the hydraulic performance of the clay. By adding the polymer, an increase of exchangeable Na^{+} in the composition of the exchange complex of the clay was observed, indicating a potential enhancement of the quality of the clay due to polymer addition.

The combination of these observations supports the hypothesis that the polymers coat and bridge the clay particles yet maintaining the interlayer between platelets open.

Swelling ability

The swelling ability of the treated clays was quantified by means of standard swell index test and swelling pressure tests. Both showed that the treatment with the anionic polymer studied here improved the swelling ability of the untreated clay. The swelling pressure test, compared to the standard swell index test, showed more accurately the swelling ability of polymer treated clays. Swelling pressure was observed to increase also with increasing polymer dosage up to an optimum value.

Hydraulic conductivity performance

Hydraulic conductivity tests were conducted on untreated and polymer treated clays. As expected, the hydraulic conductivity of untreated clays increased by permeating the samples with electrolyte solutions due to the compression of the double layer thickness. Conversely, polymer treated clays maintained low hydraulic conductivity to $CaCl_2$ and to sea water even in the long term.

The prehydration of untreated clay samples produced only a limited benefit on the hydraulic conductivity to electrolyte solutions. On the other hand, the polymer treatment and the prehydration together were able to maintain a very low hydraulic conductivity to electrolyte solutions, comparable to the hydraulic conductivity to deionized water.

The prehydration with addition of polymers and the densification of the commercial DPH GCL preserved low hydraulic conductivities even in presence of aggressive electrolyte solutions such as $CaCl_2$ solutions and sea water.

Although the prehydration with polymers and the densification effect of the DPH GCL assured a good performance on single sheet samples, the swell mechanism was of fundamental importance to guarantee a good sealing at the overlap zone. For these reasons the use of bentonite paste to seal the overlap during installation is recommended.

Chemico-osmotic efficiency and Diffusion Coefficient

The effect of partial or complete destruction of membrane behavior due to diffusion was observed in untreated clays. The clay showed in fact initial membrane behavior, that gradually decreased due to the gradual compression of the double layer thickness due to diffusion of invading cations.

On the other hand, the polymer treatment with the anionic polymer protected the clay against the destructive role of diffusion, maintaining the initial osmotic efficiency in the long term in presence 1 mM and 5 mM $CaCl_2$ solutions. The polymer treatment modified the bentonite structure such that the double layer thickness of the clay resisted collapse and the membrane efficiency was sustained.

Nevertheless, special attention should be given to the method of polymer treatment used to preserve the adsorption of the polymer onto the clay in the long term. Unlike the HYPER clay, the commercial polymer treated clays (DPH GCL and MSB) showed a decrease of the chemico-osmotic efficiency with time. This gradual decrease of the membrane efficiency was attributed to the probable release of the polymers during prolonged prehydration with deionized water before the tests.

The transport parameters of the clays were evaluated with the chemico-osmotic tests. The diffusion coefficient of the HYPER clay was lower than that of the natural clay. This result suggests that the polymer protected the exchangeable sodium of the HYPER clay from cation exchange with Ca^{2+}.

6.1.2 Theoretical interpretation

The Swell Pressure and Chemico-osmotic tests results were interpreted theoretically in a newly developed multi-ion system approach.

Swell pressure in a 3-ion system

The theoretical development presented here is based on the model proposed by Dominijanni (2005) for 2-ion systems. An extension of the model to allow for 3-ion systems was developed in cooperation with the Politecnico di Torino.

With this extension we back analyzed all experimental data of swelling pressure for natural bentonites and polymer treated bentonites.

We have calculated the swelling pressure of bentonites for 3-ion systems based on the Donnan model and the electroneutrality conditions. We assumed that the number of platelets per aggregate were constant independently of the ion concentration and valence.

The C_{X0} obtained with the back analysis of the swelling pressure tests overestimated the C_{X0} obtained in the chemico-osmotic test. We attributed this result to the special assumptions used for the theoretical interpretation of the swelling pressure. We neglected, in fact, the interparticle stresses, considering the clay structure as very dispersed.

Whereas, the theoretical interpretation of the chemico-osmotic experiments provided a better representation of the fixed charge concentration of the clays analyzed.

Nevertheless, we were able to evaluate the effect of polymer addition and densification based on the back analysis of the swelling pressure tests. Out of back analysis of the experimental data with the model, we demonstrated that the polymer treatment increased the net negative charge of the clay (C_{X0}) and limited the aggregation between clay platelets with a consequent improvement of the swelling ability of the clay. Also the densification of a clay increased its swelling pressure. For these reasons, the simultaneous effect of polymer treatment and densification improved considerably the swelling ability of the clay.

Chemico-osmotic efficiency in a 3-ion system

For the analysis of the chemico-osmotic tests results, an extension of the general model proposed by Dominijanni (2005) was developed in cooperation with Politecnico di Torino. We solved the transport equations for a 3-ion systems in order to interpret more correctly the actual multi-ion scenario expected in laboratory conditions and in situ.

Specific boundary conditions were defined to model the chemico-osmotic properties of clays in a 3-ion system. The definition of correct boundary conditions was necessary to represent actual conditions expected in the transient phase.

The Transport Equations for a 3-ion system were solved by means of a finite difference method. This model was able to represent the exchange of Na^+ with Ca^{2+} in time, in good agreement with the experiments, both on treated and untreated clays.

Finally, a parametric study and the interpretation of the results based on the new model were presented. The parametric study was intended to evaluate the impact of the fixed charge concentration of the clay and the impact of the number of clay particles per aggregate on the chemico-osmotic efficiency coefficient vs. time. Whereas, the back analysis of the experimental data allowed to define the fixed charge concentration for both the untreated and polymer treated clays.

The fixed charge concentration, C_{X0}, of the HYPER clay was higher than that of the untreated clay, whereas, the number of platelets per aggregate was lower. This theoretical interpretation suggested that not only the anionic polymer maintains the interlayer open but also it increases the negative charge concentration of the clay.

The preliminary interpretation of experimental data from laboratory tests provided a first validation of the proposed model. Nevertheless, further laboratory tests and theoretical considerations are necessary to obtain additional insights into the specific aspects that govern osmotic phenomena in modified clays.

6.2 Recommendations for future work

Hydraulic conductivity tests with various solutions are also needed, for example with higher concentrations of $CaCl_2$, or leachates or acidic solutions.

More research is needed to extend these conclusions to the long term. Possible solubility and biodegradability of the polymers in the interlayer region of the clay should be studied.

At the end of long term hydraulic conductivity test on the HYPER clay, an in depth analysis should be performed to further demonstrate the irreversible adsorption of the polymer onto the clay surface. In general, the impact of prolonged prehydration on the polymer adsorption should be studied.

The fixed charge concentration obtained by the back analysis of the swell pressure tests overestimated the C_{X0} obtained with the chemico-osmotic test. We attributed this different results to the assumption that the interparticle stresses were negligible in the swelling pressure interpretation.

The determination of the C_{X0} with the swelling pressure approach, taking into account the interparticle stresses, may be an interesting further development of the model to be able to predict the chemico-osmotic efficiency of clays based on the C_{X0} obtained out of swelling pressure tests.

The preliminary interpretation of chemico-osmotic experimental data from laboratory tests provided a first validation of the proposed model. Nevertheless, further laboratory tests and theoretical considerations are necessary to obtain additional insights into the specific aspects that govern osmotic phenomena in modified clays.

Bibliography

Ashmawy, A. K., El-Hajji, D., Sotelo, N. and Muhammad, N. (2002). Hydraulic performance of untreated and polymer-treated bentonite in inorganic landfill leachates., *Clays and Clay Minerals* **50**(5): 546–552.

Barbour, S. L. and Fredlund, D. G. (1989). Mechanisms of osmotic flow and volume change in clay soils, *Canadian Geotechnical Journal* **26**: 551–562.

Bartelt-Hunt, S. L., Burns, S. E., Culver, T. B. and Smith, J. A. (2005). Optimal design of a compacted soil liner containing sorptive amendments, *Geo-Frontiers 2005*.

Benson, C. H. (2002). Containment systems: lessons learned from north american failures, *Environmental Geotechnics (4th ICEG)*.

Benson, C. H. and Wang, X. (2000). Hydraulic conductivity assessment of hydraulic barriers constructed with paper sludge, *Geotechnics of High Water Content Materials, ASTM STP* **1374**: 91–107.

Bolt, G. H. (1956). Physico-chemical analysis of the compressibility of pure clays, *Geotechnique* **6**: 86–93.

Bouazza, A. (2001). Geosynthetic clay liners, *Geotextiles and Geomembranes, Elsevier* **20**: 3–17.

Breen, C. (1999). The characterisation and use of polycation-exchanged bentonites, *Applied Clay Science* **15**: 187–219.

Crank, J. (1975). *The mathematics of diffusion*, 2nd edn, Clarendon Press, Oxford.

Dahnert, K. and Huster, D. (1999). Comparison of the poisson-boltzmann and the donnan equilibrium of a polyelectrlyte in salt, *Journal of Colloid and Interface Science* **215**: 131–139.

Daniel, D. E., Shan, H. Y. and Anderson, J. D. (1993). Effects of partial wetting on the performance of the bentonite component of a geosynthetic clay liner, *Geosynthetics 1993* **3**: 1482–1496.

Daniel, D. E., Trautwein, S. J. and Goswami, P. (1997). Measurement of hydraulic properties of gcls using a flow box, *Testing and Acceptance Criteria for Geosynthetic Clay Liners, STP, ASTM* **1308**: 196–207.

De Groot, S. and Mazur, P. (1962). *Non-equilibrium Thermodynamics*, London: Pergamon Press.

Didier, G. and Comeaga, L. (1997). Influence of initial hydration conditions on gcl leachate permeability, *Testing and Acceptance Criteria for Geosynthetic Clay Liners, ASTM STP 1308* pp. 181–195.

Dominijanni, A. (2005). *Osmotic properties of clay soils*, PhD thesis, Politecnico di Torino.

Dominijanni, A. and Manassero, M. (2005). Modelling osmosis and solute transport through clay membrane barriers, *Geotechnical Special Publication* **130-142**: 3437–3448.

Dominijanni, A. and Manassero, M. (2008). Modeling the compressibility and the hydraulic conductivity of geosynthetic clay liners, *Proceedings of the First Pan American Geosynthetics Conference & Exhibitio,n 2-5 March 2008, Cancun, Mexico*, pp. 59–68.

Dominijanni, A., Manassero, M. and Vanni, D. (2006). Micro/macro modeling of electrolyte transport through semipermeable bentonite layers, *in* E. T. T. L. Thomas, H.R. (ed.), *Proceedings of the 5th International Congress on Environmental Geotechnics, 26th-30th June, 2006, Cardiff, Wales, UK*, Vol. 2, pp. 1123–1130.

Dormieux, L., Barboux, P., Coussy, O. and Dangla, P. (1995). A macroscopic model of the swelling phenomenon of a saturated clay, *European Journal of Mechanics, A/Solids 14(6): 981-1004.* **14**(6): 981–1004.

Egloffstein, T. A. (2001). Natural bentonites-influence of the ion exchange and partial desiccation on permeability and self-healing capacity of bentonites used in gcls, *Geomembranes and Geotextiles, Elsevier* **19**: 427–444.

Estornell, P. and Daniel, E. D. (1992). Hydraulic conductivity of three geosynthetic caly liners, *Journal of Geotechnical Engineering, ASCE* **118**(10): 1592–1606.

Ferry, J. D. (1936). Statistical evaluation of sieve constants in ultrafiltration, *J. General Physiol* **20**: 95–104.

Filippi, S., Mameli, E., Marazzato, C. and Magagnini, P. (2007). Comparison of solution-bleding and melt-intercalation for the preparation of poly(ethylene-co-acrylic acid)/organoclay nanocomposites., *European Polymer Journal. Elsevier,* **43**(5): 1645–1659.

Flynn, B. N. and Carter, G. C. (1998). Waterproofing material and method of fabrication thereof.

Fritz, S. J. (1986). Ideality of clay membranes in osmotic processes: a review, *Clays and Clay Minerals* **34**(2): 214–223.

Grace, H. P. (1953). Resistance and compressibility of filter cakes, *Chem. Engng Prog.* **49**: 303–318, 367–377.

Grathwohl (1998). *Diffusion in natural porous media, contaminant transport, sorption/desorption and dissolution kinetics.*, Kluwer academic, Norwell, MA USA.

Groenevelt, P. H. and Bolt, G. H. (1969). Non-equilibrium thermodynamics of the soil-water system, *Journal of Hydrology* **7**: 358–388.

Groenevelt, P. H., Elrick, D. E. and Laryea, K. B. (1980). Coupling phenomena in saturated homo-ionic montmorillonite. 4. the dispersion, *Soil Science Society of America Journal* **44**(6): 1168–1173.

Gu, W. Y., Lai, W. M. and Mow, V. C. (1999). Transport of multi-electrolytes in charged hydrated biological soft tissues, *Transport in Porous Media* **34**: 143–157.

Hanshaw, B. B. and Coplen, T. B. (1973). Ultrafiltration by a compacted clay membrane: Ii. sodium ion exclusion at various ionic strengths, *Geochimica et Cosmochimica Acta* **37**(10): 2311–2327.

Hiemenz, P. (1986). *Principles of Colloid and Surface Chemistry*, Marcel Dekker, New York, 2nd edn.

James, A. N., Fullerton, D. and Drake, R. (1997). Field performance of gcl under ion exchange conditions, *Journal of Geotechnical and Geoenvironmental Engineering, ASCE* **123**(10): 897–901.

Jo, H., Katsumi, T., Benson, C. H. and Edil, T. B. (2001). Hydraulic conductivity and swelling of non-prehydrated gcls premeated with single species salt solutions, *Journal of Geotechnical and Geoenvironmental Engineering, ASCE* **127**(7): 557–567.

Jo, H. Y., Benson, C. H., Shackelford, C. D., Lee, J.-M. and Edil, T. B. (2005). Long-term hydraulic conductivity of a geosynthetic clay liner permeated with inorganic salt solutions., *Journal of Geotechnical and Geoenvironmental Engineering, ASCE* **131**(4): 405–417.

Jungnickel, C., Smith, D. and Fityus, S. (2004). Coupled multi-ion electrodiffusion analysis for clay soils, *Canadian Geotechnical Journal* **41**(2): 287–298.

Katchalsky, A. and Curran, P. (1965). *Nonequilibrium Thermodynamics in Biophysics*, Harvard University Press, Cambridge, Massachusetts, 248 pp.

Katsumi, T. (2010). *Geosynthetic Clay Liners for Waste Containment Facilities (Chapter: Hydraulic conductivity of geosynthetic clay liners)*, number 4.

Katsumi, T., Ishimori, H., Onikata, M. and Fukagawa, R. (2008). Long-term barrier performance of modified bentonite materials against sodium and calcium permeant solutions, *Geotextiles and Geomembranes* **26**: 14–30.

Keijzer, T. J. S., Kleingeld, P. J. and Loch, J. P. G. (1997). *Chemical osmosis in compacted clayey material and the prediction of water transport, in Yong, R. N and Thomas, H.R. (Eds.), Geoenvironmental Engineering, Contaminated Ground: Fate of pollutants and remediation*.

Kemper, W. D. and Quirk, J. P. (1972). Ion mobilities and electric charge of external clay surfaces inferred frompotential differences and osmotic flow, *Soil Science Society ofAmerica Proceedings* **36**(3): 426–433.

Kemper, W. D. and Rollins, J. B. (1966). Osmotic efficiency coefficients across compacted clays, *Soil Science Society of America* **30**(5): 529–534.

Kharaka, Y. K. and Berry, F. F. (1973). Simultaneous flow of water and solutes through geological membranes i. experimental investigation, *Geochimica Cosmochimica Acta* **37**(12): 2577–2603.

Koerner, R. M. (2005). *Designing with Geosynthetics*, 5th edn, Prentice Hall Book Co.

Kondo, M. (1996). Method of activation of clay and activated clay.

Lagaly, G. (2006). *Colloid in clay science. Handbook of Clay Science*, Elsevier.

Laird, D. (1996). Model for crystalline swelling of 2:1 phyllosilicates, *Clays and Clay Minerals* **44**: 553–559.

Laird, D. (2006). Influence of layer charge on swelling of smectites, *Applied Clay Science* **37**: 74–87.

Lake, C. B. and Rowe, R. K. (2000). Diffusion of sodium and chloride through geosynthetic clay liners, *Geotextiles and Geomembranes* **18**: 103–131.

Lambe, T. W. and Withman, R. V. (1969). *Soil mechanics*, Wiley, New York.

Lee, J. M. (2004). *Long-term hydraulic performance of Geosynthetic Clay Liners subjected to inorgnaic salt solutions*, PhD thesis, Colorado State University, Fort Collins, Colorado, USA.

Lee, J. M. and Shackelford, C. D. (2005). Impact of bentonite quality on hydraulic conductivity of geosynthetic clay liners, *Journal of Geotechnical and Geoenvironmental Engineering* **131**(1): 64–77.

Lee, J. M., Shackelford, C. D., Benson, C. H., Jo, H. Y. and Edil, T. B. (2005). Correlating index properties and hydraulic conductivity of geosynthetic clay liners, *Journal of Geotechnical and Geoenvironmental Engineering* **131**(11): 1319–1329.

Likos, W. J., Bowders, J. J. and Gates, W. P. (2010). *Geosynthetic Clay Liners for Waste Containment Facilities. Chapter 3: Mineralogy and engineering properties of bentonite*, CRC Press, Taylor and Francis.

Lo, I. M. C., Mak, R. K. M. and H., L. S. C. (1997). Modified clays for waste containment and pollutant attenuation., *Journal of Environmental Engineering, ASCE* **123**(1): 25–32.

Lorenzetti, R. J., Bartelt-Hunt, S. L., Burns, S. E. and Smith, J. A. (2005). Hydraulic conductivities and effective diffusion coefficients of geosynthetic clay liners with organobentonite amendments, *Geotextiles and Geomembranes 23 (2005) 385400* **23**: 385–400.

Malusis, M. A. and Shackelford, C. D. (2002a). Chemico-osmotic efficiency of a geosynthetic clay liner, *Journal of Geotechnical and Geoenvironmental Engineering, ASCE* **128**(2): 97–106.

Malusis, M. A. and Shackelford, C. D. (2002b). Coupling effects during steady-state solute diffusion through a semipermeable clay membrane, *Environmental Science and Technology* **36**(6): 1312–1319.

Malusis, M. A., Shackelford, C. D. and Olsen, H. W. (2001). A laboratory apparatus to measure the chemico osmotic efficiency for cay soils., *Geotechnical Testing Journal.* **24**(3): 229–242.

Malusis, M. A., Shackelford, C. D. and Olsen, H. W. (2003). Flow and transport through clay membrane barriers, *Engineering Geology* **70**: 235–248.

Manassero, M. and Dominijanni, A. (2003). Modelling the osmosis effect on solute migration through porous media, *Geotechnique* **53**: 481–492.

Marine, I. W. and Fritz, S. J. (1981). Osmotic model to explain anomalous hydraulic heads., *Water Resources Research* **17**(1): 73–82.

Mazzieri, F., Di Emidio, G. and Van Impe, P. O. (2010). Diffusion of cacl2 in a modified bentonite: impact on osmotic efficiency and hydraulic conductivity, *Clays and Clay Minerals* **58**(2).

Mazzieri, F. and Pasqualini, E. (2006). Evaluating the permeability of an organically modified bentonite to natural seawater, *Proceedings of the 5th International Congress on Environmental Geotechnics, Cardiff, Wales, UK*.

Mazzieri, F. and Pasqualini, E. (2008). Effect of dry/wet cycles and cation exchange on the permeability of a dense prehydrated gcl, *Proceedings Eurogeo4 Fourth International Conference on Geosynthetics ed. by N. Dixon*.

Mazzieri, F., Van Impe, P. O., Van Impe, W. and Constales, D. (2003). Measurement of chemico-osmotic parameters of clayey soils, *in* R. Balkema (ed.), *Proceedings of the XIII ECSMGE, Prague*, pp. 433–438.

McBride, M. (1994). *Environmental chemistry of soils*, Oxford University Press, New York.

McRory, J. A. and Ashmawy, A. K. (2005). Polymer treatment of bentonite clay for contaminant resistant barriers, *Geo-Frontiers 2005, Geotechnical Special Publications, ASCE*, Vol. GRI-18, pp. 130–142.

Mesri, G. and Olson, R. E. (1971). Mechanisms controlling the permeability of clays, *Clay and Clay Minerals* **19**: 151–158.

Meyer, K. H. and Sievers, J. F. (1936a). La permeabilit des membranes i, theory de la permeabilit ionique, *Helvetica Chimica Acta* **19**: 649–664.

Meyer, K. H. and Sievers, J. F. (1936b). La permeabilite des membranes ii. essais avec des membranes selectives artificielles, *Helvetica Chimica Acta* **19**(1): 665–677.

Michaels, A. S. and Morelos, S. (1955). Polyelectrolyte adsorption by kaolinite, *Ind. Eng. chem.* **47**(9): 1801–1809.

Mitchell, J. (1993). *Fundamentals of Soil Behaviour*, John Wiley & Sons.

Morris, G. E. and Zbik, M. S. (2009). Smectite suspension structural behaviour, *Int. J. Miner. Process.* **93**: 20–25.

Mortensen, J. L. (1960). Adsorption of hydrolysed polyacrylonitrile on kaolinite, *Proceedngs of the 9th Natl. Conf., West Lafayette, Indiana*, pp. 530–545.

Nelson, M. (2000). *Hydraulic conductivity of paper sludges.*, Master's thesis, Univ. of Wisconsin-Madison, Madison, Wis.

Norrish, K. (1954). The swelling of montmorillonite, *Transactions Farady Society* **18**: 120–134.

Olsen, H. W. (1960). Hydraulic flow through saturated clays, *Clays and Clay Minerals* **1**: 131–161.

Olsen, H. W. (1969). Simultaneous fluxes of liquid and charge in saturated kaolinite, *Soil Science Society of America* **33**: 338–344.

Olsen, H. W., Yearsley, E. N. and Nelson, K. R. (1990). Chemico-osmosis versus diffusion-osmosis, *Transportation Research Record* **1288**: 15–22.

Onikata, M., Kondo, M., Hayashi, N. and Yamanaka, S. (1999). Complex formation of cation-exchanged montmorillonites with propylene carbonate: Osmotic swelling in aqueous electrolyte solutions., *Clay and clay minerals. Vol. 47, No.5,672-677.* **47**(5): 672–677.

Onikata, M., Kondo, M. and Kamon, M. (1996). Development and characterization of a multiswellable bentonite, *in* M. K. ed. Balkema Rotterdam (ed.), *Environmental Geotechnics*, pp. 587–590.

Onsager, L. (1931a). Reciprocal relations in irreversible processes 1, *Physical Review* **37**(4): 405–426.

Onsager, L. (1931b). Reciprocal relations in irreversible processes 11. physical review 38(12): 2265-2279., *Physical Review* **38**(12): 2265–2279.

Petrov, R. J. and Rowe, R. K. (1997). Geosynthetic clay liner (gcl) - chemical compatibility by hydraulic conductivity testing and factors impacting its performance, *Canadian Geotechnical Journal* **34**: 863–885.

Petrov, R. J., Rowe, R. K. and Quigley, R. M. (1997). Selected factors influencing gcl hydraulic conductivity, *Journal of Geotechnical and Geoenvironmental Engineering, ASCE* **123**(8): 683–695.

Porter, L. K., Kemper, W. D., Jackson, R. D. and Steward, B. A. (1960). Chloride diffusion in soils as influenced by moisture content, *Proc. Soil Sci. Soc. Am.* **24**(6): 460–463.

Pusch, R. and Schomburg, J. (1999). Impact of microstructure on the hydraulic conductivity of undisturbed and artificially prepared smectitic clays., *Engineering Geology* **54**: 167–172.

Qiu, H. and Yu, J. (2007). Polyacrylate/(cmc mmt) superabsorbent nanocomposite: Preparation and water absorbency, *Journal of Applied Polymer Science* **107**: 118–123.

Quirk, J. P. and Marcelja, S. (1997). Application of double-layer theories to the extensive crystalline swelling of li-montmorillonite, *Langmuir* **13**: 6241–6248.

Redding, A. Z. and Burns, S. E. (2000). Compressibility and index properties of organic exchanged bentonite, *Geotechnical Special Publication, ASCE* **105**: 142–150.

Robinson, R. A. and Stokes, R. H. (1959). *Electrolyte Solutions*, 2nd edn, Butterworth Scientific Publications: London UK.

Rowe, R. K. (1998). Geosynthetics and the minimization of contaminant migration through barrier systems beneath solid waste, *Proceedings of the Sixth International Conference on Geosynthetics, Atlanta*, Vol. 1, pp. 27–102.

Ruehrwein, R. A. and Ward, D. W. (1952). Mechanismo of clay aggregation by electrolytes, *Soil science* **73**: 485–492.

Ruhl, J. L. and Daniel, D. E. (1997). Geosynthetic clay liners permeated with chemical solutions and leachates, *Journal of Geotechnical and Geoenvironmental Engineering. ASCE* **123**(4): 369–381.

Satoshi, T. and Mitsuji, K. (1996). Evaluation of swelling behaviour and permeability of geosynthetic clay liner., *in* Kamon (ed.), *Environmental Geotechnics*, Vol. 1 of *609614*.

Schroeder, C., Monjoie, A., Illing, P., Dosquet, D. and Thorez, J. (2001). Testing a factory-prehydrated gcl under several conditions, *in* CISA (ed.), *Proceedings Sardinia 2001, 8th International Waste Management and Landfill Symposium, Cagliari, Italy*, Vol. 1.

Shackelford, C. D. (1991). Laboratory diffusion testing for waste disposal: A review., *Journal of Contaminant Hydrology* **7**: 177–217.

Shackelford, C. D. (2005). Environmental issues in geotechnical engineering, *Proceedings of the 16th International Conference on Soil Mechanics and Geotechnical Engineering. September 12-16, 2005, Osaka, Japan.*

Shackelford, C. D., Benson, C. H., Katsumi, T., Edil, T. B. and Lin, L. (2000). Evaluating the hydraulic conductivity of gcls permeated with non-standard liquids, *Geotextiles and Geomembranes, ELsevier* **18**: 133–161.

Shackelford, C. D. and Daniel, D. E. (1991). Diffusion in saturated soil: I. background., *Journal of Geotechnical Engineering* **117**: 467–484.

Shackelford, C. D. and Lee, J. (2003). The destructive role of diffusion on clay membrane behaviour., *Clay and Clay Minerals* **51**(2): 186–196.

Shang, J., Lo, K. and Quigley, R. (1994). Quantitative determination of potential distribution in stern-guoy double-layer model, *Canadian Geotechnical Journal* **31**: 624–636.

Simon, F. G. and Müller, W. W. (2005). Standard and alternative landfill capping design in germany, *Environmental Science and Policy, Elsevier* **7**(4): 277–290.

Sinha Ray, S. and Bousmina, M. (2005). Biodegradable polymers and their layered silicate nanocomposites: In greening the 21st century materials world, *Progress in Materials Science. Elsevier* **50**: 962–1079.

Soule, N. M. and Burns, S. E. (2001). Effects of organic cation structure on behavior of organobentonites, *Journal of Geotechnical and Geoenvironmental Engineering* **127**(4): 363–370.

Spiegler, K. S. (1958). Transport processes in ionic membranes, *Transactions of'the Faraday Society* **54**: 1408–1428.

Staverman, A. J. (1952). Non-equilibrium thermodynamics of membrane processes., *Transactions of the Faraday Society* **48**(2): 176–185.

Stumm, W. (1992). *Chemistry of the solid-water interface*, Wiley, New York.

Stutzmann, T. and Siffert, B. (1977). Contribution to the adsorption mechanism of acetamide and polyacrylamide on to clays, *Clays and Clay Minerals* **25**: 392–406.

Sumner, M. and Miller, W. (1996). *Method of Soil Analysis (Chapter: Cation exchange Capacity and Exchange Coefficients).*, Vol. 3.

Teorell, T. (1935). An attempt to formulate a quantitative theory of membrane permeability, *Proceedings of the Society for Experimental Biology and Medicine* **33**: 282–283.

Teorell, T. (1937). The properties and functions of membranes, natural and artificial, ii, *Artificial membranes, General discussion. Transactions of the Faraday Society* **33**: 1086–1088.

Terzaghi, K. T. (1923). Die berechnung der durchlassigkeitsziffer des tons aus dem verlauf der hydrodynamischen spannungserscheinungen, *Akademie der Wissenschaften in Wien. Sitzungsberichte, Mathematischnaturwissenschaftliche* **132**: 125–138.

Tessier, D. (1990). *Behavior and microstructure of clay minerals*, Plenum Press, New York.

Theng, B. K. G. (1982). Clay-polymer interactions: summary and perspectives., *Clay and Clay Minerals.* **30**(1): 1–10.

Trauger, R. and Darlington, J. (2000). Next-generation geosynthetic clay liners for improved durability and performance, *in* P. U. Geosynthetic Institute, Folsom (ed.), *Proceedings 14th GRI Conference*, pp. 255–267.

van Olphen, H. (1977). *An Introduction to Clay Colloid Chemistry, 2nd edition.*, John Wiley and Sons, Inc., New York.

Van Olphen, H. (1991). *An introduction to clay colloid chemistry*, 2nd edn.

Van Ranst, E. (2006). *Soil Mineralogy*, International Centre for Physical Land Resources.

Vasko, S. V., Jo, H. Y., Benson, C. H., Edil, T. B. and Katsumi, T. (2001). Hydraulic conductivity of partially prehydrated geosynthetic clay liners permeated with acqueous calcium chloride solutions., *Geosynthetics 2001* pp. 685–699.

Warkentin, B. P. and Schofield, R. K. (1958). Swelling pressures of dilute na-montmorillonite pastes, *Clays and Clay Minerals* **7**: 350–364.

Yalcin, T., Alemdar, A., Ece, . I. and Gngr, N. (2002). The viscosity and zeta potential of bentonite dispersions in presence of anionic surfactants, *Materials Letters* **57**: 420–424.

Yaroshchuk, A. E. (1995). Osmosis and reverse osmosis in fine-charged diaphragms and membranes, *Advances in Colloid and Interface Science, 60: 1-93.* **60**: 1–93.

Yeung, A. T. and Mitchell, J. K. (1993). Coupled fluid, electrical and chemical flows in soil, *Geotechnique* **43**(1): 121–134.

A

Numerical model calculation sheets

A.1 Flowchart

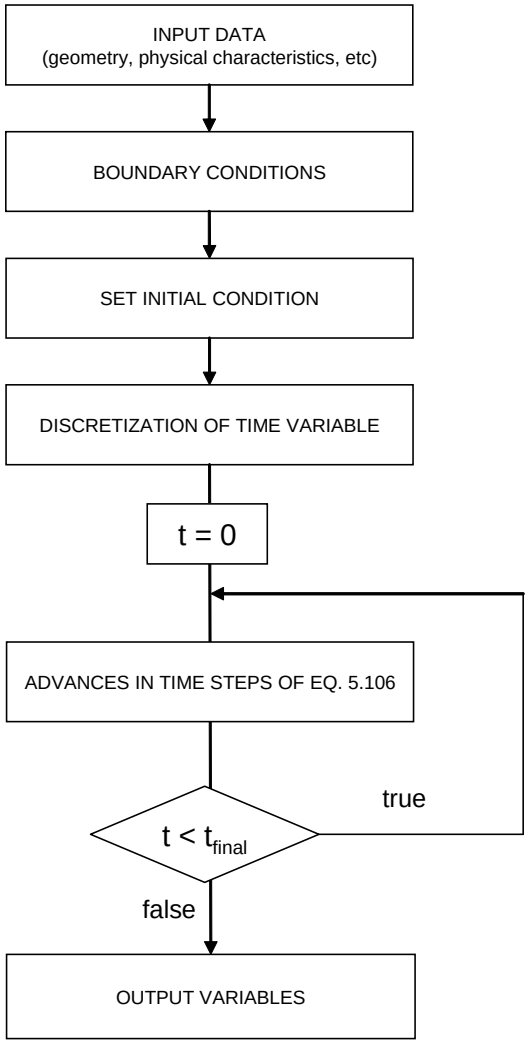

A.2 Matlab calculation sheet, parametric N

```
 % Version 1. Script for osmotic test simulation

clear all

global eps alpha
global term1 term2

% Parameters
L=0.006;                %[m]
n=0.717;                %[-]
D0Ca=7.92*10^(-10);     %[m^2/s]
D0Na=13.3*10^(-10);     %[m^2/s]
D0Cl=20.3*10^(-10);     %[m^2/s]
tau=0.015;              %[m^2/s]
CX0=0.018;             %[mol/L]
C0=0.001;               %[mol/L] CaCl2 Reference Concentration
R=8.314;                %[N*m/(mol*K)]
T=273+20;               %[C]
muw=10^(-3);            %[Pa*s]
Smax=760;               %[m^2/g]
%Nl=3;                   %[-]
ros=2.65;               %[g/cm^3]
trealfin=60;            %[day]
Kw=4.6E7;               %[kPa]
Hpp=0.006;              %[m]
npp=0.3;                %[-]
gammaw=9.81;            %kN/m^3
k=6.35*10^-12;          %m/s
A=0.0040                %m^2

% Calculated Parameters
eb=n/(1-n);                     %[-]
CX=CX0/eb;                      %[mol/L]
DCa=tau*D0Ca;                   %[m^2/s]
DNa=tau*D0Na;                   %[m^2/s]
DCl=tau*D0Cl;                   %[m^2/s]
%S=Smax/Nl;                     %[m^2/g]
ros=ros*10^6;                   %[g/m^3]
muw=10^(-6);                    %[kPa*s]
```

```
%b=eb/(ros*S);                  %[m]
%dh=tau/muw*(bˆ2)/3;            %[mˆ4/(kN*s)]
trealfins=trealfin*24*60*60;    %[s]

% Numerical Parameters
dx=1/2;
t0=Lˆ2/DCa;
t0p=npp*Hpp*gammaw*(L/2)/(Kw*k);
tfin=trealfins/t0;
dt=0.001;
nt=tfin/dt;

% Initial Conditions NL
NLpar=[1 3 5 10 20];

wMatrix=[1:nt+1];
wMatrix=wMatrix';

for i=1:5

Nl=NLpar(i);                    %[-]

S=Smax/Nl;                      %[mˆ2/g]
b=eb/(ros*S);                   %[m]
dh=tau/muw*(bˆ2)/3;             %[mˆ4/(kN*s)]


% Boundary Conditions

% TOP (A) boundary conditions
uAvCa=1;              % uvCa=CsolCa/C0;
uAvCl=2;              % uvCl=CsolCl/C0;
uAvNa=0;              % uvNa=CsolNa/C0;
eps=uAvNa/uAvCa;
alpha=CX/(uAvCa*C0);
GCl=fzero(@Donnan,0.5);
GCa=GClˆ(-2);
GNa=GClˆ(-1);
uACa=uAvCa*GCa;
uACl=uAvCl*GCl;
uANa=uAvNa*GNa;
```

```
% BOTTOM (B) boundary conditions
uBCa(1)=0;                  % uCa=CCa/C0;
uBCl=0;
uBNa(1)=CX/C0;
uBvCa=0;
uBvCl=0;
uBvNa=0;

% Initial Conditions
t(1)=0;
uCa(1)=0;
uCl(1)=0;
uNa(1)=CX/C0;
uvCa(1)=0;
uvCl(1)=0;
uvNa(1)=0;
pA(1)=0;
pB(1)=0;
deltapbis(1)=0;
wbis(1)=0;
J(1)=0;



for it=1:nt
    uCaold=uCa(it);
    uClold=uCl(it);
    uNaold=uNa(it);
    uBCaold=uBCa(it);
    uBNaold=uBNa(it);
    pAold=pA(it);
    pBold=pB(it);
    uCa12=(uACa+uCaold)/2;
    uCl12=(uACl+uClold)/2;
    uNa12=(uANa+uNaold)/2;
    uCa32=(uBCaold+uCaold)/2;
    uCl32=(uBCl+uClold)/2;
    uNa32=(uBNaold+uNaold)/2;
    kappa12=4*uCa12*DCa+uNa12*DNa+uCl12*DCl;
```

```
    kappa32=4*uCa32*DCa+uNa32*DNa+uCl32*DCl;
    tCa12=4*uCa12*DCa/kappa12;
    tCl12=uCl12*DCl/kappa12;
    tNa12=uNa12*DNa/kappa12;
    tCa32=4*uCa32*DCa/kappa32;
    tCl32=uCl32*DCl/kappa32;
    tNa32=uNa32*DNa/kappa32;
    coeffin=2*DCa*(uACa-uCaold)+DNa*(uANa-uNaold)-DCl*
    (uACl-uClold);
    coeffout=2*DCa*(uCaold-uBCaold)+DNa*(uNaold-uBNaold)-DCl*
    (uClold-uBCl);
    JCain=DCa*(uACa-uCaold)-tCa12/2*coeffin;
    JCaout=DCa*(uCaold-uBCaold)-tCa32/2*coeffout;
    J(it+1)=J(it)+JCaout;
    uCa(it+1)=uCaold+4/DCa*(JCain-JCaout)*dt;
    JClin=DCl*(uACl-uClold)+tCl12*coeffin;
    JClout=DCl*(uClold-uBCl)+tCl32*coeffout;
    uCl(it+1)=uClold+4/DCa*(JClin-JClout)*dt;
    uNa(it+1)=CX/C0+uCl(it+1)-2*uCa(it+1);
    aux1=uCa(it+1);
    aux2=uNa(it+1);
    if aux1<=CX/C0
        uBCa(it+1)=aux1;
        uBNa(it+1)=aux2;
    else
        uBCa(it+1)=CX/C0;
        uBNa(it+1)=0;
    end
    term1=uNa(it+1)*uCl(it+1);
    term2=((uCl(it+1))^2)*uCa(it+1);
    uvCl(it+1)=fzero(@Donnanv,2);
    uvCa(it+1)=term2/((uvCl(it+1))^2);
    uvNa(it+1)=uvCl(it+1)-2*uvCa(it+1);
    k12=n*dh/(1+dh*CX^2*R*T/kappa12);
    k32=n*dh/(1+dh*CX^2*R*T/kappa32);
    betaA=k12/(L/2);
    betaB=k32/(L/2);
    gammaA=-(uAvCa-uvCa(it+1)+uAvNa-uvNa(it+1)+uAvCl-uvCl(it+1))+
(uACa-uCa(it+1)+uANa-uNa(it+1)+uACl-uCl(it+1))-CX/C0/kappa12*
(2*DCa*(uACa-uCa(it+1))+DNa*(uANa-uNa(it+1))-DCl*(uACl-uCl(it+1)));
    gammaB=-(uvCa(it+1)-uBvCa+uvNa(it+1)-uBvNa+uvCl(it+1)-uBvCl)+
```

```
    (uCa(it+1)-uBCaold+uNa(it+1)
-uBNaold+uCl(it+1)-uBCl)-CX/C0/kappa32*(2*DCa*(uCa(it+1)-uBCaold)
+DNa*(uNa(it+1)
-uBNaold)-DCl*(uCl(it+1)-uBCl));
    coeffp1=betaA*betaB/(betaA+betaB);
    coeffp2=gammaA+gammaB;
    pA(it+1)=pAold-Kw/(Hpp*npp*A)*t0p*coeffp1*
    (pAold-pBold+coeffp2*R*T*C0*10^(3))*dt;
    pB(it+1)=pBold+Kw/(Hpp*npp*A)*t0p*coeffp1*
    (pAold-pBold+coeffp2*R*T*C0*10^(3))*dt;
    deltap(it+1)=pA(it+1)-pB(it+1);
    deltapbis(it+1)=-coeffp2;
    wbis(it+1)=deltapbis(it+1)/3;
    w(it+1)=deltap(it+1)/(R*T*3*C0*10^(3));
    t(it+1)=t(it)+dt;
end

wMatrix=[wMatrix w'];

end


tgiorniplot=t*t0/(60*60*24);
uCaplot=uCa*C0;
uNaplot=uNa*C0;
uClplot=uCl*C0;
%figure(1)
%plot(tgiorniplot,uCa);
%xlabel('Time (days)')
%ylabel('Calcium Relative Concentration')
%figure(2)
%plot(tgiorniplot,uNa);
%xlabel('Time (days)')
%ylabel('Sodium Relative Concentration')
%figure(3)
%plot(tgiorniplot,uCl);
%xlabel('Time (days)')
%ylabel('Chloride Relative Concentration')
%figure(4)
%plot(tgiorniplot,uCaplot);
%xlabel('Time (days)')
```

```
%ylabel('Calcium Concentration (mol/L)')
%figure(5)
%plot(tgiorniplot,uNaplot);
%xlabel('Time (days)')
%ylabel('Sodium Concentration (mol/L)')
%figure(6)
%plot(tgiorniplot,uClplot);
%xlabel('Time (days)')
%ylabel('Chloride Concentration (mol/L)')
figure(7)
plot(tgiorniplot,wMatrix(:,2),tgiorniplot, wMatrix(:,3),
tgiorniplot, wMatrix(:,4),
tgiorniplot, wMatrix(:,5), tgiorniplot, wMatrix(:,6))
xlabel('Time (days)')
ylabel('Chemico-Osmotic Efficiency Coefficient, \omega')
legend('N=1','N=3','N=5','N=10','N=20')
%figure(8)
%plot(tgiorniplot,wbis)
%xlabel('Time (days)')
%ylabel('Chemico-Osmotic Efficiency Coefficient, \omega')
%figure(9)
%plot(tgiorniplot,uBCa,tgiorniplot,uBNa)
%xlabel('Time (days)')
%ylabel('Cation Relative Concentrations');
%legend('Calcium','Sodium')
%figure(10)
%plot(tgiorniplot, J)
%xlabel('Time (days)')
%ylabel('Flux (mol/m2*s)')
%legend('Flux J')

%Results=[tgiorniplot' uCa' uNa' uCl' uCaplot' uNaplot'
uClplot' w' wbis'];
%save Res.dat Results -ascii
```

B

Hydraulic conductivity test results: pH and Eh of the outlet

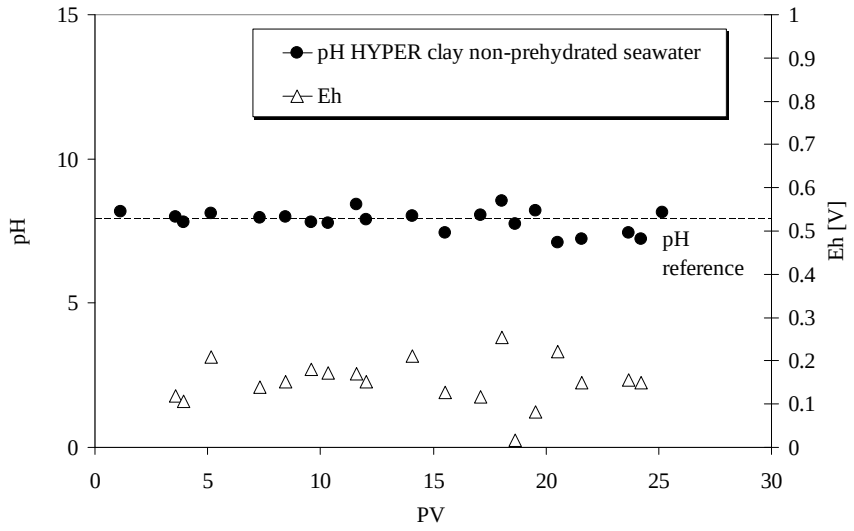

Figure B.1: Outlet pH and redox potential of the hydraulic conductivity test on the HYPER clay permeated with seawater

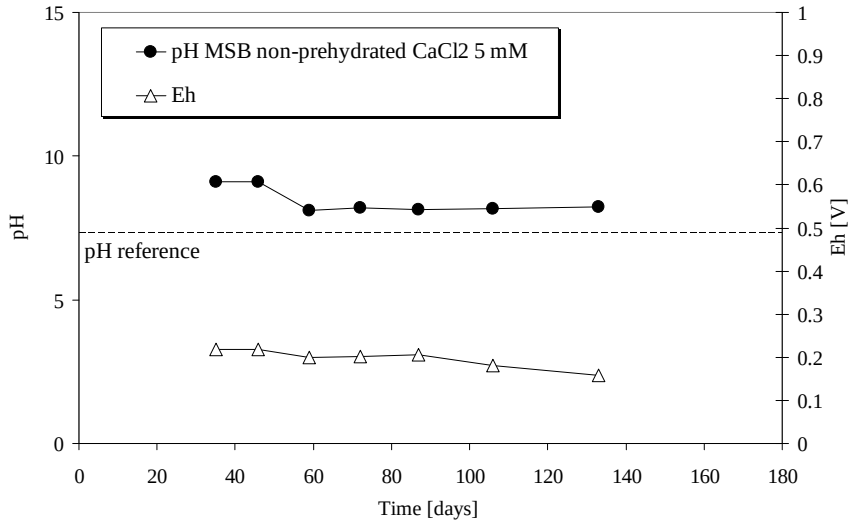

Figure B.2: Outlet pH and redox potential of the hydraulic conductivity test on the non-prehydrated MSB permeated 5 mM $CaCl_2$ solution

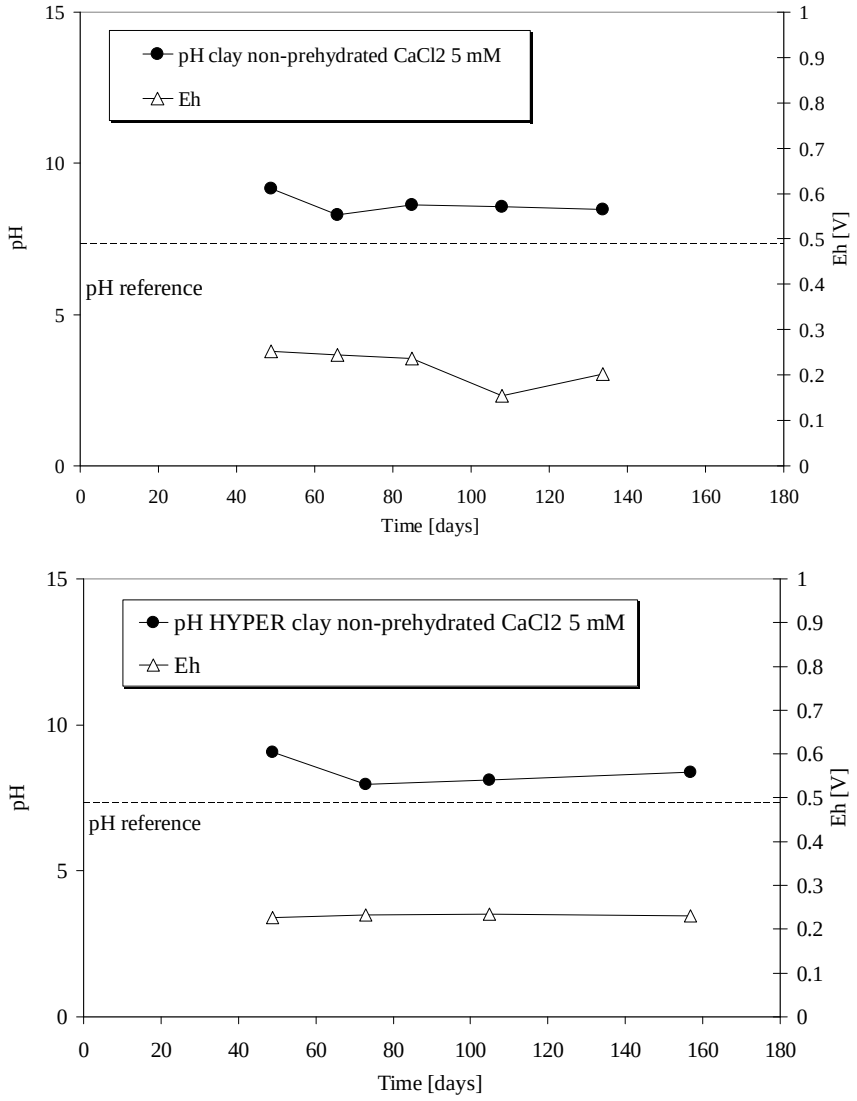

Figure B.3: Outlet pH and redox potential of the hydraulic conductivity test on the non-prehydrated (a) untreated clay and (b) HYPER clay permeated with 5 mM $CaCl_2$ solutions

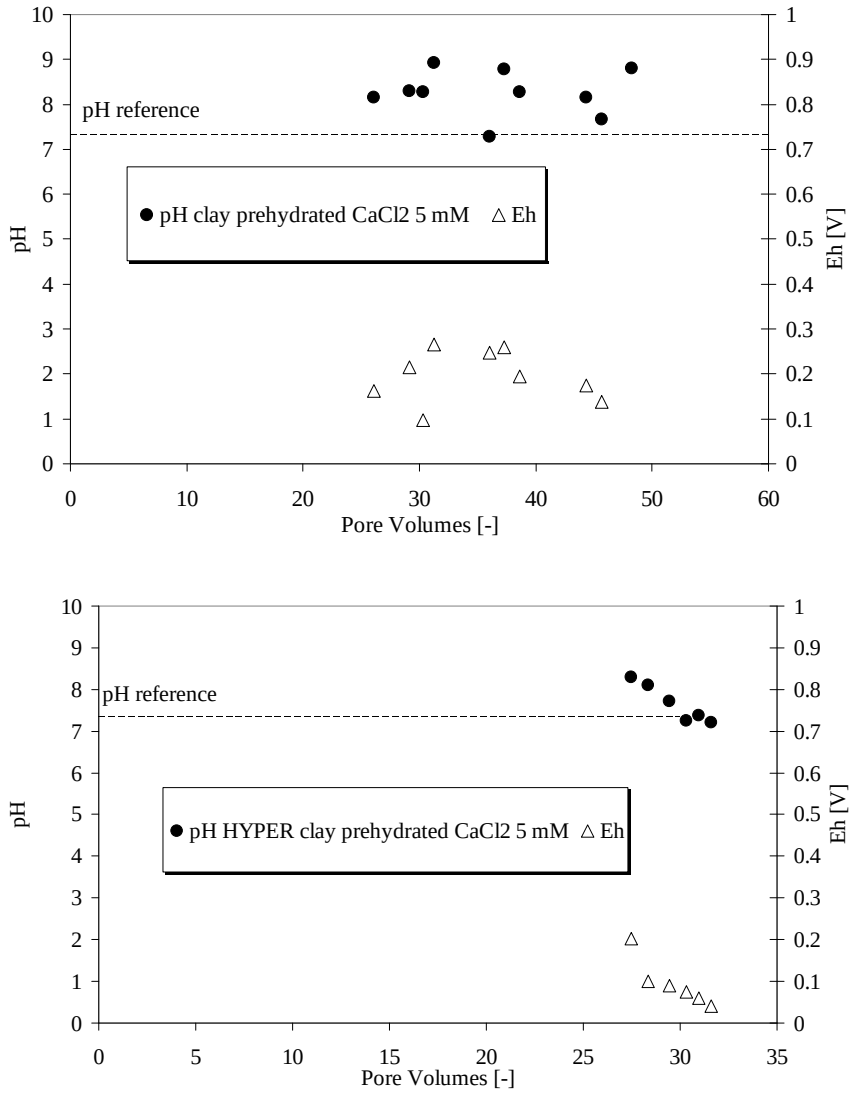

Figure B.4: Outlet pH and redox potential of the hydraulic conductivity test on the (a) untreated clay and (b) HYPER clay permeated with 5 mM $CaCl_2$ solutions after prehydrated with deionized water

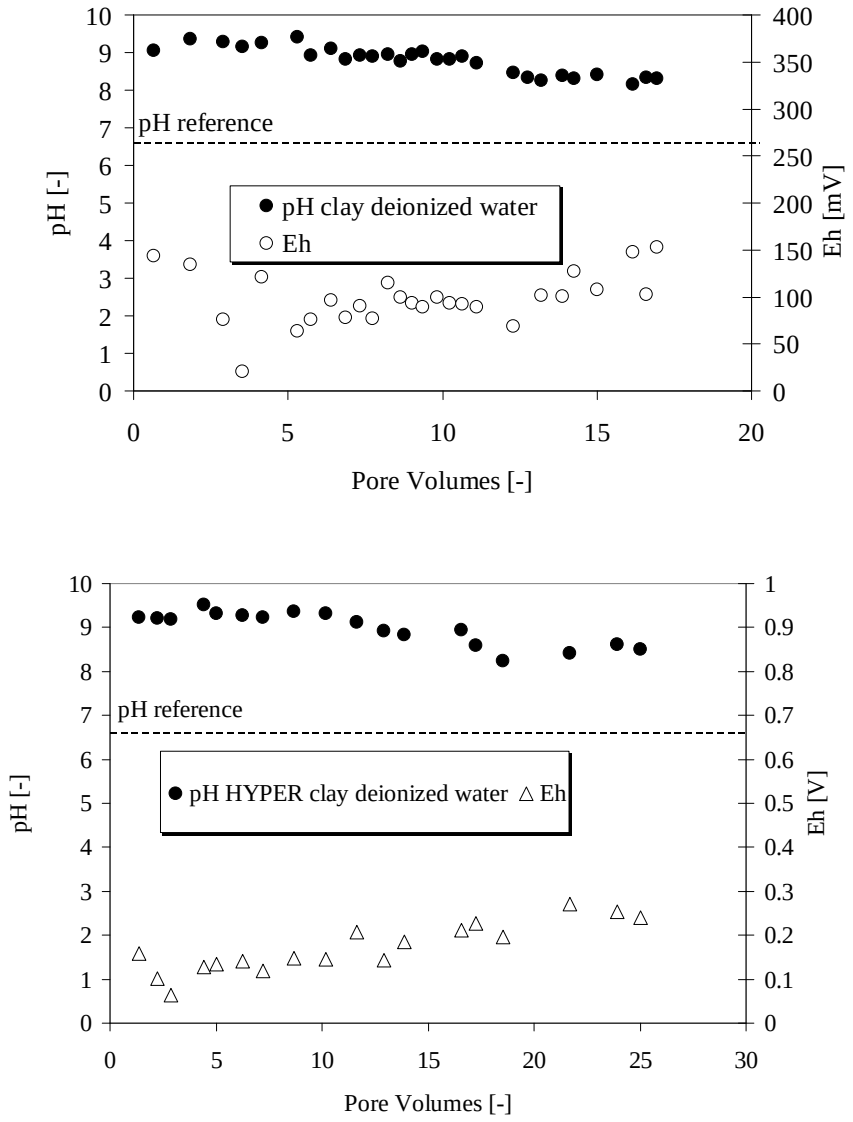

Figure B.5: Outlet pH and redox potential of the hydraulic conductivity test on the (a) untreated clay and (b) HYPER clay permeated with deionized water

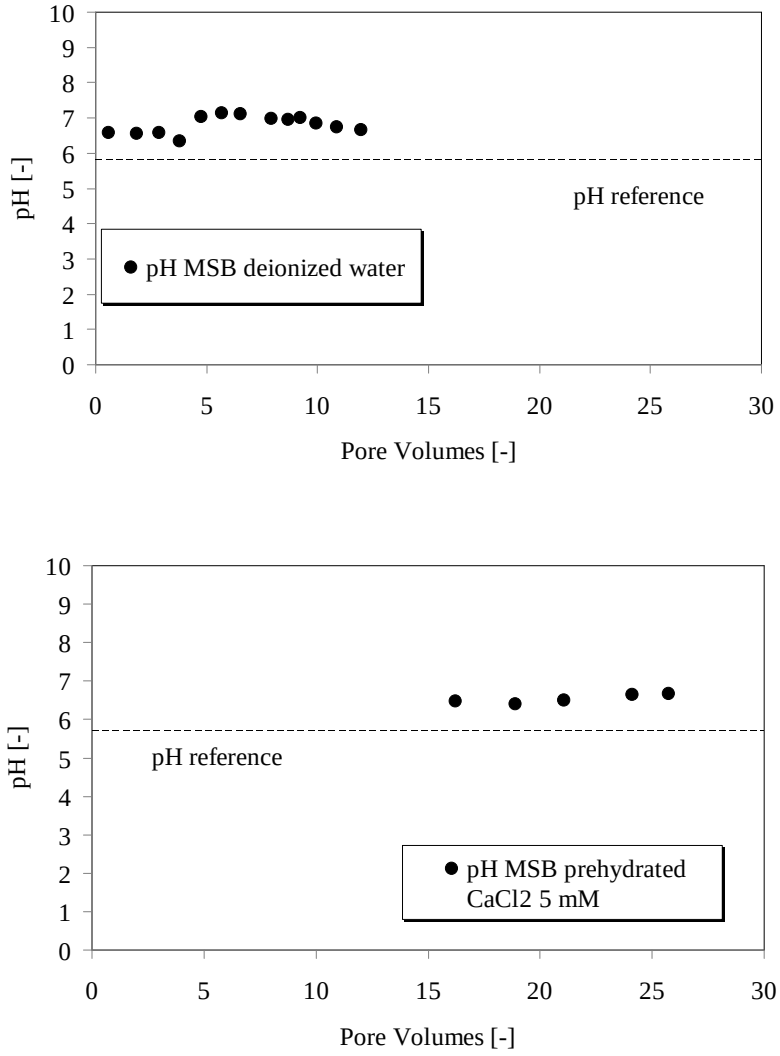

Figure B.6: Outlet pH and redox potential of the hydraulic conductivity test on the MSB bentonite permeated with (a) deionized water and (b) 5 mM $CaCl_2$ solution (after prehydration with deionized water)

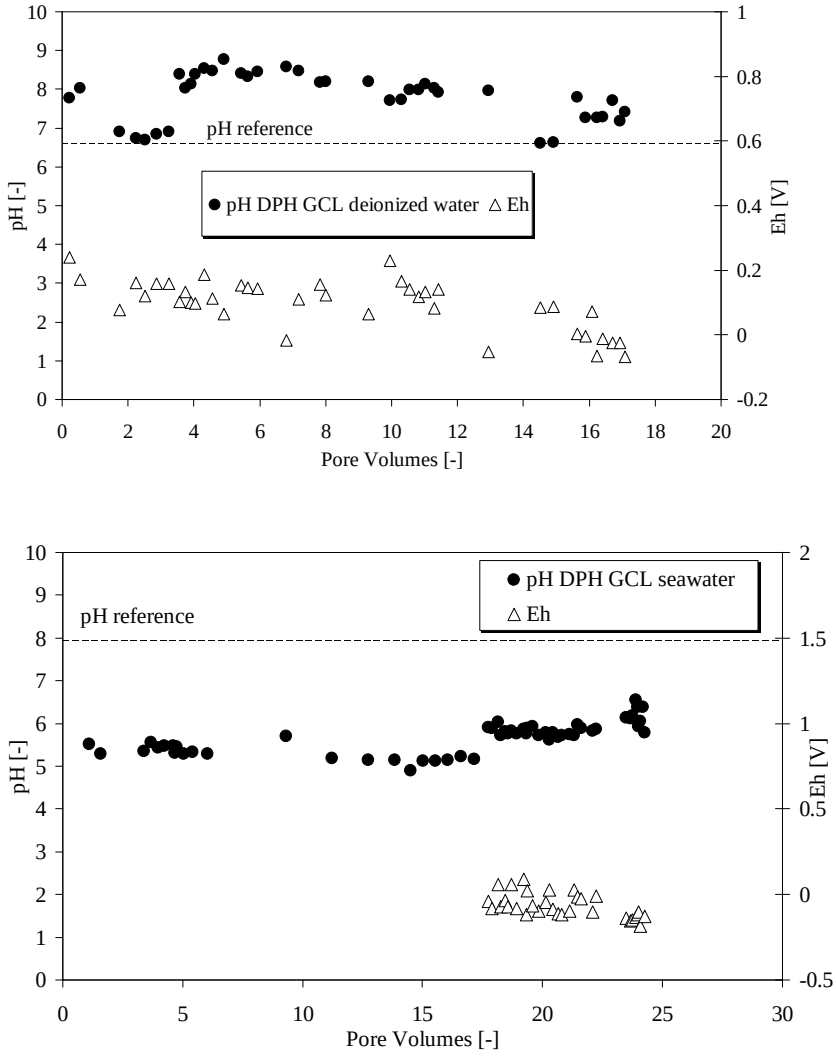

Figure B.7: Outlet pH and redox potential of the hydraulic conductivity test on the DPH GCL overlap permeated with (a) deionized water and (b) seawater

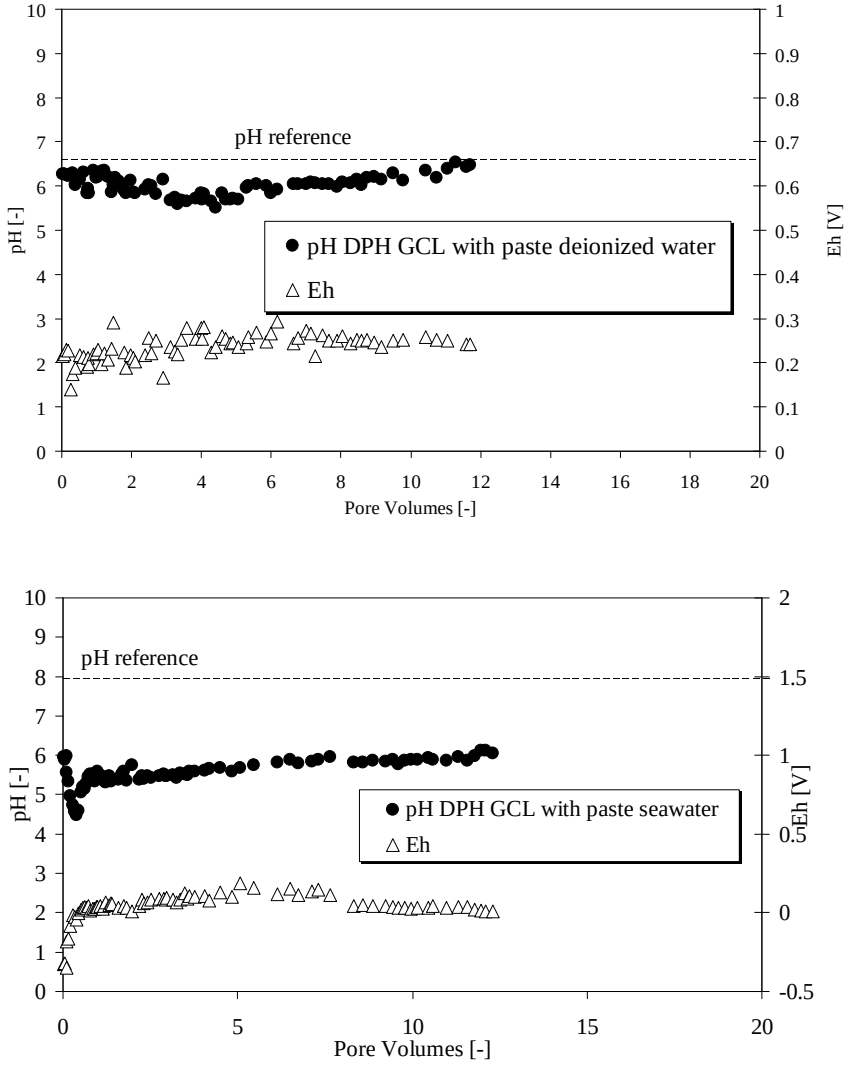

Figure B.8: Outlet pH and redox potential of the hydraulic conductivity test on the DPH GCL overlap with paste permeated with (a) deionized water and (b) seawater

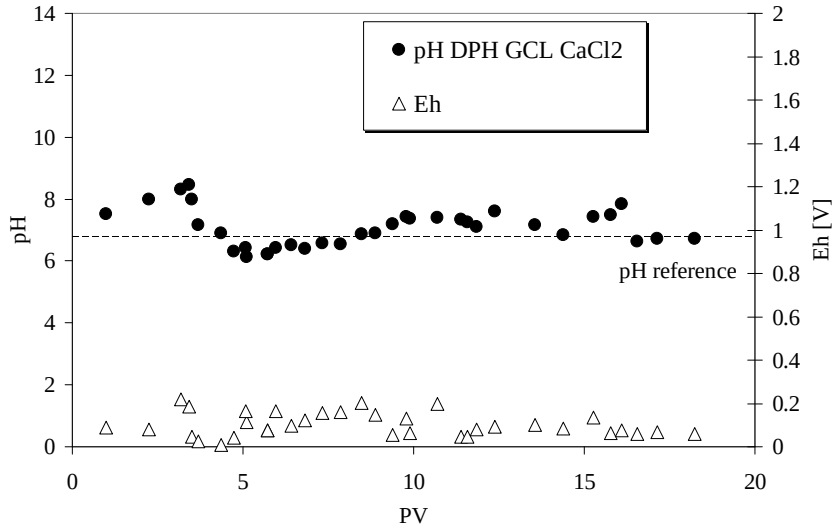

Figure B.9: Outlet pH and redox potential of the hydraulic conductivity test on the DPH GCL overlap permeated with Calcium Chloride solutions (0.01 M, 0.02 M, 0.1 M)